# Investigating the Impacts of Support Policies on Agricultural Land Use and Production with Satellite Remote Sensing:

## A Case Study in the Cross-border Area between Turkey and Bulgaria

By

Aparna Ravindra Phalke

A dissertation submitted in partial fulfillment of

the requirements for the degree of

Doctor of Philosophy

(Environment and Resources)

at the

UNIVERSITY OF WISCONSIN-MADISON

2021

Date of final oral examination: 09/01/2021

The dissertation is approved by the following members of the Final Oral Committee:

Mutlu Özdoğan, Associate Professor, Environmental Studies, Forest and Wildlife Ecology
Jeremy Foltz, Professor, Agriculture and Applied Economics
Annemarie Schneider, Associate Professor, Nelson Institute for Environmental Studies
Philip Townsend, Professor, Forest and Wildlife Ecology
Lachezar Hristov Filchev, Associate Professor, Bulgarian Academy of Sciences, Bulgaria

**Abstract**

People are the main force behind massive global transformations of land. Agricultural land is one such transformation, and its changes are driven by political and socio-economic factors as well as the capability of land to support local decisions. To this end, human dimensions of land use change can only be investigated through case studies that relate observed changes on the landscape to socio-economic and biophysical drivers. One such example is located in the cross-border area between Turkey and Bulgaria. Recent historical events in Bulgaria caused major socio-economic changes while Turkey has been a stable democracy for some time, setting the stage for a "natural experiment." What remains unknown is: How did the different pathways of socio-economic development affect agricultural land use decisions in the cross-border countries with similar agro-climatic patterns? To address this question, a detailed study involving remote sensing, crop production modeling, and comprehensive statistical analysis is presented. This dissertation addressed the following research questions: 1. What are the rates and patterns of the agricultural land use change in the cross-border between Turkey and Bulgaria in the last 20 years? 2. How has the wheat production changed in the same period? 3. What are the drivers of observed agricultural land use and production changes in the same period?

The primary contributions of this research are: i) improved understanding of support policies and their impacts on agricultural land and production; ii) new remote sensing tools with the benefit of automated crop type and yield mapping at large areas; and iii) better insights into potential biophysical underpinnings of local land use changes driven by global (country wide) decisions. This dissertation research is the first of its kind to study the cross-border area between Turkey and Bulgaria and fills an important gap in our knowledge on the effects of broad socio-economic forces on local land use decisions in a location where this information is sorely lacking.

To all the **Women** from remote parts of the world who are consistently paving the road for existence, independence and empowerment,

and

To all the **Farmers**

**Acknowledgements**

In my Ph.D. journey, I am grateful to have met many intelligent, focused, humble, and genuinely great people. This dissertation would have been incomplete without their support.

First, I would like to deeply thank my advisor, *Professor Mutlu Özdoğan*. Today, if I think I can help sustain this competitive world and have the capability to contribute in the science for societal welfare, that's only because of my advisor. In the last eight years, I got the opportunity to observe him, learn from him and be an empathetic human being like he is! His guidance on both research as well as on my career is invaluable. He always supported me and showed a right direction through my downfalls. Mutlu was the inspiration to choose the case study area of my dissertation, and he was so generous in providing detailed and careful insights on the socio-economics of the region, which benefitted my dissertation abundantly. His countless and valuable hours on my research discussions and scientific writing sessions helped me shape my dissertation as it is today. I simply can't thank him enough for his guidance, mentorship, support, strength and honesty. I hope I will become an established scientist like Mutlu, who has excellent public speaking skills, who can explain complicated science in simple terms, who is always eager to learn, and beyond professional life, who cares for his family more than anything!

I am profoundly grateful to the rest of my committee. *Professor Annemarie Schneider* is a passionate scientist and role model — a successful woman in science for early-career researchers like me. I was fortunate to have her on my committee. I was a student of her very famous land use change seminar and was amazed by her thorough scientific knowledge and simplicity. This class inspired me to collaborate with her. I really appreciate her continuous support, valuable advice and research discussion time. I am constantly motivated by her excellent research skills and writing

skills. Her research articles have been the set examples for my writing from the beginning. I wish to work closely with her in the future if I get the chance. She has my utmost respect.

I am very thankful to *Professor Philip Townsend* for all his support and guidance. Phil once gave me important advice during my prelims about "differentiating between the project work and research work" when your dissertation is funded through a project. This thought always directed me to think critically in my research work towards building the science and not just producing the results. I was a student in his well-known forest disturbances and spectroscopy seminars. I was overwhelmed by his teaching because his classes gave equal weight to theory and application. Phil always helped me whenever needed. I am grateful for his valuable support and research guidance. I really look forward to working closely with him in the future if I get the opportunity.

I would like to express my deepest appreciation to *Professor Jeremy Foltz*. Jeremy was very generous in helping me conceptualize the socio-economic research part of this dissertation. I really appreciate his valuable time for discussing my research and guiding with his detailed insights. He provided a direction to my research with his excellent knowledge of global agricultural economics. I remember emailing him with panic when I was stuck on my research questions, and he was so quick in replying and helping. I really appreciate his genuine support and encouragement during this research journey of mine.

I would like to thank *Professor Lachezar H. Filchev* for his valuable support. When I decided to work on a case study in Bulgaria, I approached to Lachezar for access to the only detailed crop calendar information of that region, which he had published in one of his papers. He was very generous in responding to my request and provided detailed datasets related to my research and introduced me to his lab work regarding the same. I was tremendously impressed with his lab's work and proposed him to be part of my dissertation committee. Since then, he has

been enormously helpful with discussing the agricultural research questions, giving access to the available datasets, providing ancillary data information, and inviting me for a field study visit. I would like to extend my profound gratitude for all his help and countless hours in discussing the research as well as providing the rare dataset of the study area. I am constantly inspired by Lachezars' teamwork and humbleness. I will carry these values from him forever. I wish to continue my collaboration with him in future.

This dissertation would not have been possible without support from the United States Geological Survey (USGS) and the National Aeronautics and Space Administration's Making Earth System Data Records for Use in Research (MEaSUREs) funding for Global Food Security-support Analysis Data (GFSAD30) project. *Dr. Prasad S. Thenkabail* is the main inspiration of my dissertation study. I am deeply thankful to Prasad for his generous support, continuous guidance, and constant encouragement during my research tenure. Prasad is always a role model to me as his research has brought the passion for remote sensing in me. I remember he always pushed me "to be proactive," and his kind words always made a deep impact on my actions. Prasad will always be a lifetime mentor and teacher to me. I am fortunate to have worked with a world-class team of scientists in the early days of my career. I would like to thank my NASA project work team – Dr. Pardhasaradhi Teluguntla, Dr. Murli Krishna Gumma, Dr. Jun Xiong, Dr. Russ Congalton, Dr. Teki Sankey, Dr. Curt Reynolds, Dr. James Tilton, Dr. Chandra Giri, Dr. Atul Jain, Dr. Mahesh Rao, Adam Oliphant, and Justin Poehnelt. Special thanks to my Ph.D. colleagues and my best friends from GFSAD30 project, without whom this journey would have been different – Dr. Richard Massey and Dr. Kamini Yadav. I would also like to give special thanks to Google Earth Engine team for their kind support – Dr. Tyler Erickson and Dr. Noel Gorelick.

I would like to thank many people from UW-Madison who helped and supported me on this journey. To start with, Center for Sustainability and the Global Environment (SAGE) and Ozdogans' lab – Yang and Yanghui were my first friends in Madison, and we went through all the struggles and happiness together. I express my deepest gratitude to both. Anke brought a joy to my Madison life. Without her, I can't imagine my PhD journey. Kaitlin, Zhiwei, Michael, Ghassan, Matthias and Ryan – all were great friends and always motivated me to work hard. I would like to thank Naparat– she brought the "Thai connection" back to my life with her friendship. I want to thank Mary, Laurel and Martina for their help and support to prepare my research trips, conferences and project related activities. Carol is a positive source of energy for SAGE – I always get motivated by her personality. I would like to thank Dr. Jonathan Foley, Dr. Chris Kucharik, Dr. Holly Gibbs and Dr. Tracey Holloway as they have always inspired me in my research journey with their sincere research work. I would like to give special thanks to all the people from the Nelson Institute for Environmental Studies who supported me and helped me. Jim, Tara and Nick were always available whenever needed, and I am extremely grateful for their help in completing all the administrative academic formalities. I would like to thank Steven Pomplun for his last-minute professional help in proof-reading my dissertation. Dr. Nathan Schulfer, Dr. Sarah J Graves, Dr. Arlyne Johnson and Dr. Aleia McCord have always provided positive support and inspiration. I am very thankful to them. I also would like to thank Dr. Paul Robbins for all his support and work for the students at the Nelson Institute. I would like to thank my sport buddies from Badminton club, Tennis club, Karate Kick Boxing club – they were my stress relief system after the hectic day. I am grateful to my best friend Dr. Akilan Thangarajah for his constant motivation and positivity.

I would like to acknowledge the support from the Dissertator Fellowship Award from the Nelson Institute for Environmental Studies. This fellowship really helped me to concentrate on research without worrying about financial needs. I'm extremely grateful to the selection team.

I would like to give special thanks to all my previous degree teachers and advisors. I have a special place for every one of you, and I am grateful to you all. I can't thank enough my support system from my home-town — people of my village — farmers of my village — women of my village. You are the real inspiration for my work. I wish to make a real impact in your lives and ease the pain with my honest work. I would like to thank all my friends and supporters for their well-wishes.

My parents, Ravindra Phalke and Seema Phalke, are the reason for everything in my life. I dedicate to them everything I own. I wish for their happiness always! This dissertation is their hard work. My sister, Archana Phalke Chavan, and brother, Rohit Phalke, are my power-houses in anything I do. I would like to thank my in-laws and family; they were the kindest and very supportive in this entire process.

Finally, I would like to express my profound gratitude to my husband, Satish Pawar. His belief in me is the force to work hard and move towards the goal. I have watched him going through toughest time of his life, and I haven't seen anybody else standing strong with such ambition and positivity. He is a constant motivation to me. This dissertation is his as much his as it is mine!

**Table of Contents**

# Chapter 1

## Introduction

### 1.1 Motivation

> "When resources are degraded, we start competing for them, whether it is at the local level [in Kenya], where we had tribal clashes over land and water, or at the global level, when we are fighting over water, oil, and minerals. So, one way to promote peace is to promote sustainable management and equitable distribution of resources."
>
> -Wangari Maathai, 2007.

Human activities have consistently modified the Earth's biosphere for food, fiber and fresh water (Foley et al., 2005; Chhabra et al., 2006; Ramankutty et al., 2018). Agricultural land use is one such modification impacting food security, sustainable development, and environmental policies (DeFries et al., 1995; Godfray et al., 2010). In the near future, 70% more food will need to be produced to meet the calorific demands of rapidly increasing population, and that can be achieved either by expansion or intensification of agricultural lands (Maxwell, 1996; Godfray et al., 2010; Wheeler et al., 2013; Meyfroidt et al., 2017). The Green Revolution was one such historical event, which accelerated agricultural intensification and doubled the world's food production (from 1961 to 1996) with only a 10% global increase in arable lands, but there was a rapid and negative impact on global ecosystem services and environmental footprint (Conway 1998; Roy et al., 2007; Thenkabail et al., 2010; Duncan et al., 2015). To this end, more studies are needed to better understand the drivers and consequences of land use transformations involving agricultural areas.

The geographic distribution of agricultural land use is a complex phenomenon, and its drivers need further exploration (Lambin et al., 2003; Meyfroit et al., 2014). For example, croplands have decreased or have been abandoned due to forest transitions, urbanization, soil degradation, global warming, and desertification in some locations (Baumann et al., 2011; Prishchepov et al., 2013), while in others they have expanded through slash-and-burn agriculture and cultivation of bio-fuel crops and boom crops (Kraemer et al., 2015; Hurni et al., 2017). Literature suggests that at local scales, land use decisions are made in hierarchical order where local actors and socio-economic factors are inter-dependent (Fernandez et al., 2007; Shen et al., 2009; Verburg et al., 2019) although socio-economic factors usually dominate (Dang et al., 2017; Therond et al., 2019). While local actors are responsible for decisions made to change land use, data on local actors is scarce (Prishchepov et al., 2017). Moreover, socio-economic and political changes are different for different locations or countries and regions (Kuemmerle et al., 2013), making it even more challenging to study the impact of support policies on land use change and crop production (Lambin, 2003). One approach to overcome these challenges is to focus on locations where rapid changes in socio-economic and political structures occurred in tandem with relatively stable socio-economic forces, creating "a natural experiment" (Prishchepov et al., 2013).

One example of such natural experiment is at the cross-border area between Turkey and Bulgaria. This region has homogeneous agro-ecological and climatic characteristics, but the amount and patterns of agricultural land use change and production may be dramatically different on each side of the border. There is certainly evidence for such dramatic differences given the socialist history of Bulgaria that was replaced with accession to the European Union (EU) in 2007. In contrast, Turkey has been a politically stable country for close to 100 years, without major socio-

economic transformations. My dissertation is focused on the study of how these contrasting political changes are manifested in agricultural land use change.

To measure the impact of support policies on changes in agricultural land use and production, it is important to make detailed farm-level measurements (Baumann et al., 2011). Although policies are developed at the national levels, the impact of these policies on land use change could be highly local. For example, if agricultural support policies are similar for two states but the farm structures and other biophysical characteristics of those farms are different, then those policies may have very different outcomes on farms in each state. Also, farm-level information can bring additional insights to build and manage support policies.

Satellite remote sensing plays an important role in studying Earth's land use and land cover, given its temporal and spatial characteristics (Schneider, 2012). In particular, the long historical record of Landsat satellite data forms a key dataset to study the trends in land use and land cover change (Baumann et al., 2014). Remote sensing, either alone or in combination with field surveys, has been at the core of identifying and mapping croplands for some time (Myers et al., 1983; Bastiaanssen et al., 2000; Morton et al., 2006; Jensen, 2009; Gao, et al., 2017). However, there are many challenges in mapping croplands with remote sensing, particularly over large areas, due to: i) great geographic variation in cultivation practices, and spatial resolution requirements in areas with small field size distributions (Ozdogan and Woodcock, 2006; Mayaoux et al., 2006; Ozdogan, 2010); ii) lack of reference data or high cost of acquiring reference data used for training that has been traditionally necessary for performing classification over large areas; and iii) 'between-scene variability' associated with Landsat image acquisitions (Phalke and Ozdogan, 2018).

With these issues in mind, this dissertation carried a research program to investigate how agricultural support policies have impacted the agricultural land use change and production between the year 2000 and the present. The following are my specific research objectives.

## 1.2 Research objectives

The overarching objective of this dissertation is to determine the drivers of cropland area and productions changes in the study area and provide the new insights into food security and support policies of the region. This dissertation carried a multi-disciplinary approach with three objectives demonstrating the satellite remote sensing application for large area agricultural monitoring at field-scale (through objective 1 and 2) and, statistical modeling to understand the drivers of agricultural land use and production (through objective 3). These objectives are discussed in detail below.

### Objective 1: Large area cropland and crop type mapping using satellite remote sensing

Timely and accurate cropland maps help to measure the change in agricultural land use from local to regional scales (Pittman et al., 2010; Waldner et al., 2015). The current era of easy access to satellite images and cloud-based image processing platforms provides convenient tools to monitor croplands, but challenges such as the availability of reference information required to map and validate large area cropland maps in a consistent and reproducible fashion remains elusive (Woodcock et al., 2001; Lobell et al., 2004; Pax-Lenney et al., 2001). This study developed a classification tool, which automatically maps cropland extent and wheat area for the last 20 years. The purpose of these maps is to quantify the rates and patterns of agricultural land use change in the study area. Therefore, the primary objective of Chapter 1 is to measure the rates and patterns of the agricultural land use and land cover change in the cross-border between Turkey and Bulgaria after 2000 using satellite remote sensing. This is achieved in three parts. In Part 1 a method for

automated large-area cropland extent mapping is introduced; In Part 2 wall-to-wall cropland extent map production is illustrated; and in Part 3 an automated wheat area mapping approach without training data is presented. Overall, this study demonstrated a large area cropland extent and crop type (wheat) mapping approach using remote sensing, machine learning, and the Google Earth Engine (GEE) platform. The results of this study separately address challenges in producing a mapping algorithm and in developing a consistent product at a global scale. The resulting cropland and wheat area statistics match well with the government statistics, and the method provides an automated and economic way to produce consistent time-series maps with little or no training data. The Part 1 findings of this study have been published in *Remote Sensing of Environment* (Phalke and Özdoğan, 2018) and Part 2 findings have been published in *ISPRS Journal of Photogrammetry and Remote Sensing* (Phalke et al., 2020). The wall-to-wall cropland mapping product is also published on NASA EOSDIS Land Processes DAAC (Phalke et al., 2017).

**Objective 2: Wheat yield prediction in the cross-border area between Turkey and Bulgaria using remotely sensed environmental variables and a neural network**

Wheat is a staple crop in the study area. Accurate and timely information on wheat yield estimates at the field scale is important for understanding regional food security and policy implications. In studies involving multiple countries or large areas, consistent data availability is a major limitation because of different methods and approaches to data collection. Also, historical datasets at the highest administrative levels such as village or districts are rarely available. For example, in Bulgaria, the agricultural statistics from 2000 are available only at the regional scale (equivalent to census regions in the United States). This study showed that a high-resolution time-series wheat yield mapping using remotely sensed inputs and a neural network is possible. Specifically, this study presented a multiple perceptron neural network (MLP-NN) method with

lowest possible administrative level public wheat yield records (such as local administrative unit [LAU-1] level for Turkey, and Nomenclature of Territorial Units for Statistics [NUTS-2] level for Bulgaria) as a dependent variable, and Landsat satellite data-derived time-series vegetation indices, soil properties, water stress variables and topographical characteristics as independent variables. The cropland and wheat maps developed in Objective 1 are used to focus the yield estimates to only the relevant locations on the landscape. The resulting wheat yield estimates agree well with the government statistics and enable us to predict village- or field-scale wheat yields in Turkey and Bulgaria. Overall, this study offers a repeatable approach to predict wheat yield at LAU-1 scale or field scale through systematic assessment of its environmental drivers and further discusses the challenges to make wheat yield maps in the context of major socio-political changes. To our knowledge, this is the first study to map wheat yield at field scales in this study area. Such granular and historical wheat yield dataset forms the basis to further identify the drivers of wheat yield change presented in the next chapter.

**Objective 3: Determining the drivers of agricultural land and production changes from the last 20 years**

Land use change is a function of environmental, biophysical, climatic, and socioeconomic drivers. In particular, the socio-economic drivers are very complex and uncertain in nature as they may be different at different times and locations. Analyzing the impact of support policies from regional to field scales can also inform reforms, if any. This study developed a holistic approach to study both biophysical and socio-economic drivers of agricultural land use change. The first and very important step of this study is to set up the hypothesis. For this purpose, it is essential to have thorough knowledge of the socio-political background of the study area. In this research, Bulgarian accession to the European Union (EU) in 2007 is observed to be an important socio-economic

breakpoint. To this end, the first hypothesis of this study is: “While the cross-border area between Turkey and Bulgaria has similar agroecological characteristics, the current state and historical patterns of agricultural land use are very different, fueled primarily by the break-neck pace of socio-economic changes in Bulgaria contrasted with relatively stable conditions in Turkey.” Specifically, this hypothesis test addressed how the trend and patterns of wheat yield change in the 2001-2007 period had different drivers compared to change in 2008-2020, which was due to implementation of the Common Agricultural Policy in Bulgaria in 2007. The second hypothesis of this study is: “The trends and patterns of the wheat yield change in the different geographic regions of the study area are different in the last 20 years, and they have socio-economic underpinnings.” This hypothesis test addressed how the drivers of wheat yield change in the last 20 years differ according to the geographic location of the study area. The first hypothesis accounted not only for different geographies, but also for different time-period. The second hypothesis derived the drivers of wheat yield change in the different locations/countries but in the same time periods. Both hypotheses were tested at regional to local scale according to socio-economic data availability.

The high-resolution wheat yield maps of the study area from Objective 2 aided in understanding the spatiotemporal distribution of wheat yield at granular scale. This chapter demonstrated three different analyses to understand the spatiotemporal trends and patterns of village scale wheat yield change in the study area. In the first analysis, a unique binning analysis is implemented, in which wheat yield data are clustered into several bins or buckets according to its wheat yield value range, and these bins and their distributions were further analyzed according to geographic location and the time-period to understand the trends and patterns. In the second analysis, we performed a trend analysis on the village-scale wheat yield time-series dataset using

the Mann-Kendall test. This test helped us to better understand the spatiotemporal trends and patterns of the wheat yield change in the study area. In the third analysis, we analyzed the distribution of wheat yield at village scale according to soil quality to understand how wheat yield is changing according to different soil quality in the study area. This granular pattern analysis in respect to soil suitability helped to strengthen the understanding of the impact of support policies on the wheat yield change of the study area. Results of this analysis provided detailed insights about the importance of environmental and socio-economic drivers in each region and explained their impacts on wheat yield at village scale. The key contribution of this research is to explain the high-level reasons for wheat yield changes in the study area since the year 2000. The main benefit of this work is its granularity and multi-scale approach. This study is the first to understand the drivers of wheat yield change in the study area and have the potential to provide new insights to policy makers and environmental investigations. The final chapter of this dissertation will summarize the findings from all the chapters and provide future directions and implications of the work.

**References**


Bastiaanssen, W. G., Molden, D. J., & Makin, I. W. (2000). Remote sensing for irrigated agriculture: examples from research and possible applications. *Agricultural Water Management*, *46*(2), 137-155.

Baumann, M., Kuemmerle, T., Elbakidze, M., Ozdogan, M., Radeloff, V. C., Keuler, N. S., ... & Hostert, P. (2011). Patterns and drivers of post-socialist farmland abandonment in Western Ukraine. *Land Use Policy*, *28*(3), 552-562.

Baumann, M., Ozdogan, M., Wolter, P. T., Krylov, A., Vladimirova, N., & Radeloff, V. C. (2014). Landsat remote sensing of forest windfall disturbance. *Remote Sensing of Environment*, *143*, 171-179.

Chhabra, A., Geist, H., Houghton, R. A., Haberl, H., Braimoh, A. K., Vlek, P. L., ... & Lambin, E. F. (2006). Multiple impacts of land-use/cover change. In *Land-use and Land-cover Change* (pp. 71-116). Springer, Berlin, Heidelberg.

Conway, G. (2019). *The doubly green revolution: food for all in the twenty-first century*. Cornell University Press.

Dang, A. N., & Kawasaki, A. (2017). Integrating biophysical and socio-economic factors for land-use and land-cover change projection in agricultural economic regions. *Ecological Modelling*, *344*, 29-37.

DeFries, R. S., Field, C. B., Fung, I., Justice, C. O., Los, S., Matson, P. A., ... & Vitousek, P. M. (1995). Mapping the land surface for global atmosphere-biosphere models: Toward continuous distributions of vegetation's functional properties. *Journal of Geophysical Research: Atmospheres*, *100*(D10), 20867-20882.

Duncan, J. M., Dash, J., & Atkinson, P. M. (2015). Elucidating the impact of temperature variability and extremes on cereal croplands through remote sensing. *Global Change Biology*, *21*(4), 1541-1551.

Fernández, J. L., Kendall, J., Davey, V., & Knapp, M. (2007). Direct payments in England: factors linked to variations in local provision. *Journal of Social Policy*, *36*(1), 97-121.

Foley, J. A., DeFries, R., Asner, G. P., Barford, C., Bonan, G., Carpenter, S. R., ... & Snyder, P. K. (2005). Global consequences of land use. *Science*, *309*(5734), 570-574.

Gao, F., Anderson, M. C., Zhang, X., Yang, Z., Alfieri, J. G., Kustas, W. P., ... & Prueger, J. H. (2017). Toward mapping crop progress at field scales through fusion of Landsat and MODIS imagery. *Remote Sensing of Environment*, *188*, 9-25.

Godfray, H. C. J., Beddington, J. R., Crute, I. R., Haddad, L., Lawrence, D., Muir, J. F., ... & Toulmin, C. (2010). Food security: the challenge of feeding 9 billion people. *Science*, *327*(5967), 812-818.

Hurni, K., Schneider, A., Heinimann, A., Nong, D. H., & Fox, J. (2017). Mapping the expansion of boom crops in mainland Southeast Asia using dense time stacks of Landsat data. *Remote Sensing*, *9*(4), 320.

Jensen, J. R. (2009). *Remote sensing of the environment: An earth resource perspective 2/e*. Pearson Education India.

Kraemer, R., Prishchepov, A. V., Müller, D., Kuemmerle, T., Radeloff, V. C., Dara, A., ... & Frühauf, M. (2015). Long-term agricultural land-cover change and potential for cropland expansion in the former Virgin Lands area of Kazakhstan. *Environmental Research Letters*, *10*(5), 054012.

Lambin, E. F., Geist, H. J., & Lepers, E. (2003). Dynamics of land-use and land-cover change in tropical regions. *Annual Review of Environment and Resources*, *28*(1), 205-241.

Maxwell, S. (1996). Food security: a post-modern perspective. *Food Policy*, *21*(2), 155-170.

Mayaux, P., Eva, H., Gallego, J., Strahler, A. H., Herold, M., Agrawal, S., ... & Roy, P. S. (2006). Validation of the global land cover 2000 map. *IEEE Transactions on Geoscience and Remote Sensing*, *44*(7), 1728-1739.

Meyfroidt, P. (2018). Trade-offs between environment and livelihoods: Bridging the global land use and food security discussions. *Global Food Security*, *16*, 9-16.

Meyfroidt, P., Carlson, K. M., Fagan, M. E., Gutiérrez-Vélez, V. H., Macedo, M. N., Curran, L. M., ... & Robiglio, V. (2014). Multiple pathways of commodity crop expansion in tropical forest landscapes. *Environmental Research Letters*, *9*(7), 074012.

Myers, V. I. (1983). Remote sensing applications in agriculture. *Manual of remote sensing*, 2111-2228.

Ozdogan, M., & Woodcock, C. E. (2006). Resolution dependent errors in remote sensing of cultivated areas. *Remote Sensing of Environment*, *103*(2), 203-217.

Ozdogan, M., Yang, Y., Allez, G., & Cervantes, C. (2010). Remote sensing of irrigated agriculture: Opportunities and challenges. *Remote Sensing*, *2*(9), 2274-2304.

Phalke, A. R., & Özdoğan, M. (2018). Large area cropland extent mapping with Landsat data and a generalized classifier. *Remote Sensing of Environment*, *219*, 180-195.

Phalke, A. R., Özdoğan, M., Thenkabail, P. S., Erickson, T., Gorelick, N., Yadav, K., & Congalton, R. G. (2020). Mapping croplands of Europe, middle east, russia, and central asia using landsat, random forest, and google earth engine. *ISPRS Journal of Photogrammetry and Remote Sensing*, *167*, 104-122.

Phalke, A., Ozdogan, M., Thenkabail, P. S., Congalton, R. G., Yadav, K., Massey, R., ... & Smith, C. (2017). NASA Making Earth System Data Records for Use in Research Environments (MEaSUREs) Global Food Security-Support Analysis Data (GFSAD)@ 30-m for

Europe. *Middle-East, Russia and Central Asia: Cropland Extent Product (GFSAD30EUCEARUMECE)*.

Pittman, K., Hansen, M. C., Becker-Reshef, I., Potapov, P. V., & Justice, C. O. (2010). Estimating global cropland extent with multi-year MODIS data. *Remote Sensing*, *2*(7), 1844-1863.

Prishchepov, A. V., Müller, D., Baumann, M., Kuemmerle, T., Alcantara, C., & Radeloff, V. C. (2017). Underlying drivers and spatial determinants of post-soviet agricultural land abandonment in temperate Eastern Europe. In *Land-cover and land-use changes in Eastern Europe after the collapse of the Soviet Union in 1991* (pp. 91-117). Springer, Cham.

Prishchepov, A. V., Müller, D., Dubinin, M., Baumann, M., & Radeloff, V. C. (2013). Determinants of agricultural land abandonment in post-Soviet European Russia. *Land Use Policy*, *30*(1), 873-884.

Ramankutty, N., Mehrabi, Z., Waha, K., Jarvis, L., Kremen, C., Herrero, M., & Rieseberg, L. H. (2018). Trends in global agricultural land use: implications for environmental health and food security. *Annual Review of Plant Biology*, *69*, 789-815.

Roy, S. S., Mahmood, R., Niyogi, D., Lei, M., Foster, S. A., Hubbard, K. G., ... & Pielke Sr, R. (2007). Impacts of the agricultural Green Revolution–induced land use changes on air temperatures in India. *Journal of Geophysical Research: Atmospheres*, *112*(D21).

Schneider, A. (2012). Monitoring land cover change in urban and peri-urban areas using dense time stacks of Landsat satellite data and a data mining approach. *Remote Sensing of Environment*, *124*, 689-704.

Shen, Q., Chen, Q., Tang, B. S., Yeung, S., Hu, Y., & Cheung, G. (2009). A system dynamics model for the sustainable land use planning and development. *Habitat International*, *33*(1), 15-25.

Thenkabail, P. S., Hanjra, M. A., Dheeravath, V., & Gumma, M. (2010). A holistic view of global croplands and their water use for ensuring global food security in the 21st century through advanced remote sensing and non-remote sensing approaches. *Remote Sensing*, *2*(1), 211-261.

Therond, O., Debril, T., Duru, M., Magrini, M. B., Plumecocq, G., & Sarthou, J. P. (2019). Socio-economic Characterisation of agriculture models. In *Agroecological transitions: From theory to practice in local Participatory design* (pp. 21-43). Springer, Cham.

Verburg, P. H., Alexander, P., Evans, T., Magliocca, N. R., Malek, Z., Rounsevell, M. D., & van Vliet, J. (2019). Beyond land cover change: towards a new generation of land use models. *Current Opinion in Environmental Sustainability*, *38*, 77-85.

Waldner, F., Fritz, S., Di Gregorio, A., & Defourny, P. (2015). Mapping priorities to focus cropland mapping activities: Fitness assessment of existing global, regional and national cropland maps. *Remote Sensing*, *7*(6), 7959-7986.

Wheeler, T., & Von Braun, J. (2013). Climate change impacts on global food security. *Science*, *341*(6145), 508-513.

**Chapter 2 (Part 1)**

**Large area cropland extent mapping with Landsat data and a generalized classifier**

Phalke, A. R., Özdoğan, M. 2018.

*Remote Sensing of Environment* 219: 180-195

**Abstract**

Accurate and up-to-date cropland maps play an important role in the study of food security. Traditional mapping of croplands using medium resolution (10 - 100 meters) remote sensing imagery involving a "one-time, one-place" approach requires significant computing and labor resources. Although high mapping accuracies can be achieved using this approach, it is tedious and expensive to collect reference information to train the classifiers at each location and to apply over large areas, such as a continent. Moreover, large area cropland mapping presents additional challenges including a wide range of agricultural management practices, climatic conditions, and crop types. To overcome these challenges, here we report on a generalized image classifier to map cropland extent, which builds a classification model using training data from one location and time period, applied to other times and locations without the need for additional training data. The study was demonstrated across eight agro-ecological zones (AEZs) in Europe, the Middle East and North Africa using Landsat data acquired between 2009 and 2011. To reduce between-scene variability associated with image availability and cloud cover, input data were reduced to salient temporal statistics derived from enhanced vegetation index (EVI) combined with topographic variables. The generalized classifier was then tested across three levels of generalization: 1. ***individual*** - where training data were extracted from and applied to the same Landsat footprint; 2. ***AEZ*** where training data were extracted from a set of Landsat footprints within an AEZ and applied to any other Landsat footprint in the same AEZ; and 3. ***regional*** where training data were extracted from a set

of Landsat footprints in the whole study area and applied to any other Landsat footprint inside the study area. Results showed that the generalized classifier is successful in identifying and mapping croplands with comparable success across all three levels of generalization with minimal cost: average loss in accuracy (as measured by overall accuracy) from the *individual* level (average overall accuracy of 80 ± 5%) to *regional* level (average overall accuracy of 74 ± 10%) is between 2 to 10% depending on the location. Results also show that generalization is not sensitive to the choice of the classification algorithm – the Linear Discriminant Analysis (LDA) model performs equally well compared to many popular machine learning algorithms found in the literature. This work suggests the generalization/signature extension framework has a great potential for rapid identification and mapping of croplands with reasonable accuracies over large areas using only easily computed vegetation indices with very little user input and ground information requirement.

### 2.1.1 Introduction

Information on the location and extent of croplands has important food security, economic, and policy implications (Lambin and Meyfroidt, 2011; Thenkabail et al., 2012; See et al., 2015). Knowledge on agricultural areas is also important for allocation of water resources, preserving biodiversity, and other social factors at regional to global scales. Remote sensing, either alone or in combination with statistical field surveys, has been at the core of identifying and mapping croplands over large areas (Myers et al., 1983; Jensen, 2009; Gao et al., 2017). Synoptic view, repeated observations, digital nature of data, and spectral bands appropriate for locating cultivated areas are just a few attributes that make remotely sensed observations attractive. Mapping of croplands over large areas using multi-date and multi-spectral remotely sensed data, remains elusive however, in part due to a great geographic variation in cultivation practices, spatial resolution requirements in areas with small parcel size distributions, large volumes of data, inconsistent availability of data across footprints and most importantly the need for a large number of training samples (Pax-Lenny et al., 2001; Mayaux et al., 2006; Ozdogan, 2010; Immitzer et al., 2016). Many currently available global cropland datasets at various spatial resolutions (e.g. Loveland et al., 2000; Friedl et al., 2002; Ramankutty et al., 2008; Biradar et al., 2009; Gong, 2009; Pittman et al., 2010; Waldner et al., 2016; Chen et al., 2014, 2015) have a number of constraints including: a) coarse resolution nature that cannot resolve small farm parcels that populate many agricultural landscapes around the world (Ozdogan and Woodcock, 2006; Griffiths et al., 2013); b) cropland category being just one class among a number of other land cover categories; c) less-than-ideal overall accuracy (between 66 to 79%), with the croplands portion being the least reliable (Frey and Smith 2007; Herold et al., 2008; Gong, 2009; Bontemps et al., 2010; Chen et al.,2015); and d) the limited use of temporal information in their making. Therefore,

there remains a pressing need to create approaches based on remote sensing to monitor croplands at moderate to high spatial resolutions over large areas, on a repeated basis, and with the ability to generalize temporally and spatially.

To overcome these challenges, here we report on a generalized image classifier based on the Linear Discriminant Analysis (LDA) algorithm to map cropland extent, which builds a classification model using training data from one location and time period and applies it to other times and locations without the need for additional training data. The general goal is to move away from the "one-time, one-place" syndrome and develop a generalized classifier that is repeatedly across space and time. In doing so, our aim is to reduce the time and resource requirements for the reference data collection process that inflicts almost all large area land cover classification problems. More specifically, we develop and demonstrate the use of a generalized and efficient cropland classification method scalable over large areas with very little training and parameterization *and* leverage medium resolution time-series data (e.g. Landsat) to map croplands while decreasing the 'between-scene' variability associated with differential image availability and cloud cover over large areas.

The generalization (or signature extension, as it is commonly known) refers to the use of spectral/temporal signatures associated with a set of land cover categories derived from one location or time period to map the same categories in other locations or time periods where no training data are available (Chittineni, 1980; Pax-Lenny et al., 2001; Woodcock et al., 2001; Knorn et al., 2009). In this sense, spectral/temporal signatures are nothing more than the predictive model derived from the training data to classify the satellite observations into land cover classes. However, the availability of training data is the major issue in a large area land cover mapping problems. The essence of generalization is to bypass the training data requirements everywhere

and at all times, and apply a trained classification model developed in one location and time to other places and periods.

The idea of generalization with medium resolution data such as Landsat in the context of agriculture is not new and has its origins in two important early developments in agricultural remote sensing. The first of these, the Large Area Crop Inventory Experiment (LACIE) of the 1970s was carried out by the National Aeronautics and Space Administration, the U.S. Department of Agriculture, and the National Oceanic and Atmospheric Administration (McDonald et al., 1975). The objective was to develop methods for estimating wheat production worldwide to demonstrate an economically important use of repetitive, multispectral, remote sensing from space. The LACIE method was generally successful in obtaining unbiased and precise area estimates but had inconsistent outcomes for predicting crop production. For example, while the experiment was successful in producing an accurate estimate of the shortfall in the Soviet spring wheat crop in 1977, the results were less successful in predicting Canadian wheat production, although the reasons were well-understood (McDonald and Hall, 1980). In general, the LACIE experiment resulted in the development of methods to estimate overall wheat production based on area and yield estimates with acceptable accuracy, without the use of ground data (Erickson, 1984). The next development was the Agriculture and Resources Inventory Surveys through Aerospace Remote Sensing experiment (AgRISTARS), jointly conducted by a number of U.S. agencies in the early 1980s. The goal of this program was to combine Landsat data with conventional ground surveys to provide timely and accurate end-of-year major crop area estimates in select U.S. states. The primary objective in each state was to obtain crop area estimates with reduced sampling errors, for example, harvested winter wheat in Kansas prior to December 1, 1980, and planted corn and soybeans in Iowa prior to December 23, 1980 (AgRISTARS Program Support Staff 1981). While

the program had many elements, crop area estimates for important state producers were generally accurate and timely. The AgRISTARS program is generally thought to have been the origin of many remote sensing applications in subsequent decades. Additional work by Bauer et al (1975) as part of the Crop Identification Technology Assessment for Remote Sensing project (CITARS) also tested the concept of generalization for crop identification and yield predictions and found that atmospheric conditions caused errors in classification accuracies and area estimates by 22 and 23% and suggested that corrections to atmospheric conditions that adjusted for sun angle differences could enhance generalized classifier applications (Bauer et al.,1975; Minter, 1978; Myers,1983). In addition, recent efforts of automated cropland mapping with temporal generalization i.e. year to year basis have been explored (Waldner et al., 2015; Xiong et al., 2017; Massey et al., 2017).

With these issues in mind, the specific objective of this study is: to develop an automated classification algorithm based on the idea of generalization to map croplands over large areas (i.e., continental scales) using remotely sensed time series observations as well as topographic and agro-climatic characteristics. The specific sub-objectives are: a) to reduce the need for reference data used for training that has been traditionally necessary for performing classification over large areas; and b) to decrease 'between-scene variability' associated with Landsat image acquisitions by reducing multispectral observations to a few salient temporal statistics derived from vegetation indices and topographic variables.

### 2.1.2 Methodology

#### 2.1.2.1 Study area

Our study area is continental in nature, spanning diverse agro-climatic and topographic characteristics as well as agricultural management practices (Figure 2.1.1). We developed and

tested the generalization approach across eight agro-ecological zones (AEZs) adapted from eight UN FAO global agro-ecological zones (GAEZ) spread across Europe, North Africa, and the Middle East (Table 2.1.1). It is noted that our methodology can be simply applied to any other parts of the globe, although in this study we have demonstrated it to this specific area based on the expertise and data availability. The croplands are defined as lands cultivated with plants harvested for food, feed, and fiber, include both seasonal crops (e.g., wheat, rice, corn, soybeans, cotton), continuous plantations (e.g., coffee, tea, rubber, cocoa, oil palms) and cropland fallows, although cropland fallows for more than three years are considered as non-croplands. The minimum mapping unit considered is 0.5 ha (or six 30-meter pixels).

#### 2.1.2.2 Generalization scheme

In this study, the conceptual framework for generalization consists of three levels (Figure 2.1.2). The first level is '*individual'* where cropland mapping within a particular Landsat footprint is performed by extracting, training, and validating data from the same Landsat footprint, similar to a traditional land cover mapping exercise. For example, to map croplands in the Landsat scene p182r029 (Bulgaria) (path 182 and row 029), the training samples are distributed inside the scene (a scene is defined as one particular acquisition within a footprint) used for classification process. The second level of generalization is '*AEZ'* where cropland mapping within Landsat footprints inside an AEZ is performed by extracting training and validation data from a set of selected Landsat footprints (2 to 4 footprints per AEZ) in a particular AEZ. More specifically, the training data from each selected scene within the AEZ are pooled and the LDA model developed from these training data is applied to another scene or composite of scenes in the AEZ that was not used in the training process. This can be repeated until all the scenes in a zone are classified. For example, zone 5 (in Central Europe) covers approximately 30 Landsat footprints (Figure 2.1.2)

and we selected only three Landsat footprints for training. We then built the LDA model using samples from these three footprints and applied it to five other randomly selected footprints in the same zone. It is noted that, practically every Landsat scene in zone 5 can be classified using the trained LDA model, not just the five selected here. The third level of generalization is '*regional'* where cropland mapping of Landsat footprints inside an entire study area or a region is performed by extracting training and validation data from a set of selected Landsat footprints covering all eight AEZs (Figure 2.1.2). The regional LDA model was constructed using the training data extracted from all the selected scenes in the region and was applied to all the remaining (non-training) scenes in the region. This process was repeated until all scenes in the AEZ or in the region used for testing at least once. For example, the entire study area covers more than 2,000 Landsat footprints but we only selected 25 footprints for training purposes by pooling reference samples and testing the resulting LDA model on the 36 representative Landsat footprints in the region that were not involved in the training process. It is noted that, practically every scene in the region can be classified using the LDA model and not just the 36 selected here.

**2.1.2.3 Classification approach**

Our approach to generalized cropland extent mapping involved three steps: 1) acquisition, pre-processing, and temporal aggregation of satellite data along with topographic variables; 2) training and application of the classification scheme across three generalization levels; and 3) validation (Figure 2.1.3).

*Satellite data and topographic variables*

Primary data used in our study were satellite images from two sensors, Landsat Thematic Mapper (TM) and Enhanced Thematic Mapper Plus (ETM+) (Table 2.1.2). Landsat data have been the workhorse of terrestrial remote sensing for over four decades. Given its spectral and temporal

characteristics, Landsat data are ideally suited for monitoring cropland extent over large areas and there are numerous examples in the literature. We selected a total of 61 Landsat footprints in our study area [25 as training scenes or core scenes and 36 as testing scenes or random scenes] (Figure 2.1.1). The selection of these footprints was primarily based on two criteria. First, we distributed the location and the number of footprints to ensure representation across diverse agro-ecological zones. Second, our preliminary analysis (not shown) involving random removal of a footprint from a larger set of available scenes revealed that three to four footprints per AEZ was sufficient in stabilizing accuracies.

The footprints belonging to the core category were used to build the classification model while those in the random category were used to test the model. For each footprint, we acquired all available Landsat 5 TM and Landsat 7 ETM+ data with less than 75% cloud cover over a three-year window [2009-11]. The reason behind using such high cloud cover threshold was to have as many valid observations as possible for each pixel in the classification input set. As will be discussed in a later section, our temporal reduction strategy that employs temporal vegetation index statistics relies on having a maximum of possible observations. The three-year window and given cloud cover threshold resulted in 2,167 Landsat images in total, with 932 in the core category and additional 1,235 in the random category spread across the study area. There was great variation in the temporal distribution of data due to differential acquisition strategies, cloud cover and the SLC-off issue involving Landsat-7 observations.

All Landsat data were downloaded as surface reflectance products as part of the Collection 1 Level-2 dataset from the United States Geological Survey (USGS) that included the cloud and cloud shadow masks developed with the Fmask algorithm (Zhu and Woodcock, 2012). We

calculated the enhanced vegetation index (EVI) (Huete et al., 2011) for each image in the collection:

$$EVI = G \times \frac{(NIR - RED)}{(NIR + C1 \times RED - C2 \times Blue + L)} \quad (1)$$

where NIR/RED/Blue (Band 4/Band 3/Band 1 respectively) correspond to surface reflectance values in the respective portions of the electromagnetic spectrum. L is the canopy background adjustment that addresses non-linear, differential NIR and RED radiant transfer through a canopy. C1, C2 are the coefficients of the aerosol resistance term, which uses the blue band to correct for aerosol influences in the red band and G is the gain factor. The coefficients used here are L=1, C1 = 6, C2 = 7.5, and G = 2.5 adopted from USGS product guide for Landsat SR derived spectral indices (https://landsat.usgs.gov/sites/default/files/documents/si_product_guide.pdf). The reason behind using EVI is that it has been shown to have improved sensitivity in high biomass regions and proved to be more reliable to study croplands compared to the normalized difference vegetation index (NDVI) because of its coupling with the canopy background signal and reduction in atmospheric influence (Kawamura et al., 2005; Wardlow et al., 2010).

The primary challenge when using Landsat for generalization questions is the spatial discontinuity of observations at footprint boundaries. For example, assume two Landsat footprints, ‘a’ and ‘b’ are adjacent to each other with one overlapping boundary. In this case, the total number of scenes and their acquisition dates in a given period for footprint ‘a’ will not be the same as the total number of scenes and imaging dates available for footprint ’b’. This discrepancy between Landsat scene locations occurs because of the differential acquisition strategies and cloud cover and often leads to a different number of input features that need to be normalized across footprints for wall-to-wall mapping efforts. To overcome this issue, we used salient temporal features

calculated from the EVI time series in each footprint. Specifically, we reduced observed EVI time series data in the collection for each footprint to seven temporal features that were deemed to be agriculturally important. These features are:

- Mean of EVI: It is the average/mean value of the time-series data of particular pixel of corresponding Landsat footprint.
- Standard deviation of EVI: It is the standard deviation of the time-series data of particular pixel of corresponding Landsat footprint.
- Maximum of EVI: It is the maximum value of the time-series data of particular pixel of corresponding Landsat footprint.
- Minimum of EVI: It is the minimum value of the time-series data of particular pixel of corresponding Landsat footprint.
- Variance of EVI: It is the variance value of the time-series data of particular pixel of corresponding Landsat footprint.
- Range of EVI: It is the range value of the time-series data of particular pixel of corresponding Landsat footprint.
- Count of EVI: It is the number of valid observations recorded on each date of particular pixel of corresponding Landsat scene.

These seven remotely sensed features were further supplemented with two additional topographic variables derived from the Shuttle Radar Topographic Mission (SRTM) digital elevation model (DEM) **(**http://www2.jpl.nasa.gov/srtm/**)** that have been shown to be important in identifying and mapping agricultural areas (e.g. Jarvis et al., 2008)

- Slope: It is the topographic variable consisting of the inclination of the surface.
- Elevation: It is the height of the surface above sea level.

The significance of this temporal reduction was twofold: first, to homogenize the differential number of observations between footprints and to reduce the number of input features for the Linear Discriminant Analysis (LDA) model. The temporal features used in the study are deemed agriculturally important because: 1) they play an important role in vegetation mapping in agricultural areas as croplands have different growth cycles over other vegetation types that are captured well using these temporal indices; 2) Landsat observations are often discontinuous in nature, making it necessary to transform temporal observations into homogenous set of features.

*Collection of reference samples*

To build the LDA model we selected 500 randomly located land parcels in each of the core footprints and 400 randomly located land parcels in each random footprint with a total of 26,900 samples (500 x 25 core footprints + 400 x 36 random footprints). To extract each sample, we first used a mean-shift image segmentation algorithm to group like-value pixels in a scene into polygons or segments with a 0.5 ha minimum mapping unit (about six Landsat pixels). In cultivated landscapes, these segments often corresponded to individual field boundaries. The input to the segmentation algorithm included two cloud-free Landsat images from different seasons (spring/summer). In the next step, each segment (parcel) was manually labeled as the cultivated or non-cultivated category on very high-resolution (VHRI) data (primarily through Google Earth Pro) using expert judgment within a double-blind approach. We used the majority rule when labeling partial segments, meaning that a label was chosen based on the dominant land cover type. When labeling, we also generated a subjective confidence score based on: 1) cropland cover fraction inside each parcel; 2) availability of VHRI data; and 3) disagreement between different analysts.

*The LDA model*

The Linear Discriminant Analysis is a general statistical tool for classification problems that has been sporadically applied to satellite image classification (Switzer, 1980). Although there is a long history of supervised classification of satellite data, particularly using a new generation of machine learning algorithms such as Support Vector Machines (SVMs) or Neural Networks, their performance often depends on the critical parameter selection that defines the model and processing these algorithms need to have a rigorous computing power. More simple classifiers, such as the LDA approach, are easy to implement and provide clear physical interpretation with reliable accuracies (Bandos et al., 2009). LDA has a wide range of remote sensing applications. Tom et al. (1984) conducted a land use mapping comparison experiment involving LDA and Bayesian maximum likelihood algorithms and found that the LDA results were superior to Bayesian maximum likelihood. LDA offered better accuracy, less machine time and cost with reduced sensitivity toward the number of variables. Recent studies that involved LDA-based classification include tropical rainforest species classification (Clark et al., 2005), water classification (Fisher et al., 2013), identification of plant part composition of forest logging residue (Acquah et al., 2016), noise removal of hyperspectral imageries (Lu et al., 2017), species classification (Deklerck et al., 2017).

In this study, we implemented the Fisher's LDA model (Fisher, 1936), primarily because of the non-Gaussian distribution of the features. More specifically, both the cropland and the non-cropland categories consist of many types (e.g., forest, urban, grasslands etc.) that result in large variability in the input features. The Fisher's LDA method does not make the normality assumption, nor does it require equal class covariance, lending itself nicely to our problem.

To implement the Fisher's LDA model, we intersected training segments or parcels with images that contain the temporal EVI features and topographic variables, then extracted the mean value for each parcel. We trained the LDA model to classify each core footprint into a binary cropland/non-cropland map across all three levels of generalizations. At the core of the LDA model is the discriminant function:

$$LDA\ score = \beta_{mean} * a + \beta_{std} * b + \beta_{max} * c + \beta_{min} * d + \beta_{var} * e + \beta_{range} * f + \beta_{count} * g + \beta_{slope} * h + \beta_{elev} * i$$

where, $\beta_{mean}$ is the coefficient of mean/average value of EVI, $\beta_{std}$ is the coefficient of standard deviation value of EVI, and so on and the letters correspond to the respective variables. An empirical threshold value ($t$), based on the stacked histogram distribution by category, was then chosen to separate cropped parcels from non-cropped parcels (Figure 2.1.4). This threshold value was applied to the $LDA_{image}$ to make the final crop/no-crop map. Note that the LDA coefficients represent the weights associated with each input variable, in essence, quantifying their discriminant power. Moreover, the separation between two classes are defined according to the probability density of the input feature space given by the ratio of the variance between the classes to the variance within classes. Note that the covariance matrix that determines the shape of the probability densities for different classes has the same shape, but are shifted versions of one another (i.e., had different mean vectors) (Figure 2.1.4).

While the application of this function was the same across all footprints and all generalization levels, the source of the LDA coefficients was different (Table A2.1.2). In the first level of generalization (*individual*), we randomly split the 500 segments into training (75%) and testing (25%) sets and evaluated the performance of the LDA model. This procedure was repeated 100 times, each time drawing a separate set (with replacement) of samples for training and testing. This process essentially captures the variability in the reference sample and results in a normal

distribution; the mean value that can be used to determine the performance of the classification model. For the second level of generalization (*zonal*), we combined segments from all core footprints in the respective AEZ to train the LDA model and tested on all the random footprints (which no training data had been drawn) in the same AEZ. For the third level (*regional*) generalization, we pooled training data from all core footprints in the study area to build the LDA model and tested on all random footprints individually.

While the *individual* level generalization is equivalent to a traditional land-cover mapping exercise, the exciting part of generalization is its ability to use thresholds repeatedly over large areas without having to retrain at each location. This ability was tested with the *zonal* and *regional* generalization models in which a single threshold was used to make a map in a AEZ or region.

#### 2.1.2.4 Assessment of timing and minimum number of satellite images

To test the impact of temporal/seasonal availability of satellite data, we performed an analysis to test the model performance with different timing of inputs. It is noted that, the seasonal analysis is undoubtedly affected by the perennial character of the vegetation cover. However, since the classifier does not consider different crops, the overall impact is relatively low. To assess the timing of imagery, we grouped the acquisition dates into four seasons: December, January, and February (DJF) as winter; March, April, May (MAM) as spring; June, July, and August (JJA) as summer; and September, October, and November (SON) as autumn. These seasons were chosen, because the differences in climatic conditions impact the availability of satellite data observations as well as crop growth conditions. It is noted that, the seasonal inputs for 2009-2011 are provided as separate variables.

At the heart of our approach, is the ability to reduce the available satellite observations into a few agriculturally important temporal features. However, as with any statistical calculation, the

number of valid inputs might affect the value of the statistical feature, which obviously varies by location in satellite observations due to cloud presence and SLC-off issues in the case of Landsat 7 data. To evaluate the stability of the EVI temporal features according to the number of valid inputs available, we performed a simulation study in which we randomly removed EVI inputs from the calculation. In one final analysis, we evaluated the minimum number of footprints required to achieve optimum overall accuracy in a particular zone by randomly reducing the number of input footprints used for training.

#### 2.1.2.5 Accuracy assessment

We evaluated the performance of the generalized LDA model in three different ways. First, we used traditional tools of accuracy assessment involving an independent set of reference samples inside a confusion matrix. We repeated this form of accuracy assessment by generalization level as well as a core/random footprint status. In assessing classification performance, we calculated overall accuracy, producer's accuracy, user's accuracy, and the Kappa score of the map. The second evaluation involved comparing generalized LDA model results with other map products that contain a cropland category. For this comparison, we used the Global Land Cover (GLC or GlobalLand30) product that was produced with Landsat data *circa* 2010 (www.globallandcover.com) (Chen et al., 2015) and CORINE land cover map (over Europe only) produced for *circa* 2012 (Buttner G., 2014). We used the map comparison kit tool (MCK) developed by the Research Institute for Knowledge Systems (**http://mck.riks.nl)** (Visser et al, 2006). We calculated two measures for quantifying the similarities and differences between two raster maps. These metrics were *average similarity*, which calculates the average similarity of cells in the map, and *fuzzy kappa*, which is the fuzzy equivalent of Kappa statistics. We performed this comparison for five representative scenes in the study area with low to high independent accuracy

values. The selected scenes for the test were: p193r024 (Germany), p202r024 (United Kingdom), p187r027 (Hungary), p182r029 (Romania) and p172r034 (Turkey). All comparisons were performed at the 250-meter resolution, primarily because of the coarse resolution nature of the CORINE product. In this process, we did not consider the potential impact of downscaling on the regional generalized cropland maps because the same downscaling procedure was used for the two products, making their errors equal. The third approach to evaluating generalized LDA model outcomes involved comparing its results to classification results returned from several machine learning algorithms. The purpose if this comparison was to address the question of how generalization will perform with other supervised classifiers. To answer this question, we compared the LDA results those from Decision Trees (DT), Support Vector Machines (SVM), and Random Forest (RF) using exactly the same inputs across two generalization levels.

### 2.1.3 Results

#### 2.1.3.1 Classification results

Results showed that the generalized LDA model performed well when mapping croplands at all three levels of generalization (Figure 2.1.5 and Table A2.1.1). The average overall accuracy across all the footprints (core + random) at the *individual* level was 80% (± 8%) while at the AEZ as well as the regional generalization was 73% (± 8%). The LDA model not only produced good results across all levels of generalization, but the spatial distribution of croplands was also as expected (Figure 2.1.6). For example, in p187r027 (Hungary) (Figure 2.1.6, column 2), the LDA model nicely captured the croplands in the south-east side and skipped the forest on the north side. Also in p192r029 (Italy) (Figure 2.1.6, column 4), the croplands in the north and south-east side were carefully mapped against the non-croplands in south-west side with the mixture of forest and grasslands.

In general, the *individual* level of generalization produced the highest accuracy compared to the other levels with a mean overall accuracy of 80% across all core footprints. The core footprint in p182r038 (Libya) had the highest overall accuracy (90%) while the p200r027 (UK) core footprint produced the poorest overall accuracy at 68%. Note that, because of the cross-validation procedure to assess accuracy at this level of generalization, each footprint had a range of overall accuracy values, and in some cases this range could be quite large (Table A2.1.1). For example, the p174r035 (Syria) footprint had a range of 68% to 90% accuracy, whereas the p200r027 (UK) footprint had a range of 50% to 80% overall accuracy values. This wide range of accuracy values within a footprint suggested that not all reference samples are created equal: some samples were great trainers while others were great testers and their quality as well as their temporal/spectral characteristics strongly affected the behavior of the LDA model (Pax-Lenney et al., 2001). Nevertheless, the mean value of the cross-validation procedure provides an estimate of how the predictive model will perform in practice. The purpose of performing classic cross-validation was to see how the model would perform in practice under various conditions. More specifically, it means that under conditions of great diversity of agricultural practices and climatic conditions within an area, some samples (selected at random) will provide greater information to the classifier to separate croplands from non-cropland areas while other samples (selected at random) will actually hurt the performance of the classification algorithm in question.

In the case of the *AEZ* level of generalization, classification results for the core footprints showed that the average overall accuracy of AEZ cropland maps was 72% (± 15%), with p182r038 (Libya) (91%) having the highest accuracy and p176r026 (Russia) (46%) the lowest overall accuracy. Zone 1 core footprints had the highest zonal average overall accuracy, whereas zone 4 core footprints had the lowest overall accuracy (Figure 2.1.5 and Table A2.1.1). For random

footprints at the *AEZ* level of generalization, average overall accuracy was 76% (± 8%), with the highest accuracy for the p177r040 (Egypt) (93%) in zone 1 and the lowest accuracy in the p207r022 footprint (UK) (54%) in zone 6. Zone 1 and 5 random footprints showed the highest average *AEZ* generalized map accuracies with 85% and 82% respectively, whereas zone 7 random footprints had the lowest accuracy of 71% (Table A2.1.1).

An interesting observation in the context of generalization is that while accuracies generally decline when moving from the *individual* level to the *AEZ* level, the decline is not equal everywhere and at all times, and the direction of change could be reversed. For example, in the Turkey footprint (p172r034), the mean accuracy at the *individual* level was 89% [range of 76% to 97%]; adding the Syria footprint from the same zone to the training set reduces the overall accuracy by 5% (Figure 2.1.7), whereas the Romania footprint (p182r029), with a mean accuracy of 84% [range 68% to 95%], exhibits similar accuracy as the *individual* level when another footprint (p182r030 from Bulgaria) from the same zone is added to the training set, *and* reduces by 25% when another footprint (p181r026 from Ukraine) from the same zone is added to the training set (Figure 2.1.7).

At the *regional* level of generalization, overall average accuracy for core footprints was 73% (± 11%) and for random footprints was 77% (± 10%). The p182r038 (Libya) footprint had the maximum accuracy (91%) followed by p182r029 (Romania), p192r029 (Italy), and p174r035 (Syria) with 83%, 82%, and 81%, respectively. All the core footprints at this level had accuracies that ranged between 70% and 90% except for the p182r029 (Russia) footprint, which had the lowest accuracy (46%). In the case of random footprints, overall accuracies ranged from 91% in p171r035 (Syria) to 63% in the p207r022 (UK), with average overall accuracy of 77% (± 10%). In general, random footprints in p201r038 (Morocco) (88%), p177r040 (Egypt) (87%), p185028

(Romania) (84%), and p196r035 (Algeria) (83%) had high overall accuracies. The random footprints in zones 2 and 5 had the highest accuracies, each with 80%, while the lowest accuracies were found in zone 7 with 66% (Figure 2.1.8).

It is interesting to note that for core footprints, average change in overall accuracy when moving from *individual* to the *AEZ* models was about 8%, but negligible (less than 1%) when moving from the *AEZ* to the *regional* level. There were a few locations, such as p177r039 (Egypt), p182r038 (Libya), p201r027 (Morocco), p191r036 (Tunisia), p187r027 (Hungary), and p182r029 (Romania), that had a negligible change (less than 2%) in overall accuracy when moving from the *individual* to *AEZ* or the *regional* level. p200r033 (Spain) had exceptionally large loss in accuracy when moving from the *individual* level to *AEZ* (18% loss) and *regional* (27% loss) levels (Figure 2.1.8). One potential reason for this significant decline in accuracy is that agriculture in this particular footprint is quite different in terms of its specific spectral/temporal characteristics from agriculture in other footprints located in the same zone. This inhibits generalization between footprints because adding more variability to the model negatively affects model performance. This finding has important implications for signature extension in general and points to the fact that any generalization works best in cases where similar agro-ecological conditions or cultivation practices occur.

When moving from *AEZ* level to *regional* level the change in overall accuracies was minor for all locations except for p198r024 (Netherlands) (12%), and p200r033 (Spain) and p182r021 (Russia) (both 9%). Results also demonstrated that for random footprints, when moving from the *AEZ* to the *regional* generalization, average loss of accuracy was negligible (less than 1%). Zone 4 random footprints had better results with the *AEZ* generalization classification model compared to the *regional* with an average gain in accuracy of 8%, but zone 6 random footprints demonstrated

better results using the *regional* generalized classification model compared to the *AEZ* model with an average accuracy gain of 4%. It is interesting to note that, for random footprints, *regional* level generalized croplands maps provided better overall accuracies than *AEZ* maps except for zones 1, 2, and 4 (Figure 2.1.8 and Table A2.1.1).

Lastly**,** results also showed that there are a few cases (~3%) where LDA did not give a good separation between classes. For example, the p200r027 (UK) footprint provided poor discrimination (the high overlap between cropland and non-cropland histograms in Figure 2.1.4) but the p177r039 (Egypt) footprint showed a very strong discrimination (low overlap between cropland and non-cropland histograms) between crop and non-crop parcels (Figure 2.1.4). One reason for this is related to the difference in the number of valid observations at each location: the p200r027 footprint had a total of 18 Landsat scenes but the number of valid observations for each pixel was significantly lower [between 2 and 8]; the p177r039 footprint had a total of 26 acquisitions in the same period, most of which were valid observations.

Further, the average overall producer's accuracy across all the footprints (core + random) at the *individual* level was 74% (±8%), while at the *AEZ* as well as the *regional* generalization was 73% (±12%) and 72% (±11%), respectively. Zone 1 and 5 footprints had the highest producer's accuracy range from 75% to 85%, while zone 4 footprints had lowest producer's accuracies, ranging from 40% to 60%. The average overall user's accuracy across all the footprints (core + random) at the *individual* level was 80% (± 6%), while at the *AEZ* as well as the *regional* generalization was 76% (±10%) and 73% (±12%), respectively. Zone 1 core footprints had lowest user's accuracies range from 45% to 55%, whereas zone 1 random footprints had highest user's accuracies range from 85% to 95% (Figure 2.1.8).

#### 2.1.3.2 Assessment of timing and minimum number of satellite images required

The results of the assessment of timing of imagery tests showed that the overall accuracies using inputs from a single season led only to a slight decrease in accuracy compared to the model trained with inputs from all seasons (Table 2.1.3). For example, in the case of Turkey (p172r034), the overall accuracy using data only from season two (MAM) was 87%, the highest among the four seasons, while overall accuracy with input from all seasons was 88%. The same test using other seasons individually had overall accuracy of 83%. This analysis also revealed that the timing of imagery was more important than the number of valid observations in a season. Following from the same footprint, the second season (MAM) had the lowest number of valid observations but produced a crop map with the highest overall accuracy among all other seasons (Table 2.1.3).

The analysis to understand the minimum number of observations required, suggested that all EVI statistics (except for the minEVI) stabilized after about 15 observations across all footprints. This suggested that the value of the variable of interest (e.g., EVI standard deviation) could change dramatically, depending on the magnitude and the number of inputs if the total number of inputs was less than approximately 15 observations. This has important implications for the success of generalization in locations with persistent cloud cover (e.g., UK).

Our analysis (not shown) also revealed that a minimum of 3 to 4 footprints were required to achieve optimum overall accuracies at the *AEZ* level of generalization. While this number varied between different zones, additional number of footprints, regardless of their geographic position, did not lead to improvements in accuracy. Note that this analysis was performed with a pre-selected set of footprints and did not include all the possible footprints in a zone. It is possible that the results will be slightly different if this analysis was repeated with a full set of footprints in each zone.

### 2.1.3.3 Comparison of regional generalized map with traditional *individual* generalized map and other cropland products such as GLC and CORINE

The cropland extent maps produced by the regional generalization option using the LDA model were highly similar to the other cropland maps (Figure 2.1.9).

The mean value of average similarity between the *individual* and *regional* generalized map was 93%. Average similarity between the *regional* generalized map and the CORINE and the GLC maps were 89% and 86%, respectively (Table A2.1.3). The highest average similarity was 93% for p193r024 and the lowest average similarity was 80% for p172r034 when the *regional* generalized maps were compared to the CORINE land cover product. For the GLC maps, the highest and lowest average similarities were for p193r024 (94%) and for p200r024 (80%), respectively. The fuzzy kappa metric followed the same pattern (Table A2.1.3).

### 2.1.3.4 Comparison of the LDA model against other supervised classifiers

When compared against a several popular supervised classifiers involving machine learning algorithms, the LDA model performed well, if not better, across the range of locations tested (Figure 2.1.10) with a few exceptions. Footprint p182r038 (Libya) had 32% lower accuracy when classified with the Support Vector Machines (SVM) algorithm, while p191r036 (Tunisia) had 16% higher accuracy with SVM than the LDA model. Interestingly, p200r033 (Spain) averaged 10% greater accuracy with other classification algorithms than the LDA model. In sum, the result of the LDA model was competitive compared to other machine learning algorithms, while enjoying much greater cost efficiency. It is also noted that, all the classifiers including the LDA model exhibited similar amount of reduction in overall accuracies (between 2% to 10%), when moving from *individual* scene classification to *regional* generalization.

### 2.1.4 Discussion

Mapping croplands over large areas using remotely sensed observations with medium resolution satellite observations presents several challenges when the traditional one-time, one-place approach is used. These challenges include a large volume of data, calibration issues across sensors, inconsistent data availability, cost of training samples, and diverse agro-climatic conditions. Currently available global cropland datasets mainly produced with huge training sample inputs, for example, GLC global land cover map has cultivated land as one class and this dataset was developed with the help of 100s of thousands of reference samples and thousands of men hours, which significantly limits its reproducibility (Chen et al., 2010). Our study evaluated a generalization approach to overcome some of these challenges to produce cropland maps at 30-meter spatial resolution over large areas with the intent to offer operational applications. While there are successful examples of generalization in forest mapping applications in the literature (e.g. Pax-Lenny et al., 2001; Woodcock et al., 2001), generalization based cropland mapping has received less attention. Although Landsat and similar observations with fairly useful temporal and spatial resolution provide a tremendous opportunity to study complicated landscapes such as croplands, the gaps in the time-series data, primarily due to cloud cover, pose a major challenge (Pax-Lenny et al., 2001). Our approach attempts to overcome this challenge by reducing the original time series observations into agriculturally relevant temporal vegetation index statistics to produce cheaper and better cropland classification, while exploiting the concept of signature extension. The results show that these temporal EVI statistics, together with topographic variables, provide sufficient information for the cropland classification problem involving the LDA model in a generalization framework. Standard deviation, maximum, and range of EVI had the greatest separation power over other variables in discriminating croplands from non-croplands areas. At

the same time, the use of only temporal EVI statistics in the classification process came with limitations that included the need for a minimum number of valid observations at each pixel to ensure stable temporal statistics, sufficient seasonal distribution of valid observations, and the need for geographical variation in the value and the distribution of these temporal indices.

Moreover, the evaluation of the timing of imagery showed that there was little difference between single season and full year inputs, as long as the single season was representative of the crops, and cultivation practices in an area as some seasons were much more important than others. This suggests that information on the climatic conditions and cropping pattern is important in the classification process if one were to choose only one or two seasons as inputs (Baumann et al., 2012). In locations where the number of observations is significantly reduced or available only in certain periods of the year, due primarily to persistent cloud cover, the generalization scheme involving LDA performs poorly (e.g. the UK and Ireland). Our detailed analysis to evaluate the minimum number of valid observations required to perform at acceptable levels of accuracy suggests that on an average in all test locations, a minimum number of 15 observations are needed, *regardless of the period in which these observations are made*. Therefore, it is possible to use the number of valid observations, together with their temporal distributions, as an early indication of expected classification accuracy by location, and thus implement potential mitigation strategies such as an increased observation period (e.g., from three to five years) as well as other inputs that may help with the classification decision.

This study used the Fisher's LDA model to perform classification process that proved to be as reliable as more modern machine learning algorithms used in the literature (Tom et al., 1984; Fisher et al., 2013). One can argue that the primary reason the machine learning algorithms produced results similar to the LDA model is that they were given only a limited set of inputs (EVI

temporal statistics plus topographic features) and they could easily outperform the LDA model if given additional, and perhaps more relevant features. While we did not test this theory, in a simple case like the one presented here, the LDA model not only produced equally good results, but also brought additional benefits, including ease of implementation, a logical explanation of the relationship between input features and predicted outcomes (as opposed to a black box, for example, a clear discrimination between two classes through LDA score histogram in Figure 2.1.4), and minimal computational cost (Tom et al., 1984; Fisher et al., 2013), especially when considering applications over large areas. Recently, the remote sensing community has seen many developments in cloud computing, the most popular of which is the Google Earth Engine (GEE) (Gorelick et al., 2017). While GEE certainly reduces the burden of large data volume and expensive computation, classification over large areas with acceptable accuracies still requires a large number of training data, which must be collected manually. In fact, under the traditional mapping scenario, our entire study area with thousands of Landsat scenes would require millions of training samples. An important implication of our approach using the generalized model is not only to significantly reduce the training data requirements but also the time to produce wall-to-wall cropland extent maps.

The performance of the LDA model (and the classification accuracies) is highly dependent on the LDA scores threshold values (Fisher et al., 2013). In general, this threshold value depends on the variability of the input data and the geographic distribution of training samples. Our core footprints spanned diverse agro-climatic conditions of the study area and this diversity greatly improved the performance of the model. At the same time, the ability to define a precise threshold was reduced with increasing diversity as the generalization level moved from *individual* level to *AEZ* and to the *regional* level. We call this reduction as the cost of generalization. This means that

while our study was successful in finding the correct threshold value and produced reliable levels of accuracy at all levels of generalization, there is always a tradeoff between generalization and accuracy. That there were many cases where the generalization benefited from the diversity of temporal distribution of observations (e.g., zone five) and in those cases the cost of generalization was generally small. In this regard, there may be an opportunity to modify the *regional* generalization model by studying the distribution of training data samples and characteristics of input variables. Moreover, our approach can be used to produce cropland maps over time (even on an annual basis) just by applying the LDA coefficients and adjusting the thresholds. While this approach may not result in the most accurate croplands product, its repeatability, ease of production, and clear and meaningful signature (the LDA scores) does not diminish its value.

In this study, we used the LDA algorithm to perform generalization, but the ideas proposed here are not limited to LDA, as the generalization framework does not seem sensitive to the choice of classifier. While we demonstrated the efficacy of the generalized classifier across Europe, the Middle East and North Africa, the concept of generalization can be applied and replicated easily in any other country or continent across the globe with minimal inputs and effort. To this end, the future work can include testing the generalization approach with following advancements: 1) enhance the input feature space by incorporating raw spectral band information in addition to EVI; 2) explore objective ways to quantify the LDA score threshold to discriminate croplands; 3) extend the generalization framework across time and sensors involving medium resolution observations such as those provided with Sentinel-1 and Sentinel-2; and 4) increase the categorical detail by focusing on more refined cropland variables such as crop type and irrigation status.

Finally, to our knowledge, this study is the first attempt to use the ideas of generalization to map croplands over large areas using a few agriculturally relevant indices derived from Landsat

observations and topographic data. The results suggest that the use of salient temporal features together with topographical characteristics was sufficient to separate cultivated areas from non-cropped locations on a parcel-by-parcel basis. In this regard, the study has major implications for solving the problem of limitation by differential data availability among footprints. The medium spatial resolution satellite missions such as the Landsat and Sentinel programs have tremendous potential to monitor cultivated areas worldwide but have temporal acquisition limits. This study contributes to our ability to map croplands across continental areas by not only reducing between-scene variability but also by reducing the need to retrain the classification model. The cropland maps produced through this approach have reliable accuracies, contain high spatial detail, and are easy to produce over very large areas on an operational basis that are so important for food security questions.

### 2.1.5 Conclusions

In this study, we tested the idea of generalization (or signature extension, as it generally known) using the linear discriminant analysis (LDA) algorithm to produce cropland maps. The rationale of the generalization approach is that the methods can be applied over large areas quickly and efficiently without having to re-train and re-parameterize a model. The goal is to use the generalized LDA parameters established in one location or time period to other locations and times. The expected decrease in accuracy, as we generalize from a single scene to a zone and to regions appears to be within acceptable levels for large scale mapping. Moreover, the proposed generalization approach, while only tested with the LDA model here, can be applied with any classification algorithm of choice. Finally, the generalized classifier built on LDA lends itself nicely to cloud computing based remote sensing image processing platforms such as GEE. While these platforms have built-in capabilities to apply classification algorithms at scale, they do not

reduce the need for large amounts of high-quality training data. In this context, one additional benefit of the proposed method is to remove this burden.

The proposed generalization framework has important implications for cropland mapping over large areas at 30-meter spatial resolution while requiring very little user input. The methodology can further be extended for mapping more refined cropland attributes like crop types and their irrigation status that have been shown to be important for answering food security questions at continental to global scales.

### 2.1.6 Acknowledgments

This research was partially funded by USGS cooperative agreement number G13AC00061. This publication was made possible by the GFSAD30 project led by Prof. Prasad Thenkabail. The authors thank three anonymous reviewers as well as Dr. Sarah Graves, whose suggestions and edits significantly improved the content and readability of this manuscript.

**References**

AgRISTARS Program Support Staff 1981. AgRISTARS: Agriculture and resources inventory surveys through aerospace remote sensing, annual report—fiscal year 1980 NASA, Lyndon B. Johnson Space Center, Houston, TX (1981)

Bandos, T. V., Bruzzone, L., & Camps-Valls, G. (2009). Classification of hyperspectral images with regularized linear discriminant analysis. *IEEE Transactions on Geoscience and Remote Sensing*, *47*(3), 862-873.

Bauer, M. E., Cary, T. K., Davis, B. J., & Swain, P. H. (1975). Crop identification technology assessment for remote sensing (CITARS). Volume 6: Data processing at the laboratory for applications of remote sensing.

Baumann, M., Ozdogan, M., Kuemmerle, T., Wendland, K. J., Esipova, E., & Radeloff, V. C. (2012). Using the Landsat record to detect forest-cover changes during and after the collapse of the Soviet Union in the temperate zone of European Russia. *Remote Sensing of Environment*, *124*, 174-184.

Biradar, C. M., Thenkabail, P. S., Noojipady, P., Li, Y., Dheeravath, V., Turral, H., ... & Mohideen, S. (2009). A global map of rainfed cropland areas (GMRCA) at the end of last millennium using remote sensing. *International Journal of Applied Earth Observation and Geoinformation*, *11*(2), 114-129.

Bontemps, S., Defourny, P., Van Bogaert, E., Arino, O., & Kalogirou, V. (2010). gLoBCoVER 2009 Products Description Manual Version 1.0. *ESA and UCLouvain) Available at http://dup. esrin. esa. it/files/p68/GLOBCOVER2009_Product_Description_Manual_1. 0. pdf [Verified July 2012]*.

Büttner, G. (2014). CORINE land cover and land cover change products. In *Land use and land cover mapping in Europe* (pp. 55-74). Springer, Dordrecht.

Chen, J., Chen, J., Liao, A., Cao, X., Chen, L., Chen, X., ... & Mills, J. (2015). Global land cover mapping at 30 m resolution: A POK-based operational approach. *ISPRS Journal of Photogrammetry and Remote Sensing*, *103*, 7-27.

Chittineni, C. B. (1980). Signature extension in remote sensing. *Pattern Recognition*, *12*(4), 243-249.

Clark, M. L., Roberts, D. A., & Clark, D. B. (2005). Hyperspectral discrimination of tropical rain forest tree species at leaf to crown scales. *Remote Sensing of Environment*, *96*(3-4), 375-398.

Congalton, R. G. (2001). Accuracy assessment and validation of remotely sensed and other spatial information. *International Journal of Wildland Fire*, *10*(4), 321-328.

Deklerck, V., Finch, K., Gasson, P., Van den Bulcke, J., Van Acker, J., Beeckman, H., & Espinoza, E. (2017). Comparison of species classification models of mass spectrometry data: Kernel Discriminant Analysis vs Random Forest; A case study of Afrormosia (Pericopsis elata (Harms) Meeuwen). *Rapid Communications in Mass Spectrometry*, *31*(19), 1582-1588.

Erickson, J. D. (1984). The LACIE experiment in satellite aided monitoring of global crop production. *The role of terrestrial vegetation in the global carbon cycle: measurement by remote sensing*, *23*, 191-217.

Fischer, G., Nachtergaele, F., Prieler, S., Van Velthuizen, H.T., Verelst, L. and Wiberg, D. (2008). Global agro-ecological zones assessment for agriculture (GAEZ 2008). *IIASA, Laxenburg, Austria and FAO, Rome, Italy*, *10*.

Fisher, R.A. (1936). The use of multiple measurements in taxonomic problems. *Annals of Eugenics*, *7*(2), 179-188.

Frey, K.E. and Smith, L.C. (2007). How well do we know northern land cover? Comparison of four global vegetation and wetland products with a new ground-truth database for West Siberia. *Global Biogeochemical Cycles*, *21*(1).

Friedl, M.A., McIver, D.K., Hodges, J.C., Zhang, X.Y., Muchoney, D., Strahler, A.H., Woodcock, C.E., Gopal, S., Schneider, A., Cooper, A. and Baccini, A. (2002). Global land cover mapping from MODIS: algorithms and early results. *Remote Sensing of Environment*, *83*(1-2), 287-302.

Gao, F., Anderson, M.C., Zhang, X., Yang, Z., Alfieri, J.G., Kustas, W.P., Mueller, R., Johnson, D.M. and Prueger, J.H. (2017). Toward mapping crop progress at field scales through fusion of Landsat and MODIS imagery. *Remote Sensing of Environment*, *188*, 9-25.

Gong, P., Pu, R. and Yu, B. (1997). Conifer species recognition: An exploratory analysis of in situ hyperspectral data. *Remote Sensing of Environment*, *62*(2), 189-200.

Gorelick, N., Hancher, M., Dixon, M., Ilyushchenko, S., Thau, D. and Moore, R. (2017). Google Earth Engine: Planetary-scale geospatial analysis for everyone. *Remote Sensing of Environment*, *202*, 18-27.

Gray, J. and Song, C. (2013). Consistent classification of image time series with automatic adaptive signature generalization. *Remote Sensing of Environment*, *134*, 333-341.

Griffiths, P., van der Linden, S., Kuemmerle, T. and Hostert, P. (2013). A pixel-based Landsat compositing algorithm for large area land cover mapping. *IEEE Journal of Selected Topics in Applied Earth Observations and Remote Sensing*, *6*(5), 2088-2101.

Herold, M., Mayaux, P., Woodcock, C.E., Baccini, A. and Schmullius, C. (2008). Some challenges in global land cover mapping: An assessment of agreement and accuracy in existing 1 km datasets. *Remote Sensing of Environment*, *112*(5), 2538-2556.

Huete, A., Didan, K., van Leeuwen, W., Miura, T. and Glenn, E. (2010). MODIS vegetation indices. In *Land remote sensing and global environmental change*, 579-602. Springer, New York, NY.

Immitzer, M., Vuolo, F. and Atzberger, C. (2016). First experience with Sentinel-2 data for crop and tree species classifications in central Europe. *Remote Sensing*, *8*(3), 166.

Jarvis, A., Reuter, H.I., Nelson, A. and Guevara, E. (2008). Hole-filled seamless SRTM data V4, International Centre for tropical Agriculture (CIAT).

Jensen, R. (2009). *Remote sensing of the environment- An earth resource perspective 2/e*. Pearson Education India.

Jonsson, P. and Eklundh, L. (2002). Seasonality extraction by function fitting to time-series of satellite sensor data. *IEEE transactions on Geoscience and Remote Sensing*, 40(8), 1824-1832.

Jun, C., Ban, Y., & Li, S. (2014). Open access to Earth land-cover map. *Nature*, *514*(7523), 434-434.

Kawamura, K., Akiyama, T., Yokota, H.O., Tsutsumi, M., Yasuda, T., Watanabe, O. and Wang, S. (2005). Comparing MODIS vegetation indices with AVHRR NDVI for monitoring the forage quantity and quality in Inner Mongolia grassland, China. *Grassland Science*, *51*(1), 33-40.

Knorn, J., Rabe, A., Radeloff, V.C., Kuemmerle, T., Kozak, J. and Hostert, P. (2009). Land cover mapping of large areas using chain classification of neighboring Landsat satellite images. *Remote Sensing of Environment*, *113*(5), 957-964.

Lambin, E.F. and Meyfroidt, P. (2011). Global land use change, economic globalization, and the looming land scarcity. *Proceedings of the National Academy of Sciences*, *108*(9), 3465-3472.

Loveland, T.R., Reed, B.C., Brown, J.F., Ohlen, D.O., Zhu, Z., Yang, L.W.M.J. and Merchant, J.W. (2000). Development of a global land cover characteristics database and IGBP DISCover from 1 km AVHRR data. *International Journal of Remote Sensing*, *21*(6-7), 1303-1330.

Lu, M., Hu, L., Yue, T., Chen, Z., Chen, B., Lu, X. and Xu, B. (2017). Penalized Linear Discriminant Analysis of Hyperspectral Imagery for Noise Removal. *IEEE Geoscience and Remote Sensing Letters*, *14*(3), 359-363.

MacDonald, R.B. and Hall, F.G. (1980). Global crop forecasting. *Science*, *208*(4445), 670-679.

Massey, R., Sankey, T.T., Congalton, R.G., Yadav, K., Thenkabail, P.S., Ozdogan, M. and Meador, A.J.S. (2017). MODIS phenology-derived, multi-year distribution of conterminous US crop types. *Remote Sensing of Environment*, *198*, 490-503.

Mayaux, P., Eva, H., Gallego, J., Strahler, A.H., Herold, M., Agrawal, S., Naumov, S., De Miranda, E.E., Di Bella, C.M., Ordoyne, C. and Kopin, Y. (2006). Validation of the global land cover 2000 map. *IEEE Transactions on Geoscience and Remote Sensing*, *44*(7), 1728-1739.

Myers, V.I. (1983). Remote sensing applications in agriculture. *Manual of remote sensing*, 2111-2228.

Ozdogan, M. (2010). The spatial distribution of crop types from MODIS data: Temporal unmixing using Independent Component Analysis. *Remote Sensing of Environment*, *114*(6), 1190-1204.

Ozdogan, M. and Woodcock, C.E. (2006). Resolution dependent errors in remote sensing of cultivated areas. *Remote Sensing of Environment*, *103*(2), 203-217.

Pax-Lenney, M., Woodcock, C.E., Macomber, S.A., Gopal, S. and Song, C. (2001). Forest mapping with a generalized classifier and Landsat TM data. *Remote Sensing of Environment*, *77*(3), 241-250.

Pittman, K., Hansen, M.C., Becker-Reshef, I., Potapov, P.V. and Justice, C.O. (2010). Estimating global cropland extent with multi-year MODIS data. *Remote Sensing*, *2*(7), 1844-1863.

Ramankutty, N., Evan, A.T., Monfreda, C. and Foley, J.A. (2008). Farming the planet: 1. Geographic distribution of global agricultural lands in the year 2000. *Global Biogeochemical Cycles*, *22*(1).

Scharlemann, J.P., Benz, D., Hay, S.I., Purse, B.V., Tatem, A.J., Wint, G.W. and Rogers, D.J. (2008). Global data for ecology and epidemiology: a novel algorithm for temporal Fourier processing MODIS data. *PloS one*, *3*(1), 1408.

See, L., Fritz, S., You, L., Ramankutty, N., Herrero, M., Justice, C., Becker-Reshef, I., Thornton, P., Erb, K., Gong, P. and Tang, H. (2015). Improved global cropland data as an essential ingredient for food security. *Global Food Security*, *4*, 37-45.

Switzer, P. (1980). Extensions of linear discriminant analysis for statistical classification of remotely sensed satellite imagery. *Journal of the International Association for Mathematical Geology*, *12*(4), 367-376.

Thenkabail, P.S. and Wu, Z. (2012). An automated cropland classification algorithm (ACCA) for Tajikistan by combining Landsat, MODIS, and secondary data. *Remote Sensing*, *4*(10), 2890-2918.

Tom, C.H. and Miller, L.D. (1984). An automated land-use mapping comparison of the Bayesian maximum likelihood and linear discriminant analysis algorithms. *Photogrammetric Engineering and Remote Sensing*, *50*(2), 193-207.

Visser, H. and De Nijs, T. (2006). The map comparison kit. *Environmental Modelling & Software*, *21*(3), 346-358.

Waldner, F., Canto, G.S. and Defourny, P. (2015). Automated annual cropland mapping using knowledge-based temporal features. *ISPRS Journal of Photogrammetry and Remote Sensing*, *110*, 1-13.

Waldner, F., Fritz, S., Di Gregorio, A., Plotnikov, D., Bartalev, S., Kussul, N., Gong, P., Thenkabail, P., Hazeu, G., Klein, I. and Löw, F. (2016). A unified cropland layer at 250 m for global agriculture monitoring. *Data*, *1*(1), 3.

Wardlow, B.D. and Egbert, S.L. (2010). A comparison of MODIS 250-m EVI and NDVI data for crop mapping: a case study for southwest Kansas. *International Journal of Remote Sensing*, *31*(3), 805-830.

Weiss, D.J., Atkinson, P.M., Bhatt, S., Mappin, B., Hay, S.I. and Gething, P.W. (2014). An effective approach for gap-filling continental scale remotely sensed time-series. *ISPRS Journal of Photogrammetry and Remote Sensing*, 98, 106-118.

Woodcock, C.E., Macomber, S.A., Pax-Lenney, M. and Cohen, W.B. (2001). Monitoring large areas for forest change using Landsat: Generalization across space, time and Landsat sensors. *Remote Sensing of Environment*, *78*(1-2), 194-203.

Xiong, J., Thenkabail, P.S., Gumma, M.K., Teluguntla, P., Poehnelt, J., Congalton, R.G., Yadav, K. and Thau, D. (2017). Automated cropland mapping of continental Africa using Google Earth Engine cloud computing. *ISPRS Journal of Photogrammetry and Remote Sensing*, *126*, 225-244.

Zhu, Z. and Woodcock, C.E. (2012). Object-based cloud and cloud shadow detection in Landsat imagery. *Remote Sensing of Environment*, 118, 83-94.

## Figures

**Figure 2.1.1** Map of the study area showing eight agro-ecological zones (AEZ) adapted from the Food and Agricultural Organization (FAO) of the United Nation's agro-ecological zones (Fischer et al., 2008) overlaid with country boundaries in the background. Also shown are the selected core (dark red) and random (white) footprints used in the analysis.

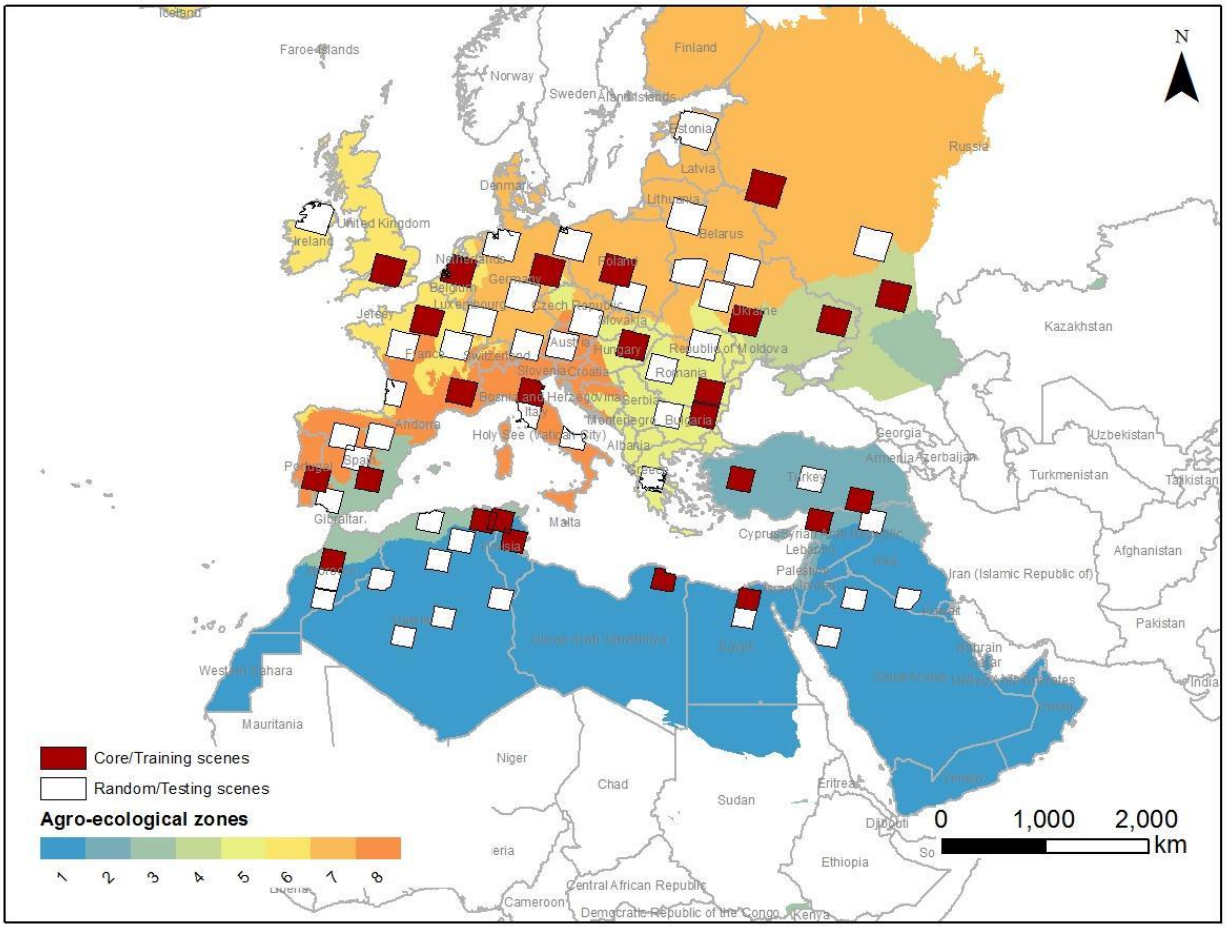

**Figure 2.1.2** Demonstration of Generalization in our study. This figure shows the source of training data for classifying sample footprint p182r029 (located in zone 5 inside Romania) selected for demonstration. The same approach used for applying generalized classifier for classifying any Landsat footprint according to the level of generalization.

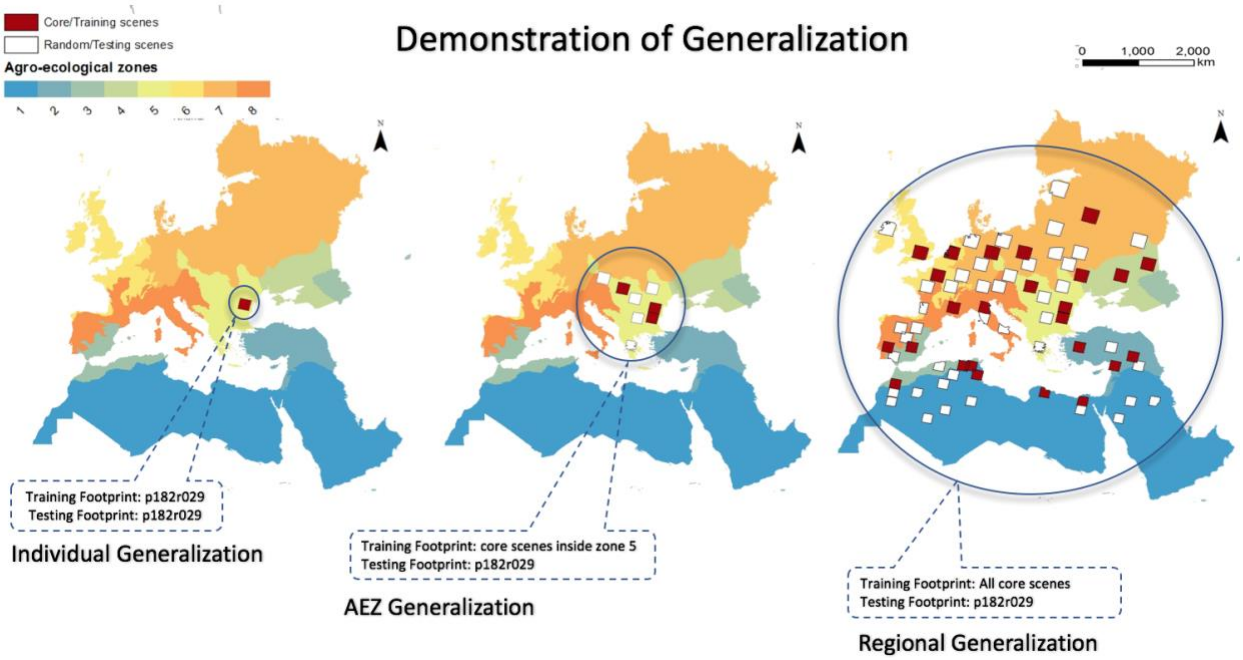

**Figure 2.1.3** General methodology of our study. Three important phases in the methodology: 1) acquisition, pre-processing, and temporal aggregation of satellite data along with topographic variables; 2) training and application of the classification scheme across three generalization levels; and 3) validation.

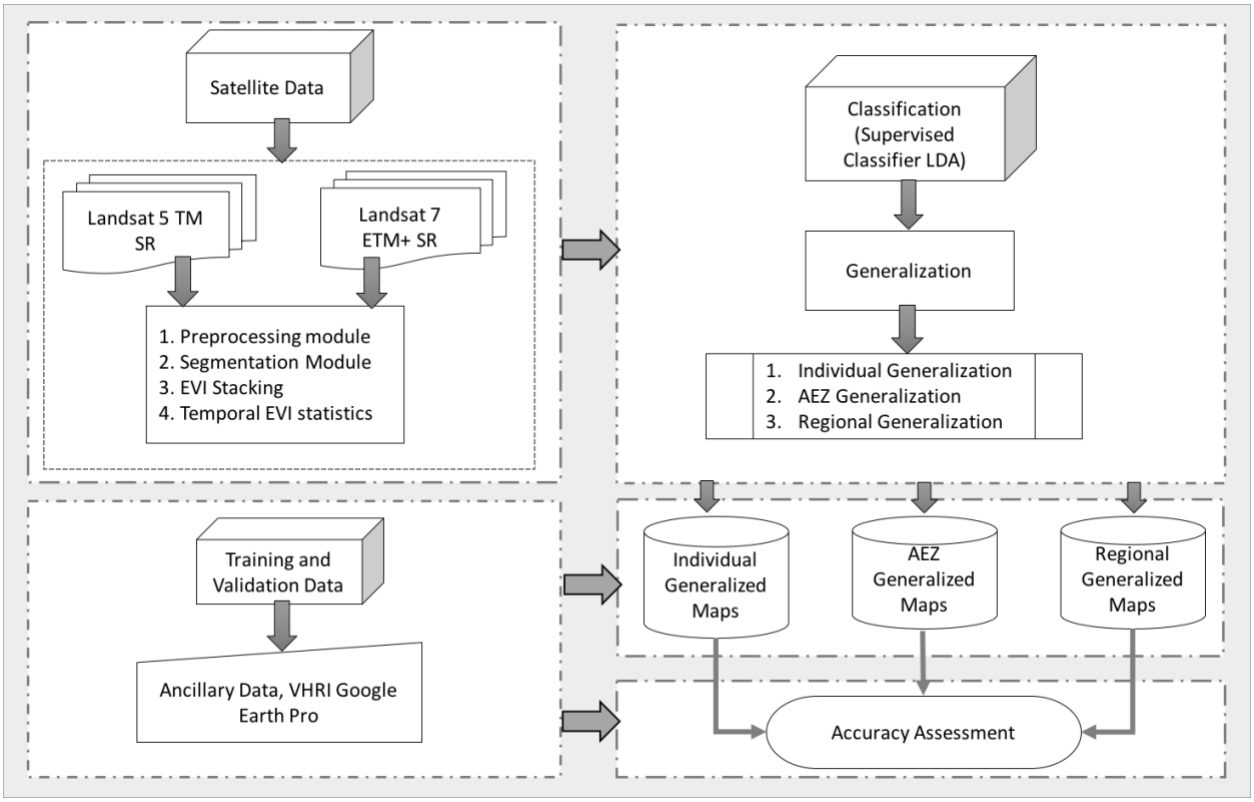

**Figure 2.1.4** LDA score histogram for discrimination of croplands and non-croplands. Left-side figure shows LDA score histogram for scene p177r039 which falls in the Egypt with very good discrimination between crop and non-crop whereas, right-side figure shows the LDA score histogram for scene p202r024 which falls in the United Kingdom with very less discrimination between croplands and non-croplands classes. These are two extreme cases of LDA score discrimination observed in the study area.

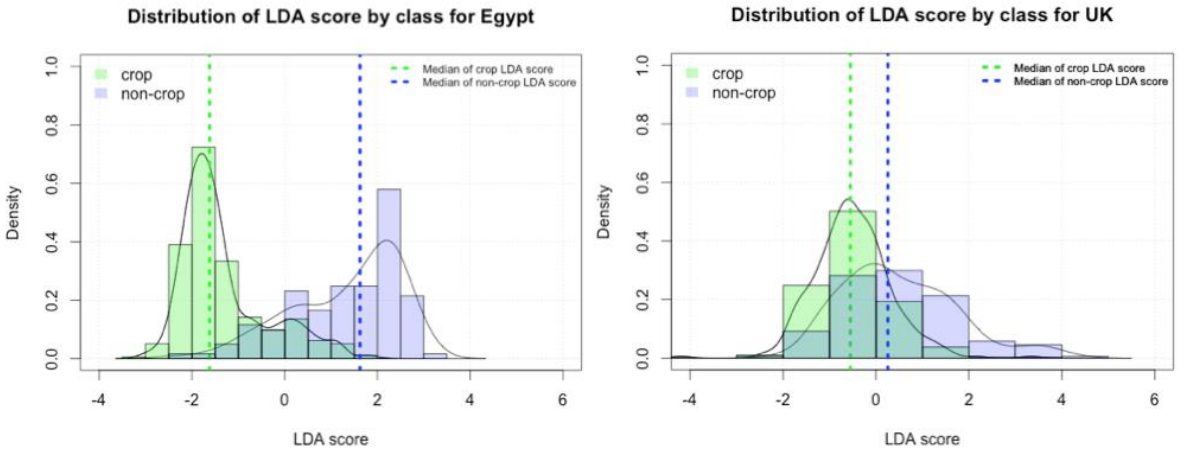

**Figure 2.1.5** Accuracy assessment of the cropland maps at each generalization levels for all the footprints (25 core footprints in light green color and 36 random footprints in light yellow color).

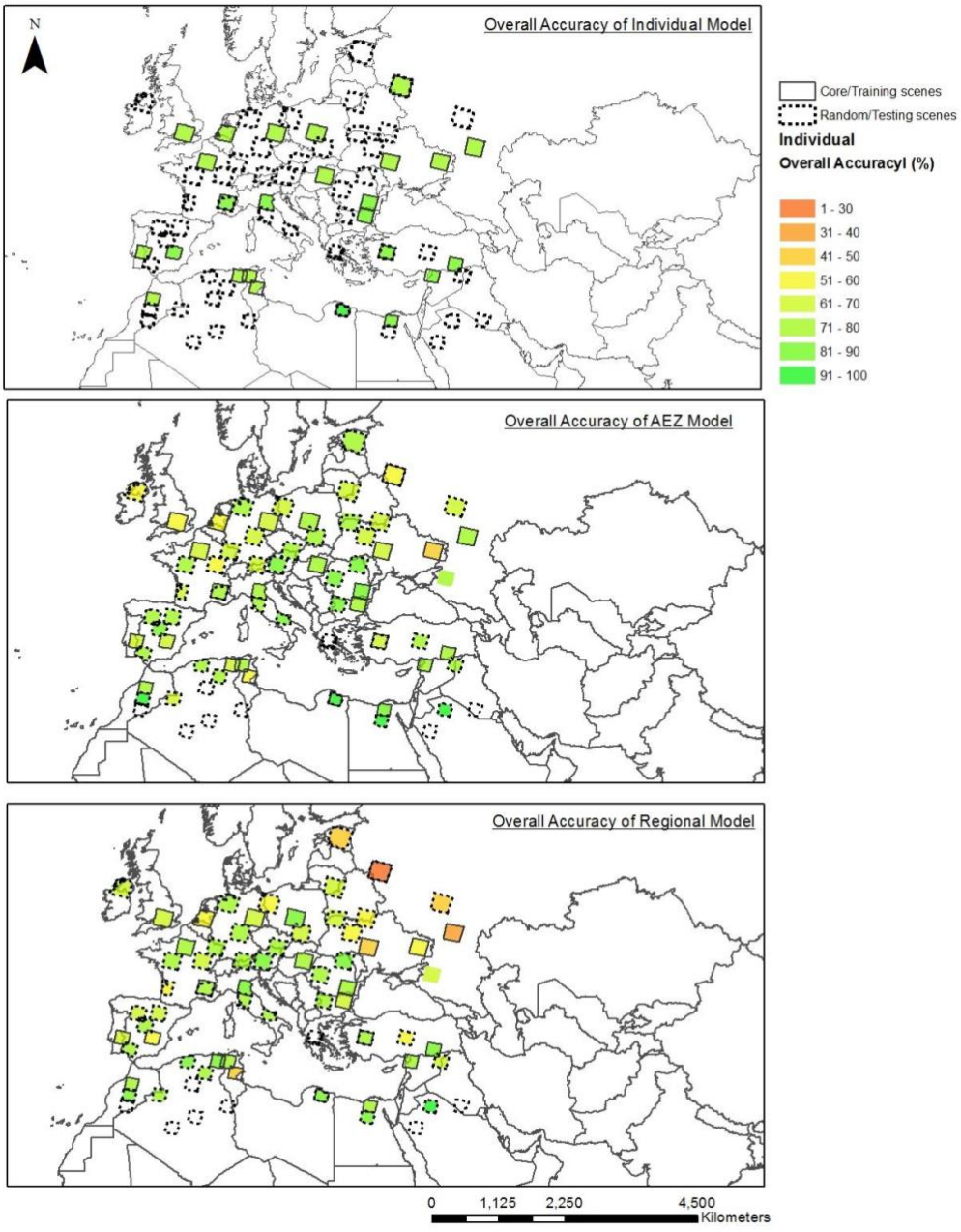

**Figure 2.1.6** Sample cropland extent maps across different AEZs (columns) in the study area and across all generalization levels (rows) along with the Landsat False Color Composite (FCC) for reference (first row). Also provided are various accuracy metrics for the respected sample.

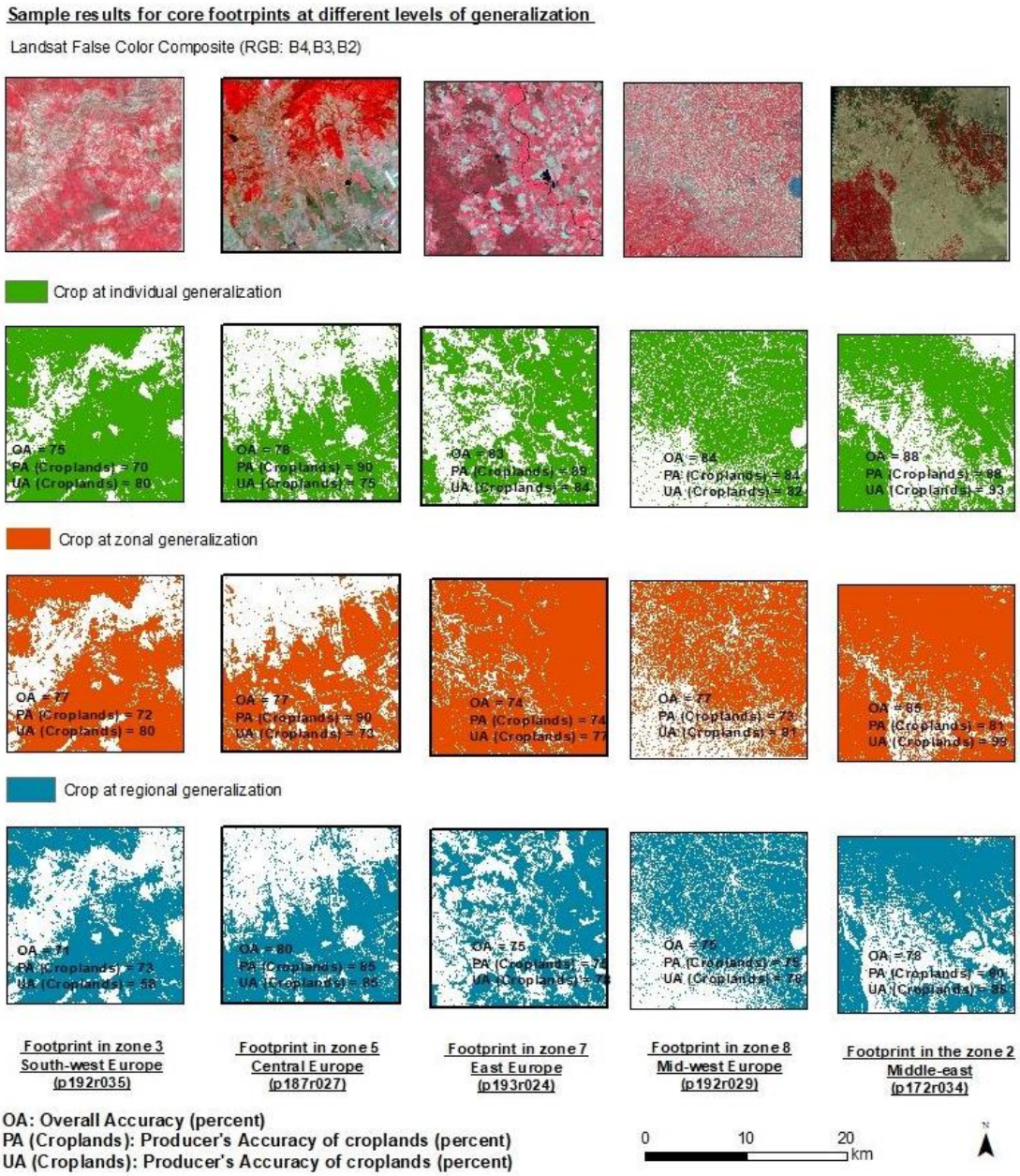

**Figure 2.1.7** Changes in overall accuracy between *individual* and *AEZ* level generalization. In each panel, the green bars and the light black line represent the histogram distribution of overall accuracy at the *individual* generalization level resulting from the cross-validation procedure. The red vertical bar depicts the overall accuracy of the same footprint at the *AEZ* level generalization when another footprint is added to the training set. The additional footprint in question is provided on the figure.

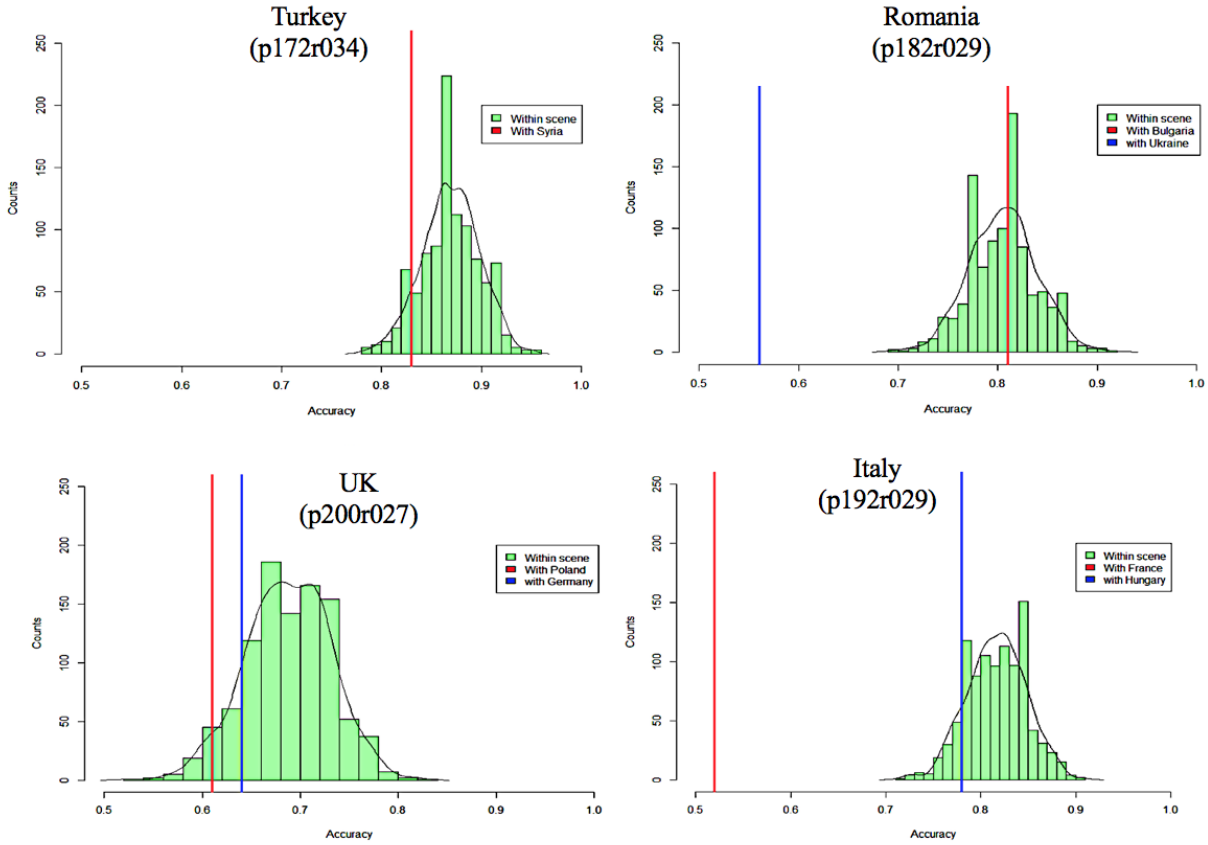

**Figure 2.1.8** Accuracy metrics at each level of generalization and at each agro-ecological zone for the core (first column) and random scenes (second column). Combined (core + random) accuracies are provided in the last column. Yellow circles represent *individual* level accuracies, green circles represent *AEZ* level accuracies and grey circles represent *regional* level accuracies for each AEZ. Diameter of each circle represents the standard deviation of accuracy in respective AEZ. First row displays overall accuracy, second row displays the producer's accuracy and third row displays the user's accuracy.

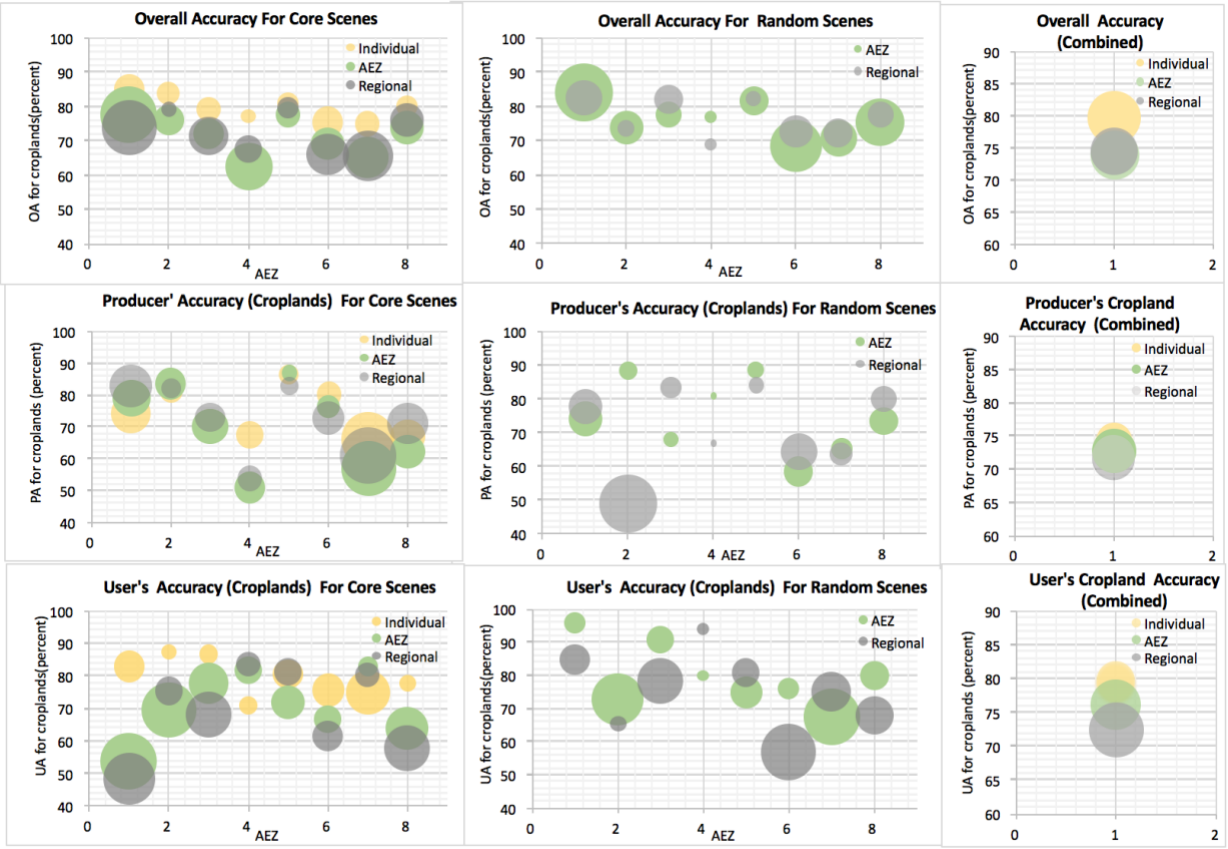


**Note: Diameter of the circle represents the standard deviation of accuracy values**
OA : Overall Accuracy ; PA: Producer's Accurancy; UA: User's Accuracy

**Figure 2.1.9** Visual comparison of *individual* and *regional* LDA cropland maps with CORINE and GLC croplands at 250m. Each row is for a different location while the columns are for a different map product. Also included is the Landsat false color composite for reference. Each box is approximately 8100 km$^2$.

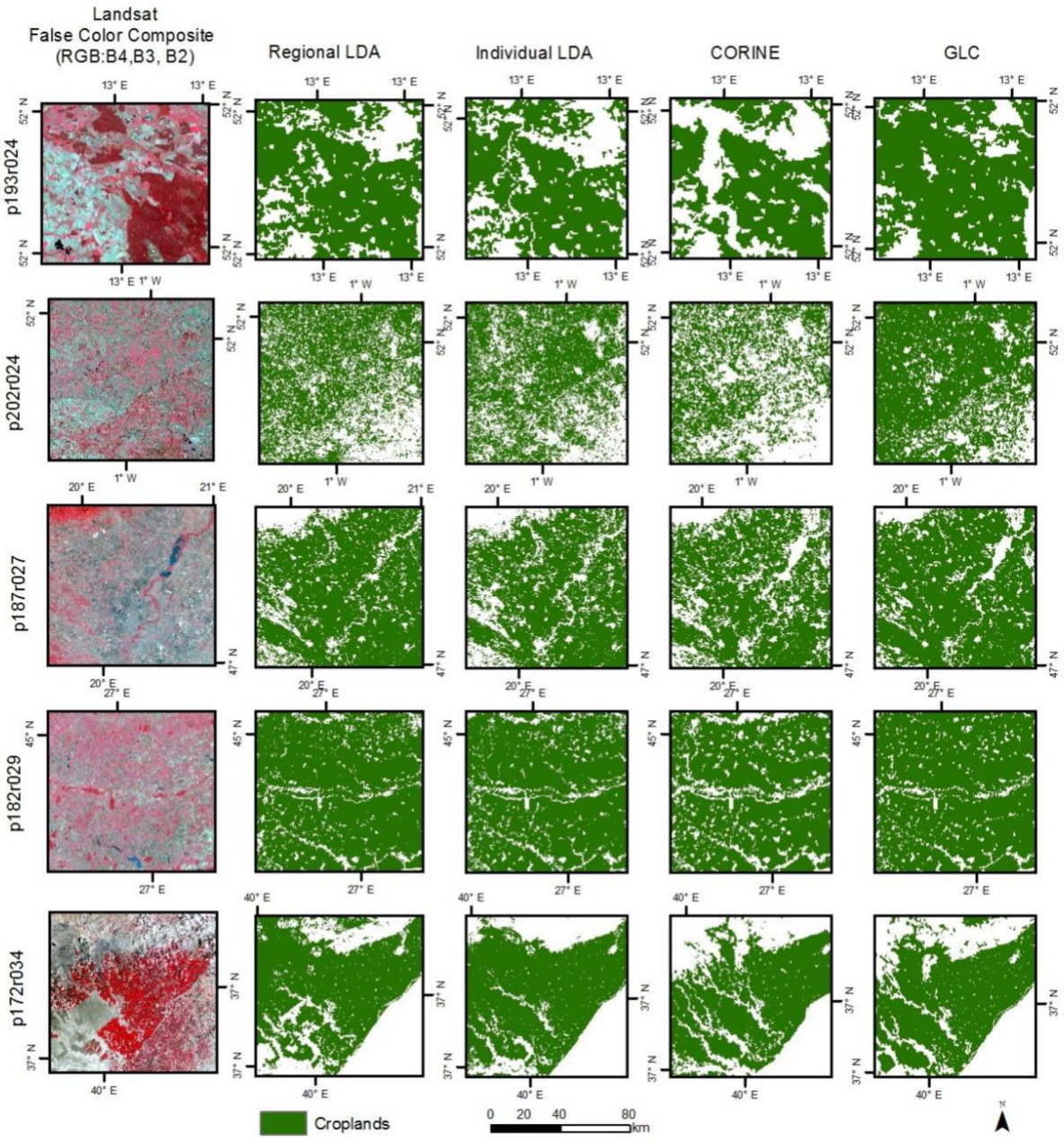

**Figure 2.1.10** Comparison of percent accuracies of cropland map classified using different classifiers random forest (RF), decision trees (DT) and support vector machines (SVM) with *regional* LDA generalized classified cropland maps.

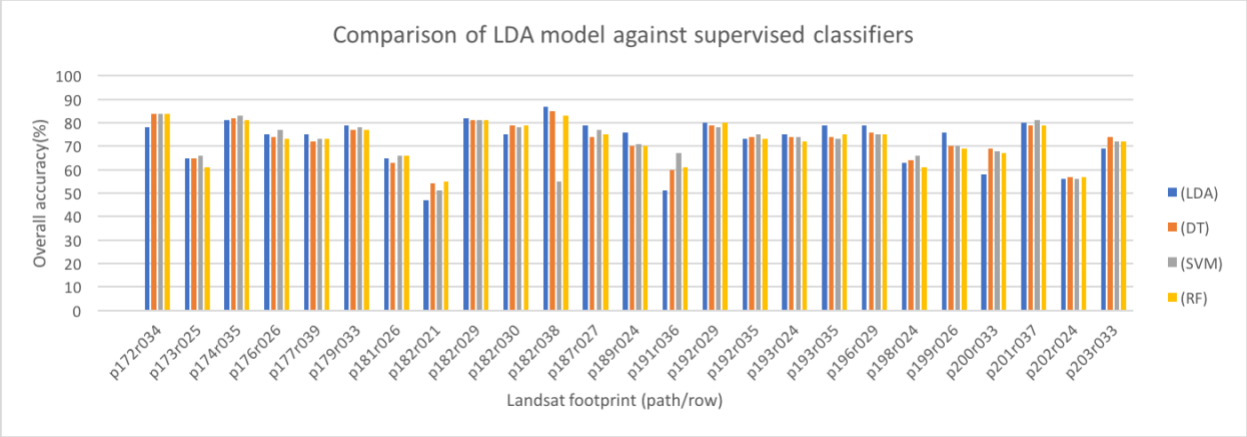

## Tables

**Table 2.1.1** Agro-ecological zones of the study area.

| AEZ | Moisture Regime | Length of growing period (days) | Major Sub-continents |
|---|---|---|---|
| Zone 1 | Arid | 1- 60 days | North Africa, the Middle-east |
| Zone 2 | Semi-Arid | 60 -119 days | the Middle-east |
| Zone 3 | Mediterranean in North and south and Semi-Arid in East | 119-179 days | South-west Europe |
| Zone 4 | Semi-Arid | 119-239 days | South-east Europe |
| Zone 5 | Humid continental in North, Mediterranean in South, Humid subtropical in west | 90-179 days | Central Europe |
| Zone 6 | Marine West-coast | 150-365 days | North-west Europe |
| Zone 7 | Humid-continental | 150-239 days | East Europe |
| Zone 8 | Mediterranean | 150-299 days | Mid- west Europe |

**Table 2.1.2** List of Landsat footprints with two Landsat sensors (LT5 and LE7) along with their associated agro-eco zones (AEZ) for time-period 2009-2011. The Core footprints refer to those with training segments. Random footprints refer to those without a training set. Last two columns show the overall average number of Landsat scenes for each sensor and each AEZ.

| | | Core Scenes | | | | | | Random Scenes | | | | | | | |
|---|---|---|---|---|---|---|---|---|---|---|---|---|---|---|---|
| AEZ | Sub-continent | LT5 | LE7 | LT5 | LE7 | LT5 | LE7 | LT5 | LE7 | LT5 | LE7 | LT5 | LE7 | LT5 | LE7 |
| z1 | North Africa | 2 | 10 | 6 | 7 | 3 | 11 | 6 | 10 | 6 | 6 | 5 | 9 | 5 | 9 |
| z2 | the Middle-east | 5 | 10 | 6 | 9 | 6 | 12 | 5 | 8 | 5 | 6 | 6 | 11 | 7 | 9 |
| z3 | SW Europe | 9 | 7 | 9 | 7 | 11 | 7 | 6 | 8 | 5 | 9 | 8 | 8 | 8 | 8 |
| z4 | SE Europe | 5 | 6 | 7 | 4 | 6 | 9 | 4 | 2 | 4 | 8 | 2 | 5 | 5 | 6 |
| z5 | Central Europe | 7 | 8 | 7 | 7 | 7 | 8 | 5 | 7 | 4 | 5 | 7 | 9 | 7 | 7 |
| z6 | NW Europe | 2 | 2 | 2 | 2 | 1 | 4 | 2 | 5 | 2 | 4 | 3 | 6 | 3 | 4 |
| z7 | East Europe | 4 | 4 | 4 | 4 | 6 | 6 | 5 | 5 | 5 | 4 | 6 | 6 | 5 | 5 |
| z8 | MW Europe | 4 | 6 | 5 | 6 | 5 | 7 | 6 | 6 | 5 | 6 | 5 | 9 | 6 | 6 |
| | | 2009 | | 2010 | | 2011 | | 2009 | | 2010 | | 2011 | | Overall Average | |

SW: south-west
SE: south-east
NW: north-west
MW: mid-west

Low — High

Number of Landsat scenes

**Table 2.1.3** Seasonal model generalized accuracies. Seasonal models are named according to temporal domain of EVI (Enhanced vegetation index) observations used to form inputs. 'S1' corresponds to season1 LDA model with EVI observations from December, January and February, 'S2' is season2 with EVI observations from March, April and May, 'S3' is seasons3 with EVI observations from Jun, July and August, 'S4' is season4 with EVI observations from September, October and November, and 'All' corresponds to EVI observations in all seasons. Average count is the average of the number of valid observations for the total number of training segments (often 500) of respective Landsat footprint in each season.

p172r034

| | S1 | S2 | S3 | S4 | All |
|---|---|---|---|---|---|
| OA | 83 | 87 | 84 | 83 | 88 |
| PA (crop) | 87 | 87 | 86 | 86 | 89 |
| PA (non-crop) | 74 | 86 | 80 | 80 | 86 |
| UA (crop) | 91 | 93 | 88 | 88 | 92 |
| UA (non-crop) | 65 | 77 | 77 | 76 | 81 |
| Average Count | 3 | 6 | 24 | 13 | 44 |

P181r026

| | S1 | S2 | S3 | S4 | All |
|---|---|---|---|---|---|
| OA | 54 | 60 | 75 | 76 | 76 |
| PA (crop) | 53 | 57 | 75 | 73 | 76 |
| PA (non-crop) | 56 | 63 | 75 | 79 | 77 |
| UA (crop) | 51 | 61 | 70 | 77 | 73 |
| UA (non-crop) | 58 | 58 | 80 | 75 | 80 |
| Average Count | 2 | 7 | 12 | 7 | 28 |

p177r039

| | S1 | S2 | S3 | S4 | All |
|---|---|---|---|---|---|
| OA | 85 | 86 | 83 | 85 | 87 |
| PA (crop) | 93 | 93 | 90 | 93 | 93 |
| PA (non-crop) | 65 | 68 | 66 | 67 | 73 |
| UA (crop) | 86 | 88 | 86 | 86 | 90 |
| UA (non-crop) | 80 | 80 | 74 | 80 | 79 |
| Average Count | 5 | 5 | 3 | 4 | 16 |

P200r033

| | S1 | S2 | S3 | S4 | All |
|---|---|---|---|---|---|
| OA | 86 | 84 | 83 | 84 | 85 |
| PA (crop) | 84 | 84 | 81 | 82 | 84 |
| PA (non-crop) | 89 | 85 | 89 | 89 | 87 |
| UA (crop) | 95 | 92 | 94 | 94 | 93 |
| UA (non-crop) | 71 | 73 | 67 | 68 | 73 |
| Average Count | 5 | 5 | 9 | 9 | 27 |

p189r024

| | S1 | S2 | S3 | S4 | All |
|---|---|---|---|---|---|
| OA | | 71 | 80 | 71 | 76 |
| PA (crop) | | 88 | 94 | 89 | 92 |
| PA (non-crop) | | 38 | 51 | 38 | 46 |
| UA (crop) | | 73 | 80 | 72 | 76 |
| UA (non-crop) | | 63 | 79 | 67 | 75 |
| Average Count | 0 | 6 | 7 | 5 | 18 |

P182r030

| | S1 | S2 | S3 | S4 | All |
|---|---|---|---|---|---|
| OA | 71 | 72 | 81 | 76 | 82 |
| PA (crop) | 66 | 67 | 78 | 72 | 81 |
| PA (non-crop) | 79 | 79 | 85 | 80 | 84 |
| UA (crop) | 85 | 82 | 86 | 82 | 83 |
| UA (non-crop) | 57 | 61 | 77 | 69 | 82 |
| Average Count | 3 | 6 | 15 | 8 | 31 |

Accuracy
Low High

Average Count
Low High

OA: Overall Accuracy (Percer
PA: Producer's Accuracy (Pe
UA: User's Accuracy (Percen

| | | Months |
|---|---|---|
| S1: | Season1 | Dec Jan Feb |
| S2: | Season2 | March April May |
| S3: | Season3 | Jun Jul Aug |
| S4: | Season4 | Sept Oct Nov |
| All: | All seasons | |

## Appendix A2.1

**Table A2.1.1** Accuracy assessment results of cropland maps at all generalization levels for the core (green) and the random (yellow) footprints.

| Landsat footprint | Country | Generalization level | Crop classified as crop | Non-crop classified as crop | Crop classified as non-crop | Non-crop classified as non-crop | Overall accuracy | Kappa |
|---|---|---|---|---|---|---|---|---|
| p177r039 | Egypt | Individual | 333 | 26 | 34 | 97 | 88 % | 0.68 |
| | | AEZ | 354 | 39 | 13 | 84 | 89% | 0.70 |
| | | Regional | 275 | 11 | 92 | 112 | 79% | 0.54 |
| p182r038 | Libya | Individual | 38 | 30 | 12 | 384 | 91% | 0.59 |
| | | AEZ | 24 | 17 | 26 | 397 | 91% | 0.48 |
| | | Regional | 13 | 8 | 37 | 406 | 90% | 0.32 |
| p191r036 | Tunisia | Individual | 228 | 67 | 35 | 149 | 79% | 0.56 |
| | | AEZ | 45 | 6 | 218 | 210 | 53% | 0.13 |
| | | Regional | 20 | 1 | 243 | 215 | 49% | 0.06 |
| p172r034 | Turkey | Individual | 288 | 38 | 18 | 150 | 89% | 0.75 |
| | | AEZ | 303 | 97 | 3 | 91 | 80% | 0.52 |
| | | Regional | 248 | 34 | 58 | 154 | 81% | 0.61 |
| p174r035 | Syria | Individual | 197 | 47 | 37 | 188 | 82% | 0.64 |
| | | AEZ | 192 | 53 | 42 | 182 | 80% | 0.59 |
| | | Regional | 135 | 11 | 99 | 224 | 77% | 0.53 |
| p179r033 | Turkey | Individual | 178 | 56 | 28 | 230 | 83% | 0.66 |
| | | AEZ | 57 | 2 | 149 | 284 | 69% | 0.30 |
| | | Regional | 87 | 12 | 119 | 274 | 73% | 0.41 |
| p200r033 | Spain | Individual | 276 | 53 | 18 | 141 | 85% | 0.69 |
| | | AEZ | 144 | 15 | 150 | 179 | 66% | 0.37 |
| | | Regional | 62 | 9 | 232 | 185 | 51% | 0.14 |
| p201r037 | Morocco | Individual | 157 | 75 | 21 | 239 | 80% | 0.60 |
| | | AEZ | 158 | 87 | 20 | 227 | 78% | 0.56 |
| | | Regional | 147 | 69 | 31 | 245 | 80% | 0.58 |
| p193r035 | Algeria | Individual | 163 | 84 | 25 | 224 | 78% | 0.56 |
| | | AEZ | 174 | 142 | 14 | 166 | 69% | 0.41 |
| | | Regional | 134 | 42 | 54 | 266 | 81% | 0.58 |
| p192r035 | Tunisia | Individual | 182 | 77 | 43 | 192 | 76% | 0.52 |
| | | AEZ | 181 | 77 | 44 | 192 | 76% | 0.51 |
| | | Regional | 134 | 48 | 91 | 221 | 72% | 0.42 |
| p181r026 | Ukraine | Individual | 163 | 49 | 59 | 203 | 77% | 0.54 |
| | | AEZ | 192 | 124 | 30 | 128 | 68% | 0.36 |
| | | Regional | 219 | 247 | 3 | 5 | 47% | 0.01 |
| p176r026 | Russia | Individual | 121 | 46 | 47 | 260 | 80% | 0.57 |
| | | AEZ | 147 | 236 | 21 | 70 | 46% | 0.08 |
| | | Regional | 140 | 181 | 28 | 125 | 56% | 0.20 |
| p173r025 | Russia | Individual | 58 | 39 | 24 | 163 | 78% | 0.49 |
| | | AEZ | 58 | 49 | 24 | 153 | 74% | 0.43 |
| | | Regional | 74 | 170 | 8 | 32 | 37% | 0.04 |
| p182r030 | Bulgaria | Individual | 196 | 43 | 39 | 207 | 83% | 0.66 |
| | | AEZ | 134 | 25 | 101 | 225 | 74% | 0.47 |
| | | Regional | 230 | 182 | 5 | 68 | 61% | 0.25 |

| | | | | | | | | |
|---|---|---|---|---|---|---|---|---|
| p187r027 | Hungary | Individual | 249 | 32 | 75 | 132 | 78% | 0.54 |
| | | AEZ | 236 | 26 | 88 | 138 | 77% | 0.52 |
| | | Regional | 309 | 120 | 15 | 44 | 72% | 0.26 |
| p182r029 | Romania | Individual | 267 | 29 | 51 | 142 | 84% | 0.65 |
| | | AEZ | 274 | 42 | 44 | 129 | 82% | 0.61 |
| | | Regional | 312 | 123 | 6 | 48 | 74% | 0.31 |
| p199r026 | France | Individual | 227 | 25 | 69 | 160 | 80% | 0.60 |
| | | AEZ | 220 | 84 | 76 | 101 | 67% | 0.29 |
| | | Regional | 222 | 42 | 74 | 143 | 76% | 0.51 |
| p202r024 | UK | Individual | 231 | 70 | 70 | 107 | 71% | 0.37 |
| | | AEZ | 145 | 46 | 156 | 131 | 58% | 0.20 |
| | | Regional | 189 | 66 | 112 | 111 | 63% | 0.24 |
| p198r024 | Netherlands | Individual | 175 | 50 | 43 | 205 | 80% | 0.61 |
| | | AEZ | 2 | 0 | 216 | 255 | 54% | 0.01 |
| | | Regional | 10 | 1 | 208 | 254 | 56% | 0.05 |
| p189r024 | Poland | Individual | 297 | 22 | 93 | 83 | 77% | 0.44 |
| | | AEZ | 305 | 22 | 85 | 83 | 78% | 0.47 |
| | | Regional | 373 | 75 | 17 | 30 | 81% | 0.30 |
| p193r024 | Germany | Individual | 199 | 38 | 60 | 195 | 80% | 0.60 |
| | | AEZ | 217 | 148 | 42 | 85 | 61% | 0.21 |
| | | Regional | 235 | 127 | 24 | 106 | 69% | 0.37 |
| p182r021 | Russia | Individual | 43 | 123 | 12 | 307 | 72% | 0.26 |
| | | AEZ | 48 | 205 | 7 | 225 | 56% | 0.15 |
| | | Regional | 55 | 387 | 0 | 43 | 20% | 0.02 |
| p203r033 | Portugal | Individual | 119 | 72 | 30 | 275 | 79% | 0.55 |
| | | AEZ | 112 | 134 | 37 | 213 | 66% | 0.31 |
| | | Regional | 107 | 129 | 42 | 218 | 66% | 0.30 |
| p192r029 | Italy | Individual | 193 | 37 | 41 | 220 | 84% | 0.68 |
| | | AEZ | 185 | 69 | 49 | 188 | 76% | 0.52 |
| | | Regional | 205 | 66 | 29 | 191 | 81% | 0.61 |
| p196r029 | France | Individual | 93 | 63 | 30 | 298 | 81% | 0.53 |
| | | AEZ | 47 | 22 | 76 | 339 | 80% | 0.38 |
| | | Regional | 35 | 15 | 88 | 346 | 79% | 0.30 |
| p171r039 | Saudi Arabia | AEZ | 182 | 15 | 4 | 188 | 95% | 0.90 |
| | | Regional | 168 | 15 | 18 | 188 | 92% | 0.83 |
| p177r040 | Egypt | AEZ | 273 | 21 | 16 | 273 | 94% | 0.87 |
| | | Regional | 237 | 9 | 52 | 285 | 90% | 0.79 |
| p194r036 | Algeria | AEZ | 144 | 95 | 11 | 141 | 73% | 0.48 |
| | | Regional | 117 | 43 | 38 | 193 | 79% | 0.57 |
| p198r038 | Algeria | AEZ | 79 | 124 | 0 | 189 | 68% | 0.38 |
| | | Regional | 74 | 97 | 5 | 216 | 74% | 0.44 |
| p201r038 | Morocco | AEZ | 188 | 30 | 6 | 168 | 91% | 0.82 |
| | | Regional | 167 | 21 | 27 | 177 | 88% | 0.76 |
| p171r035 | Syria/Iraq | AEZ | 249 | 50 | 34 | 49 | 78% | 0.40 |
| | | Regional | 161 | 7 | 122 | 92 | 66% | 0.36 |
| p175r033 | Turkey | AEZ | 149 | 10 | 101 | 126 | 71% | 0.45 |
| | | Regional | 99 | 12 | 151 | 124 | 58% | 0.25 |
| p196r035 | Algeria | AEZ | 230 | 124 | 10 | 226 | 77% | 0.56 |
| | | Regional | 177 | 42 | 63 | 308 | 82% | 0.63 |
| p202r034 | Spain | AEZ | 246 | 112 | 20 | 207 | 77% | 0.56 |
| | | Regional | 197 | 57 | 69 | 262 | 78% | 0.56 |
| p200r031 | Spain | AEZ | 145 | 53 | 28 | 169 | 79% | 0.59 |

| | | | | | | | | |
|---|---|---|---|---|---|---|---|---|
| | | Regional | 63 | 18 | 110 | 204 | 68% | 0.30 |
| p174r028 | Russia | AEZ | 191 | 46 | 48 | 115 | 77% | 0.51 |
| | | Regional | 226 | 140 | 13 | 21 | 62% | 0.09 |
| p190r026 | Czech | AEZ | 181 | 19 | 61 | 131 | 80% | 0.59 |
| | Republic | Regional | 215 | 63 | 27 | 87 | 77% | 0.49 |
| p183r027 | Moldova | AEZ | 254 | 25 | 75 | 228 | 83% | 0.66 |
| | | Regional | 300 | 78 | 29 | 175 | 82% | 0.62 |
| p185r028 | Romania | AEZ | 180 | 13 | 85 | 307 | 83% | 0.65 |
| | | Regional | 252 | 114 | 13 | 206 | 78% | 0.58 |
| p184r030 | Bulgaria | AEZ | 160 | 40 | 29 | 168 | 83% | 0.65 |
| | | Regional | 175 | 76 | 14 | 132 | 77% | 0.55 |
| p196r026 | Germany | AEZ | 169 | 132 | 6 | 85 | 65% | 0.33 |
| | | Regional | 154 | 72 | 21 | 145 | 76% | 0.53 |
| p197r027 | France | AEZ | 145 | 173 | 11 | 57 | 52% | 0.15 |
| | | Regional | 116 | 82 | 40 | 148 | 68% | 0.37 |
| p200r027 | France | AEZ | 75 | 36 | 18 | 67 | 72% | 0.45 |
| | | Regional | 84 | 42 | 9 | 61 | 74% | 0.49 |
| p207r022 | UK | AEZ | 69 | 150 | 32 | 133 | 53% | 0.11 |
| | | Regional | 49 | 93 | 52 | 190 | 62% | 0.14 |
| p187r019 | Estonia | AEZ | 79 | 60 | 84 | 372 | 76% | 0.36 |
| | | Regional | 155 | 332 | 8 | 100 | 43% | 0.11 |
| p182r024 | Belarus | AEZ | 181 | 151 | 28 | 226 | 69% | 0.41 |
| | | Regional | 202 | 237 | 7 | 140 | 58% | 0.27 |
| p183r025 | Ukraine | AEZ | 248 | 167 | 34 | 132 | 65% | 0.32 |
| | | Regional | 276 | 226 | 6 | 73 | 60% | 0.22 |
| p185r024 | Ukraine | AEZ | 204 | 57 | 76 | 244 | 77% | 0.54 |
| | | Regional | 274 | 219 | 6 | 82 | 61% | 0.24 |
| p186r022 | Lithuania | AEZ | 134 | 63 | 68 | 123 | 66% | 0.32 |
| | | Regional | 198 | 142 | 4 | 44 | 62% | 0.22 |
| p188r025 | Poland | AEZ | 143 | 57 | 55 | 138 | 72% | 0.43 |
| | | Regional | 170 | 105 | 28 | 90 | 66% | 0.32 |
| p192r023 | Poland | AEZ | 213 | 154 | 35 | 175 | 67% | 0.37 |
| | | Regional | 234 | 233 | 14 | 96 | 57% | 0.21 |
| p196r023 | Germany | AEZ | 185 | 120 | 27 | 242 | 74% | 0.50 |
| | | Regional | 203 | 156 | 9 | 206 | 71% | 0.46 |
| p194r025 | Germany | AEZ | 20 | 5 | 168 | 379 | 70% | 0.12 |
| | | Regional | 101 | 53 | 87 | 331 | 76% | 0.42 |
| p175r023 | Russia | AEZ | 110 | 55 | 116 | 287 | 70% | 0.34 |
| | | Regional | 212 | 300 | 14 | 42 | 45% | 0.05 |
| p191r027 | Austria | AEZ | 238 | 55 | 45 | 227 | 82% | 0.65 |
| | | Regional | 255 | 47 | 28 | 235 | 87% | 0.73 |
| p189r031 | Italy | AEZ | 353 | 66 | 65 | 206 | 81% | 0.60 |
| | | Regional | 275 | 17 | 143 | 255 | 77% | 0.55 |
| p192r030 | Italy | AEZ | 154 | 40 | 37 | 157 | 80% | 0.60 |
| | | Regional | 115 | 32 | 76 | 165 | 72% | 0.44 |
| p200r029 | France | AEZ | 93 | 97 | 32 | 166 | 67% | 0.33 |
| | | Regional | 87 | 123 | 38 | 140 | 59% | 0.19 |
| p202r031 | Spain | AEZ | 168 | 26 | 66 | 124 | 76% | 0.52 |
| | | Regional | 131 | 24 | 103 | 126 | 67% | 0.37 |
| p201r032 | Spain | AEZ | 170 | 24 | 50 | 149 | 81% | 0.62 |
| | | Regional | 169 | 48 | 51 | 125 | 75% | 0.49 |
| p193r027 | Germany | AEZ | 183 | 177 | 23 | 176 | 64% | 0.33 |
| | | Regional | 194 | 130 | 12 | 223 | 75% | 0.51 |

**Table A2.1.2** LDA coefficients at zonal and regional level of generalization.

| Generalization level | Input Variable | | | | | | | | |
|---|---|---|---|---|---|---|---|---|---|
| | Mean EVI | SD EVI | Max EVI | Min EVI | Var EVI | Range EVI | Count EVI | Slope | Elevation |
| Zone 1 | 7.22 | -16.41 | -4.23 | -11.95 | 78.20 | -4.37 | -0.02 | 0.10 | 0.000 |
| Zone 2 | 7.26 | -33.30 | 0.35 | -1.01 | 51.39 | 0.49 | 0.01 | 0.10 | 0.001 |
| Zone 3 | 9.84 | -4.90 | -2.60 | -1.26 | 10.01 | -2.48 | 0.03 | 0.13 | 0.000 |
| Zone 4 | 15.73 | -14.56 | -5.07 | -3.93 | 6.04 | -0.10 | 0.03 | 0.07 | -0.003 |
| Zone 5 | 13.65 | -29.82 | -4.51 | -3.68 | 66.31 | -1.18 | 0.02 | 0.13 | 0.001 |
| Zone 6 | 0.07 | -23.79 | 5.61 | -7.83 | -0.05 | -2.57 | -0.05 | 0.14 | -0.003 |
| Zone 7 | 20.30 | -7.54 | -7.46 | -16.52 | 9.86 | -3.99 | -0.09 | 0.25 | 0.001 |
| Zone 8 | 10.87 | -1.51 | -5.34 | -2.48 | 4.09 | -3.73 | 0.05 | 0.06 | 0.000 |
| Regional | 0.47 | -12.24 | 7.13 | -7.69 | 9.07 | -7.68 | -0.01 | 0.13 | 0.000 |

Note:

| | |
|---|---|
| Mean EVI | Average value of EVI time-series data |
| SD EVI | Standard deviation value of EVI time-series data |
| Max EVI | Maximum value of EVI time-series data |
| Min EVI | Minimum value of EVI time-series data |
| Var EVI | Variance value of EVI time-series data |
| Range EVI | Range value of EVI time-series data |
| Count EVI | Number of valid observations in the EVI time-series data |

**Table A2.1.3** Comparison of *regional* and *individual* generalized maps with other croplands maps from the GLC and CORINE land cover products.

| Footprints | Country | *Individual* LDA | | | CORINE | | | GLC | | |
|---|---|---|---|---|---|---|---|---|---|---|
| | | Average Similarity (percent) | Fuzzy Kappa (percent) | Croplands Area (1000ha) | Average Similarity (percent) | Fuzzy Kappa (percent) | Croplands Area (1000ha) | Average Similarity (percent) | Fuzzy Kappa (percent) | Croplands Area (1000ha) |
| p193r024 | Germany | 97 | 91 | 1613 | 93 | 77 | 1523 | 94 | 89 | 1808 |
| p202r024 | UK | 84 | 40 | 1937 | 88 | 60 | 1463 | 80 | 40 | 2181 |
| p187r027 | Hungary | 97 | 90 | 1832 | 90 | 71 | 1797 | 87 | 61 | 2081 |
| p182r029 | Romania | 96 | 87 | 2193 | 92 | 74 | 2119 | 89 | 63 | 2269 |
| p172r034 | Turkey | 89 | 72 | 1616 | 80 | 51 | 1371 | 81 | 52 | 1470 |

**Chapter 2 (Part 2)**

## Mapping croplands of Europe, Middle East, Russia, and Central Asia using Landsat, Random Forest, and Google Earth Engine

Phalke, A. R., Özdoğan M., Thenkabail, P. S., Erickson, T., Gorelick, N., Yadav, K., Congalton, R. G. 2020.

*ISPRS Journal of Photogrammetry and Remote Sensing* 167: 104-122

### Abstract

Accurate and timely information on croplands is important for environmental, food security, and policy studies. Spatially explicit cropland datasets are also required to derive information on crop type, crop yield, cropping intensity, as well as irrigated areas. Large area – defined as continental to global – cropland mapping is challenging due to differential manifestation of croplands, wide range of cultivation practices and limited reference data availability. This study presents the results of a cropland extent mapping of 64 countries covering large parts of Europe, Middle East, Russia and Central Asia. To cover such a vast area, roughly 160,000 Landsat scenes from 3,351 footprints between 2014 and 2016 were processed within the Google Earth Engine (GEE) platform. We used a pixel-based Random Forest (RF) machine learning algorithm with a set of satellite data inputs capturing diverse spectral, temporal and topographical characteristics across twelve agroecological zones (AEZs). The reference data to train the classification model were collected from very high spatial resolution imagery (VHRI) and ancillary datasets. The result is a binary map showing cultivated/non-cultivated areas ca. 2015. The map produced an overall accuracy of 93.8 % with roughly 14 % omission and commission errors for the cropland class based on a large set of independent validation samples. The map suggests the entire study area has a total 546 million hectares (Mha) of net croplands (nearly 30% of global net cropland areas) occupying 18 % of the

study land area. Comparison between national cropland area estimates from United Nations Food and Agricultural Organizations (FAO) and those derived from this work also showed an R-square value of 0.95. This Landsat-derived 30-m cropland product (GFSAD30) provided 10-30% greater cropland areas compared to UN FAO in the 64 Countries. Finally, the map-to-map comparison between GFSAD30 with several other cropland products revealed that the best *similarity matrix* was with the 30m global land cover (GLC30) product providing an overall similarity of 88.8 % (Kappa 0.7) with producer's cropland similarity of 89.2 % (errors of omissions = 10.8%) and user's cropland similarity of 81.8 % (errors of commissions = 8.1%). GFSAD30 captured the missing croplands in GLC30 product around significantly irrigated agricultural areas in Germany and Belgium and rainfed agriculture in Italy. This study also established that the real strengths of GFSAD30 product, compared to other products, were: 1. identifying precise location of croplands, and 2. capturing fragmented croplands. The cropland extent map dataset is available through NASA's Land Processes Distributed Active Archive Center (LP DAAC) at **https://doi.org/10.5067/MEaSUREs/GFSAD/GFSAD30EUCEARUMECE.001**, while the training and reference data as well as visualization are available at the Global Croplands <**https://croplands.org**> website, GEE code is accessible at: https://code.earthengine.google.com/1666e8bed34e0ce2b2aaf1235ad8c6bd.

### 2.2.1 Introduction

Agricultural is an essential part of the terrestrial ecosystem and plays an important role in human livelihood (Meyer et al., 1992; Lambin et al., 2003; Alexander et al., 2015; Ramankutty et al., 2018). Presence of agricultural lands and their change over time are driven by a number of factors ranging from biophysical and climatic characteristics to socio-economic and political forces (Veldkamp et al., 2001; Meyfroit et al., 2013; Vliet et al., 2015; Gomes et al., 2019). For example, in some parts of the globe (e.g., South Asia and Africa) rapid increase in population leads to expansion and intensification of agricultural lands to produce more food (Maxwell, 1996; Godfray et al., 2010; Wheeler et al., 2013; Meyfroidt et al., 2017; Thenkabail, 2018). In other locations (e.g. Europe and Central Asia), major political events (for example, breakdown of the Soviet Union or European Union integration) caused changes in support policies, which impacted agricultural land use and crop production (Hatna and Bakker, 2011; Baumann et al., 2011; Prishchepov et al., 2012; Griffiths et al., 2013). Knowledge on the area and spatial patterns of agriculture also support sustainable development initiatives as well as environmental resource planning and management (Smit et al., 1996; Fischer et al., 2005; Lambin et al., 2011; German et al., 2017; Hunter et al., 2017; Ramankutty et al., 2018). Moreover, information on cropland extent is needed to derive additional characteristics of agricultural areas including crop type, crop yield and cropping intensities (Xiong et al., 2017; Massey et al., 2018; Teluguntla et al., 2018, Gumma et al., 2019, Oliphant et al., 2019; Thenkabail et al., 2020). To this end, it is critical to study croplands over space and time for improved understanding of the agricultural land use change and its drivers. This study aims to generate one such cropland extent, covering large parts of Europe, Middle East, Russia, and Central Asia.

The study area (Figure 2.2.1) spans approximately a quarter of the Earth's ice-free terrestrial surface (FAO, 2019). Agricultural lands in this area have undergone major changes associated with environmental and socio-economic transformations of the recent and historical past (Csaki, 1990; Kuemmerle et al., 2007; Verburg et al., 2010; Prishchepove et al., 2012). There are numerous examples of agricultural abandonment (e.g., Eastern Europe) (Baumann et al., 2012; Griffiths et al., 2013; Gutman and Radeloff, 2016; Prishchepov et al., 2017), loss of production due to urbanization (e.g., Eastern Mediterranean) (Alphan, 2003; Bilgili et al., 2018), agricultural expansion (e.g., Central Asia) (Latruffe et al., 2010;-Kraemer et al., 2015; Dara et al., 2018), and degradation (e.g., Middle East) (Croiteru et al., 2010; Zdruli, 2014). Spatially explicit cropland information forms the basis to better understand such dynamics of agricultural land use change and its drivers in the study area.

Satellite remote sensing provides the ability to derive accurate and timely agricultural information (Moran et al., 1997; Steven and Clark, 2013; Thenkabail and Lyon, 2016). The wide range of spectral, spatial, and temporal characteristics of remotely sensed observations facilitate land use and land cover mapping involving agriculture at local to regional scales with various levels of uncertainty (Friedl et al., 2002; Herold et al., 2008; Schneider, 2012; Congalton et al., 2014, 2019). It is also becoming increasingly clear that medium resolution observations – defined as 10 – 100-meter spatial resolution such as those provided by Landsat and Sentinel-2 missions are critical in capturing agricultural areas dominated by small to medium sized farms (Wulder et al., 2003; Ozdogan and Woodcock, 2006; Griffiths et al., 2019). However, mapping croplands over large areas with medium resolution data remains challenging due to different agricultural and management practices, climate characteristics, satellite sensor issues, acquisition strategies, and data product continuity. Previous studies provide many examples of large-scale land use and land

cover mapping with low- to moderate-resolution observations in which croplands are presented as one category out of many (e.g., Friedl et al., 2002; Thenkabail et al., 2008, 2012; Ozdogan et al., 2008; Pittman at al., 2010; Portmann et al., 2010; Siebert et al., 2010; Bontemps et al., 2011; Gong et al., 2013). Some of these datasets combine agricultural inventory datasets with remote sensing observations (Ramanakutty and Foley, 1998, Frolking et al., 2002; See et al., 2015). Others use satellite data as a base layer for visual interpretation, such as the Coordination of Information on the Environment (CORINE) Programme Land Cover (CLC) dataset for 39 European countries (Buttner, 2014). Yet others use brute force approach to classify the entire globe into a few generalized categories such as the Finer Resolution Observation and Monitoring (FROM) of Global Land Cover project (Gong et al. 2013). These existing land cover maps tend to be less reliable and have certain drawbacks including: 1. the cultivated category is just one class in a number of land cover categories; 2. the accuracy of the cropland class varies from 60-80 % (Friedl et al., 2002; MaCallum et al., 2006; Bontemps et al., 2010); and 3. cultivated areas have high uncertainty because of different methods, different datasets used, different definitions of classes mapped, different time-periods across products development, and significant disagreement of calculated cropland areas with national statistics (Gong et al., 2013; Chen et al., 2015; Waldner et al., 2015, 2016). To overcome some of these challenges, our goal here is to generate an accurate and seamless cropland extent area map in Europe, Middle East, Russia and Central Asia using Landsat satellite data *circa* year 2015.

### 2.2.2 Study area

Study area covers roughly 3,300 Mha of land area spread across Europe, Middle East, Russia and Central Asia (Figure 2.2.1). The landscape is composed of highly diverse climatic, environmental, topographic, and cultural characteristics. It consists of temperate climate of

European landscapes to dry climates of Central Asia and Scottish Highlands, Ural Mountains in Europe to steppes in the Russia along with large deserts in Middle East and Central Asia. The agricultural landscape in Europe and Russia are characterized by medium sized farms (2 ha-25 ha) while small farms (<2ha) dominate in Central Asia and Middle East. Row crops interspersed with orchards are common in European landscapes while Middle East and Central Asia have most of the irrigated lands. Wheat is the major crop produced in the region covering the largest growing area (40 %) of the world (FAO, 2019). Additionally, major parts of the study area experienced large socio-economic transition associated with the breakdown of the Soviet Union and integration with the European Union with important consequences for land use and land cover changes in agricultural areas (Lyon, 1994; Mueller, 1973; Baumann et al., 2011; Palmer, 2016; Gutman and Radeloff, 2016; Hartwell, 2017; Prishchepov et al., 2017; Griffiths et al., 2019).

### 2.2.3 Methods

This study used a pixel-based Random Forest (RF) classification method to produce a cropland extent map with Landsat data by computing in the Google Earth Engine (GEE) platform (Gorelick et al., 2017). First, we stratified the entire study area into twelve agro-ecological zones or AEZs (Figure 2.2.1). In the next step, we collected and pre-processed Landsat satellite data to extract agriculturally relevant information and used VHRI as a "background" to visually interpret the class labels of samples. Then, we performed image classification using a RF machine learning algorithm, informed with high quality training samples followed by post processing using Kernel filter. RF model results tested for primary accuracy assessment using K-fold cross-validation procedure. Finally, we evaluated the cropland extent map for accuracy, performed by an independent team with validation data hidden from the production team, and compared with other cropland datasets (Figure 2.2.2).

#### 2.2.3.1 Definition of croplands

Clear definition of the cropland extent is necessary to set the distinction between cropland and non-cropland land use labels considered here. This study is part of the Global Food Security Analysis Data project at 30-m (GFSAD30) (www.cropland.org). The definition of croplands used here is "*lands cultivated with plants harvested for food, feed, and fiber, including both annual crops as well as continuous plantations (e.g., coffee, tea, rubber, cocoa, oil palms). Cropland fallows, defined as areas equipped for cultivation (including plantations) but are not cultivated for a season or two are included in the cropland category"* (Teluguntla et al., 2015; Thenkabail et al., 2020).

#### 2.2.3.2 Agro-ecological zoning

To facilitate the classification of Landsat data while considering region specific differences in agricultural practices and climatic conditions, we stratified the study area into 12 agro-ecoregions (Figure 2.2.1), using the UN FAO definitions, but modified (mostly merged) along the administrative boundaries (Fischer at al., 2012) to allow for national crop area estimates.

#### 2.2.3.3 Data

This study used Landsat surface reflectance (SR) data from two sensors (Landsat-8 OLI and Landsat-7 ETM+) acquired between 2014 and 2016 along with a topographic dataset from the Shuttle Radar Topographic Mission (SRTM) derived Digital Elevation Model (DEM) (http://www2.jpl.nasa.gov/srtm/), all within the GEE platform. The entire collection of Landsat data accounted to 160,000 individual images collected over 3,351 Landsat tiles (Table 2.2.1). The temporal distribution of cloud free images varied widely across the 12 agro-ecological zones. Each image in the collection were screened for cloud and cloud shadows using the image masks provided with the SR products.

To deal with inconsistent observations across the zones, we used seasonal composites along with temporal statistics that allowed us to produce single set of inputs, consisting of 56 bands to be presented to the RF classifier across all zones (Table 2.2.2). Note that, the representative value of each reference sample input feature was based on the average value of all the pixels in respective sampling unit. The selection of these features was based on extensive testing with several different spectral band combinations as well as vegetation and water indices and their impact on accuracy on the cropland category. The main satellite-based indices from these selected 56 bands are the bimonthly composites of the Normalized Difference Vegetation Index (NDVI) and the Normalized Difference Water Index (NDWI), mainly due to its capability to capture the vegetation and water related characteristics of the landscape. These indices were calculated using the following well known formulas:

$$\mathrm{NDVI} = \frac{\mathrm{NIR} - \mathrm{RED}}{\mathrm{NIR} + \mathrm{RED}} \quad (1)$$

$$\mathrm{NDWI} = \frac{\mathrm{NIR} - \mathrm{SWIR}}{\mathrm{NIR} + \mathrm{SWIR}} \quad (2)$$

Where, NIR, RED and SWIR represents Landsat near infrared, red and short-wave infrared bands, respectively. Entire processing was conducted in GEE using image collections and reducers as well as on-the-fly polygon drawing capabilities over the background of sub-meter to 5-m very high spatial-resolution satellite imagery to augment the reference samples as needed.

In the next step, reference data were collected and labeled with cropland and non-cropland category using background of Google Earth VHRI and ancillary information from expert judgment within a double-blind approach. Each reference sample used a sampling unit composed of 3 × 3 pixel. These samples were selected using a random sampling design in each zone. We augmented the reference data using ancillary data from sources such as the Land Use and Coverage Area

Frame Survey (LUCAS) (**http://ec.europa.eu/eurostat/web/lucas)** by Eurostat. In total, over 64,000 reference samples (~32,500 croplands and ~31,000 non-croplands) were collected for training the RF classifier (Table 2.2.3). Note that roughly 20% of the reference data were set aside and used in test mode to evaluate the importance of input features and parameter settings for the RF algorithm.

#### 2.2.3.4 Supervised classification using Random Forest

It is becoming increasingly clear that machine learning algorithms provide superior outcomes over traditional classifiers based on a number of land use and land cover mapping studies (Friedl et al., 2002; Adam et al., 2014; Li et al., 2014; Xiong et al., 2017; Akilan et al., 2018; Massey et al., 2018; Phalke and Ozdogan, 2018). In general, machine learning algorithms have been shown to perform better for large datasets with substantial noise compared to traditional parametric classifiers like maximum likelihood (Pelletier, 2016).

We used the pixel-based supervised Random Forest (RF) algorithm for classifying cultivated areas, based on successful results from prior research as part of the same project but applied to different continents (Xiong et al., 2017; Phalke and Ozdogan, 2018; Teluguntla et al., 2018; Oliphant et al., 2019 and, Gumma et al., 2019) and also comparing three commonly used machine learning algorithms such as RF, support vector machines (SVM) and Classification & Regression Tress (CART) on selected five sample agroecological zones from the study area with similar input features (Table A.2.2.3). The results of this machine learning algorithms comparison test concluded that the RF method not only outperform the other classifiers for the binary classification problem at hand, but it also has the best computing performance with little or no parameter setting requirements (Table A.2.2.3). Similar observations were made in other recent studies involving land cover classification problems (Pellletier et al., 2016; Fu et al., 2016; Massey

et al., 2018). For this study, we selected 100 trees per node by internal testing (Figure A.2.2.1). This study leveraged GEE implementation of the RF algorithm to scale both the training and the prediction phases to classify agricultural lands in the study area. Finally, we used three measures to define variable importance: a) mean decrease in accuracy due to removal of a variable from set of inputs, b) mean decrease in Gini coefficient (Dorfaman,1979)– a measure of how each variable contributes to the homogeneity of the nodes, used for calculation of splits during training; and c) discrimination power of each variable through boxplots.

#### 2.2.3.5 Accuracy assessment

To perform the accuracy assessment, we focused on three key elements: 1) method of sampling; 2) selection of number of samples; and 3) sampling unit (Yadav and Congalton, 2018). The production of high-quality validation samples were carried out by visual interpretation of class labels using the background of sub-meter to 5-m very high-resolution imagery (VHRI) from the US National Geospatial Agency (NGA). It is noted that VHRI is not used in classification as input but only used as a "background" to label the class. The accuracy assessment was performed individually for each of the twelve zones as well as for the overall study area. The accuracy assessment team had the stratified (across zones), random (within zones), and balanced (across cropland area distribution) set of 3,000 samples (250 samples per zone), and these samples were hidden from the production team through the entire process (Yadav and Congalton, 2018). The samples characteristics are called stratified, random, and balanced – because i) each zone has 250 testing samples collected – called as stratified across zones; ii) all the 250 samples were randomly distributed inside or within the zone – thus called as random within zones; and iii) the number of croplands and non-croplands samples were selected according to the areal distribution ratio of reference cropland area dataset. For example, if zone 1 has 70% cropland area and 30%

noncroplands area according to reference sources, the samples were collected distributed accordingly. Further, we used a sampling unit composed of 3 × 3 pixels to minimize adverse impact from positional inaccuracy. The heterogeneous samples with mixed cropland and non-cropland classes were removed from the selection. The selection of balanced samples was proportional to cropland and non-cropland areas in each zone. The measures of accuracies included: producer's accuracy (PA) or errors of omission, user's accuracy (UA) or errors of commission, and overall accuracy (OA) for croplands and non-croplands (Story and Congalton, 1986; Olofsson et al, 2014; Congalton, 2014) as:

$$OA = Sd \times 100\% \ (1)\ n \quad \textbf{(3)}$$

$$UA = Xij \times 100\% \ (2)\ Xj \quad \textbf{(4)}$$

$$PA = Xij \times 100\% \ (3)\ Xi \quad \textbf{(5)}$$

where *Sd* is the total number of correctly classified pixels, *n* = total number of validation pixels, *Xij* = observation in row *i* column *j*; *Xi* = marginal total of row *i*; *Xj* = marginal total of column *j*.

**2.2.3.6 Country-wide areal statistics comparison**

We compared cropland area estimates from this Landsat-derived 30-m product with estimates from other sources including the FAO (FAO, 2015) as well as other remote sensing-based datasets at the country level. These datasets were: 1) Monthly irrigated and rain-fed crop areas for 2014 (MIRCA2014) (Portman et al., 2010); 2) global croplands derived from Global Irrigated Area Mapping (GIAM) (Thenkabail et al., 2008, 2009, 2011 and Biradar et al., 2009); 3) Global Map of Rainfed Cropland Areas (GMRCA) (Thenkabail et al., 2009, 2011 and Biradar et al., 2009); 4) Global rain-fed, irrigated, and paddy croplands (GRIPC) (Salmon et al., 2015); 5)

Global Land Cover for circa 2010 (GLC30) (Chen et al., 2015); and 6) CORINE Land cover ca 2012 by the European Commission (Buttner et al., 2014) (Table 2.2.4).

#### 2.2.3.7 Map-to-map comparison

Map to map comparisons provide a degree of similarity between two or more maps. To perform such comparison, we extracted 1,500 samples from each zone and compared our map with other remote sensing-based land cover products that contain a cropland category using a confusion matrix setup, which we refer to as *similarity matrix* because of the predicted nature of maps being compared. The other remote-sensing based map products were: 1) the global land cover (GLC30) circa 2010 (www.globallandcover.com) (Chen et al., 2015); 2) regional cropland products for Europe as part of the CORINE land cover dataset at 100m resolution (https://www.eea.europa.eu/data-and-maps/data/clc-2012-raster) (Buttner, 2014); 3) a regional land cover product for Central Asia (Klein et al., 2012) at 250m resolution; and 4) a local crop type map product for the Fergana Valley in Central Asia at 30-m (Biradar et al., 2016) (Table 2.2.4). Note that some of these products did not necessarily match the crop definition used here, had various spatial resolutions, were developed for different target years, and a wide range of methods were used in their development. To account for these differences, we had to spatially resample our map product at times and only consider those that were close in time as well as definition in the comparison.

### 2.2.4 Results

#### 2.2.4.1 Variable importance

The first set of results concerns the variable importance as revealed by the RF classifier. Results show that across all AEZs the *NDVI Range* and topographic *slope* features have the higher mean decrease in accuracy (40 and 25 respectively) and the higher mean decrease Gini coefficient

values (380 and 400 respectively) while the *Blue* and *SWIR1* surface reflectance quantities showed lower mean decrease in accuracy values and Gini coefficient values (Figure 2.2.3). Further, *NDVI* and *NDWI* showed higher discrimination (0.3 and 0.4 respectively) between classes across all zones, whereas *Blue* surface reflectance showed lower discrimination (0.001) (Figure 2.2.3). It is observed that there were noticeable outliers in the sampling data (Figure 2.2.3a). The reason behind the noticeable outliers is the data impurities from a few band values and the mixing of crop and non-crop related feature characteristics. This was one of the challenges in developing the croplands classification model. In a few cases, we replaced or removed samples to avoid the outliers and it took several iterations of the model. Data preprocessing incorporated this.

#### 2.2.4.2 Classification results

The result of this study is a new cropland extent map of Europe, Middle East, Russia and Central Asia at 30-m (Figure 2.2.4). Visual assessment of the current cropland product reveals cultivated areas are correctly captured across a variety of agricultural landscapes extending from flat cropland areas in Central Europe to desert areas in the Middle East and Central Asia (Figure 2.2.4). Moreover, clear distinction between the agroforestry and agricultural lands in Spain and parts of Scandinavia are clearly made (Figure 2.2.4b), an issue commonly identified in other medium resolution land cover maps (Chen et al., 2015). Difficult to map dryland agriculture in Northern Syria and Iraq were successfully identified (Figure 2.2.4b) while irrigated croplands in Saudi Arabia deserts, date plantations in Oman, and rainfed agriculture in Syria and Kazakhstan were mapped as expected (Figure 2.2.4b). Extensive wheat cultivated areas in southwest Russia were also mapped correctly (Figure 2.2.4b, left panel 2).

Net cropland area of the entire study region is calculated at 546 Mha (17.8% of the net land area) with a range of distribution across the 12 zones. Zones 3, 4 and 10 cover large area (14.4%,

16.5 % and 17.2 % respectively) and zone 1,5,7,9 and 12 cover very low area (3.5 %, 1.2 %, 1 %, 2.4 % and 0.02 % respectively).

#### 2.2.4.3 Independent accuracy assessment

The results of the accuracy assessment showed that the overall accuracy of the entire study area cropland extent map was 93.8 % with various levels of user's (a measure of commission error) and producer's (a measure of omission error) accuracies as provided in Table 2.2.5. Map accuracy also varies by zone, having the highest overall accuracy (99.8%) in zone 12 (Northeast Russia where only 0.02% croplands exist) and the lowest overall accuracy (76.1%) in zone 10 (western Russia with roughly 17% croplands) (Table 5). Ninety-two percent of croplands of the entire study area were concentrated in just seven zones (zones 2 to 4, 6, 8, 10 and 11). Zone 10 had the lowest accuracy primarily because high cloud cover and very less frequency of satellite observation. It has overall accuracies of 76.1% with user's cropland accuracy 75.2% and producer's cropland accuracy 80.9%. The highest producer's cropland accuracies were observed in zone 1(92.3%) and zone 8 (90.1%) with 3.5% and 13.2% respectively of net croplands of the entire study area. The highest user's cropland accuracies were observed in zone 4 (93%) and zone 7 (100%) with percent of croplands equal to 16.5% and 1%, respectively of net cropland areas of the entire study area. For the entire Landsat-derived 30-m product the overall accuracy was 93.8% with cropland class providing producer's accuracy of 86.5% (errors of omission = 13.5%) and user's accuracy of 85.7% (errors of commission = 14.3%).

#### 2.2.4.4 Comparison of cropland areas

The net cropland area for Europe, Middle East, Russia and Central Asia were estimated at 546 Mha or 17.5 % of the land area of the entire study area. This estimate is in line with other remote sensing-based estimates, although major differences exist (Table 2.2.6a and 2.2.6b). The

comparison of national cropland areas derived in this study with those reported from the FAO (2014) and MIRCA2014 (which is derived from the FAO figures) for 64 countries showed a high degree of correlation (Figure 2.2.5). At the same time, our study found 10 to 30% more cropland areas when compared to reported estimates from the FAO (Figure 2.2.5). Same is true when national cropland area estimates are compared to those derived from other land cover datasets (Figure 2.2.5). Of the products, the best relationships were: 1. GLC30 with an intercept of 0.987 and R-square value of 0.93 (Figure 2.2.5c) and 2. CORINE with an intercept of 0.90 and R-square value of 0.97 (Figure 2.2.5d). This is expected given GLC30 is a 30m land cover product compared to this (GFSAD30) 30m cropland product. The variability in area estimates between GFSAD30 versus GLC30, the two 30m products, are minimal with near 1:1 line fit (Figure 2.2.5c). CORINE 100m is developed by European countries with extensive use of remote sensing, national statistics, and field collected reference data. The variability in area estimates between GFSAD30 versus CORINE, the 30m and 100m products, shows slightly higher cropland estimates of GFSAD30. Compared to the two statistical products (FAO in Figure 2.2.5a and MIRCA in Figure 2.2.5b), the GFSAD30 consistently over-estimates cropland areas by 10-30%. This is on expected lines, given the consistent under-reporting of cropland areas by countries as established in other remote sensing studies (Thenkabail et al., 2011, 2012). So, we see a slope of only 0.66 between GFSAD30 versus FAO (Figure 2.2.5a) and GFSAD30 versus MIRCA (Figure 2.2.5b) even though R-square values were high with 0.95 for FAO (Figure 2.2.5a) and 0.94 for MIRCA (Figure 2.2.5b). The highest variability in cropland areas between GFSAD30 was with: (1) GIAM and GMRCA (Figure 2.2.5e), and (2) GRIPC (Figure 2.2.5f). This is mainly because GMRCA and GRIPC are mapped using 1 to 10-km data. In addition, those products were for nominal year 2000 and 2005 when compared to this product (GFSAD30) mapped for nominal year 2015.

#### 2.2.4.5 Map-to-map comparison results

Comparison of the cropland map derived in this study with the cropland label of the GLC30 map suggests overall similarity of 88.8% (Kappa 0.7) across the entire study area with producer's cropland similarity as 89.2% (errors of omissions = 10.8%) and user's cropland similarity 81.8% (errors of commissions = 8.1%) (Figure 2.2.6). The highest similarity was observed in zone 5 (northern Europe) at 98.3% with Kappa 0.9, whereas lowest similarity was observed in zone 2 (Portugal and Spain) at 83.2% (Figure 2.2.6). A closer look at both maps reveals that our cropland extent maps were successful in capturing the missing croplands in GLC30 product around significantly irrigated agricultural areas in Germany and Belgium and rainfed agriculture in Italy (Figure 2.2.6b).

Comparison of our results to the CORINE land cover map in Europe showed that the overall similarity was 87.3% (Kappa 0.8) with producer's cropland similarity as 93.3% (errors of omissions = 6.7%) and user's cropland similarity 78.6% (errors of commissions = 21.4%) (Figure 2.2.7a). The highest similarity was 97.7% observed in zone 5 (northern Europe) while lowest similarity was observed in zone 2 (Portugal and Spain) at 81.4%. The reason behind this dissimilarity is lack of representation of dry agricultural areas in Spain in the CORINE map, which are accurately captured in the GFSAD30 product (Figure 2.2.7b upper panel).

The regional croplands of Central Asia from this study and from Klein et al. (2012) (at 250 m) also showed a high degree of similarity at 87.4 (kappa 0.7) with producer's cropland similarity as 91.3% (errors of omissions = 8.7%) and user's cropland similarity 80.9% (errors of commissions = 19.1%) (Figure 2.2.8a). While this was not explicitly tested, the difference in similarity here can be attributed to the different year of the development of the compared map in question (Klein et al. map is from 2012).

Comparison to a local cropland map in Fergana Valley in Central Asia at 30m (Biradar et al., 2016) also shows a high similarity at 93.2% (Kappa 0.7) with producer's cropland similarity as 90.6% (errors of omissions = 9.4%) and user's cropland similarity 77.6% (errors of commissions = 22.4%). Visual assessment further confirms the close spatial distribution of croplands in both maps, primarily aided by close similarities in cropland definition, spatial resolution, and target year (Figure 2.2.8b).

### 2.2.5 Discussion

This study produced a wall-to-wall cropland extent map at 30-m spatial resolution for 64 countries in Europe, Middle East, Russia, and Central Asia using time-series Landsat data for the nominal year 2015 and the RF algorithm implemented in Google Earth Engine (Figure 2.2.1). The net cropland areas for the nominal year 2015 derived from this map was 546 Mha, covering 17.8% of the net land area in the study and nearly 30% of the 1.873 billion hectares of the net global cropland areas of the world (Thenkabail et al., 2020). The cropland extent map is highly accurate with a weighted overall accuracy of 93.8%. The discrepancies in the cropland areas between this study and other sources can mainly attributed to: 1. the year of production of the datasets; 2. the differences in cultivated class definitions; 3. the method of development; 4. type of data used; and 5. the purpose of classification or map. The key innovations in this study are: 1) first attempt to produce highly accurate and precise 30-m map with special focus on the croplands in a very large study area with twelve agroecological zones using Landsat satellite data; 2) successful demonstration of the methodological capability to process large area croplands with unique features through homogenization of remotely sensed time series observations while incorporating topographic and agro-climatic characteristics using Random Forest machine learning algorithm and the Google Earth Engine platform and, 3) the independent and careful scientific accuracy

assessment and validation of the resulting map while comparing it with six other global as well as regional remote sensing based croplands data resources. We highlight these contributions and the current need for producing open-source large area croplands mapping data and algorithms at the beginning of our manuscript to clearly emphasize the importance of our work. We believe that the cropland mapping product presented in this study have the potential to provide valuable contributions for global food and water security analysis and land cover change monitoring.

Further, comparison of GFSAD30 to other products allowed us to understand both its benefits as well as its limitations. For example, the GFSAD30 map accurately captures the occasionally missing croplands from products such as CORINE and GLC30. For example, in Iraq, although most of the land is a desert, our study shows that croplands in Iraq are about 12% of the total land area whereas, GLC30 shows 10% and FAO shows 8%. We have a little overestimation compared to other two products, partly because of the difference in cropland definition we use, different year of mapping and mainly due to capturing of dryland area with better precision than other products (as shown in Figure 2.2.4b). At the same time, our focus on reduced omission errors from the onset might have produced a map with excessive commission errors in certain locations. One example of this is in Kazakhstan where some grassland areas were mapped as croplands (Figure 2.2.4b). Our approach balances omission and commissions errors to a minimum. Thereby, the final product had a producer's accuracy of 86.5% (errors of omissions = 13.5%) and user's accuracy of 85.7% (errors of commissions = 14.3%).

We also note that the accuracy and the level of omission/commission errors of the current map is highly dependent on Landsat data availability (primarily due to clouds). While the use of seasonal composites partly addressed this issue, it is nevertheless present, especially in areas known to have high cloud cover (e.g., the UK, Northern Europe, and parts of Russia). This issue

can certainly be resolved with more observations, for example by adding Sentinel 2 observations into the classification process.

Large area classifications usually suffer from lack of high-quality reference training and testing data. In this study we addressed this problem by generating a very large sample of high-quality training data, as well as through classifying based on agroecological zones (AEZs) and using secondary data such as the SRTM derived elevation and slope. This approach is resource intensive in terms of need for high quality reference training and validation data. However, recently efforts in gathering global reference (training and validation) data through machine learning hubs (e.g., https://www.mlhub.earth/, https://croplands.org/app/data/search) and spectral-signature data banks (https://lpdaac.usgs.gov/products/ghisaconusv001/) of agricultural crops, especially through ground data mobile apps (https://www.croplands.org/mobile), is expected to help continuity of this approach in the future. This type of study targeting large areas could potentially benefit from the ideas of generalization or signature extension (Phalke and Ozdogan, 2018). Moreover, we note that the RF algorithm was sensitive to the number and distribution of training samples. In particular, it was more important have a balanced number of samples covering diverse manifestation of the other (non-cropland) categories as well as different types of cropping practices than a large number of samples with narrow class representations. The greatest difficulties in cropland mapping in the study area were in separating grasslands from croplands, in desert margins (e.g., Iraq, Kazakhstan where rainfed agriculture is limited to a very short season when anything will grow), cropland fallows (e.g., whether a fallow is 1 year or 5-year or permanent), and intensive agroforestry practices in the Mediterranean. In such cases, greater number of interactions of RF runs by tweaking the knowledge base for the algorithm is required to keep the errors of omissions and commissions to a minimum possible.

While it may appear excessive, our evaluation of many different forms of inputs suggested that the 56 features used here were necessary to balance accuracy against the need for changing input feature space across all zones: the 56 inputs performed better across all regions compared to other combinations. An additional benefit of this set of inputs is that they are scalable and can be implemented easily in GEE for any given study area with appropriate change in reference training and validation data of the region of study. We note that the methods presented here can be replicated for any other year or study location and can be automated to rapidly produce cropland maps in future studies.

Lastly, monitoring croplands in the study region was very challenging not only because of the diversity in agricultural practices across the region but also because of crop dynamics, driven by environmental as well as socio-economic heterogeneity. The cropland information presented here will be of vital importance to understand the environmental, climatic, land use change, and policy implications in the study area.

### 2.2.6 Conclusions

This study produced the first cropland extent map at 30-m using Landsat-7 and Landsat-8 data for the nominal year 2015 over 64 countries of Europe, Middle East, Russia and Central Asia. The study demonstrated the power of agricultural cropland mapping over very large areas using high-resolution 30m satellite-sensor big-data processing using the pixel-based Random Forest (RF) machine learning algorithms on the Google Earth Engine (GEE). The study developed a unique approach involving RF machine learning algorithm, a set of 56 input bands derived from seasonal composites of remotely sensed observations, topographic variables, 63,403 reference training samples, 3000 reference validation samples across 12 agro-ecological zones to produce cropland versus non-cropland maps. The independent accuracy assessment showed the overall

accuracy of the final map was 93.8 % with cropland class providing producer's accuracy of 86.5% (errors of omissions = 13.5%) and user's accuracy of 85.7% (errors of commissions = 14.3%). The cropland map established that study area has a total 546 Mha net cultivated area, which is 17.8% net land area of the study region and nearly 30% of all global croplands. The current map shows that vast flat topographic areas of Central, East, and West Europe, irrigated zones in Central Asia and the Middle East, and highly productive soils of southwest Russia contain the highest concentrations of croplands. In contrast, Northern Europe, large parts of the Middle East and Far East Russia have a very little agriculture. Nevertheless, the high-resolution nature of the GFSAD30 map allowed us to capture narrow concentrations of cultivated areas even in these locations. The classification approach used in this study can be replicated to map net croplands for other years in the same study areas as well as in any other region and time given the inputs, especial considering the computing power and ever-growing archive of satellite observation available in GEE. The results presented here are crucial for the societal use and scientific community especially in studies related to agriculture, water, food security, land use and land cover change, climate change, environmental monitoring, and policy development. The cropland extent map of Europe, Middle East, Russia and Central Asia is available to download through NASA's Land Processes Distributed Active Archive Center (LP DAAC) at https://doi.org/10.5067/MEaSUREs/GFSAD/GFSAD30EUCEARUMECE.001 and data visualization and information available at global croplands website: https://croplands.org. Also, the training datasets as well as the GEE code used for classification can be downloaded from the global croplands website: https://code.earthengine.google.com/1666e8bed34e0ce2b2aaf1235ad8c6bd.

### 2.2.7 Acknowledgments

The study was funded by the National Aeronautics and Space Administration (NASA) grant number: NNH13AV82I through its MEaSUREs (Making Earth System Data Records for Use in Research Environments) initiative. The United States Geological Survey (USGS) provided supplemental funding from other direct and indirect means through the Climate and Land Use Change Mission Area, including the Land Change Science (LCS) and Land Remote Sensing (LRS) programs. The project was led by United States Geological Survey (USGS) in collaboration with NASA AMES, University of New Hampshire (UNH), California State University Monterey Bay (CSUMB), University of Wisconsin (UW), NASA GSFC, and Northern Arizona University. There were a number of international partners including the International Crops Research Institute for the Semi-Arid Tropics (ICRISAT). Also, we want to acknowledge Dr. Chandrashekhar Biradar from the International Center for Agricultural Research in the Dry Areas (ICARDA) and Dr. Igor Klein from the German Aerospace Center (DLR), German Remote Sensing Data Center for sharing the cropland related data. This research is also a part of **Global Food Security Analysis Data Project (GFSAD30)** for Europe, Middle East, Russia, and Central Asia. Any use of trade, firm, or product names is for descriptive purposes only and does not imply endorsement by the U.S. Government.

**References**

Adam, E., Mutanga, O., Odindi, J., & Abdel-Rahman, E. M. (2014). Land-use/cover classification in a heterogeneous coastal landscape using RapidEye imagery: evaluating the performance of random forest and support vector machines classifiers. *International Journal of Remote Sensing*, *35*(10), 3440-3458.

Akilan, T., Wu, Q. J., & Zhang, H. (2018). Effect of fusing features from multiple DCNN architectures in image classification. *IET Image Processing*, *12*(7), 1102-1110.

Alexander, P., Rounsevell, M. D., Dislich, C., Dodson, J. R., Engström, K., & Moran, D. (2015). Drivers for global agricultural land use change: The nexus of diet, population, yield and bioenergy. *Global Environmental Change*, *35*, 138-147.

Baumann, M., Kuemmerle, T., Elbakidze, M., Ozdogan, M., Radeloff, V. C., Keuler, N. S., & Hostert, P. (2011). Patterns and drivers of post-socialist farmland abandonment in Western Ukraine. *Land use policy*, *28*(3), 552-562.

Biradar, C. (2015). Crop type map of Fergana valley Central Asia for the year 2011.

Bontemps, S., Defourny, P., Van Bogaert, E., Arino, O., & Kalogirou, V. (2010). GlobCover 2009: product description manual, version 1.0. *ESA and UCLouvain) Available at http://dup. esrin. esa. it/files/p68/GLOBCOVER2009_Product_Description_Manual_1. 0. pdf [Verified July 2012]*.

Bontemps, S., Defourny, P., Van Bogaert, E., Arino, O., Kalogirou, V., & Perez, J. R. (2011). GLOBCOVER 2009 Products description and validation report. *URL: http://ionia1. esrin. esa. int/docs/GLOBCOVER2009_Validation_Report_2*, *2*.

Büttner, G. (2014). CORINE land cover and land cover change products. In *Land use and land cover mapping in Europe* (pp. 55-74). Springer Netherlands.

Cardille, J. A., & Foley, J. A. (2003). Agricultural land-use change in Brazilian Amazonia between 1980 and 1995: Evidence from integrated satellite and census data. *Remote Sensing of Environment*, *87*(4), 551-562.

Chen, J., Chen, J., Liao, A., Cao, X., Chen, L., Chen, X., & Zhang, W. (2015). Global land cover mapping at 30m resolution: A POK-based operational approach. *ISPRS Journal of Photogrammetry and Remote Sensing*, *103*, 7-27.

Congalton, R. G., Gu, J., Yadav, K., Thenkabail, P., & Ozdogan, M. (2014). Global land cover mapping: A review and uncertainty analysis. *Remote Sensing*, *6*(12), 12070-12093.

Congalton, R. and K. Green. 2019. *Assessing the accuracy of remotely sensed data: principles and practices. 3rd edition*. CRC/Taylor & Francis, Boca Raton, FL. 328p.

Dorfman, R. (1979). A formula for the Gini coefficient. *The Review of Economics and Statistics*, 146-149.

Fischer, G., Nachtergaele, F. O., Prieler, S., Teixeira, E., Tóth, G., Van Velthuizen, H., & Wiberg, D. (2012). Global Agro-ecological Zones (GAEZ v3. 0)-Model Documentation.

Fischer, G., Shah, M., Tubiello, F. N., & Van Velhuizen, H. (2005). Socio-economic and climate change impacts on agriculture: an integrated assessment, 1990–2080. *Philosophical Transactions of the Royal Society of London B: Biological Sciences*, *360*(1463), 2067-2083.

Food and Agricultural Organization (FAO). (2019). Europe and Central Asia food and agriculture. *Food and Agriculture Organization of the United Nations Regional Office for Europe and Central Asia Budapest, E-ISBN*, 978-92.

Friedl, M. A., McIver, D. K., Hodges, J. C., Zhang, X. Y., Muchoney, D., Strahler, A. H., & Baccini, A. (2002). Global land cover mapping from MODIS: algorithms and early results. *Remote Sensing of Environment*, *83*(1), 287-302.

Frolking, S., Qiu, J., Boles, S., Xiao, X., Liu, J., Zhuang, Y., & Qin, X. (2002). Combining remote sensing and ground census data to develop new maps of the distribution of rice agriculture in China. *Global Biogeochemical Cycles*, *16*(4).

Fu, P., & Weng, Q. (2016). A time series analysis of urbanization induced land use and land cover change and its impact on land surface temperature with Landsat imagery. *Remote Sensing of Environment*, *175*, 205-214.

German, R. N., Thompson, C. E., & Benton, T. G. (2017). Relationships among multiple aspects of agriculture's environmental impact and productivity: a meta-analysis to guide sustainable agriculture. *Biological Reviews*, *92*(2), 716-738.

Global Cropland Extent Map at 30m (GCEM30) derived using Landsat Satellite Time-series Data for the Year 2015 using Multiple Machine Learning Algorithms on the Google Earth Engine (GEE) Cloud. Research Paper #, United States Geological Survey (USGS). Upcoming.

Godfray, H. C. J., Beddington, J. R., Crute, I. R., Haddad, L., Lawrence, D., Muir, J. F., & Toulmin, C. (2010). Food security: the challenge of feeding 9 billion people. *Science*, *327*(5967), 812-818.

Gomes, E., Abrantes, P., Banos, A., Rocha, J., & Buxton, M. (2019). Farming under urban pressure: Farmers' land use and land cover change intentions. *Applied Geography*, *102*, 58-70.

Gong, P., Wang, J., Yu, L., Zhao, Y., Zhao, Y., Liang, L., & Li, C. (2013). Finer resolution observation and monitoring of global land cover: first mapping results with Landsat TM and ETM+ data. *International Journal of Remote Sensing*, *34*(7), 2607-2654.

Gorelick, N., Hancher, M., Dixon, M., Ilyushchenko, S., Thau, D., & Moore, R. (2017). Google Earth Engine: Planetary-scale geospatial analysis for everyone. *Remote Sensing of Environment*, *202*, 18-27.

Griffiths, P., Müller, D., Kuemmerle, T., & Hostert, P. (2013). Agricultural land change in the Carpathian ecoregion after the breakdown of socialism and expansion of the European Union. *Environmental Research Letters*, *8*(4), 045024.

Griffiths, P., Nendel, C., & Hostert, P. (2019). Intra-annual reflectance composites from Sentinel-2 and Landsat for national-scale crop and land cover mapping. *Remote Sensing of Environment*, *220*, 135-151.

Gumma, M.K., Thenkabail, P.S., Teluguntla, P., Oliphant, A., Xiong, J., Giri, C., Pyla, V., Dixit, S., Whitbread, A.M. (2019). Agricultural cropland extent and areas of South Asia derived using Landsat satellite 30-m time-series big-data using random forest machine learning algorithms on the Google Earth Engine cloud. *GIScience and Remote Sensing*, ISSN: 1548-1603 (Print) 1943-7226. https://doi.org/10.1080/15481603.2019.1690780**.**

Gutman, G., & Radeloff, V. (Eds.). (2016). *Land-cover and land-use changes in Eastern Europe after the collapse of the Soviet Union in 1991*. Springer.

Hatna, E., & Bakker, M. M. (2011). Abandonment and expansion of arable land in Europe. *Ecosystems*, *14*(5), 720-731.

Herold, M., P. Mayaux, C. E. Woodcock, A. Baccini, and C. Schmullius. "Some challenges in global land cover mapping: An assessment of agreement and accuracy in existing 1 km datasets." *Remote Sensing of Environment* 112, no. 5 (2008): 2538-2556.

Hunter, M. C., Smith, R. G., Schipanski, M. E., Atwood, L. W., & Mortensen, D. A. (2017). Agriculture in 2050: Recalibrating Targets for Sustainable Intensification. *BioScience*, *67*(4), 386-391.

Klein, I., Gessner, U., & Kuenzer, C. (2012). Regional land cover mapping and change detection in Central Asia using MODIS time-series. *Applied Geography*, *35*(1), 219-234.

Kuemmerle, T., Hostert, P., Radeloff, V. C., Perzanowski, K., & Kruhlov, I. (2007). Post-socialist forest disturbance in the Carpathian border region of Poland, Slovakia, and Ukraine. *Ecological Applications*, *17*(5), 1279-1295.

Lambin, E. F., & Meyfroidt, P. (2011). Global land use change, economic globalization, and the looming land scarcity. *Proceedings of the National Academy of Sciences*, *108*(9), 3465-3472.

Lambin, E. F., Geist, H. J., & Lepers, E. (2003). Dynamics of land-use and land-cover change in tropical regions. *Annual Review of Environment and Resources*, *28*(1), 205-241.

Latruffe, L., Davidova, S., Douarin, E., & Gorton, M. (2010). Farm expansion in Lithuania after accession to the EU: The role of CAP payments in alleviating potential credit constraints. *Europe-Asia Studies*, *62*(2), 351-365.

Li, C., Wang, J., Wang, L., Hu, L. and Gong, P., 2014. Comparison of classification algorithms and training sample sizes in urban land classification with Landsat thematic mapper imagery. *Remote Sensing*, *6*(2), 964-983.

Massey, R., Sankey, T. T., Yadav, K., Congalton, R. G., & Tilton, J. C. (2018). Integrating cloud-based workflows in continental-scale cropland extent classification. *Remote Sensing of Environment*, *219*, 162-179.

Maxwell, S. (1996). Food security: a post-modern perspective. *Food Policy*, *21*(2), 155-170.

Meyer, W. B., & Turner, B. L. (1992). Human population growth and global land-use/cover change. *Annual Review of Ecology and Systematics*, *23*(1), 39-61.

Meyfroidt, P. (2017). Trade-offs between environment and livelihoods: Bridging the global land use and food security discussions. *Global Food Security*, *16*, 9-16.

Moran, M. S., Inoue, Y., & Barnes, E. M. (1997). Opportunities and limitations for image-based remote sensing in precision crop management. *Remote Sensing of Environment*, *61*(3), 319-346.

Mueller, J. E. (1973). *War, presidents, and public opinion*. John Wiley & Sons.

Oliphant, A., Thenkabail, P.S., Teluguntla, P., Xiong, J., Gumma, M.K., Congalton, R., and Yadav, K. (2019). Mapping cropland extent of Southeast and Northeast Asia using multi-year time-series Landsat 30-m data using random forest classifier on Google Earth Engine. *International Journal of Applied Earth Observation and Geoinformation*. Vol. 81: 110-124. https://doi.org/10.1016/j.jag.2018.11.014

Olofsson, P., Foody, G. M., Herold, M., Stehman, S. V., Woodcock, C. E., & Wulder, M. A. (2014). Good practices for estimating area and assessing accuracy of land change. *Remote Sensing of Environment*, *148*, 42-57.

Özdoğan, M., & Woodcock, C. E. (2006). Resolution dependent errors in remote sensing of cultivated areas. *Remote Sensing of Environment*, *103*(2), 203-217.

Özdoğan, M., & Gutman, G. (2008). A new methodology to map irrigated areas using multi-temporal MODIS and ancillary data: An application example in the continental US. *Remote Sensing of Environment*, *112*(9), 3520-3537.

Palmer, R. R. (2016). *The world of the French Revolution*. Routledge.

Pelletier, C., Valero, S., Inglada, J., Champion, N., & Dedieu, G. (2016). Assessing the robustness of Random Forests to map land cover with high resolution satellite image time series over large areas. *Remote Sensing of Environment*, *187*, 156-168.

Phalke, A. R., & Özdoğan, M. (2018). Large area cropland extent mapping with Landsat data and a generalized classifier. *Remote Sensing of Environment*, *219*, 180-195.

Phalke, A., Özdoğan, M., Thenkabail, S., P., G., Congalton, R., Yadav, K., Massey, R., Teluguntla, P., Poehnelt, J., Smith, C. (2017). NASA Making Earth System Data Records for Use in Research Environments (MEaSUREs) Global Food Security-support Analysis Data (GFSAD) Cropland Extent 2015 Europe, Central Asia, Russia, Middle East 30 m V001 [Data set]. NASA

EOSDIS Land Processes DAAC. Accessed 2019-12-04 from https://doi.org/10.5067/MEaSUREs/GFSAD/GFSAD30EUCEARUMECE.001

Pittman, K., Hansen, M. C., Becker-Reshef, I., Potapov, P. V., & Justice, C. O. (2010). Estimating global cropland extent with multi-year MODIS data. *Remote Sensing*, *2*(7), 1844-1863.

Portmann, F. T., Siebert, S., & Döll, P. (2010). MIRCA2000—Global monthly irrigated and rainfed crop areas around the year 2000: A new high-resolution data set for agricultural and hydrological modeling. *Global Biogeochemical Cycles*, *24*(1).

Prishchepov, A. V., Müller, D., Baumann, M., Kuemmerle, T., Alcantara, C., & Radeloff, V. C. (2017). Underlying drivers and spatial determinants of post-Soviet agricultural land abandonment in temperate Eastern Europe. In *Land-cover and Land-use changes in Eastern Europe after the collapse of the Soviet Union in 1991* (pp. 91-117). Springer International Publishing.

Prishchepov, A. V., Radeloff, V. C., Baumann, M., Kuemmerle, T., & Müller, D. (2012). Effects of institutional changes on land use: agricultural land abandonment during the transition from state-command to market-driven economies in post-Soviet Eastern Europe. *Environmental Research Letters*, *7*(2), 024021.

Prishchepov, A. V., Radeloff, V. C., Dubinin, M., & Alcantara, C. (2012). The effect of Landsat ETM/ETM+ image acquisition dates on the detection of agricultural land abandonment in Eastern Europe. *Remote Sensing of Environment*, *126*, 195-209.

Ramankutty, N., Mehrabi, Z., Waha, K., Jarvis, L., Kremen, C., Herrero, M., & Rieseberg, L. H. (2018). Trends in global agricultural land use: implications for environmental health and food security. *Annual Review of Plant Biology*, *69*, 789-815.

Salmon, J. M., Friedl, M. A., Frolking, S., Wisser, D., & Douglas, E. M. (2015). Global rain-fed, irrigated, and paddy croplands: A new high resolution map derived from remote sensing, crop inventories and climate data. *International Journal of Applied Earth Observation and Geoinformation*, *38*, 321-334.

Schneider, A. (2012). Monitoring land cover change in urban and peri-urban areas using dense time stacks of Landsat satellite data and a data mining approach. *Remote Sensing of Environment*, *124*, 689-704.

See, L., Fritz, S., You, L., Ramankutty, N., Herrero, M., Justice, C., Becker-Reshef, I., Thornton, P., Erb, K., Gong, P. and Tang, H., 2015. Improved global cropland data as an essential ingredient for food security. *Global Food Security, 4*, 37-45.

Siebert, S., Portmann, F. T., & Döll, P. (2010). Global patterns of cropland use intensity. *Remote Sensing*, *2*(7), 1625-1643.

Smit, J., Nasr, J., & Ratta, A. (1996). *Urban agriculture: food, jobs and sustainable cities*. The Urban Agriculture Network, Inc., New York, , pp. 35-37.

Steven, M. D., & Clark, J. A. (Eds.). (2013). *Applications of remote sensing in agriculture*. Elsevier.

Story, M., & Congalton, R. G. (1986). Accuracy assessment: a user's perspective. *Photogrammetric Engineering and Remote Sensing*, *52*(3), 397-399.

Teluguntla, P., Thenkabail, P. S., Xiong, J., Gumma, M. K., Giri, C., Milesi, C., ... & Tilton, J. (2015). Global Food Security Support Analysis Data (GFSAD) at Nominal 1 km (GCAD) derived from remote sensing in support of food security in the twenty-first century: Current achievements and future possibilities.

Teluguntla, P., Thenkabail, P. S., Oliphant, A., Xiong, J., Gumma, M. K., Congalton, R. G., ... & Huete, A. (2018). A 30-m landsat-derived cropland extent product of Australia and China using random forest machine learning algorithm on Google Earth Engine cloud computing platform. *ISPRS Journal of Photogrammetry and Remote Sensing*, *144*, 325-340.

Thenkabail, P. S., Biradar, C. M., Noojipady, P., Dheeravath, V., Li, Y. J., Velpuri, M., & Vithanage, J. (2008). *A Global Irrigated Area Map (GIAM) using remote sensing at the end of the last millennium*. Colombo, Sri Lanka: International Water Management Institute.

Thenkabail, P.S., Biradar C.M., Noojipady, P., Dheeravath, V., Li, Y.J., Velpuri, M., Gumma, M., Reddy, G.P.O., Turral, H., Cai, X. L., Vithanage, J., Schull, M., and Dutta, R. (2009). Global irrigated area map (GIAM), derived from remote sensing, for the end of the last millennium. *International Journal of Remote Sensing, 30*(14): 3679-3733.

Thenkabail, P.S., Hanjra, M.A., Dheeravath, V., Gumma, M. (2011). Global croplands and their water use remote sensing and non-remote sensing perspectives. *Advances in environmental remote sensing: sensors, algorithms, and applications*. Taylor and Francis, pp. 383-419.

Thenkabail, P. S., & Wu, Z. (2012). An automated cropland classification algorithm (ACCA) for Tajikistan by combining Landsat, MODIS, and secondary data. *Remote Sensing*, *4*(10), 2890-2918.

Thenkabail, P. S., & Lyon, J. G. (2016). *Hyperspectral remote sensing of vegetation*. CRC press.

Thenkabail, P. (2018). Global Food Security Support Analysis Data at Nominal 1 km (GFSAD1km) Derived from Remote Sensing in Support of Food Security in the Twenty-First Century: Current Achievements and Future Possibilities. In *Remote sensing handbook (three volume set)*, pp. 865-894. CRC Press.

Veldkamp, A., & Lambin, E. F. (2001). Predicting land-use change. *Agriculture, Ecosystem & Environment*, 85(1), 1-6.

Verburg, P. H., van Berkel, D. B., van Doorn, A. M., van Eupen, M., & van den Heiligenberg, H. A. (2010). Trajectories of land use change in Europe: a model-based exploration of rural futures. *Landscape Ecology*, *25*(2), 217-232.

Waldner, F., Canto, G. S., & Defourny, P. (2015). Automated annual cropland mapping using knowledge-based temporal features. *ISPRS Journal of Photogrammetry and Remote Sensing*, *110*, 1-13.

Waldner, F., De Abelleyra, D., Verón, S. R., Zhang, M., Wu, B., Plotnikov, D., ... & Le Maire, G. (2016). Towards a set of agrosystem-specific cropland mapping methods to address the global cropland diversity. *International Journal of Remote Sensing*, *37*(14), 3196-3231.

Wheeler, T., & Von Braun, J. (2013). Climate change impacts on global food security. *Science*, *341*(6145), 508-513.

Wulder, M. A., J. A. Dechka, M. A. Gillis, J. E. Luther, R. J. Hall, A. Beaudoin, and S. E. Franklin. "Operational mapping of the land cover of the forested area of Canada with Landsat data: EOSD land cover program." *The Forestry Chronicle* 79, no. 6 (2003): 1075-1083.

Xiong, J., Thenkabail, P., Tilton, J., Gumma, M., Teluguntla, P., Oliphant, A., & Gorelick, N. (2017). Nominal 30-m cropland extent map of continental Africa by integrating pixel-based and object-based algorithms using Sentinel-2 and Landsat-8 data on Google Earth Engine. *Remote Sensing*, *9*(10), 1065.

Yadav, K., & Congalton, R. (2018). Accuracy assessment of global food security-support analysis data (GFSAD) cropland extent maps produced at three different spatial resolutions. *Remote Sensing*, *10*(11), 1800.

Yang, H., Ma, B., Du, Q., & Yang, C. (2010). Improving urban land use and land cover classification from high-spatial-resolution hyperspectral imagery using contextual information. *Journal of Applied Remote Sensing*, *4*(1), 041890.

**Figures**

**Figure 2.2.1** Study area with twelve agroecological zones (AEZs) spread across Europe, Middle East, Russia and Central Asia, study, covering a total 3,351 Landsat tiles. Each color represents different AEZ group of countries.

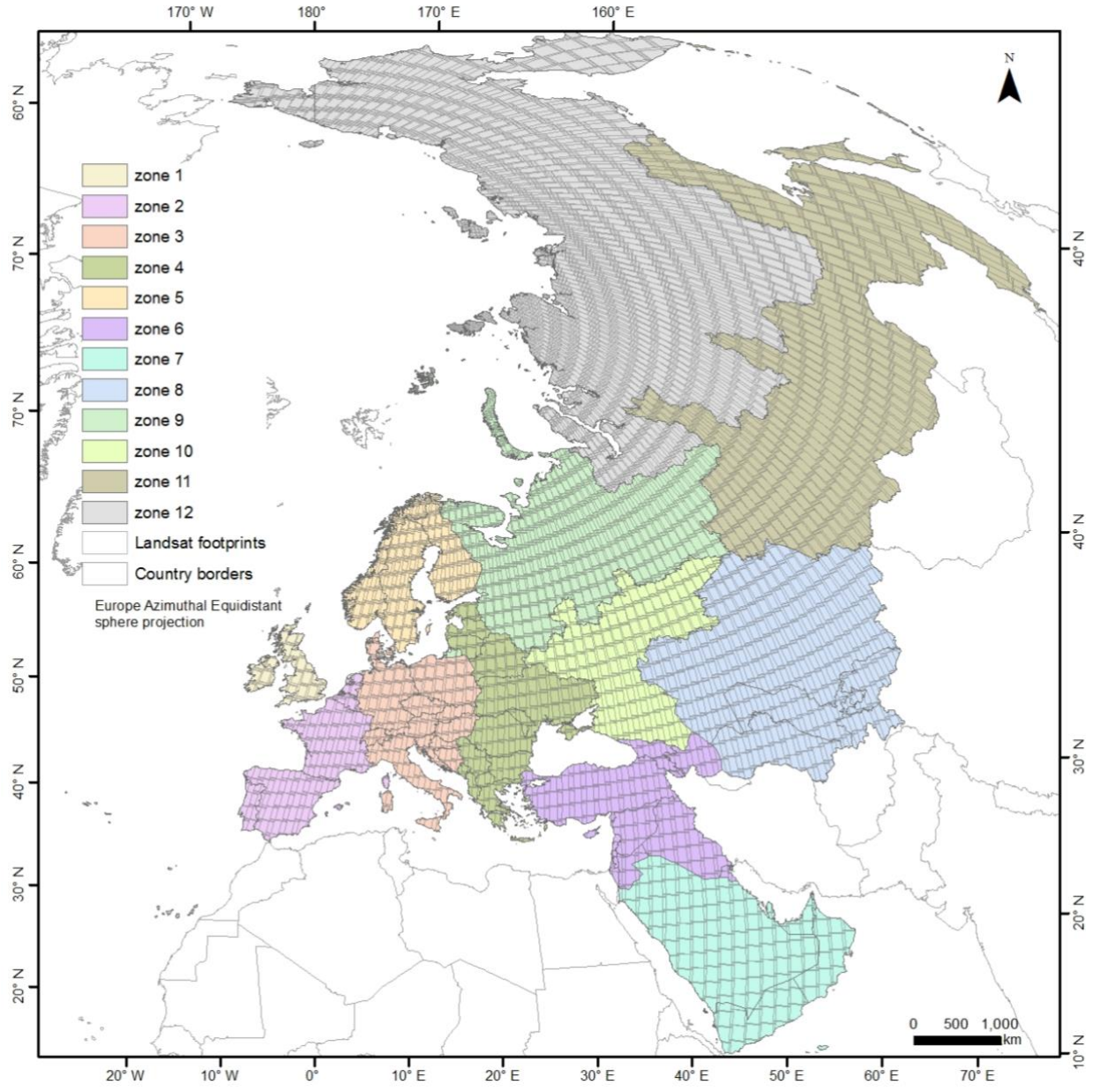

**Figure 2.2.2** Flowchart showing the overall methodology employed in this study. Three major steps involved are: i) data collection, ii) data processing and, iii) accuracy assessment and evaluation.

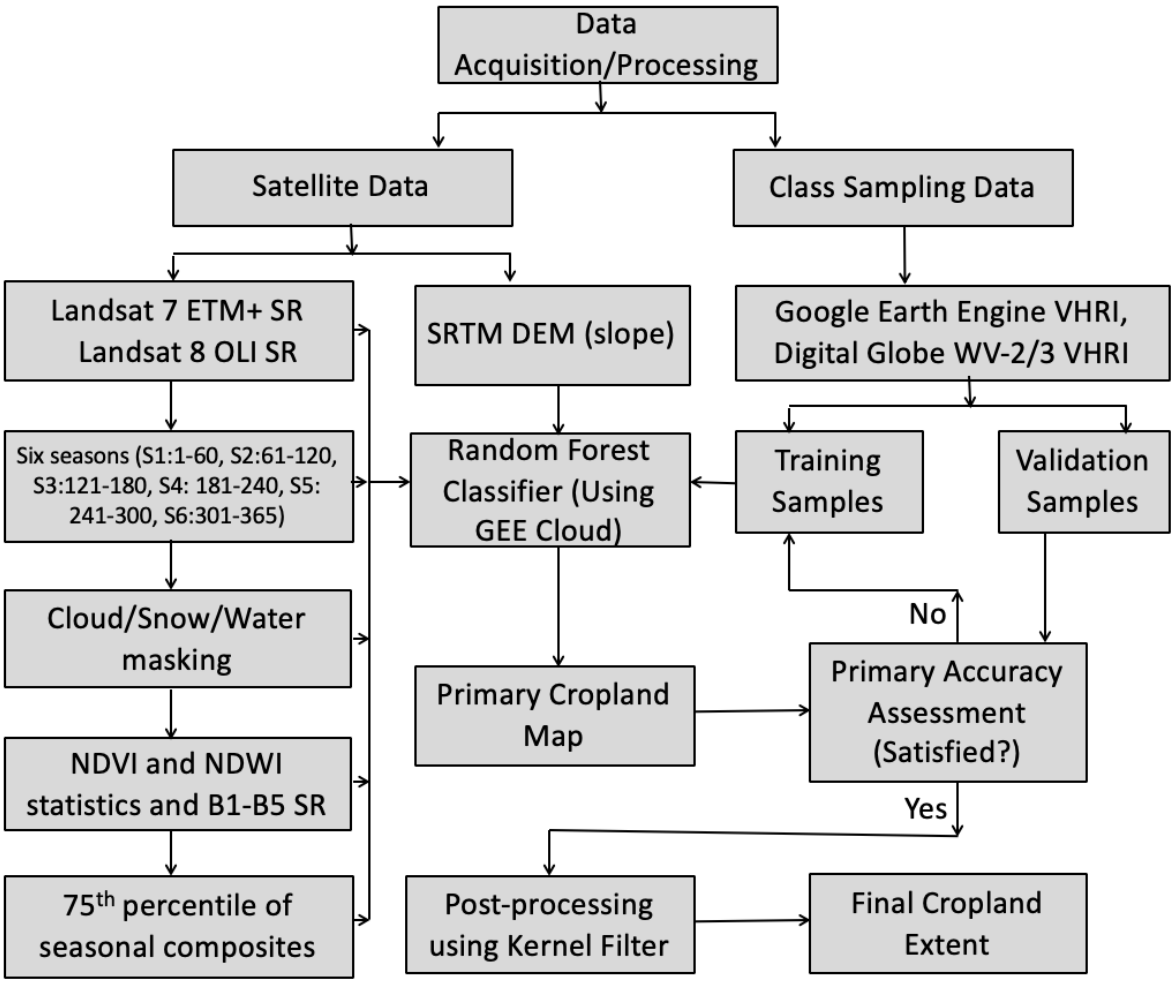

**Figure 2.2.3** Characteristics of input features in the RF classifier for AEZ 5. Panel a shows the box plot of the discrimination of croplands and non-croplands by each input variable (where B1, B2, B3,B4, B5 and B7 are spectral reflectance of blue, green, red, NIR, SWIR1 and SWIR2 Bands of Landsat data; NDVI is the normalized vegetation index; NDWI is the normalized water index; all these values were calculated to the average of full dataset except range, min, stddev are the range, minimum and standard deviation of full dataset of NDVI values respectively.). Panels b and c present the importance of input variables by mean decrease accuracy values and mean decrease Gini coefficient values.

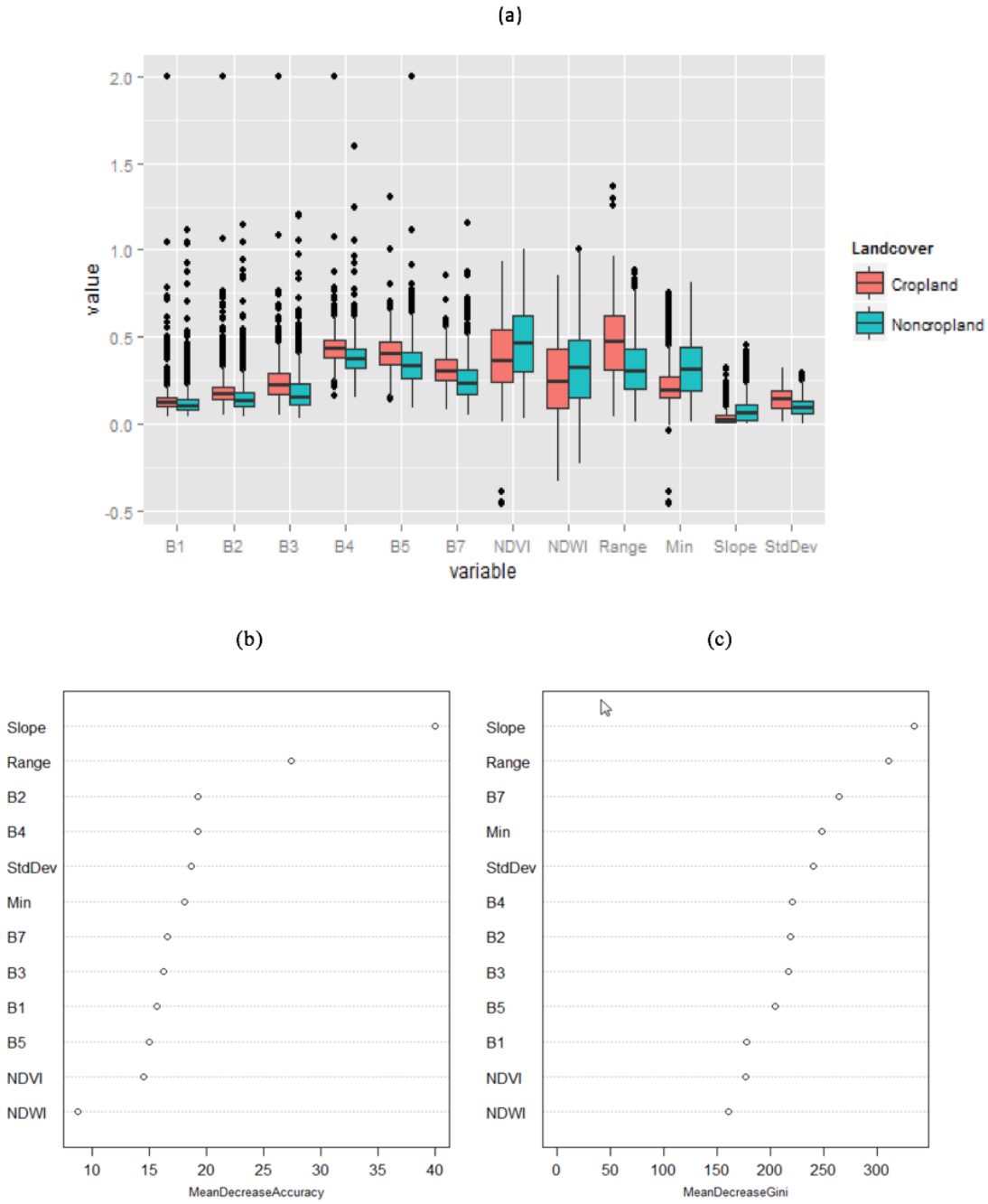

**Figure 2.2.4** (a) the distribution of cropland areas of study area at 30m and; (b) visual assessment of the cropland extent product at 30-m in few sample locations, showing the detail. Green color represents the cropland mask and background is the natural color composite high resolution satellite image.

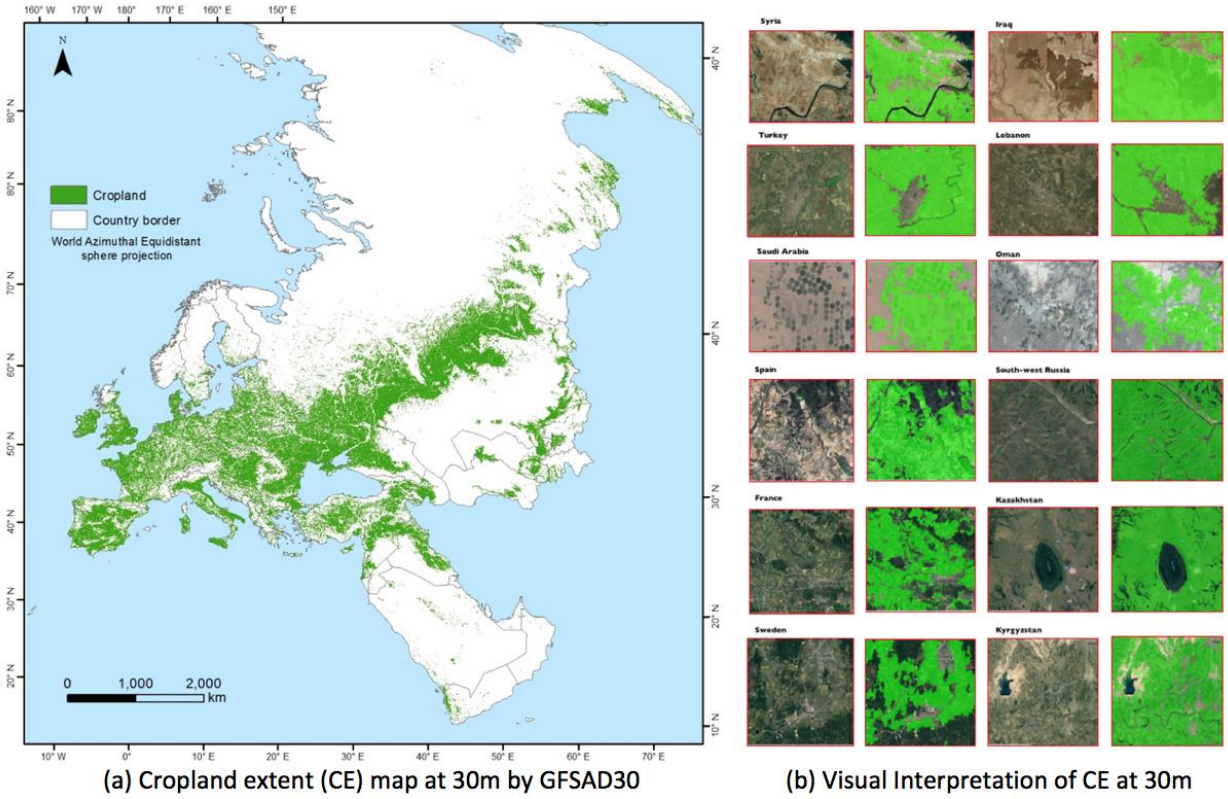


(a) Cropland extent (CE) map at 30m by GFSAD30 (b) Visual Interpretation of CE at 30m

**Figure 2.2.5** Comparison between cropland areas (Mha) by this study (GFSAD30) (X-axis) and other sources (Y-axis). Blue dots represent the respective countries croplands in GFSAD30 (our study) map area (on X-axis) and other source map croplands area on Y-axis. The top row shows comparison of GFSAD30 with national census data by FAOSTAT (a) and MIRCA2014 (b) respectively. Panels in the middle row show comparison of GFSAD30 with GLC30 (c) and CORINE (d) respectively. The bottom row shows comparison of GFSAD30 with GIAM-GMRCA (e) and GRIPC2005 (f) Cropland areas respectively. Note that the cropland area for Russia was removed from each graph due to its large net area.

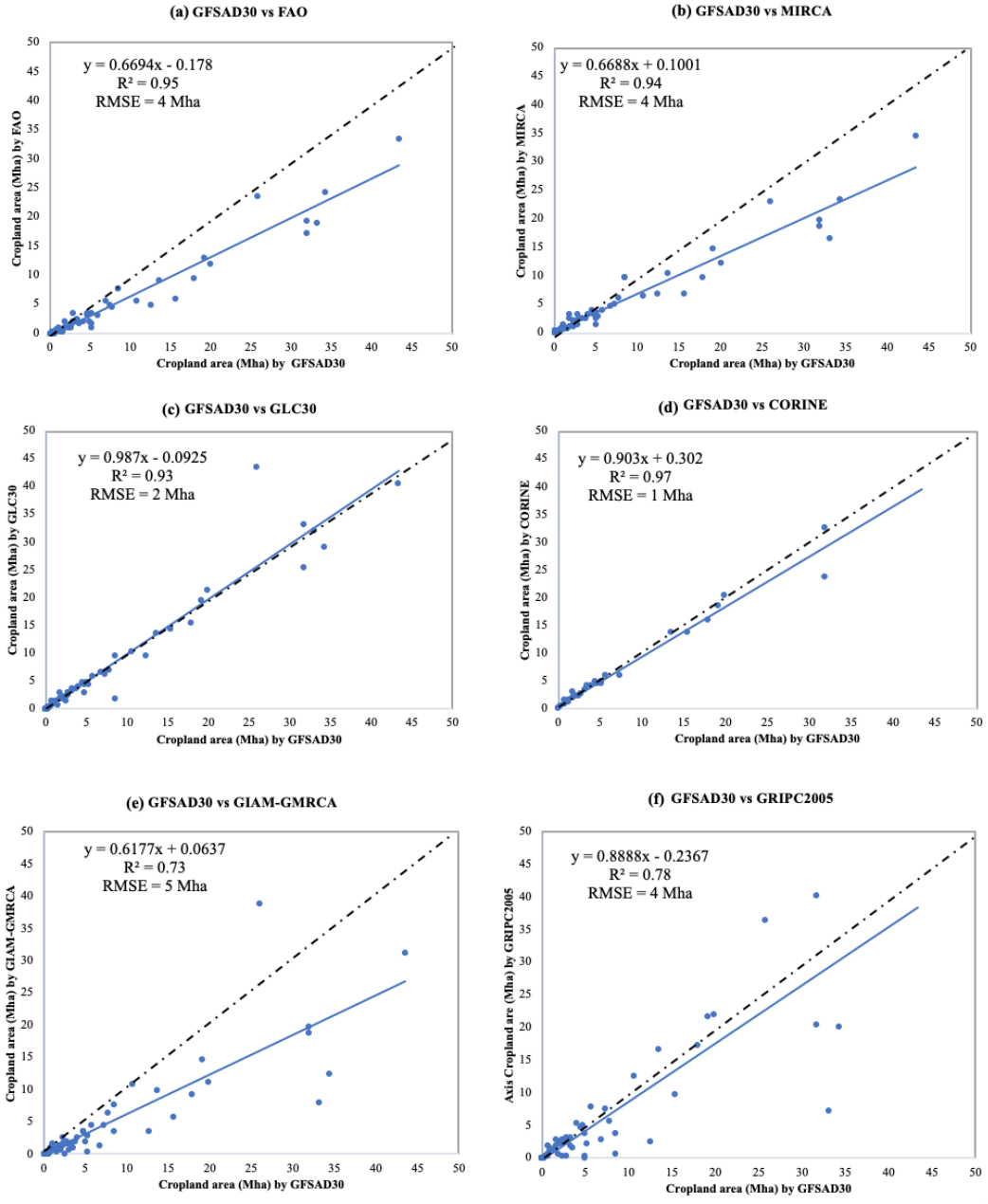

**Figure 2.2.6** Similarity matrices resulting from map to map comparison for the entire study area between GFSAD30 cropland extent (this study) for the nominal year 2015 and GLC30 derived cropland extent (CE) at 30m for circa 2015. Panel (a) shows the similarity matrices for each zone and panel (b) shows the visual comparison between GFSAD30 CE (yellow color) and GLC30 CE (green color).

**(a) Similarity matrices of map to map comparison of GFSAD30 CE with GLC30 CE at 30m**

Zone 1

| Map Data | Reference Data: Crop | Reference Data: Non-crop | Total | User's Accuracy |
|---|---|---|---|---|
| Crop | 834 | 143 | 977 | 85.4% |
| Non-crop | 61 | 462 | 523 | 88.3% |
| Total | 895 | 605 | 1500 | |
| Producer's Accuracy | 93.2% | 76.4% | | |
| Overall Similarity | | | | 86.4% |
| Kappa | | | | 0.7 |

Zone 4

| Map Data | Reference Data: Crop | Reference Data: Non-crop | Total | User's Accuracy |
|---|---|---|---|---|
| Crop | 776 | 126 | 902 | 86.0% |
| Non-crop | 96 | 502 | 598 | 83.9% |
| Total | 872 | 628 | 1500 | |
| Producer's Accuracy | 89.0% | 79.9% | | |
| Overall Similarity | | | | 85.2% |
| Kappa | | | | 0.7 |

Zone7

| Map Data | Reference Data: Crop | Reference Data: Non-crop | Total | User's Accuracy |
|---|---|---|---|---|
| Crop | 570 | 135 | 705 | 80.9% |
| Non-crop | 54 | 741 | 795 | 93.2% |
| Total | 624 | 876 | 1500 | |
| Producer's Accuracy | 91.3% | 84.6% | | |
| Overall Similarity | | | | 87.4% |
| Kappa | | | | 0.8 |

Zone 2

| Map Data | Reference Data: Crop | Reference Data: Non-crop | Total | User's Accuracy |
|---|---|---|---|---|
| Crop | 726 | 162 | 888 | 81.8% |
| Non-crop | 86 | 526 | 612 | 85.9% |
| Total | 812 | 688 | 1500 | |
| Producer's Accuracy | 89.4% | 76.5% | | |
| Overall Similarity | | | | 83.5% |
| Kappa | | | | 0.7 |

Zone 5

| Map Data | Reference Data: Crop | Reference Data: Non-crop | Total | User's Accuracy |
|---|---|---|---|---|
| Crop | 92 | 0 | 92 | 100% |
| Non-crop | 25 | 1383 | 1408 | 98.2% |
| Total | 117 | 1383 | 1500 | |
| Producer's Accuracy | 78.6% | 100.0% | | |
| Overall Similarity | | | | 98.3% |
| Kappa | | | | 0.9 |

Zone8

| Map Data | Reference Data: Crop | Reference Data: Non-crop | Total | User's Accuracy |
|---|---|---|---|---|
| Crop | 186 | 84 | 270 | 68.9% |
| Non-crop | 24 | 1206 | 1230 | 98.0% |
| Total | 210 | 1290 | 1500 | |
| Producer's Accuracy | 88.6% | 93.5% | | |
| Overall Similarity | | | | 92.8% |
| Kappa | | | | 0.7 |

Zone 3

| Map Data | Reference Data: Crop | Reference Data: Non-crop | Total | User's Accuracy |
|---|---|---|---|---|
| Crop | 734 | 119 | 853 | 86.0% |
| Non-crop | 85 | 562 | 647 | 86.9% |
| Total | 819 | 681 | 1500 | |
| Producer's Accuracy | 89.6% | 82.5% | | |
| Overall Similarity | | | | 86.4% |
| Kappa | | | | 0.7 |

Zone 6

| Map Data | Reference Data: Crop | Reference Data: Non-crop | Total | User's Accuracy |
|---|---|---|---|---|
| Crop | 351 | 186 | 537 | 65.4% |
| Non-crop | 78 | 885 | 963 | 91.9% |
| Total | 429 | 1071 | 1500 | |
| Producer's Accuracy | 81.8% | 82.6% | | |
| Overall Similarity | | | | 82.4% |
| Kappa | | | | 0.6 |

Zone 9,10,11

| Map Data | Reference Data: Crop | Reference Data: Non-crop | Total | User's Accuracy |
|---|---|---|---|---|
| Crop | 122 | 25 | 147 | 83.0% |
| Non-crop | 25 | 1328 | 1353 | 98.2% |
| Total | 147 | 1353 | 1500 | |
| Producer's Accuracy | 83.0% | 98.2% | | |
| Overall Similarity | | | | 96.7% |
| Kappa | | | | 0.8 |

Overall

| Map Data | Reference Data: Crop | Reference Data: Non-crop | Total | User's Accuracy |
|---|---|---|---|---|
| Crop | 4391 | 980 | 5371 | 81.8% |
| Non-crop | 534 | 7595 | 8129 | 93.4% |
| Total | 4925 | 8575 | 13500 | |
| Producer's Accuracy | 89.2% | 88.6% | | |
| Overall Similarity | | | | 88.8% |
| Kappa | | | | 0.7 |

**(b) Visual Interpretation of comparison between GFSAD30 CE and GLC30 CE at 30m**

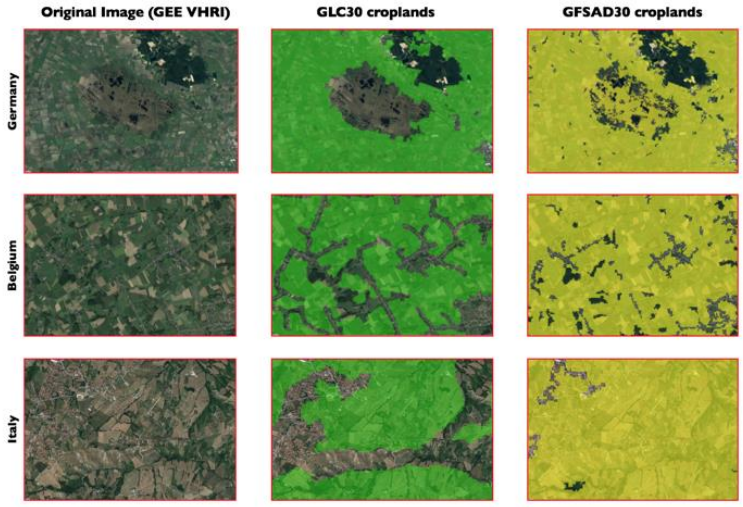

**Figure 2.2.7** Map to map comparison for the entire study area between GFSAD30 (this study) and CORINE-derived cropland extent at 30m. Panel (a) shows the similarity matrices for the zones and panel (b) shows the visual comparison between GFSAD30 and CORINE croplands.

**(a) Similarity matrices of map to map comparison of GFSAD30 CE with CORINE CE at 100m**

Zone 1

| Map Data \ Reference Data | Crop | Non-crop | Total | User's Accuracy |
|---|---|---|---|---|
| Crop | 789 | 188 | 977 | 80.8% |
| Non-crop | 39 | 484 | 523 | 92.5% |
| Total | 828 | 672 | 1500 | |
| Producer's Accuracy | 95.3% | 72.0% | | |
| Overall Similarity | | | | 84.9% |
| Kappa | | | | 0.7 |

Zone 4

| Map Data \ Reference Data | Crop | Non-crop | Total | User's Accuracy |
|---|---|---|---|---|
| Crop | 570 | 135 | 705 | 80.9% |
| Non-crop | 54 | 741 | 795 | 93.2% |
| Total | 624 | 876 | 1500 | |
| Producer's Accuracy | 91.3% | 84.6% | | |
| Overall Similarity | | | | 87.4% |
| Kappa | | | | 0.7 |

Zone 2

| Map Data \ Reference Data | Crop | Non-crop | Total | User's Accuracy |
|---|---|---|---|---|
| Crop | 655 | 233 | 888 | 73.8% |
| Non-crop | 46 | 566 | 612 | 92.5% |
| Total | 701 | 799 | 1500 | |
| Producer's Accuracy | 93.4% | 70.8% | | |
| Overall Similarity | | | | 81.4% |
| Kappa | | | | 0.63 |

Zone 5

| Map Data \ Reference Data | Crop | Non-crop | Total | User's Accuracy |
|---|---|---|---|---|
| Crop | 69 | 23 | 92 | 75% |
| Non-crop | 11 | 1397 | 1408 | 99.2% |
| Total | 80 | 1420 | 1500 | |
| Producer's Accuracy | 86.3% | 98.4% | | |
| Overall Similarity | | | | 97.7% |
| Kappa | | | | 0.8 |

Zone 3

| Map Data \ Reference Data | Crop | Non-crop | Total | User's Accuracy |
|---|---|---|---|---|
| Crop | 679 | 174 | 853 | 79.6% |
| Non-crop | 47 | 600 | 647 | 92.7% |
| Total | 726 | 774 | 1500 | |
| Producer's Accuracy | 93.5% | 77.5% | | |
| Overall Similarity | | | | 85.3% |
| Kappa | | | | 0.7 |

Overall

| Map Data \ Reference Data | Crop | Non-crop | Total | User's Accuracy |
|---|---|---|---|---|
| Crop | 2762 | 753 | 3515 | 78.6% |
| Non-crop | 197 | 3788 | 3985 | 95.1% |
| Total | 2959 | 4541 | 7500 | |
| Producer's Accuracy | 93.3% | 83.4% | | |
| Overall Similarity | | | | 87.3% |
| Kappa | | | | 0.8 |

**(b) Visual Interpretation of comparison between GFSAD30 CE and CORINE CE at 100m**

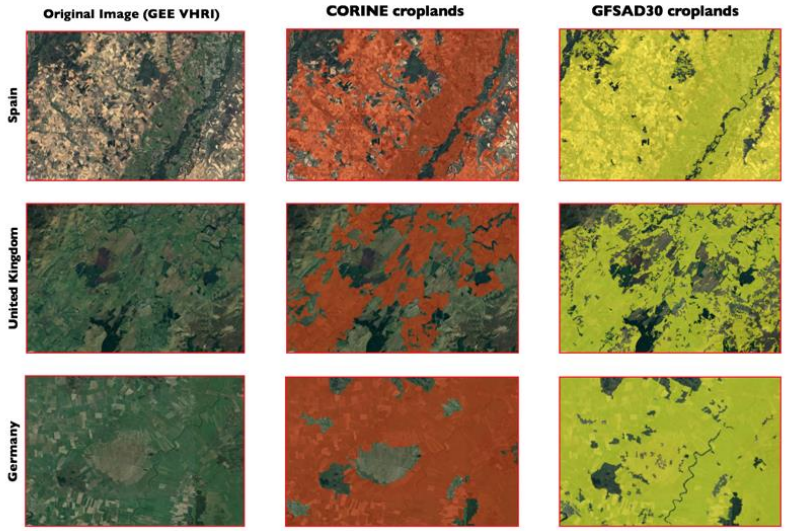

**Figure 2.2.8** Map to map comparison for cropland extent developed by GFSAD30 and croplands in the Central Asia. Panel (a) shows the comparison between GFSAD30 croplands and croplands of Central Asia by Igor Klein et al (2012) and panel (b) shows the comparison between GFSAD30 (this study) croplands and croplands by Biradar et al (2016) of Fergana Valley in Central Asia.

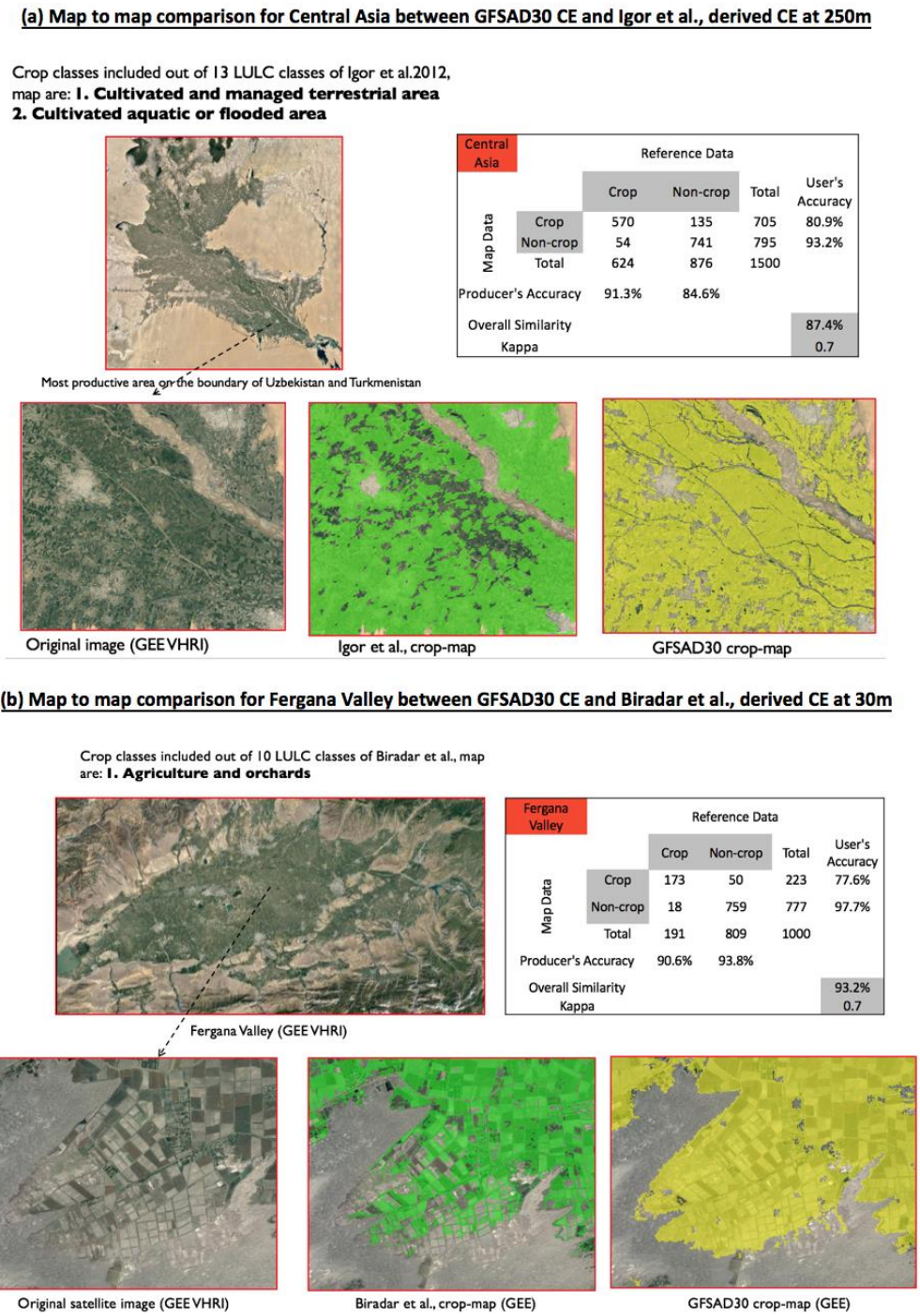

**Tables**

**Table 2.2.1** Characteristics of multi-temporal Landsat data used in the study. Color code ranging from green to red represents low to high values.

| Zones | Landsat tiles | Number of Landsat satellite images | | | | | |
|---|---|---|---|---|---|---|---|
| | | 2014 | | 2015 | | 2016 | |
| | | LE7 | LC8 | LE7 | LC8 | LE7 | LC8 |
| z1 | 57 | 488 | 713 | 530 | 717 | 535 | 698 |
| z2 | 135 | 1844 | 2112 | 1859 | 2217 | 1832 | 2191 |
| z3 | 151 | 2208 | 2514 | 2223 | 2600 | 2272 | 2539 |
| z4 | 167 | 2154 | 2668 | 2478 | 2666 | 2575 | 2575 |
| z5 | 168 | 996 | 1866 | 1481 | 1806 | 1663 | 1816 |
| z6 | 139 | 2359 | 2866 | 2574 | 2729 | 2389 | 2771 |
| z7 | 152 | 1868 | 3305 | 2977 | 3137 | 2942 | 3282 |
| z8 | 290 | 3274 | 5299 | 4737 | 5004 | 4434 | 5088 |
| z9 | 430 | 892 | 2054 | 1460 | 1959 | 1530 | 3006 |
| z10 | 183 | 1499 | 2330 | 2000 | 2198 | 1697 | 2212 |
| z11 | 513 | 2401 | 3656 | 3274 | 3905 | 3218 | 5372 |
| z12 | 966 | 18 | 44 | 28 | 124 | 21 | 4987 |
| Total | 3351 | 20001 | 29427 | 25621 | 29062 | 25108 | 36537 |

**Table 2.2.2** Input bands or variables used to classify croplands of the entire study area.

| | |
|---|---|
| Number of seasons | Six seasons: (Season 1: January-February, Season 2: March-April, Season 3: May-June, Season 4: July-August, Season 5: September-October and Season 6: November-December) |
| Number of input bands | 1.Bimonthly (six per year) NDVI and NDWI (36 total)<br>2. Slope derived from SRTM DEM (1 total)<br>3. Standard deviation, Range, and Minimum of NDVI derived from the full dataset (3 bands total)<br>4. $75^{th}$ percentile value of each reflective band + NDVI + NDWI bands derived from the full dataset for two years (16 bands total) |

**Table 2.2.3** Reference training and validation data for the study area.

| Zones | Reference samples | |
|---|---|---|
| | Cropland | Non-cropland |
| 1 | 3466 | 1854 |
| 2 | 4267 | 2211 |
| 3 | 5780 | 953 |
| 4 | 7665 | 3818 |
| 5 | 2265 | 3139 |
| 6 | 4072 | 4459 |
| 7 | 1257 | 3315 |
| 8 | 2792 | 4193 |
| 9 | 163 | 1856 |
| 10 | 632 | 484 |
| 11 | 184 | 1900 |
| 12 | 2 | 2676 |
| Total | 63403 | |

**Table 2.2.4** Data sources used for comparisons with the GFSAD30 croplands (this paper).

| | Name of data source | Author | Resolution | Year of development | Cropland definition associated classes | Comparison Type |
|---|---|---|---|---|---|---|
| 1 | Monthly irrigated and rain-fed crop areas for 2014 (MIRCA2014) | Portman et al., 2010 | Country | 2014 | Irrigated and rainfed croplands | Coutnry-wise areal statistics comparison |
| 2 | Food and Agricultural Organization (FAO) Agricultural land area excluding pasture based on FAO2013 statistics consider nominal 2015 | FAOSTAT, 2015 | Country | 2015 | Harvested lands | Coutnry-wise areal statistics comparison |
| 3 | Global croplands derived from Global Irrigated Area Mapping (GIAM) and Global Map of Rainfed Cropland Areas (GMRCA) | Thenkabail et al., 2009, 2011 and Biradar et al., 2009 | 1km | 2000 | Irrigated and rainfed croplands | Country-wise areal statistics and Map to map similarity matrix comparison |
| 4 | Global Land Cover for circa 2010 (GLC30) | Chen et al., 2015 | 30m | 2010 | Cultivated lands | Country-wise areal statistics and Map-map comparison |
| 5 | CORINE Land cover | Buttner et al., 2014 | 100m | 2012 | 211, 212, 213, 221, 222, 223, 241, 242, 243, 244 | Country-wise areal statistics and Map to map similarity matrix comparison |
| 6 | A regional land cover product for Central Asia | Klein et al., 2012 | 250m | 2010 | Cultivated lands | Map to map similarity matrixcomparisons |
| 7 | A regional crop type map product for the Fergana Valley in Central Asia at 30-m | Biradar et al., 2016 | 30m | 2014 | Crop type classes | Map to map similarity matrix comparisons |

**Table 2.2.5** Independent accuracy assessment results for each zone as well as for the entire study area.

Zone 1, % of TCA*=3.5%

| Map Data \ Reference Data | Crop | No-Crop | Total | User Accuracy |
|---|---|---|---|---|
| Crop | 156 | 15 | 171 | 91.2% |
| No-Crop | 13 | 66 | 79 | 83.5% |
| Total | 169 | 81 | 250 | |
| Producer Accuracy | 92.3% | 81.5% | | **88.8%** |

Zone 2, % of TCA*=12.5%

| Map Data \ Reference Data | Crop | No-Crop | Total | User Accuracy |
|---|---|---|---|---|
| Crop | 129 | 24 | 153 | 84.3% |
| No-Crop | 28 | 69 | 97 | 71.1% |
| Total | 157 | 93 | 250 | |
| Producer Accuracy | 82.2% | 74.2% | | **79.2%** |

Zone 3, % of TCA*=14.4%

| Map Data \ Reference Data | Crop | No-Crop | Total | User Accuracy |
|---|---|---|---|---|
| Crop | 144 | 12 | 156 | 92.3% |
| No-Crop | 20 | 74 | 94 | 78.8% |
| Total | 164 | 86 | 250 | |
| Producer Accuracy | 87.8% | 86.1% | | **87.2%** |

Zone 4, % of TCA*=16.5%

| Map Data \ Reference Data | Crop | No-Crop | Total | User Accuracy |
|---|---|---|---|---|
| Crop | 145 | 11 | 156 | 93% |
| No-Crop | 21 | 73 | 94 | 77.7% |
| Total | 166 | 84 | 250 | |
| Producer Accuracy | 87.4% | 87.0% | | **87.2%** |

Zone 5, % of TCA*=1.2%

| Map Data \ Reference Data | Crop | No-Crop | Total | User Accuracy |
|---|---|---|---|---|
| Crop | 18 | 1 | 19 | 94.7% |
| No-Crop | 2 | 229 | 231 | 99.1% |
| Total | 20 | 230 | 250 | |
| Producer Accuracy | 90% | 99.6% | | **98.8%** |

Zone 6, % of TCA*=11%

| Map Data \ Reference Data | Crop | No-Crop | Total | User Accuracy |
|---|---|---|---|---|
| Crop | 87 | 22 | 109 | 79.8% |
| No-Crop | 10 | 131 | 141 | 92.9% |
| Total | 97 | 153 | 250 | |
| Producer Accuracy | 89.7% | 85.6% | | **87.2%** |

Zone 7, % of TCA*=1%

| Map Data \ Reference Data | Crop | No-Crop | Total | User Accuracy |
|---|---|---|---|---|
| Crop | 8 | 0 | 8 | 100% |
| No-Crop | 1 | 241 | 242 | 99.6% |
| Total | 9 | 241 | 250 | |
| Producer Accuracy | 88.9% | 100% | | **99.6%** |

Zone 8, % of TCA*=13.2%

| Map Data \ Reference Data | Crop | No-Crop | Total | User Accuracy |
|---|---|---|---|---|
| Crop | 36 | 11 | 47 | 76.6% |
| No-Crop | 4 | 199 | 203 | 98% |
| Total | 40 | 210 | 250 | |
| Producer Accuracy | 90% | 94.8% | | **94%** |

Zone 9, % of TCA*=2.4%

| Map Data \ Reference Data | Crop | No-Crop | Total | User Accuracy |
|---|---|---|---|---|
| Crop | 7 | 6 | 13 | 53.9% |
| No-Crop | 4 | 233 | 237 | 98.3% |
| Total | 11 | 239 | 250 | |
| Producer Accuracy | 63.6% | 97.5% | | **96%** |

Zone 10, % of TCA*=17.2%

| Map Data \ Reference Data | Crop | No-Crop | Total | User Accuracy |
|---|---|---|---|---|
| Crop | 106 | 35 | 141 | 75.2% |
| No-Crop | 25 | 84 | 109 | 77.1% |
| Total | 131 | 119 | 250 | |
| Producer Accuracy | 80.9% | 70.6% | | **76%** |

Zone 11, % of TCA*=7.2%

| Map Data \ Reference Data | Crop | No-Crop | Total | User Accuracy |
|---|---|---|---|---|
| Crop | 21 | 6 | 27 | 77.8% |
| No-Crop | 5 | 217 | 222 | 97.8% |
| Total | 26 | 223 | 249 | |
| Producer Accuracy | 80.8% | 97.3% | | **95.6%** |

Zone 12, % of TCA*=0.02%

| Map Data \ Reference Data | Crop | No-Crop | Total | User Accuracy |
|---|---|---|---|---|
| Crop | 0 | 0 | 0 | NA |
| No-Crop | 0 | 250 | 250 | 100% |
| Total | 0 | 250 | 250 | |
| Producer Accuracy | NA | 100% | | **100%** |

All zones, % of TCA*=16.5%

| Map Data \ Reference Data | Crop | No-Crop | Total | User Accuracy |
|---|---|---|---|---|
| Crop | 857 | 143 | 1,000 | 85.7% |
| No-Crop | 134 | 1,866 | 2,000 | 93.3% |
| Total | 991 | 2,009 | 3,000 | |
| Producer Accuracy | 86.5% | 92.9% | | **90.8%** |
| | | | Weighted Accuracy** | **93.8%** |

Note: *TCA (Total Croplands Area) = 546 Mha

** The all-zones Weighted Accuracy is weighted by proportion of croplands in each zone

## Appendix A2.2

**Table A.2.2.1** Net cropland areas (NCAs) derived based on 30-m GFSAD30 cropland product and comparison with other cropland products for countries in the Europe.

| Region name | Country Name | Land Area[1] | GFSAD30[2] | MIRCA2014[3] | FAO[4] | CORINE[5] | GLC30[6] | GIAM-GMRCA[7] | GRIPC 2005[8] |
|---|---|---|---|---|---|---|---|---|---|
| | | Mha | Mha | Mha | Mha | Mha | Mha | Mha | Mha |
| Europe | Albania | 2.7 | 0.7 | 0.8 | 0.7 | 0.8 | 0.7 | 1.1 | 1.9 |
| Europe | Andorra | 0.047 | 0.001 | 0.001 | 0.001 | NA | 0.002 | 0.006 | 0.004 |
| Europe | Austria | 8.3 | 2.7 | 1.5 | 1.4 | 2.7 | 2.7 | 1.9 | 2.7 |
| Europe | Belarus | 20.3 | 10.7 | 6.3 | 5.7 | NA | 10.5 | 11.1 | 12.7 |
| Europe | Belgium | 3.0 | 1.7 | 3.2 | 0.9 | 1.8 | 1.8 | 1.4 | 2.0 |
| Europe | Bosnia & Herzegovina | 5.1 | 1.8 | 1.1 | 1.1 | 1.8 | 1.9 | 1.3 | 2.9 |
| Europe | Bulgaria | 10.9 | 5.8 | 3.7 | 3.3 | 5.8 | 5.8 | 4.7 | 7.9 |
| Europe | Croatia | 5.6 | 2.3 | 1.6 | 1.0 | 2.3 | 2.3 | 1.6 | 3.1 |
| Europe | Cyprus | 0.9 | 0.5 | 0.2 | 0.1 | NA | 0.5 | 0.2 | 0.3 |
| Europe | Czech Republic | 7.7 | 4.7 | 3.2 | 3.3 | 4.5 | 4.5 | 3.6 | 5.0 |
| Europe | Denmark | 4.2 | 3.3 | 2.6 | 2.4 | 3.2 | 3.2 | 1.7 | 3.4 |
| Europe | Estonia | 4.2 | 1.4 | 0.8 | 0.6 | 1.4 | 1.5 | 1.1 | 1.3 |
| Europe | Finland | 30.2 | 1.9 | 2.3 | 2.3 | 2.8 | 3 | 0.8 | 0.7 |
| Europe | France | 54.8 | 31.8 | 19.6 | 19.4 | 32.6 | 33.3 | 20.0 | 40.3 |
| Europe | Germany | 34.9 | 19.9 | 12.3 | 12.1 | 20.4 | 21.4 | 11.2 | 22.1 |
| Europe | Greece | 12.9 | 4.6 | 3.8 | 3.7 | 5 | 5 | 3.7 | 4.9 |
| Europe | Hungary | 9.1 | 7.3 | 4.9 | 4.8 | 6.1 | 6.3 | 4.6 | 7.7 |
| Europe | Ireland | 6.9 | 5.1 | 1.2 | 1.1 | 4.7 | 4.8 | 0.6 | 0.5 |
| Europe | Italy | 29.4 | 17.9 | 9.6 | 9.5 | 15.9 | 15.4 | 9.3 | 17.3 |
| Europe | Latvia | 6.2 | 2.7 | 1.9 | 1.2 | 2.7 | 2.8 | 2.1 | 2.8 |
| Europe | Liechtenstein | 0.015 | 0.005 | 0.004 | 0.003 | 0.004 | 0.005 | 0.005 | 0.006 |
| Europe | Lithuania | 6.3 | 4.0 | 3.0 | 2.1 | 3.9 | 4 | 2.7 | 5.6 |
| Europe | Luxembourg | 0.3 | 0.1 | 0.1 | 0.1 | 0.1 | 0.1 | 0.1 | 0.2 |
| Europe | Moldova | 3.3 | 2.9 | 2.2 | 2.1 | NA | 2.6 | 1.8 | 3.2 |
| Europe | Montenegro | 1.3 | 0.2 | 0.4 | 0.2 | 0.2 | 0.2 | 0.4 | 0.0 |
| Europe | Netherlands | 3.4 | 2.2 | 1.0 | 1.1 | 2.4 | 2.4 | 1.4 | 2.3 |
| Europe | Norway | 30.7 | 0.8 | 0.7 | 0.8 | 1.5 | 1.5 | 0.5 | 0.3 |
| Europe | Poland | 30.4 | 19.1 | 14.5 | 12.9 | 18.6 | 19.7 | 14.8 | 21.8 |
| Europe | Portugal | 9.1 | 5.2 | 2.7 | 1.9 | 4.6 | 4.5 | 3.1 | 2.3 |
| Europe | Romania | 23.0 | 13.6 | 10.2 | 9.2 | 13.6 | 13.6 | 9.9 | 16.7 |
| Europe | San Marino | 0.006 | 0.005 | 0.002 | 0.001 | NA | NA | 0.003 | 0.005 |
| Europe | Serbia | 8.7 | 5.1 | 3.4 | 3.6 | 4.7 | 4.9 | 3.1 | 0.0 |
| Europe | Slovakia | 4.8 | 2.5 | 1.5 | 1.4 | 2.3 | 2.4 | 1.8 | 2.5 |

| | | | | | | | | | |
|---|---|---|---|---|---|---|---|---|---|
| Europe | Slovenia | 2.0 | 0.7 | 0.2 | 0.2 | 0.7 | 0.7 | 0.5 | 0.7 |
| Europe | Spain | 49.9 | 31.8 | 18.7 | 17.2 | 23.8 | 25.7 | 18.8 | 20.6 |
| Europe | Sweden | 41.1 | 3.4 | 2.6 | 2.6 | 3.9 | 3.9 | 1.1 | 2.1 |
| Europe | Switzerland | 4.0 | 1.4 | 0.5 | 0.4 | 1.2 | 1.2 | 0.7 | 1.3 |
| Europe | Turkey | 76.9 | 34.3 | 23.2 | 24.3 | NA | 29.2 | 12.4 | 20.2 |
| Europe | Ukraine | 58.0 | 43.4 | 34.5 | 33.4 | NA | 40.6 | 31.3 | 50.1 |
| Europe | United Kingdom | 24.2 | 15.5 | 6.6 | 6.1 | 13.7 | 14.3 | 6.0 | 9.9 |

1= total land area is land area excluding area under inland water bodies

2=current study

3=Monthly irrigated and rainfed crop areas (MIRCA) around the year derived by Portman et al.

4=FAO Agricultural land area excluding pasture based on FAO2013 statistics consider nominal 2015 (http://www.fao.org/faostat/en/#data/QC)

5= CORINE land cover (CLC) at 100m resolution by European Commission (https://www.eea.europa.eu/data-and-maps/data/clc-2012-raster)

6= Global Land Cover(GLC30) product derived from Landsat data circa 2010 (www.globallandcover.com) (Chen et al., 2015),

7= global croplands derived from Global Irrigated Area Mapping (GIAM) and Global Map of Rainfed Cropland Areas (GMRCA) by Thenkabail et al.,2009 and Biradar et al., 2009

8= Global rain-fed, irrigated, and paddy croplands (GRIPC) derived by Solomon et al.,2015

**Table A.2.2.2** Net cropland areas (NCAs) derived based on 30-m GFSAD30 cropland product and comparison with other cropland products for countries in the Middle East, Russia and Central Asia.

| Region Name | Country Name | Land Area[1] | GFSAD30[2] | MIRCA2014[3] | FAO[4] | GLC30[6] | GIAM-GMRCA[7] | GRIPC 2005[8] |
|---|---|---|---|---|---|---|---|---|
| | | Mha | Mha | Mha | Mha | Mha | Mha | Mha |
| Middle East | Syria | 18.4 | 6.8 | 4.7 | 5.7 | 6.5 | 1.4 | 2.9 |
| Middle East | Saudi Arabia | 214.9 | 2.9 | 3.3 | 3.5 | 2.9 | 0.7 | 0.3 |
| Middle East | Yemen | 52.8 | 2.5 | 1.7 | 1.5 | 1.4 | 0.3 | 0.3 |
| Middle East | Macedonia | 2.5 | 0.9 | 0.6 | 0.5 | 0.9 | 0.9 | 1.7 |
| Middle East | Israel | 2.2 | 0.6 | 0.4 | 0.4 | 0.4 | 0.2 | 0.5 |
| Middle East | Jordan | 8.9 | 0.5 | 0.4 | 0.3 | 0.4 | 0.1 | 0.4 |
| Middle East | United Arab Emirates | 8.4 | 0.2 | 0.4 | 0.3 | 0.2 | 0.1 | 0.0 |
| Middle East | Lebanon | 1.0 | 0.2 | 0.3 | 0.3 | 0.3 | 0.2 | 0.2 |
| Middle East | Oman | 31.1 | 0.2 | 0.1 | 0.1 | 0.2 | 0.1 | 0.03 |
| Middle East | West Bank | 0.6 | 0.1 | 0 | 0 | 0.1 | 0.1 | 0 |
| Middle East | Kuwait | 1.8 | 0.041 | 0.017 | 0.015 | 0 | 0.037 | 0.001 |
| Middle East | Qatar | 1.2 | 0.027 | 0.013 | 0.015 | 0 | 0.039 | 0.0004 |
| Middle East | Gaza Strip | 0 | 0.023 | 0 | 0 | 0 | 0.007 | 0.011 |
| Middle East | Azerbaijan | 8.3 | 4.9 | 2.5 | 2.1 | 3.1 | 2.2 | 4.0 |
| Middle East | Armenia | 2.8 | 1.5 | 0.7 | 0.5 | 0.7 | 0.5 | 1.3 |
| Middle East | Georgia | 65.2 | 8.5 | 9.5 | 7.9 | 1.9 | 7.9 | 3.8 |
| Middle East | Bahrain | 0.1 | 0.006 | 0.008 | 0.004 | 0 | 0.000 | 0.000 |
| Russia | Russia | 1,633.0 | 155.8 | 127.5 | 123.5 | 0.7 | 128.7 | 235.9 |
| West Asia | Iraq | 43.5 | 12.5 | 6.6 | 4.8 | 9.5 | 3.6 | 2.5 |
| Central Asia | Kazakhstan | 270.1 | 25.9 | 23.1 | 23.6 | 43.5 | 39.0 | 36.4 |
| Central Asia | Uzbekistan | 42.6 | 7.8 | 6.1 | 4.7 | 7 | 6.4 | 5.9 |
| Central Asia | Turkmenistan | 47.0 | 3.7 | 2.6 | 1.9 | 3.6 | 2.1 | 1.7 |
| Central Asia | Kyrgyzstan | 19.2 | 2.2 | 2.1 | 1.3 | 1.8 | 2.7 | 2.6 |
| Central Asia | Tajikistan | 14.0 | 1.1 | 1.4 | 0.9 | 1.2 | 1.6 | 1.5 |

1= total land area is land area excluding area under inland water bodies

2=current study

3=Monthly irrigated and rainfed crop areas (MIRCA) around the year derived by Portman et al.

4=FAO Agricultural land area excluding pasture based on FAO2013 statistics consider nominal 2015 (http://www.fao.org/faostat/en/#data/QC)

6= Global Land Cover(GLC30) product derived from Landsat data circa 2010 (www.globallandcover.com) (Chen et al., 2015),

7= global croplands derived from Global Irrigated Area Mapping (GIAM) and Global Map of Rainfed Cropland Areas (GMRCA) by Thenkabail et al.,2009 and Biradar et al., 2009

8= Global rain-fed, irrigated, and paddy croplands (GRIPC) derived by Solomon et al.,2015

**Table A.2.2.3** Comparison of different machine learning algorithms at five representative zones in the study area

| Accuracy assessment | Zone | RF | CART | SVM |
|---|---|---|---|---|
| User's Cropland Accuracy | Zone 1 | 77 | 68 | 67 |
| | Zone 2 | 47 | 40 | 44 |
| | Zone 3 | 73 | 61 | 61 |
| | Zone 4 | 67 | 47 | 53 |
| | Zone 6 | 88 | 81 | 72 |
| Producer's Crop Accuracy | Zone 1 | 80 | 75 | 59 |
| | Zone 2 | 95 | 89 | 73 |
| | Zone 3 | 74 | 74 | 56 |
| | Zone 4 | 56 | 64 | 42 |
| | Zone 6 | 86 | 81 | 79 |
| User's Non-crop Accuracy | Zone 1 | 85 | 83 | 64 |
| | Zone 2 | 99 | 98 | 94 |
| | Zone 3 | 82 | 85 | 66 |
| | Zone 4 | 71 | 86 | 61 |
| | Zone 6 | 80 | 74 | 74 |
| Producer's Non-crop Accuracy | Zone 1 | 83 | 77 | 72 |
| | Zone 2 | 83 | 81 | 81 |
| | Zone 3 | 81 | 75 | 70 |
| | Zone 4 | 80 | 75 | 71 |
| | Zone 6 | 83 | 74 | 66 |
| Overall Accuracy | Zone 1 | 82 | 76 | 65 |
| | Zone 2 | 85 | 82 | 80 |
| | Zone 3 | 78 | 75 | 64 |
| | Zone 4 | 70 | 72 | 58 |
| | Zone 6 | 85 | 78 | 73 |

**Table A.2.2.4** Countries under each zone

| Zone ID | Coutries |
|---|---|
| 1 | UK, Ireland |
| 2 | Portugal, Spain, France, Andorra, Netherlands, Luxemburg, Belgium |
| 3 | Denmark, Poland, Czech Republic, Germany, Slovakia, Hungary, Austria, Liechtenstein, Slovenia, Switzerland, Bosnia and Herzegovina, Croatia, Italy,San Mario |
| 4 | Estonia, Latvia, Lithuania, Belarus, Ukraine, Serbia, Romania, Bulgaria, Montenegro, Macedonia, Albania, Greece, Moldova |
| 5 | Finland, Norway, Sweden |
| 6 | Turkey, Syria, Iraq, Cyprus, Lebanon, Jordan, Gaza Strip, Armenia, Israel, West Bank, Azerbaijan, Kuwait |
| 7 | Oman, Saudi Arabia, Bahrain, Qatar, Yemen, UAE |
| 8,9,10,11 | Russia |
| 12 | Kazakhstan, Kyrgyzstan, Uzbekistan, Turkmenistan, Tajikistan |

**Figure A.2.2.1** Selection of number of trees per node in RF model (X-axis is "n_estimator" variable which is the number of trees per node and Y-axis is "accuracy" which is accuracy of final output map of the model.

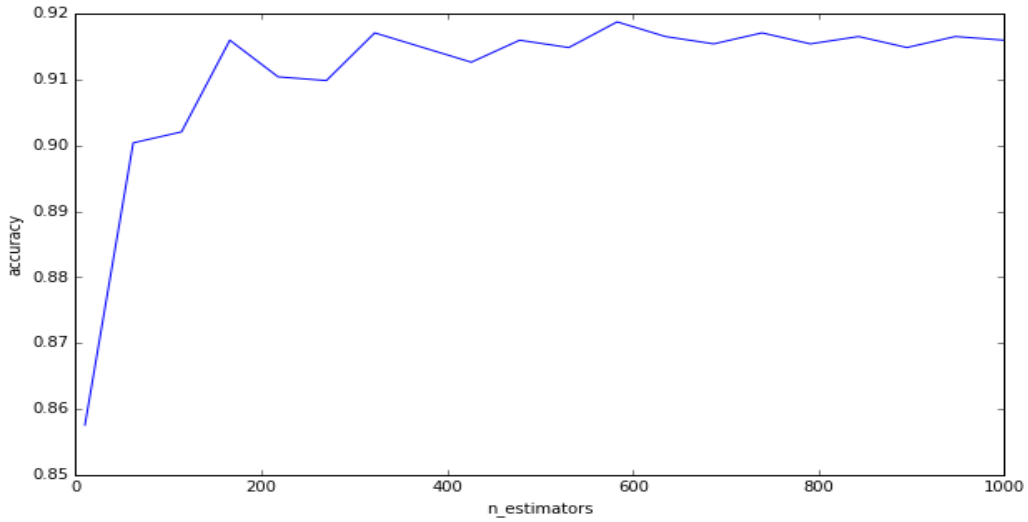

## Chapter 2 (Part 3)

## Mapping wheat cultivated areas in Southeastern Europe with remote sensing and minimal training data

### Abstract

Accurate and up-to date wheat area estimate is a critical input for food security and policy-related studies. Wheat as a staple crop covers 60% of agricultural lands in the cross-border area between Turkey and Bulgaria. For this study area, wheat area statistics in Bulgaria are available at regional scale (equivalent to census regions in the United States) until year 2017, and for Turkey, wheat area statistics are available at the district scale (equivalent to county in the United States) from year 2004 to 2020. Remote sensing provides the extraordinary capability to map field-scale temporally consistent wheat area, but traditional large area mapping methods using remote sensing require a large volume of training data and large computing resources. This study presents a new approach called “Peak Value Method” (PVM) to automatically map wheat cultivated areas in the cross-border area between Turkey and Bulgaria with little or no need for training data. The proposed method is based on the seasonal trajectory of vegetation activity observed from Landsat-derived enhanced vegetation index (EVI) time series, and the maximum value threshold. The maximum value threshold was calculated with the help of a cropping calendar of wheat in the study area. We processed ~5800 Landsat scenes within Google Earth Engine (GEE) to automatically map wheat cultivated areas between 2001 and 2020 using PVM. The maps are validated with independent accuracy assessment as well as comparison with available wheat area statistics and similar remote sensing-based wheat mapping products. The results of this study are successful demonstration of PVM and 20 years of wheat maps at 30-m resolution covering the cross-border area. The wheat maps in Bulgaria produced an overall accuracy of 86% with 10%

omission error and 12% commission error in year 2018, and overall accuracy of 90% with 5% omission error and 8% commission error in year 2019 (~1000 field survey samples in each year). The wheat maps in Turkey produced an overall accuracy of 98.5% with negligible omission errors and 8% commission errors in year 2017 (~160 field survey samples). Comparison between government-derived wheat area statistics and this study yielded an average (between 2001 and 2020) R-square of ~0.85 and average root mean square error (RMSE) of 8,000 ha. The highest R-square (~0.92) was observed in 2014 and the lowest R square (~0.80) was observed in 2007. The lowest RMSE (~4,000 ha) was observed in 2019 and the highest RMSE (~18,000 ha) was observed in 2007. Comparison to a remote sensing-based wheat map by Rufin et al (2015) produced around 85% of overall similarity value with ~10% omission and 12% commission errors. The high commission errors in the wheat maps appear to be related to the commission errors in the cropland extent masks used as part of the proposed method. Wheat area in Turkey and Bulgaria decreased by ~0.1Mha (~10%) from 2001 and 2020. The main limitation of this study is its dependence on the prior knowledge of agronomical characteristics of wheat in the study area, availability of satellite data during the peak growing season, and availability of a high-quality cropland map. The results of this study have important implications for field-scale crop type mapping over large areas without the need for extensive training data and have the ability to improve our understanding of policy implications of wheat growing in Southeastern Europe.

### 2.3.1 Introduction

Agricultural land use and its dynamics are principal elements impacting the environment, food security and support policies (Agarwal, 2002; Ericksen et al, 2009; Teluguntla et al.,2015). It is observed that field-scale time-series information about land use and land cover is essential to understand the detailed impact of changing environment and climate in the area (Foley et al., 2011; Ray et al., 2012). In order to evaluate the agricultural support policies in the region, it is critical to understand the capability of each farm to cultivate and produce the agricultural commodity (Hostert et al., 2011; Prishchepov et al., 2012; Sieber et al.,2013). To this end, spatially explicit agricultural knowledge is vital for environmental and socio-economic studies.

Wheat as a staple crop covering the 60% of the cultivated area in the study region plays a significant role in the livelihood and sustainability of the region (NSI, 2020; TurkStat, 2020). Accurate and timely information on wheat area at the field scale is also important for understanding regional food security implications (Khan et al., 2016; Qiu et al.,2017; Zhong et al., 2019). In studies involving multiple countries or large areas, consistent data availability is a major limitation because of different acquisition strategies and sources. (Ramankutty and Foley, 1999; Gibbs and Salmon, 2016). It is observed that historical area statistics at the highest administrative levels are rarely available. For example, in our study area, wheat estimates are available at only planning region scale (equivalent to census regions in the United States) on the Bulgaria side and district scale on the Turkey side with limited time coverage (NSI, 2020; TurkStat, 2020). The spatiotemporal granularity in such conventional datasets is needed for its wider use. It is observed that the places with agroecological similarity can have different trends in land use and land cover change over the same period. For example, in our study area, wheat estimates from 2000 to 2020 are different in southern Bulgaria and northern Bulgaria, or in Turkey and Bulgaria (NSI, 2020;

TurkStat, 2020). To this end, it is important to study the field scale time-series wheat information in this study area in order to summarize the reasons for change through different environmental modeling approaches.

Satellite remote sensing provides significant opportunities to visit the history of environmental change through historical imagery (Ozdogan et al., 2010; Mulla, 2013; Roy et al., 2017). Landsat satellite data are rich with its consistent Earth imagery records, with a series of sensors from the 1980s to today. Continuous Landsat missions provide land use data free of cost and with improved quality (Schneider, 2012; Loveland et al., 2016; Wulder et al., 2019). The current era of easy access to satellite images and cloud-based image processing platforms provides convenient tools to monitor croplands, but the challenges such as the availability of reference information required to map and validate large area cropland maps in a consistent and reproducible fashion remains elusive (Pax-Lenney et al., 2001; Woodcock et al., 2001; Lobell et al., 2004). Many studies have demonstrated the use of Landsat data to map global (Yu et al., 2013; Xiong, 2017; Phalke et al., 2020) to local agricultural lands (Wasser et al., 2004; Coulter et al., 2016; Yang et al., 2019) and their different attributes (Baumann et al., 2014; Yan et al., 2016; Graesser et al., 2017; Cai et al., 2018; Rufin et al, 2021).

Every vegetation type has different growth phenology, and remote sensing allows us to capture this growth signature through the derived time-series vegetation indices (Oetter et al., 2001; Kennedy et al., 2007; Kontgis et al., 2015). Generally, it is relatively complicated to differentiate vegetation types using vegetation index trajectories, mainly due to missing data values in the time-series (Loveland et al., 2016; Roy et al., 2017). Many studies used gap-filling algorithms for this purpose (Maxwell et al., 2007; Griffiths et al., 2019; Pipia et al., 2019, 2021). These gap-filling algorithms sometimes use fusion of two satellite data with similar characteristics

(Xin et al., 2013; Gao et al., 2017) or use different statistical data imputation methods to fill the missing values (Baumann et al., 2017; Belgiu et al., 2018; Martinez-Ferrer et al., 2020). In both of these techniques, the cost of computation is relatively higher, and the method might add uncertainty in the outputs due to synthetic data fillings.

For our study area, only limited studies have mapped croplands or crop types using Landsat at the country scales (Rufin et al., 2015; Phalke et al., 2018, Phalke et al., 2020). Some studies have used other satellite datasets (other than Landsat) to map wheat crop (Esetlili et al., 2018, Gikov et al., 2019; Dimitrov et al., 2021), and still others have mapped wheat in a very small region in the country but with great accuracy (Vassilev, 2015; Roumenina et al., 2015; Roumenina et al., 2020; Unal et al., 2017). Most of these studies cover a single time period and need large volumes of training data. To this end, the goals of this study are: i) to investigate the difficulties in wheat area mapping in the region; ii) to demonstrate an automated wheat area mapping algorithm; and iii) to generate accurate and seamless wheat area maps covering the last 20 years in the study region using Landsat satellite data.

### 2.3.2 Study area

The study area is geographically situated in Mediterranean Europe (Figure 2.3.1) at the cross-border region between Turkey and Bulgaria. These cross-border areas are also known as Northern Thracia (Bulgaria) and Eastern Thracia (Turkey). This study area is situated on the southeast border of the European Union. Agriculture is an important land use in the study region, covering more than 40% of the landscape in Bulgaria and Turkey, with wheat as a staple crop covering approximately 60% of the cultivated lands, operated under very similar agro-ecological and climatic patterns (FAO, 2019).

The Bulgaria-side covers northcentral, northeast, southeast and southcentral planning regions with 18 provinces and 177 municipalities. The prominent topographical features defining Bulgaria's climate (mostly humid-continental but sub-tropical in the southernmost part) are the Danubian Plain (in the north), the Balkan Mountains (in the center), the Thracian Plain (in the southeast) and the Rhodope Mountains (in the southwest), with elevation ranging from sea level (Thracian Plains) to 2,900 m (Mount Musala in southwest Bulgaria). The major river flowing at the cross-border region between Bulgaria and Turkey is Maritsa with its tributaries. The average temperature and precipitation in Bulgaria are 3.45ºC and 630 mm respectively. Northern Bulgaria is cooler and has higher precipitation compared to southern Bulgaria. Southern Bulgaria has 63% of the country's total population, with population density of 81.5 people per km². Bulgaria's population rate has been continuously declining at a constant pace.

The Turkish side covers the northwest subregion with three provinces (NUTS-3) (Edirne, Tekirdag and Kiklareli) and 26 districts. This part of Turkey is also known as European Turkey or Turkish Thrace. Although it covers only 3% of the total area (23,764 $km^2$) of Turkey, 14% of the country's total population (i.e., about 11 million people) lives here, with average population density of 470 people per km² (with the highest density in European Istanbul with 1,564 people per km²). The total population of Turkey is rapidly increasing since 1950. Eastern Thrace shares a border with Greece (212 km) and Bulgaria (269 km), as well as the Aegean Sea and Black Sea. Because of its unique geographic location (at the transitional area between two continents) and sea-based trade corridor for many countries (Russia, Ukraine, Romania, Bulgaria and Georgia), the region is the main link of connection for intercontinental and intercountry transports. Climatic conditions in the region are mostly Mediterranean, with highest temperature of 35 ºC and lowest temperature of 12 ºC.

### 2.3.3 Methods

This study used a simple classification method using time-series EVI trajectories derived from Landsat data from 2001 to 2020 and processed using a GEE platform. In the first step, we collected seasonal time-series Landsat data from January to August in each year from 2001 to 2020. In the next step, we preprocessed this satellite data to produce the seasonal trajectories of vegetation index for each pixel/location in the image. This vegetation seasonal trajectory is further studied in relation to the crop growth cycle and simple thresholding algorithm used while masking the entire image stack for high-quality cropland masks. In this study, we developed high-quality cropland masks of the study area using our past study results (Phalke et al, 2018). Lastly, we performed an independent accuracy assessment and compared the map with area statistics and other products to evaluate the developed time-series wheat maps of the study area (Figure 2.3.2).

#### 2.3.3.1 Data

This study used two main data inputs: i) satellite data inputs, and ii) agronomic data inputs.

*Satellite data*

Satellite-based time-series vegetation indices are suitable to observe the changes in crop biomass and cropping cycles. This study used Landsat surface reflectance (SR) data from three sensors (Landat-5 TM, Landsat-7 ETM+ and Landsat-8 OLI) acquired between 2001 and 2020 from January to August each year. The temporal distribution of cloud-free images and valid satellite data value images varied widely across the countries. The entire collection of Landsat data accounted for about 5800 individual Landsat scenes collected over six Landsat tiles ranging from path 181 to 183 and row 30 to 31 (Table 2.3.1). Each image in the collection was screened for cloud and cloud shadow using the image masks provided by SR products. This study calculated

Enhanced Vegetation Index (EVI) using blue, red, and near-infrared (NIR) bands of respective Landsat SR products (Equation 1)

$$EVI = G \times \frac{(NIR - RED)}{(NIR - C1 \times RED - C2 \times Blue + L)} \quad (1)$$

where NIR, RED and Blue correspond to surface reflectance values in the Landsat near infrared, red and blue electromagnetic spectrums, respectively. L is the canopy background adjustment that addresses non-linear, differential NIR and RED radiant transfer through a canopy. C1, C2 are the coefficients of the aerosol resistance term, which uses the blue band to correct for aerosol influences in the red band and G is the gain factor. The coefficients used here are L=1, C1 = 6, C2 = 7.5, and G = 2.5 adopted from USGS product guide for Landsat SR derived spectral indices (https://landsat.usgs.gov/sites/default/files/documents/si_product_guide.pdf). The reason behind using EVI is that it has been shown to have improved sensitivity in high biomass regions and proved to be reliable to study croplands because of its coupling with the canopy background signal and reduction in atmospheric influence (Kawamura et al., 2005; Wardlow et al., 2010). The entire composites were further masked with the temporal cropland masks presented in the Chapter 2 (Part 1) of this dissertation (Phalke et al., 2018).

In the next step, this study composed two image inputs for each year and each location: i) maximum EVI input, and ii) maximum day of the year (DOY) input. Maximum EVI input is the reduced image with maximum EVI value of the entire seasonal collection of the images. Maximum DOY input is the DOY or time of the image when the EVI is the maximum in the entire image collected stack. DOY is also simply the day of year or time-stamp extracted from Max EVI image composite. The entire data process ranging from Landsat data collection, preprocessing, indices calculation and extraction was conducted on Google Earth Engine (GEE) platform.

*Agronomic data*

This study collected the basic agronomic data representing the growth cycle of wheat crop in the study area in two ways: i) crop calendar of wheat, and ii) aggregated growing degree days (AGDD) for wheat. In this study, we derived accumulated growing degree days using ERA5 daily datasets (Copernicus Climate Service, 2017) for ~160 ground samples in Turkey and tested its relation to the day of the year (DOY). The results showed that AGDD provides useful crop growth characteristics. While this study used the DOY concept as an input to classifier AGDD can also be used as an alternative, especially when considering interannual variation in planting and maximum greenness dates (Figure 2.3.3). We derived crop calendar for wheat from each country's government data archives, ancillary datasets, literature (Roumenin et al., 2013), FAO crop calendars, and other sources such as the United States Department of Agriculture (USDA) (Table 2.3.2).

**2.3.3.2 Mapping framework**

The classification framework of this study is based on the estimates of EVI time-series trajectory and crop growth characteristics. The classification method introduced in this study is called "peak value method" (PVM). There are two simple steps in this method: i) deriving the EVI time series trajectory with available satellite data in the study region masked with high-quality cropland masks; and ii) deriving the suitable threshold value for maximum value composite of EVI time-series trajectory using peak growth timing of the wheat from cropping calendar (Figure 2.3.2).

*EVI time series trajectory*

EVI time series trajectory is derived in two steps: i) high-quality cropland mask generation for 2001-2020 in the study area; and ii) EVI calculation. In this study, we produced high-quality cropland masks using previous work by the author (Phalke et al., 2018). For this purpose, we applied a zonal generalization method of cropland classification, and crop maps were validated using very high-resolution samples collected through GEE. In the next step, EVI is calculated for all those pixels or locations in the study area within the cropland mask.

To understand the satellite data signatures of wheat crop in the study, we derived EVI time-series for available ground samples of different crop types in the study area (Figure 2.3.4). The high-quality ground sample data obtained through a field survey (Ozdogan et al., 2017 unpublished data; Lachezar et al., 2018 unpublished data) provided us the opportunity to evaluate the temporal growing conditions of different crop types grown in the study area through satellite data signatures.

*Peak Value Method (PVM)*

This study derived an index called “peak value threshold” for each pixel in the study using maximum EVI composite of the study area and maximum DOY composite of the study area for each mapping year (calculated in section 3.1 of this chapter). This threshold uses agronomic knowledge of the crop type (Table 2.3.2). Specifically, this threshold is based on maximum EVI value range and maximum DOY value range in the growing season of the crop. For example, in our study area, it is expected that wheat crop can reach its peak growth in the months between March to June and during that time, maximum EVI will be more than 0.3. This threshold usually will remain the same if harvested wheat varieties and cropping conditions are similar. For our study area, wheat is the major winter crop harvested, and winter cropping practices are homogeneous in the entire area. Therefore, the estimated threshold can be the same for overall application.

#### 2.3.3.3 Accuracy assessment

This study evaluated wheat mapping results in three different ways: i) independent accuracy assessment; ii) areal statistics comparisons; and iii) map-to-map comparisons.

*Independent accuracy assessment*

On the Bulgarian side, ~1000 wheat survey samples were collected by Dr. Lachezar (Lachezar et al., 2018 unpublished data) for years 2018 and 2019. On the Turkish side, ~400 different crop type samples were collected by Dr. Ozdogan (Ozdogan et al., 2017 unpublished data), of which approximately 160 samples were for wheat. We extracted 3 × 3 pixels centered at these ground reference points as the sampling unit. The heterogeneous samples with mixed classes were removed from the selection. The selections of balanced samples were proportional to wheat and non-wheat areas in each region of the study area. The measure of accuracies included: producer's accuracy (PA) or errors of omission, user's accuracy (UA) or errors of commission, and overall accuracy (OA) for croplands and non-croplands (Story and Congalton, 1986; Olofsson et al, 2014; Congalton, 2014) as:

$$OA = Sd \times 100\% \ (1)\ n \tag{2}$$

$$UA = Xij \times 100\% \ (2)\ Xj \tag{3}$$

$$PA = Xij \times 100\% \ (3)\ Xi \tag{4}$$

where $Sd$ is the total number of correctly classified pixels, $n$ = total number of validation pixels, $Xij$ = observation in row $i$ column $j$; $Xi$ = marginal total of row $i$; $Xj$ = marginal total of column $j$.

*Areal statistics comparison*

We compared wheat area estimates derived in this study to government-derived statistics and other remote sensing-based mapping products in the study area. Specifically, we compared wheat areas in NW Turkey derived by Rufin et al. (2015), who used image classification methods applied to Landsat but used class definition that was for broader for winter crops (e.g., wheat and barley).

*Map-to-map comparison*

We compared our wheat map with the winter crop map by Rufin et al (2015) using the similarity matrix analysis (Phalke et al., 2020). First, we extracted about 1000 randomly distributed samples from NW Turkey covering wheat and non-wheat areas from our map and compared their labels to the winter crop map from Rufin et al (2015) within traditional confusion matrix setup (which we refer to as a *similarity matrix)*.

### 2.3.4 Results

#### 2.3.4.1 Classification results

*Wheat area maps*

The primary results of this study presented 30-meter scale wheat area maps from 2001 to 2020 covering the cross-border area between Turkey and Bulgaria. Figure 2.3.5 represents wheat area maps zoomed to a selected location for years 2001 to 2020 and shows the example of finest mapped areas as well as areas with missing wheat extent or problematic regions due to satellite data quality. Visual assessment of these maps indicated that wheat areas are consistently mapped across the study area except in 2012, mainly due to SLC-Off stripes in Landsat 7 images. Overall, wheat areas in Bulgaria had a decreasing trend until the year 2007. After 2007, the Bulgarian-side

wheat area showed stable signals. Wheat area on the Turkish side had overall stable signals from year 2004 except for Bababeski (Kirklareli), Luleburgaz (Kirkalareli), Marmara (Tekirdag) and Hayrabolu (Tekirdag) districts, which had a slight increasing wheat area trend after 2011. Visual assessment also clarified that wheat areas in both countries have a clear distinction between wheat and non-wheat croplands for each year.

#### 2.3.4.2 Accuracy assessment results

The results of accuracy assessment and map evaluation are summarized in three ways: i) independent accuracy assessment; ii) areal comparisons with government statistical datasets; and iii) map-to-map comparison with a similar remote sensing wheat map product in NW Turkey.

*Independent accuracy assessment*

On the Bulgarian side, independent accuracy assessment for 2018 showed the overall accuracy of ~86% with 10% omission and commission errors. For 2019, wheat maps in Bulgaria had overall accuracy of 90% with roughly 5% commission and omission errors. On the Turkish side wheat maps had overall accuracy of 98.5% in the year 2017 with negligible omission and commission errors. In general, this study produced wheat maps with more commission errors than omission errors, primarily due to larger omission errors in the underlying cropland masks.

*Comparison of wheat area*

The comparison between wheat areas derived in this study and government statistics at the district level had average (for the 2001-2020) R square value of ~0.85 with the highest R square (0.92) in 2014 and lowest (~0.80) in 2007. The RMSE values observed to be lowest (4000 ha) in 2019 and highest (13,000 ha) in 2013 (Figure 2.3.7 and 2.3.8).

*Map-to-map comparison*

The results of a similarity matrix showed ~85% overall similarity score with omission and commission errors of about 10%. The visual assessment of wheat cultivated areas produced in this study and those by Rufin et al (2015) indicates that this study has captured some missing wheat crop in Kirklareli compared to Rufin maps, and the Rufin et al. map has captured missing wheat areas in the southern part of NW Turkey compared to this study's wheat maps. Overall, both maps showed a strong agreement (Figure 2.3.9).

### 2.3.5 Discussion

In this study, we propose a new classifier to map wheat in the cross-border region between Turkey and Bulgaria. The classifier is simple to implement, built on GEE, and does not require extensive training data. The wheat cultivated areas with the help of the proposed classifier showed high agreement with government reports, and high overall map accuracy (ranging from 86 to 98%) based on ground samples. The differences in wheat areas derived in this study and government statistics are mainly due to differences in class definitions, measuring methods, and satellite data availability. In general, wheat maps generated in this study tend to overestimate wheat areas reported in government statistics in both countries and this is primarily due to commission errors in the baseline cropland extent maps. The baseline cropland extent masks used in this study had primary application for food security related studies (Phalke et al., 2018) and therefore, more commission errors were allowed (Phalke et al., 2020).

The classification method developed in this study comes with several advantages and disadvantages. The advantages of this method are: a) training data are not needed to map wheat areas; b) simple implementation on GEE; and c) easy to automate and scale to be used in other

locations. The disadvantages include: a) high-quality crop masks are required; b) dependency on the availability of the satellite data during the peak season of crop; c) dependency on crop calendar knowledge; and d) difficulty separating crop types with similar crop growth phenologies. Some of these disadvantages can be addressed, such as developing high-quality crop masks (e.g., Phalke and Ozdogan, 2018) and satellite data fusion methods can be implemented to fill the gaps. In this study, our mapping results provided desired outputs with simple implementation, but in the future, the PVM based on satellite data fusion can be tested for new areas. For example, mapping the wheat cultivated areas in 2012 was challenging, mainly because only Landsat 7 ETM+ sensor data were available in that year. The Landsat 7 ETM+ sensor has scan line issues and thus the stripes were detected in the wheat area map.

It is also observed that some crops may have similar peak periods, but the vegetation greenness values can be different. PVM is advantageous in the sense that it combines the peak greenness with time of peak growth. While not tested here, AGDD is an important input that can be considered to further enhance the proposed method. The strength of the AGDD approach over the DOY approach to identify the peak growing period is that shifting climatic patterns (e.g., warmer years vs cooler years) and geographies can be captured in a single metric without relying on fixed calendar dates. For a broader application of the PVM, the growth cycle of the crop of interest must be considered. However, the growth cycle of crops is impacted by several parameters such as temperature, precipitation, soil conditions, crop management practices and agricultural inputs. Usually crop growth cycles are same in similar agroclimatic areas and in this case, same peak value threshold based on AGDD can be useful. But, to map the same crop in different agroecological zones may require a different peak value threshold. Machine learning models can also help to quantify the peak value threshold using AGDD across different spatiotemporal scales.

The observed wheat area trends in government statistics showed strong agreement with the wheat trends from this study's wheat area maps. Overall, wheat trends are similar throughout Bulgaria, but in NW Turkey, slight differences were observed between the south and north regions of NW Turkey. This study's area maps provide an opportunity to further explore the distribution of these wheat areas at much more granular levels such as villages or even individual farms. For example, close observation of Bulgarian wheat area maps provided different insights on the different trends in southcentral Bulgaria farms versus farms in other regions of the country. To this end, availability of such granular datasets of wheat areas can aid policy-related implications in the region.

### 2.3.6 Conclusions

In this study we developed a new classifier – the peak value method or (PVM) – to map wheat areas in the cross-border area between Turkey and Bulgaria. The resulting wheat maps showed strong agreement with government statistics (R-square range 0.8-0.92) as well as another remote sensing-based winter crop map in the region (86% overall similarity). The independent accuracy assessment results showed high overall accuracies ranging from 86% to 98% with less than 10% commission errors and negligible omission errors. This method is able to map wheat crops without any use of training data in the area where wheat is the main winter cereal. The proposed method can potentially be replicated in other regions to map wheat cultivated areas, given an accurate cropland mask and absence of crops with wheat-like phenology (e.g. barley). The results of this study also add a great value climate change, environment, and sustainability studies in the region.

**References**

Agarwal, C. (2002). A review and assessment of land-use change models: dynamics of space, time, and human choice. *General technical report NE-297*. U.S. Department of Agriculture.

Baumann, M., Ozdogan, M., Richardson, A. D., & Radeloff, V. C. (2017). Phenology from Landsat when data is scarce: Using MODIS and dynamic time-warping to combine multi-year Landsat imagery to derive annual phenology curves. *International Journal of Applied Earth Observation and Geoinformation*, *54*, 72-83.

Baumann, M., Ozdogan, M., Wolter, P. T., Krylov, A., Vladimirova, N., & Radeloff, V. C. (2014). Landsat remote sensing of forest windfall disturbance. *Remote Sensing of Environment*, *143*, 171-179.

Belgiu, M., & Csillik, O. (2018). Sentinel-2 cropland mapping using pixel-based and object-based time-weighted dynamic time warping analysis. *Remote Sensing of Environment*, *204*, 509-523.

Cai, Y., Guan, K., Peng, J., Wang, S., Seifert, C., Wardlow, B., & Li, Z. (2018). A high-performance and in-season classification system of field-level crop types using time-series Landsat data and a machine learning approach. *Remote Sensing of Environment*, *210*, 35-47.

Copernicus Climate Change Service (C3S) (2017): ERA5: Fifth generation of ECMWF atmospheric reanalyses of the global climate. Copernicus Climate Change Service Climate Data Store (CDS), (date of access), https://cds.climate.copernicus.eu/cdsapp#!/home

Coulter, L. L., Stow, D. A., Tsai, Y. H., Ibanez, N., Shih, H. C., Kerr, A., ... & Mensah, F. (2016). Classification and assessment of land cover and land use change in southern Ghana using dense stacks of Landsat 7 ETM+ imagery. *Remote Sensing of Environment*, *184*, 396-409.

Dimitrov, P., Filchev, L., Roumenina, E., & Jelev, G. Crop type mapping in Bulgaria using Sentinel-1/2 data. Bulgarian Academy of Sciences, http://journal.space.bas.bg/arhiv/n%2033/Articles/4_Dimitrov.pdf.

Dimitrov, P., Kamenova, I., Vassilev, V., Roumenina, E., Banov, M., & Jelev, G. (2015). Crop Type Mapping by PROBA-V Satellite Data with 100 m and 300 m Spatial Resolution at Zlatia Test Site, Bulgaria. In *Proceedings of the tenth anniversary scientific conference with international participation: Space, ecology, safety (SES 2014). Published by SRTI-BAS* (pp. 260-267).

Diuk-Wasser, M. A., Bagayoko, M., Sogoba, N., Dolo, G., Toure, M. B., Traore, S. F., & Taylor, C. E. (2004). Mapping rice field anopheline breeding habitats in Mali, West Africa, using Landsat ETM+ sensor data. *International Journal of Remote Sensing*, *25*(2), 359-376.

Diuk-Wasser, M. A., Bagayoko, M., Sogoba, N., Dolo, G., Toure, M. B., Traore, S. F., & Taylor, C. E. (2004). Mapping rice field anopheline breeding habitats in Mali, West Africa, using Landsat ETM+ sensor data. *International Journal of Remote Sensing*, *25*(2), 359-376.

Ericksen, P. J., Ingram, J. S., & Liverman, D. M. (2009). Food security and global environmental change: emerging challenges. *Environmental Science & Policy*, *12*(4), 373-377.

Esetlili, M. T., Balcik, F. B., Sanli, F. B., KALKAN, K., USTUNER, M., Goksel, C., ... & Kurucu, Y. (2018). Comparison of object and pixel-based classifications for mapping crops using Rapideye imagery: a case study of Menemen Plain, Turkey. *International Journal of Environment and Geoinformatics*, *5*(2), 231-243.

Foley, J. A., Ramankutty, N., Brauman, K. A., Cassidy, E. S., Gerber, J. S., Johnston, M., ... & Zaks, D. P. (2011). Solutions for a cultivated planet. *Nature*, *478*(7369), 337-342.

Gao, F., Anderson, M. C., Zhang, X., Yang, Z., Alfieri, J. G., Kustas, W. P., ... & Prueger, J. H. (2017). Toward mapping crop progress at field scales through fusion of Landsat and MODIS imagery. *Remote Sensing of Environment*, *188*, 9-25.

Gibbs, H. K., & Salmon, J. M. (2015). Mapping the world's degraded lands. *Applied Geography*, *57*, 12-21.

Gikov, A., Dimitrov, P., Filchev, L., Roumenina, E., & Jelev, G. (2019). Crop type mapping using multi-date imagery from the Sentinel-2 satellites. *Comptes rendus de l'Academie bulgare des Sciences*, *72*(6), 787-795.

Graesser, J., & Ramankutty, N. (2017). Detection of cropland field parcels from Landsat imagery. *Remote Sensing of Environment*, *201*, 165-180.

Griffiths, P., Nendel, C., & Hostert, P. (2019). Intra-annual reflectance composites from Sentinel-2 and Landsat for national-scale crop and land cover mapping. *Remote Sensing of Environment*, *220*, 135-151.

Hostert, P., Kuemmerle, T., Prishchepov, A., Sieber, A., Lambin, E. F., & Radeloff, V. C. (2011). Rapid land use change after socio-economic disturbances: the collapse of the Soviet Union versus Chernobyl. *Environmental Research Letters*, *6*(4), 045201.

Kennedy, R. E., Cohen, W. B., & Schroeder, T. A. (2007). Trajectory-based change detection for automated characterization of forest disturbance dynamics. *Remote Sensing of Environment*, *110*(3), 370-386.

Khan, A., Hansen, M. C., Potapov, P., Stehman, S. V., & Chatta, A. A. (2016). Landsat-based wheat mapping in the heterogeneous cropping system of Punjab, Pakistan. *International Journal of Remote Sensing*, *37*(6), 1391-1410.

Kontgis, C., Schneider, A., & Ozdogan, M. (2015). Mapping rice paddy extent and intensification in the Vietnamese Mekong River Delta with dense time stacks of Landsat data. *Remote Sensing of Environment*, *169*, 255-269.

Lobell, D. B., & Asner, G. P. (2004). Cropland distributions from temporal unmixing of MODIS data. *Remote Sensing of Environment*, *93*(3), 412-422.

Loveland, T. R., & Irons, J. R. (2016). Landsat 8: The plans, the reality, and the legacy. *Remote Sensing of Environment*, *185*, 1-6.

Martínez-Ferrer, L., Piles, M., & Camps-Valls, G. (2020). Crop yield estimation and interpretability with Gaussian processes. *IEEE Geoscience and Remote Sensing Letters*, doi:10.1109/LGRS.2020.3016140.

Maxwell, S. K., Schmidt, G. L., & Storey, J. C. (2007). A multi-scale segmentation approach to filling gaps in Landsat ETM+ SLC-off images. *International Journal of Remote Sensing*, *28*(23), 5339-5356.

Mulla, D. J. (2013). Twenty five years of remote sensing in precision agriculture: Key advances and remaining knowledge gaps. *Biosystems Engineering*, *114*(4), 358-371.

National Statistical Institute (NSI), Bulgaria, (2020) https://infostat.nsi.bg/infostat/pages/module.jsf?x_2=6.

Oetter, D. R., Cohen, W. B., Berterretche, M., Maiersperger, T. K., & Kennedy, R. E. (2001). Land cover mapping in an agricultural setting using multiseasonal Thematic Mapper data. *Remote Sensing of Environment*, *76*(2), 139-155.

Ozdogan, M., Yang, Y., Allez, G., & Cervantes, C. (2010). Remote sensing of irrigated agriculture: Opportunities and challenges. *Remote Sensing*, *2*(9), 2274-2304.

Pax-Lenney, M., Woodcock, C. E., Macomber, S. A., Gopal, S., & Song, C. (2001). Forest mapping with a generalized classifier and Landsat TM data. *Remote Sensing of Environment*, *77*(3), 241-250.

Phalke, A. R., & Özdoğan, M. (2018). Large area cropland extent mapping with Landsat data and a generalized classifier. *Remote Sensing of Environment*, *219*, 180-195.

Phalke, A. R., Özdoğan, M., Thenkabail, P. S., Erickson, T., Gorelick, N., Yadav, K., & Congalton, R. G. (2020). Mapping croplands of Europe, Middle East, Russia, and Central Asia using Landsat, Random Forest, and Google Earth Engine. *ISPRS Journal of Photogrammetry and Remote Sensing*, *167*, 104-122.

Pipia, L., Amin, E., Belda, S., Salinero-Delgado, M., & Verrelst, J. (2021). Green LAI mapping and cloud gap-filling using Gaussian process regression in Google Earth Engine. *Remote Sensing*, *13*(3), 403.

Pipia, L., Muñoz-Marí, J., Amin, E., Belda, S., Camps-Valls, G., & Verrelst, J. (2019). Fusing optical and SAR time series for LAI gap filling with multioutput Gaussian processes. *Remote Sensing of Environment*, *235*, 111452.

Prishchepov, A. V., Radeloff, V. C., Baumann, M., Kuemmerle, T., & Müller, D. (2012). Effects of institutional changes on land use: agricultural land abandonment during the transition from state-command to market-driven economies in post-Soviet Eastern Europe. *Environmental Research Letters*, *7*(2), 024021.

Qiu, B., Luo, Y., Tang, Z., Chen, C., Lu, D., Huang, H., ... & Xu, W. (2017). Winter wheat mapping combining variations before and after estimated heading dates. *ISPRS Journal of Photogrammetry and Remote Sensing*, *123*, 35-46.

Ramankutty, N., & Foley, J. A. (1999). Estimating historical changes in global land cover: Croplands from 1700 to 1992. *Global Biogeochemical Cycles*, *13*(4), 997-1027.

Ray, D. K., Ramankutty, N., Mueller, N. D., West, P. C., & Foley, J. A. (2012). Recent patterns of crop yield growth and stagnation. *Nature Communications*, *3*(1), 1-7.

Roumenina, E., Atzberger, C., Vassilev, V., Dimitrov, P., Kamenova, I., Banov, M., ... & Jelev, G. (2015). Single-and multi-date crop identification using PROBA-V 100 and 300 m S1 products on Zlatia test site, Bulgaria. *Remote Sensing*, *7*(10), 13843-13862.

Roumenina, E., Jelev, G., Dimitrov, P., Filchev, L., Kamenova, I., Gikov, A., ... & Kolchakov, V. (2020). Qualitative evaluation and within-feld mapping of winter wheat crop condition using multispectral remote sensing data. *Bulgarian Journal of Agricultural Science*, *26*(6), 1129-1142.

Roumenina, E., Kazandjiev, V., Dimitrov, P., Filchev, L., Vassilev, V., Jelev, G., ... & Lukarski, H. (2013). Validation of LAI and assessment of winter wheat status using spectral data and vegetation indices from SPOT VEGETATION and simulated PROBA-V images. *International Journal of Remote Sensing*, *34*(8), 2888-2904.

Roy, P. S., Behera, M. D., & Srivastav, S. K. (2017). Satellite remote sensing: sensors, applications and techniques, 465-472.

Rufin, P., Müller, D., Schwieder, M., Pflugmacher, D., & Hostert, P. (2021). Landsat time series reveal simultaneous expansion and intensification of irrigated dry season cropping in Southeastern Turkey. *Journal of Land Use Science*, *16*(1), 94-110.

Schneider, A. (2012). Monitoring land cover change in urban and peri-urban areas using dense time stacks of Landsat satellite data and a data mining approach. *Remote Sensing of Environment*, *124*, 689-704.

Sieber, A., Kuemmerle, T., Prishchepov, A. V., Wendland, K. J., Baumann, M., Radeloff, V. C., ... & Hostert, P. (2013). Landsat-based mapping of post-Soviet land-use change to assess the effectiveness of the Oksky and Mordovsky protected areas in European Russia. *Remote Sensing of Environment*, *133*, 38-51.

Teluguntla, P., Thenkabail, P. S., Xiong, J., Gumma, M. K., Giri, C., Milesi, C., ... & Tilton, J. (2015). Global food security support analysis data (GFSAD) at nominal 1 km (GCAD) derived from remote sensing in support of food security in the twenty-first century: Current

achievements and future possibilities. In *Land resources monitoring, modeling, and mapping with remote sensing.* CRC Press.

Turkish Statistical Institute (TURKSTAT), Turkey, (2020) https://www.tuik.gov.tr/Home/Index .

Ünal, E., & Debie, C. A. J. M. (2017). Mapping wheat growing areas of Turkey by integrating multi-temporal NDVI data and official crop statistics. *Journal of Field Crops Central Research Institute*, *26*(1), 11-23.

Vassilev, V. S. (2015). Crop identification mapping on the arable territory of Bulgaria using multi-temporal 100 m PROBA-V NDVI data for 2014. *Comptes rendus de l'Académie bulgare des Sciences*, *68*(6), 761-769.

Woodcock, C. E., Macomber, S. A., Pax-Lenney, M., & Cohen, W. B. (2001). Monitoring large areas for forest change using Landsat: Generalization across space, time and Landsat sensors. *Remote Sensing of Environment*, *78*(1-2), 194-203.

Wulder, M. A., Loveland, T. R., Roy, D. P., Crawford, C. J., Masek, J. G., Woodcock, C. E., ... & Zhu, Z. (2019). Current status of Landsat program, science, and applications. *Remote Sensing of Environment*, *225*, 127-147.

Xin, Q., Olofsson, P., Zhu, Z., Tan, B., & Woodcock, C. E. (2013). Toward near real-time monitoring of forest disturbance by fusion of MODIS and Landsat data. *Remote Sensing of Environment*, *135*, 234-247.

Yan, L., & Roy, D. P. (2016). Conterminous United States crop field size quantification from multi-temporal Landsat data. *Remote Sensing of Environment*, *172*, 67-86.

Yang, L., Wang, L., Huang, J., Mansaray, L. R., & Mijiti, R. (2019). Monitoring policy-driven crop area adjustments in northeast China using Landsat-8 imagery. *International Journal of Applied Earth Observation and Geoinformation*, *82*, 101892.

Yu, L., Wang, J., & Gong, P. (2013). Improving 30 m global land-cover map FROM-GLC with time series MODIS and auxiliary data sets: a segmentation-based approach. *International Journal of Remote Sensing*, *34*(16), 5851-5867.

Zhong, L., Hu, L., Zhou, H., & Tao, X. (2019). Deep learning based winter wheat mapping using statistical data as ground references in Kansas and northern Texas, US. *Remote Sensing of Environment*, *233*, 111411.

**Figures**

**Figure 2.3.1** Study area covering the cross-border region between Turkey and Bulgaria. The Bulgaria side covers southeast Bulgaria, southcentral Bulgaria, northcentral Bulgaria and northeast Bulgaria. The Turkey side of the study area covers northwest Turkey.

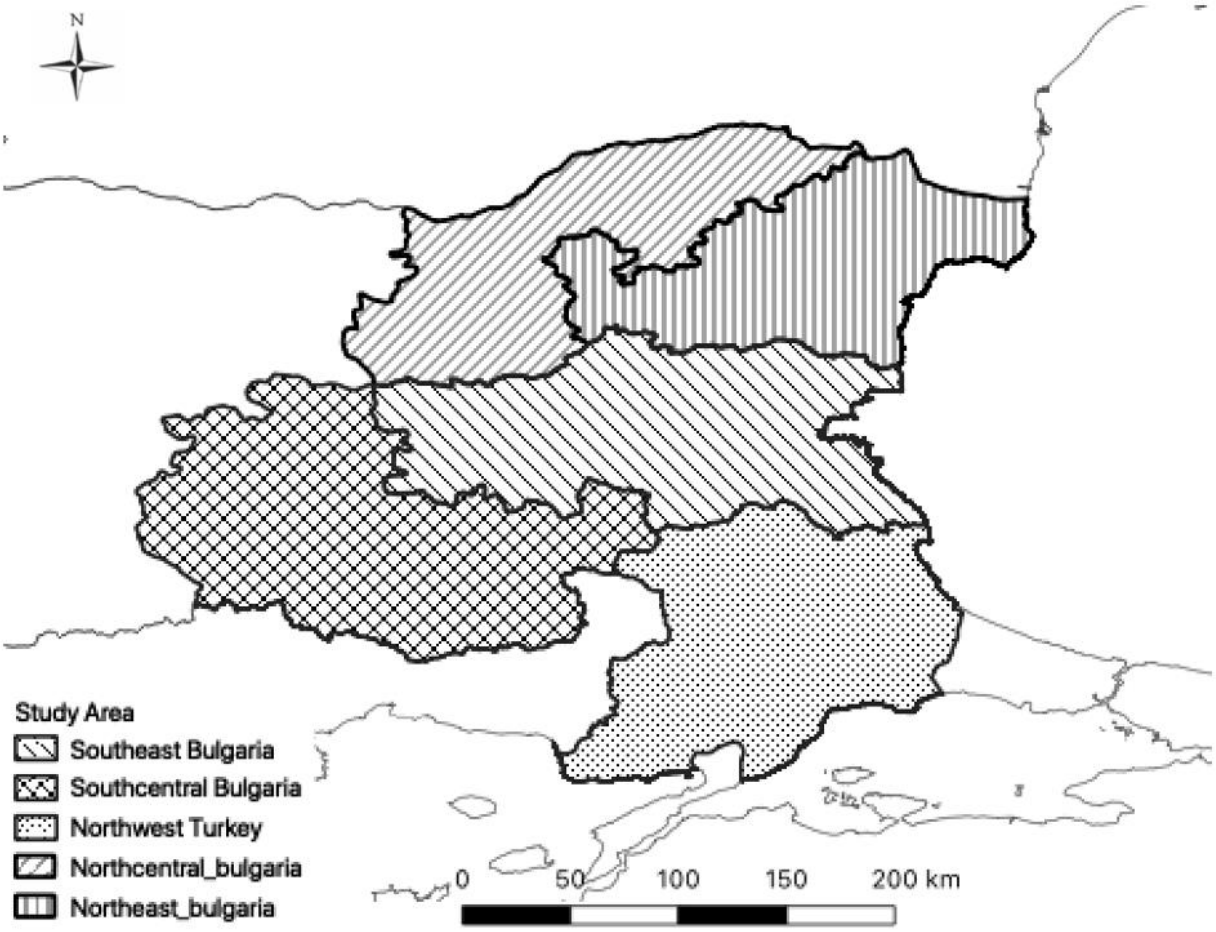

**Figure 2.3.2** Flowchart showing the overall methodology employed to map wheat areas in this study. Three major steps involved are: i) data collection; ii) data processing; and iii) accuracy assessment and evaluation.

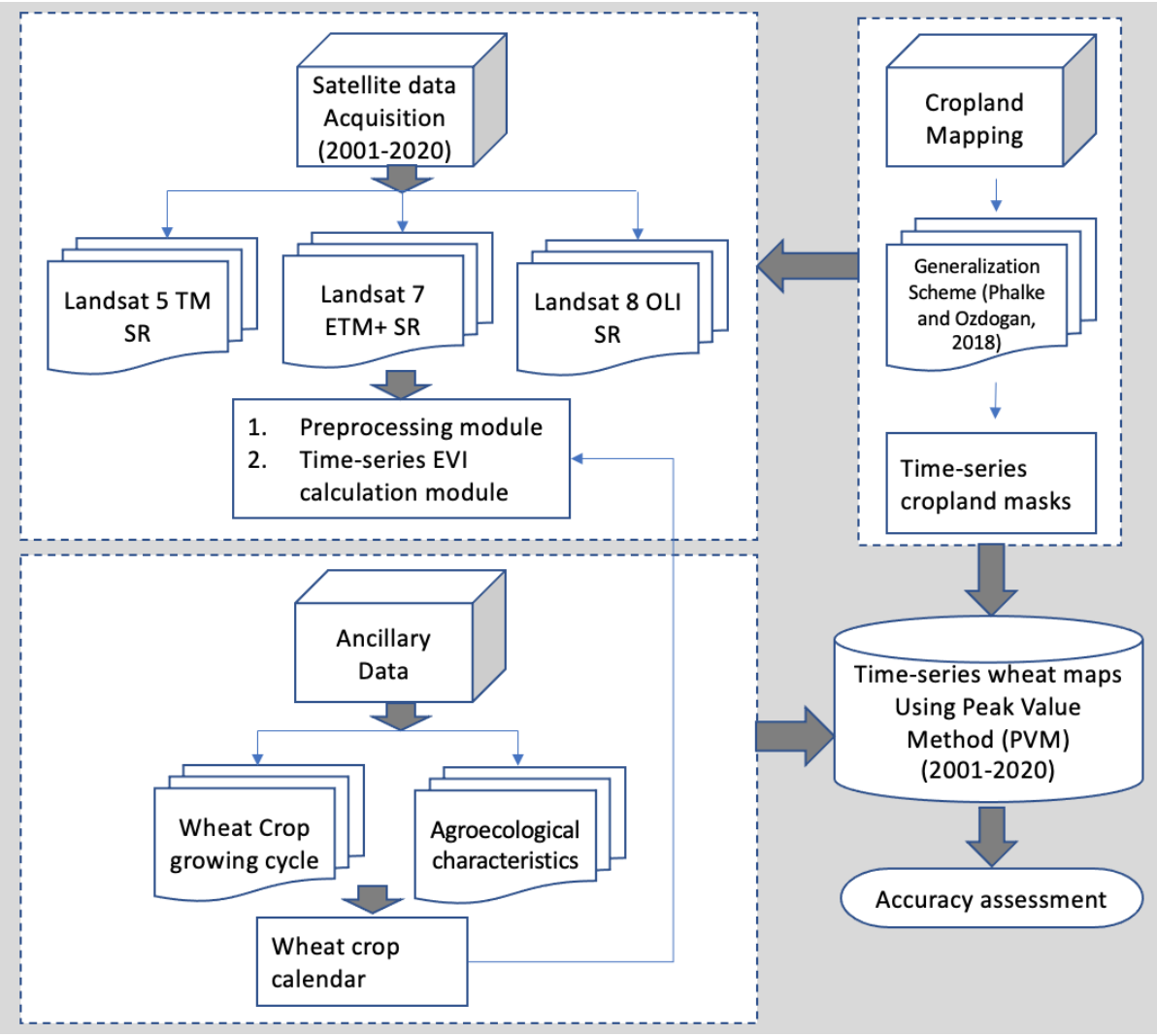

**Figure 2.3.3** Accumulated growing degree days (AGDD) of different crops in northwest Turkey for year 2017. The X-axis refers to day of the year, and the Y-axis is AGDD. Bule color dots refer to wheat samples, orange dots refer to maize samples, grey dots refer to barley, yellow dots refer to paddy, and red dots refer to sunflower.

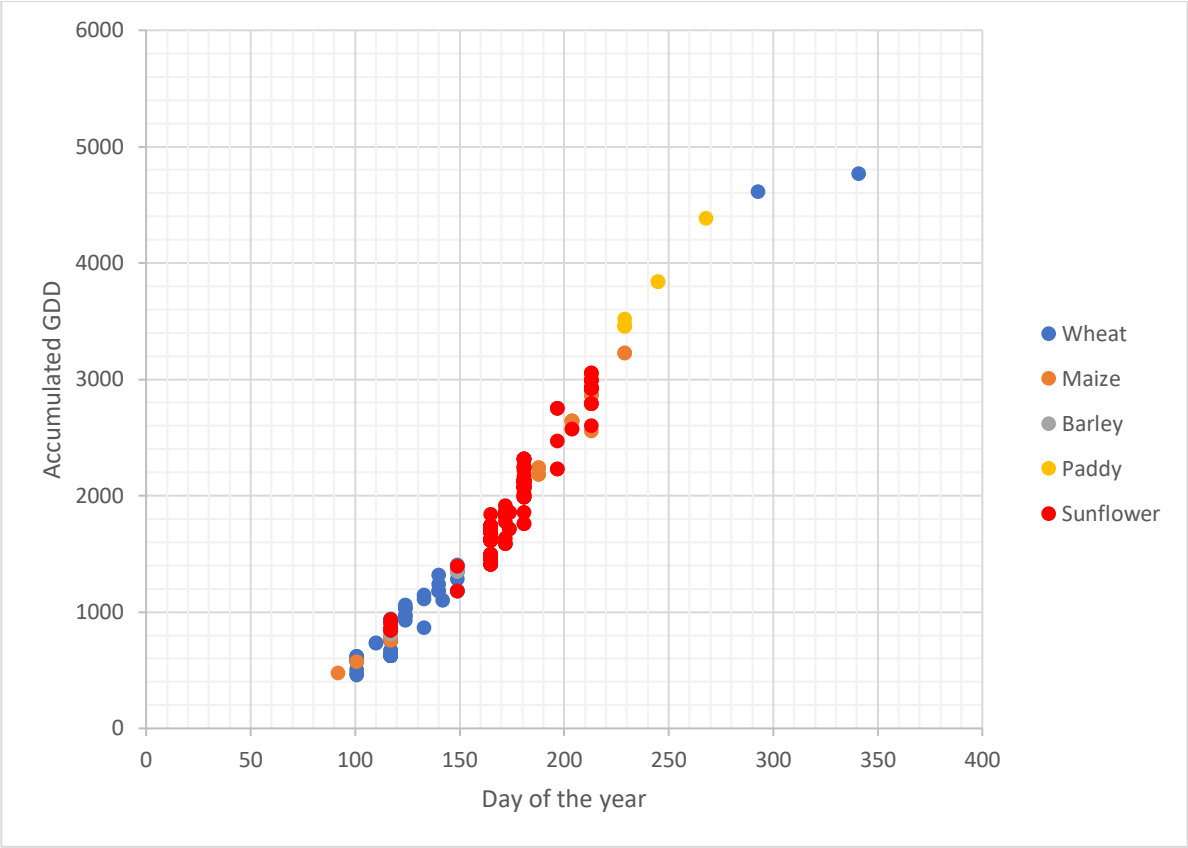

**Figure 2.3.4** EVI time-series trajectory of crop-types in Turkey derived from Landsat dataset for year 2017. The top panel refers to wheat and sunflower EVI signatures, the middle panel refers to maize and canola EVI signatures, and the bottom panel refers to paddy and barley EVI signatures. X-axis refers to day of the year and Y-axis refers to EVI value.

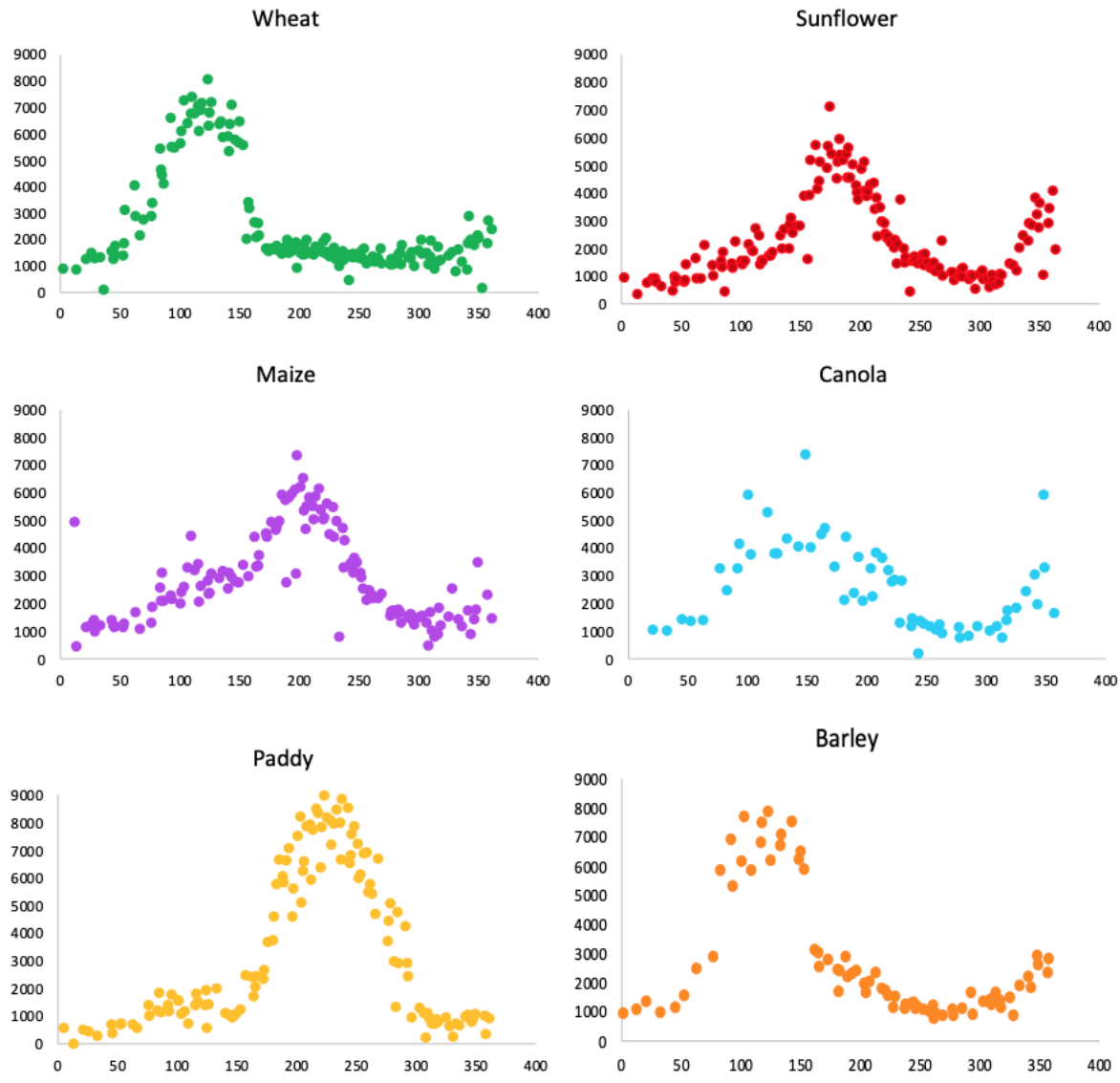

**Figure 2.3.5** Wheat mapping results for years 2001-2020 for a selected location in the study area covering Turkey, northcentral Bulgaria, northeast Bulgaria, southcentral Bulgaria and southeast Bulgaria. (The first column refers the very-high-resolution imagery background (VHRI) from GEE background display and remaining columns represents the mapping year. Each row represents the region in the study area).

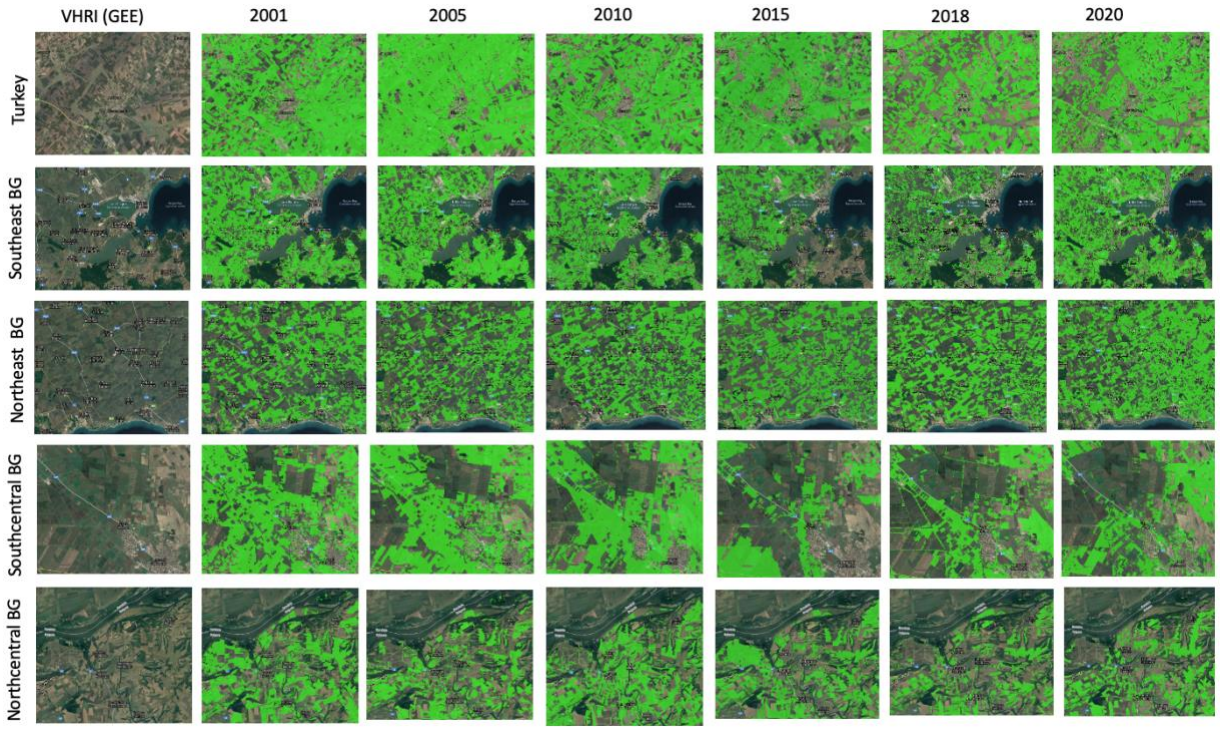

**Figure 2.3.6** Cropland extent mapping results in the study area. The left column refers to cropland extent change map from 2000 to 2010 and the right column refers to cropland extent change map from 2010 to 2018. The top panel refers to entire region change maps and bottom panels are zoom-in insets of the respective change maps.

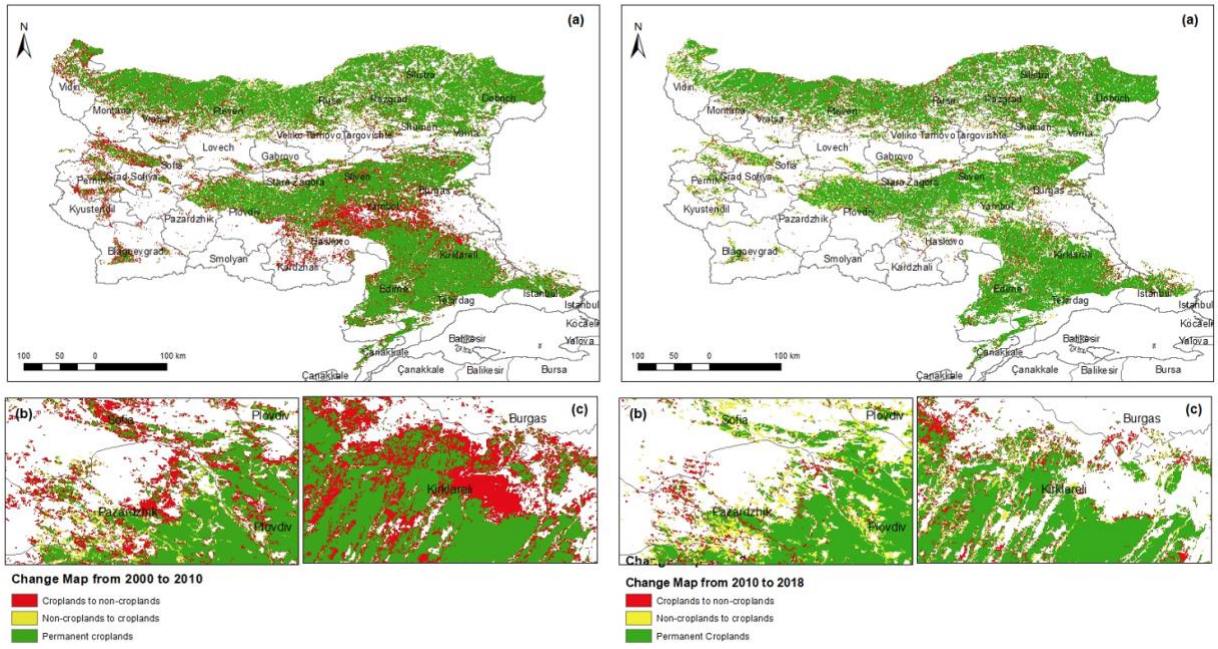

**Figure 2.3.7** Areal statistic comparisons between wheat area estimates derived from government statistics and those produced in this study for years 2004 to 2012 (X-axis refers observed wheat areas from government and Y-axis refers to mapped wheat areas in this study. The top panel refers years 2004, 2005 and 2006; the middle panel refers to years 2007, 2008 and 2009; and the bottom panel refers to years 2010, 2011 and 2012).

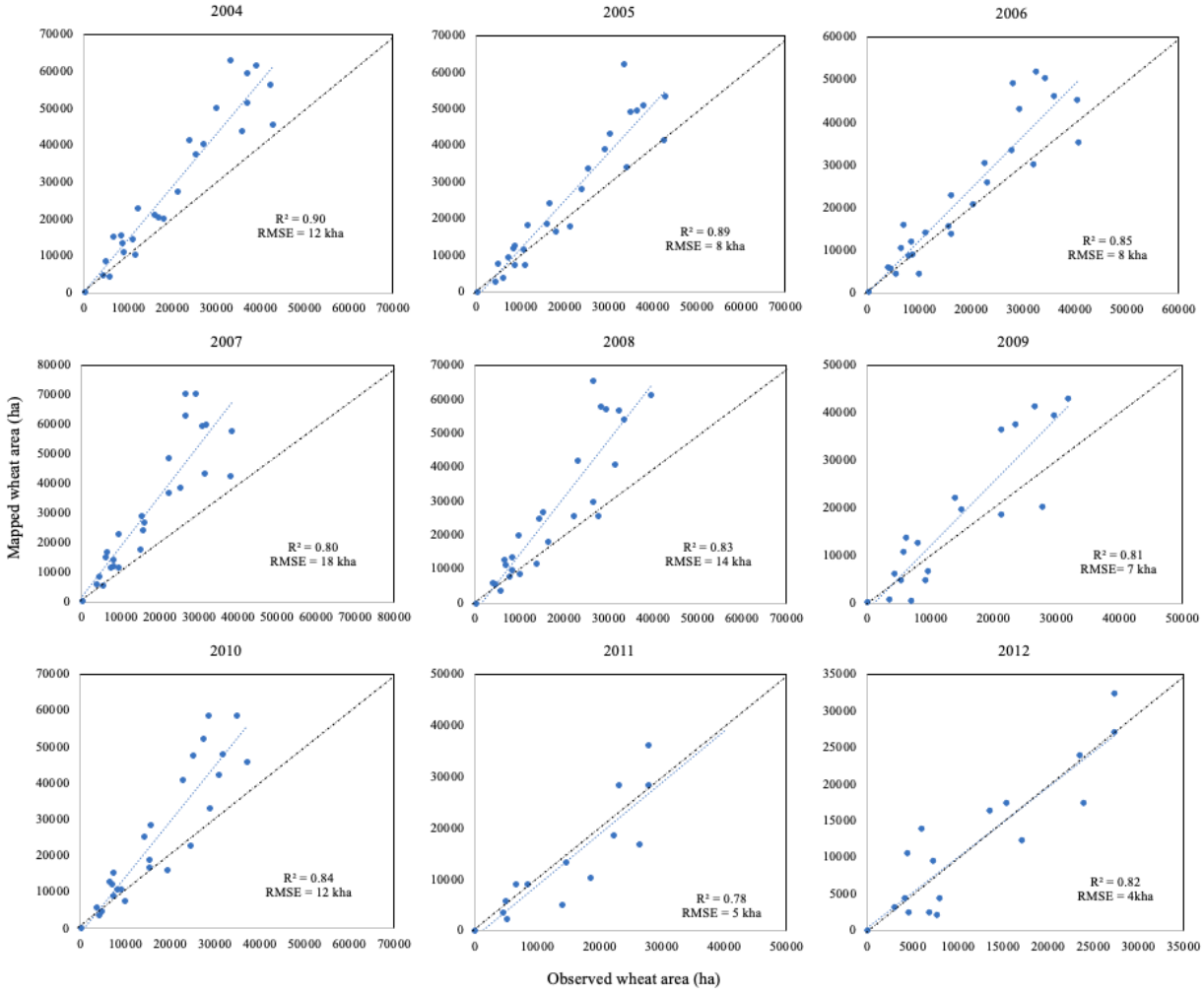

**Figure 2.3.8** Areal statistic comparisons between wheat area estimates derived from government statistics and those produced in this study for years 2013 to 2020 (the X-axis refers to observed wheat areas from government date and the Y-axis refers to mapped wheat areas in this study. The top panel refers to years 2013, 2014 and 2015; the middle panel refers to years 2016, 2017 and 2018; and the bottom panel refers to years 2019 and 2020).

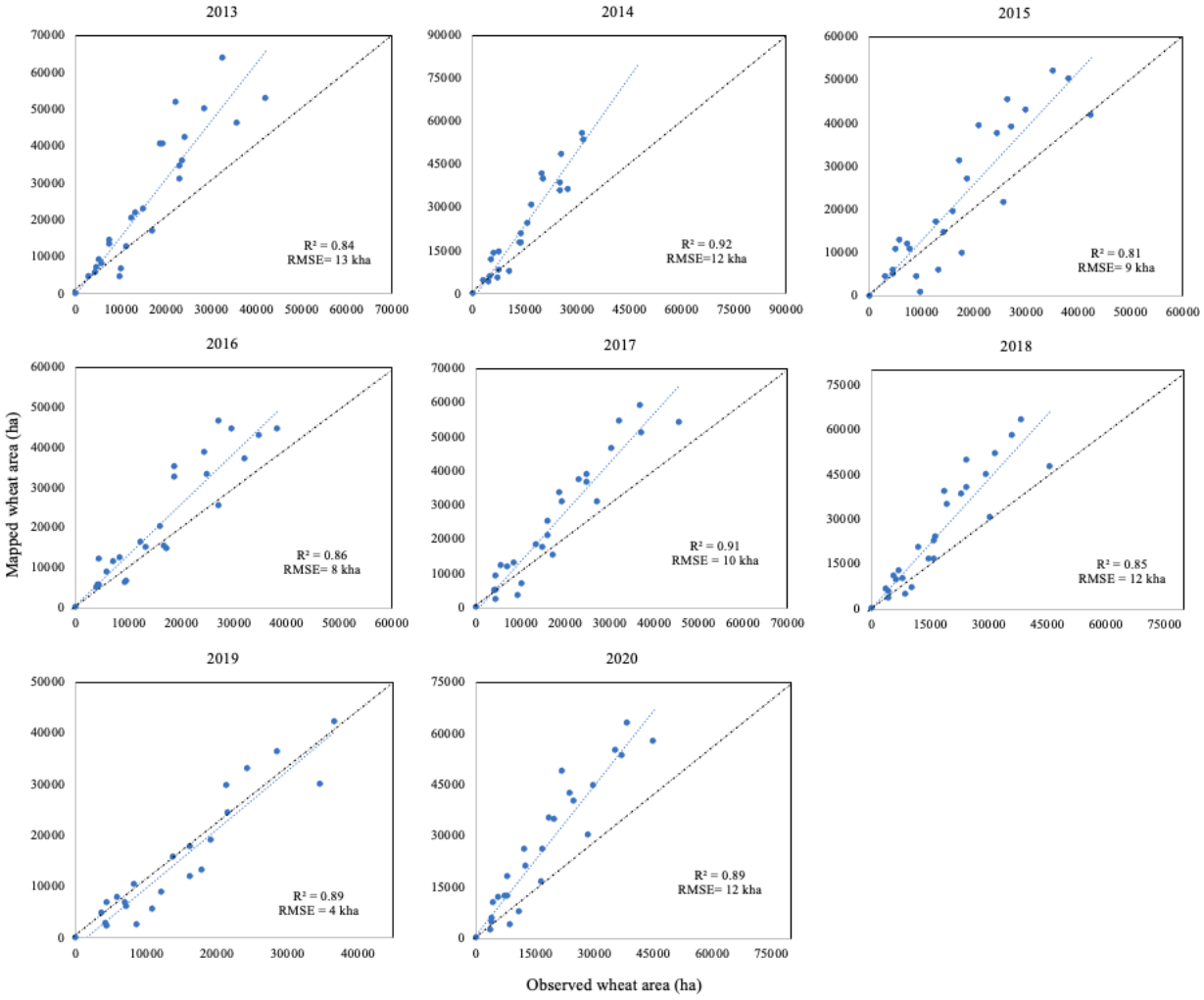

**Figure 2.3.9** Map-to-map comparison between this study area wheat map and the Rufin et al. winter crop map for year 2015 in NW Turkey. Left panel refers to areal statistics comparisons for each district in NW Turkey, with the X-axis referring to wheat areas estimates from this study and the Y-axis referring to wheat area estimates from the Rufin et al study. The right panel refers to visual representation of wheat area map from sample location in NW Turkey. The first column refers to VHRI from GEE; the second column refers to wheat mapped in this study; and the third column refers to wheat map from the Rufin et al. study.

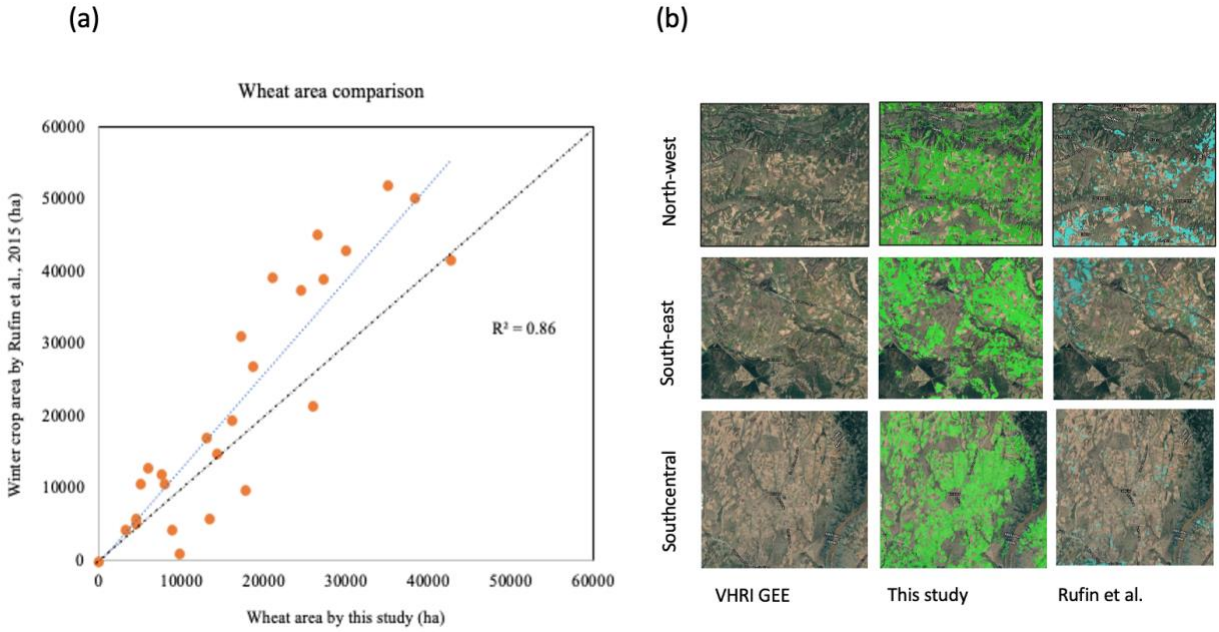

## Tables

**Table 2.3.1** Characteristics of multi-temporal Landsat data with three Landsat sensors (LC8, LT5 and LE7) for all the mapping years between 2001-2020 used in the study. Color code ranging from yellow to green represents low to high values.

| | Jan | | | Feb | | | March | | | April | | | May | | | Jun | | | Jul | | | Aug | | | Total |
|---|---|---|---|---|---|---|---|---|---|---|---|---|---|---|---|---|---|---|---|---|---|---|---|---|---|
| | L5 | L7 | L8 | L5 | L7 | L8 | L5 | L7 | L8 | L5 | L7 | L8 | L5 | L7 | L8 | L5 | L7 | L8 | L5 | L7 | L8 | L5 | L7 | L8 | |
| 2001 | 10 | 15 | 0 | 7 | 18 | 0 | 11 | 20 | 0 | 8 | 25 | 0 | 14 | 26 | 0 | 22 | 29 | 0 | 24 | 31 | 0 | 21 | 23 | 0 | 304 |
| 2002 | 20 | 19 | 0 | 19 | 27 | 0 | 8 | 15 | 0 | 0 | 21 | 0 | 9 | 30 | 0 | 19 | 14 | 0 | 13 | 26 | 0 | 5 | 23 | 0 | 268 |
| 2003 | 0 | 11 | 0 | 0 | 16 | 0 | 0 | 21 | 0 | 0 | 25 | 0 | 0 | 17 | 0 | 6 | 4 | 0 | 25 | 3 | 0 | 24 | 9 | 0 | 161 |
| 2004 | 9 | 6 | 0 | 15 | 5 | 0 | 15 | 18 | 0 | 13 | 16 | 0 | 21 | 8 | 0 | 18 | 20 | 0 | 23 | 21 | 0 | 19 | 20 | 0 | 247 |
| 2005 | 11 | 12 | 0 | 7 | 8 | 0 | 15 | 19 | 0 | 15 | 16 | 0 | 14 | 17 | 0 | 27 | 16 | 0 | 16 | 14 | 0 | 18 | 27 | 0 | 252 |
| 2006 | 5 | 6 | 0 | 15 | 13 | 0 | 3 | 13 | 0 | 10 | 8 | 0 | 17 | 15 | 0 | 18 | 24 | 0 | 24 | 12 | 0 | 28 | 26 | 0 | 237 |
| 2007 | 19 | 11 | 0 | 14 | 13 | 0 | 17 | 16 | 0 | 11 | 23 | 0 | 24 | 17 | 0 | 27 | 20 | 0 | 27 | 21 | 0 | 29 | 19 | 0 | 308 |
| 2008 | 0 | 10 | 0 | 0 | 15 | 0 | 13 | 15 | 0 | 16 | 9 | 0 | 23 | 22 | 0 | 14 | 22 | 0 | 16 | 18 | 0 | 22 | 29 | 0 | 244 |
| 2009 | 8 | 8 | 0 | 11 | 10 | 0 | 9 | 6 | 0 | 20 | 21 | 0 | 26 | 23 | 0 | 25 | 24 | 0 | 27 | 25 | 0 | 30 | 23 | 0 | 296 |
| 2010 | 5 | 4 | 0 | 13 | 4 | 0 | 12 | 10 | 0 | 20 | 16 | 0 | 14 | 20 | 0 | 14 | 14 | 0 | 21 | 18 | 0 | 17 | 25 | 0 | 227 |
| 2011 | 10 | 6 | 0 | 13 | 9 | 0 | 13 | 13 | 0 | 9 | 15 | 0 | 21 | 14 | 0 | 14 | 16 | 0 | 15 | 20 | 0 | 28 | 28 | 0 | 244 |
| 2012 | 0 | 12 | 0 | 0 | 13 | 0 | 0 | 22 | 0 | 0 | 24 | 0 | 0 | 24 | 0 | 0 | 28 | 0 | 0 | 29 | 0 | 0 | 22 | 0 | 174 |
| 2013 | 0 | 6 | 0 | 0 | 11 | 0 | 0 | 8 | 0 | 0 | 19 | 14 | 0 | 26 | 20 | 0 | 29 | 28 | 0 | 31 | 28 | 0 | 21 | 32 | 273 |
| 2014 | 0 | 15 | 23 | 0 | 17 | 21 | 0 | 18 | 17 | 0 | 13 | 21 | 0 | 28 | 27 | 0 | 19 | 22 | 0 | 25 | 26 | 0 | 31 | 29 | 352 |
| 2015 | 0 | 19 | 25 | 0 | 10 | 13 | 0 | 21 | 22 | 0 | 19 | 24 | 0 | 27 | 27 | 0 | 26 | 28 | 0 | 30 | 30 | 0 | 30 | 29 | 380 |
| 2016 | 0 | 15 | 23 | 0 | 12 | 18 | 0 | 18 | 21 | 0 | 25 | 21 | 0 | 22 | 27 | 0 | 15 | 29 | 0 | 29 | 27 | 0 | 28 | 30 | 360 |
| 2017 | 0 | 13 | 18 | 0 | 18 | 23 | 0 | 11 | 20 | 0 | 23 | 26 | 0 | 19 | 27 | 0 | 26 | 28 | 0 | 27 | 26 | 0 | 30 | 32 | 367 |
| 2018 | 0 | 13 | 21 | 0 | 13 | 19 | 0 | 17 | 16 | 0 | 28 | 32 | 0 | 22 | 24 | 0 | 26 | 28 | 0 | 26 | 27 | 0 | 31 | 30 | 373 |
| 2019 | 0 | 15 | 14 | 0 | 22 | 26 | 0 | 27 | 27 | 0 | 15 | 21 | 0 | 26 | 30 | 0 | 29 | 32 | 0 | 25 | 27 | 0 | 32 | 26 | 394 |
| 2020 | 0 | 17 | 22 | 0 | 17 | 22 | 0 | 17 | 21 | 0 | 26 | 29 | 0 | 24 | 23 | 0 | 25 | 26 | 0 | 29 | 29 | 0 | 31 | 29 | 387 |
| Total | 97 | 233 | 146 | 114 | 271 | 142 | 116 | 325 | 144 | 122 | 387 | 188 | 183 | 427 | 205 | 204 | 426 | 221 | 231 | 460 | 220 | 241 | 508 | 237 | 5848 |

**Table 2.3.2** Crop calendar derived from USDA (Source: https://ipad.fas.usda.gov/ogamaps/cropcalendar.aspx).

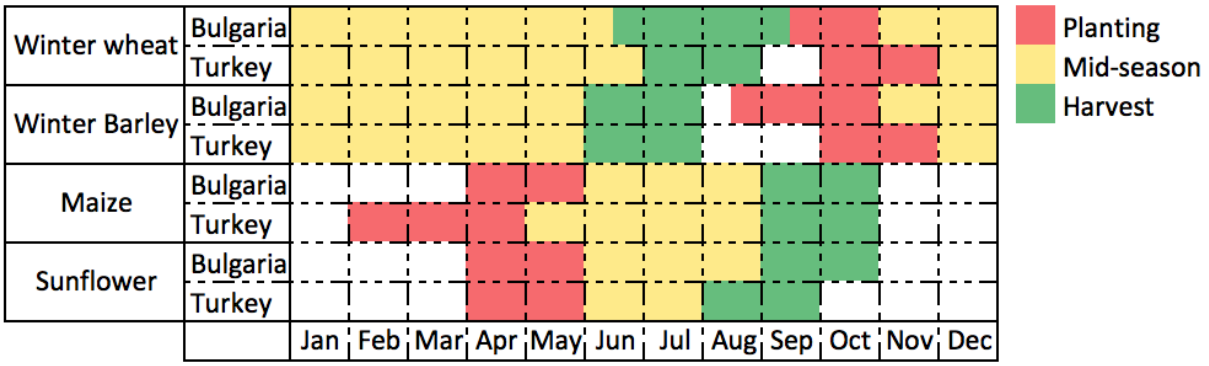

**Table 2.3.3** Accuracy assessment of temporal generalized model map for the base year (2018) and historical cropland maps in the study region. (PA refers to producer's accuracy and UA refers to user's accuracy).

| | Overall Accuracy | PA (crop) | PA (noncrop) | UA (crop) | UA (noncrop) |
|---|---|---|---|---|---|
| Final generalized model | | | | | |
| 2018 | 89% | 84% | 93% | 88% | 90% |
| Historical maps | | | | | |
| 1990 | 86% | 78% | 90% | 85% | 86% |
| 2000 | 90% | 86% | 92% | 88% | 91% |
| 2010 | 87% | 82% | 91% | 85% | 88% |

## Chapter 3

## Field-level wheat yield mapping in the cross-border area between Bulgaria and Turkey based on remote sensing and government statistics using a neural network approach

### Abstract

Wheat as a staple crop in the study area has approximately 60% share in the total cereal production of the region. While wheat yield data in Bulgaria is hardly available at the planning region (NUTS-2) scale (equivalent to census regions in the United States) and for a limited period (2001-2017), consistent and finer-scale crop yield estimates remain unavailable. Requirement of a large number of training samples, reduced correlation between yield and predictor variables, and generally lack of methods capable of capturing the non-linear relationships between input and output variables are few of the constraints in the development of fine scale crop yield estimates. To address these limitations, we developed a wheat yield estimation model based on remotely sensed observations, environmental characteristics, and government statistics and demonstrate its application at the village scale in the cross-border area. The model uses a multiple perceptron neural network (MLP-NN) approach trained with finest possible administrative-level public wheat yield records (such as LAU-1 for Turkey and NUTS-2 for Bulgaria) as the dependent variable, and satellite data-derived time-series vegetation indices, water stress variables, and topographical characteristics as independent variables. We evaluated the yield estimation model for spatial predictions as well as temporal predictions at two levels. In the first level, we used the training data only from Turkey at the districts level; and in the second level, we used a full set of training data from Turkey and Bulgaria. In the first dimension (temporal), we evaluated the model for one test year with the training dataset from all the other years; and in the second dimension (spatial), we tested the model for selected statistical units (districts/planning regions) with the training dataset from all the

remaining statistical units in the study region. Results show that number of inputs are less important than the quality of the inputs, and therefore, data preparation is a critical step identified in the model development. Time-series observations of respective variables from March to July were more significant than other months in the wheat growing cycle. MLP-NN approach performed better (R square of ~0.86) over Random Forest (RF) and linear regression (R square of ~0.65). For the temporal dimension, predictions at both levels have average $R^2$ ~0.62 with standard deviation (SD) of 0.07. The root mean square errors for the temporal dimension evaluation varied from 250 kg/ha to 900kg/ha. For the spatial dimension, predictions for the first level (i.e., Turkey-level) has average $R^2$ ~ 0.62 with SD of 0.07, and for the second level (full-dataset level) has average $R^2$ ~ 0.66 with SD of 0.09. The root mean square errors for spatial dimension evaluation varied from 200 kg/ha to 400kg/ha. The demonstrated village-scale final predictions aggregate when compared with observed wheat yield have $R^2$ ~ 0.86 for Turkey and ~0.78 for Bulgaria and t-test shows these two populations are not statistically different at the level of significance of 0.001. The uncertainty in wheat yield estimates is mainly due to the different modes of observed wheat yield records in the respective countries. The proposed wheat yield model has the potential to provide acceptable wheat yield predictions at any resolution from individual pixels to fields to villages or statistical regions. Such estimates offer the opportunity to assess the drivers of wheat yield change at the farm level in the study area.

## 3.1 Introduction

Crop yield is a basic indicator of support policy and global food security-related studies (Gibbs et al., 2008; Deryng et al., 2011; Ray et al., 2012). Detailed crop yield estimates of major food crops according to season and location are essential for regional- to global-scale environmental impact assessments (Kumar, 2016; Stuart et al., 2016). Accurate and timely crop yield estimates help to understand environmental stress and design a suitable adaptation framework for sustainable livelihood (Weiss et al., 2020; Ma et al., 2021). Administrative unit-level crop estimate datasets can be easily available from government statistical departments, but they come with certain drawbacks such as inconsistent methods of data collection (Doraiswamy et al., 2003; Ilizumi et al., 2016; Meyfroidt et al., 2019); different definitions of land use types in different countries or geographic units (Verburg et al., 2011; Burke et al., 2017); lower granularity such as administrative level units (for example, province or district level) (Hunt et al., 2019); and limited historical records (Ray et al., 2015; Lobell et al., 2013).

Wheat is the major harvested commodity in the cross-border study area between Turkey (Özdoğan, 2011; Vanli et al., 2020) and Bulgaria (Alexandrov et al., 2000). It is observed that wheat yield estimate in the last 20 years has distinct trends and patterns in the six regions (northeast Bulgaria, northcentral Bulgaria, southeast Bulgaria, southcentral Bulgaria, and northwest Turkey) of the study area, although they have similar agroclimatic characteristics (FAOSTAT, 2020; TurkStat, 2020; NSI, 2020). For example, wheat yield in southeast (SE) Bulgaria rapidly increased (about 10%) from 2007 to 2012 but, wheat yield in southcentral (SC) Bulgaria decreased in the same period (NSI, 2020). It is noted that both regions had similar agricultural support policy implementation (for 2001 to 2017), the individual impacts of these policies may look quite different. It is observed that overall wheat yield estimate in northwest (NW) Turkey has increasing

trends in the last 20-years, but wheat yield trends in Bulgaria increase only after 2007 (NSI, 2020; TurkStat, 2020). To explore this between- and within-country disparity in wheat yield trends and to assess the drivers of change at regional to field scales, consistent wheat yield estimates are essential. Field-level wheat information also allows examination of environmental variables within districts, which may not be captured at coarser country-level datasets (Duncan et al., 2015; Anderson et al.,2016). In our study area, wheat yield estimates are only available at planning-region (NUTS-2) scale in Bulgaria (NSI, 2020). To perform finer-scale policy analysis or to design a decision-making framework for farmers it is important to have high-resolution crop yield estimates.

Many studies recently presented crop yield prediction frameworks for different locations and crop types using either physiological crop model simulations (Hansen and Jones, 2000; Srinivasan et al., 2010; Moriondo et. al., 2011; Kang et al.,2019, Fuzzo et al., 2020) or empirical approaches (Bolton and Friedl, 2013; Lobell et al., 2015; Shook et al., 2021). Crop simulation models are highly dependent on large-scale crop canopy-related information and are limited for large area application (Xia et al., 2019). Empirical approaches to predict crop yield are getting popular within remote sensing community due to the availability of quality satellite data from Landsat and Sentinel data missions and advancements in machine learning models (Cai et al., 2018; Shao et al., 2019; Khaki et al., 2020).

The Landsat satellite mission has a long historical record, bi-weekly temporal resolution, a range of bands, data consistency, and public availability (Irons and Masek, 2006). These data characteristics provide great potential for its use in yield prediction through different vegetation and water indices (Roy and Yan, 2020). Also, MODIS and Sentinel-2 data missions provide consistent information about environmental variables (Chen et al., 2020; Gómez et al., 2021). Crop

yield model developments also benefit greatly from climate and water balance-related data inputs derived from satellite and ancillary data simulations. A few examples of such data are: TerraClimate (Abatzoglou et al.,2018), ERA5 (Muñoz Sabater, J., 2019), Global Land Data Assimilation systems (GLDAS) (Rodell et al., 2004), and Parameter-elevation Regressions on Independent Slopes Model (PRISM) (Daly et al., 2015).

Machine learning models have great potential to make field-scale yield estimates with linear or non-linear relationships between observed crop yield and related time-series environmental information about soil, water, and crop type (Basso et al., 2019; Dang et al., 2020; Wang et al., 2020). Simple statistical models using linear regression analysis are usually sensitive to noise and inconsistency (Sellam et al., 2016). A neural network approach has been observed to be effective for crop yield predictions due to its strength in non-linear data handling (Kaul et al., 2005; Khosla et al., 2019). Deep learning models with multiple-layer structures are usually exceptional in their performance over traditional neural networks and other methods, but they can be costly and require large amounts of training data (Chollet, 2017).

In our study area, the literature presents limited studies on crop yield prediction (Ozkan et al., 2002; Özdoğan, 2011; Çakır, 2014; Yildirak et al.,2015; Kogan et al.,2016). Particularly in Bulgaria, only one study (Kogan, 2016) performed a simple statistical model development to predict maize yield in the Pleven region of northern Bulgaria using Advanced Very High Resolution Radiometer (AVHRR)-based time-series vegetation indices and corn yield data acquired from local field experiments. Moreover, wheat yield prediction at LAU-2 scale or field scale remains unknown for the study area.

To address the wheat yield data availability and accessibility limitations in the cross-border area, this study aims to build a robust framework to model wheat yield estimates at LAU-1 scale

(county scale) based on an empirical modeling approach and remote-sensed environmental variables. For our study area, the set-up with one side of the cross-border area (Turkey) having local (LAU-1 level) wheat yield estimate availability, and the other side (Bulgaria) with only regional (NUTS-2 level) wheat yield estimates, provides the perfect opportunity to build and test a local-scale wheat yield estimate model for the entire study area. We used the MLP-NN approach and evaluated the model at local scale to predict the unknown year and unknown statistical unit wheat yield estimate in the study area. Specifically, we used satellite-derived environmental data inputs with time-series information related to crop biomass, water stress, heat stress, and crop phenology-related indices from Landsat time-series. Lastly, we evaluated the local-scale wheat yield trends and patterns of the study area. It is noted that the wheat yield model was validated at district (LAU-1) scale, and final predictions were performed at village scale (LAU-2 of Bulgaria) in order to understand the local wheat yield trends and patterns of the study area.

## 3.2 Methodology

### 3.2.1 Study Area

The study area is geographically situated in Mediterranean Europe (Figure 3.1) across the border between Turkey and Bulgaria. These cross-border areas are also known as Northern Thracia (Bulgaria) and Eastern Thracia (Turkey). The Bulgaria-side cross-border area covers northcentral (BG32, NUTS-2), northeast (BG33, NUTS-2), southeast (BG34, NUTS-2) and southcentral (BG42, NUTS-2) planning regions with 18 provinces (NUTS-3) and 177 municipalities (LAU-1). The Turkey-side cross border area covers the northwest or Tekirdag subregion (TR21, NUTS-2) with 3 provinces (NUTS-3) (Edirne, Tekirdag and Kirklareli) and 26 districts (LAU-1). Agriculture is an important land use in the study region, covering more than 60% of the landscape in Bulgaria and Turkey, operated under very similar agro-ecological and climatic patterns (FAO,

2019). Wheat is the major crop harvested in the winter in the study region. This study area is situated on the border of the European Union. It is observed that the Bulgaria side of the cross-border area had major changes in agricultural support policies after its accession to the European Union in 2007, but the Turkey-side cross-border area did not have any such transitions (Table 3.1). While similar environmental characteristics in both cross-border areas suggest equal trends in wheat area and yield, the observed trends and patterns for Bulgaria and Turkey are distinct. This suggests underlying socio-economic implications for the wheat yield change in both countries. Although Bulgaria had similar country-wide agricultural policy transitions after 2007, the local wheat trends are different. This suggests that socio-economics may have different implications on different statistical-unit-level (inter-country and inter-region) yield trends, and detailed or high-resolution crop yield measurements would be beneficial to study the policy and food security at the local scale in the study area. Further, Bulgaria has a very low-resolution (only NUTS-2 level) time-series wheat yield dataset and Turkey has a high-resolution (LAU-1 level) yield dataset publicly available. Therefore, this study area provides a great opportunity to build a LAU-1 level wheat yield model with the help of remotely sensed environmental variables and predict higher-resolution wheat yield estimates.

### 3.2.2 Datasets

To build the wheat yield estimate model of the study area, two main types of data inputs are necessary: 1. the highest possible administrative-level wheat yield records archived from respective statistical departments of each country, and 2. environmental and topographical variables extracted using satellite imageries or other ancillary datasets (Table 3.2 and Table 3.3).

*Wheat yield records*

On the Turkish side, we collected all available LAU-1 level wheat yield records from 2004 to 2020. There are 26 districts (LAU-1 scale units) in Turkey, with three provinces (or NUTS-3 level units). On the Bulgarian side, we collected planning region-scale (NUTS-2 level) wheat yield records from 2001 to 2017. There are four planning regions and 155 municipalities (LAU-1 level units) in Bulgaria. The distribution of average wheat yield in each statistical unit in the study area is shown in Figure 3.1.

*Satellite data inputs*

Crop-biomass-related variables are widely used in crop yield prediction models. Satellite-based time series vegetation indices are suitable to observe the changes in crop biomass and cropping cycles. This study used Landsat surface reflectance (SR) data from three sensors (Landsat-5 TM, Landsat-7 ETM+ and Landsat-8 OLI) acquired between 2001 and 2020. The entire collection of Landsat data amounted to 7,502 individual images collected over six Landsat tiles ranging from paths 181 to 183 and rows 30 to 31. Each image in the collection was screened for cloud and cloud shadow using the image masks provided by SR products. This study calculated Enhanced Vegetation Index (EVI), Normalized Difference Vegetation Index (NDVI), Normalized difference Water Index (NDWI), and Green Chlorophyll Index (GCI) using blue, red, green, near infrared (NIR), and shortwave infrared (SWIR) bands of respective Landsat SR products (Equations 1 to 4 below)

$$EVI = G \times \frac{(NIR - RED)}{(NIR - C1 \times RED - C2 \times Blue + L)} \quad (1)$$

$$NDVI = \frac{NIR - RED}{NIR + RED} \quad (2)$$

$$NDWI = \frac{NIR - SWIR}{NIR + SWIR} \quad (3)$$

$$GCI = \frac{NIR}{Green} \quad (4)$$

where NIR, RED, Blue, Green, and SWIR corresponds to surface reflectance values in the Landsat near infrared, red, blue, green, and short-wave infrared electromagnetic spectrums, respectively. L is the canopy background adjustment that addresses non-linear, differential NIR and RED radiant transfer through a canopy. C1, C2 are the coefficients of the aerosol resistance term, which uses the blue band to correct for aerosol influences in the red band and G is the gain factor. The coefficients used here are L=1, C1 = 6, C2 = 7.5, and G = 2.5 adopted from USGS product guide for Landsat SR derived spectral indices (https://landsat.usgs.gov/sites/default/files/documents/si_product_guide.pdf). The reason for using EVI is that it has been shown to have higher sensitivity in high-biomass regions and proved to be reliable to study croplands because of its coupling with the canopy background signal and reduction in atmospheric influence (Kawamura et al., 2005; Wardlow et al., 2010). NDVI and NDWI measure the vegetation greenness and moisture content and are widely used among the crop yield modeling community to monitor crop phenology and crop water content. GCI measures the canopy chlorophyll content of crops using light-use efficiency, and it can be used to indicate crop health (Gitelson et al., 2005). Further, the vegetation indices were aggregated temporally to get monthly and seasonal composites, and spatially to get the values for each selected statistical unit (districts or regions) in the yield prediction model. The seasonal composites included valid satellite data inputs from January to August according to wheat cropping cycles in the study region (Table 3.3). The entire composites were further masked with the temporal wheat area and cropland masks

created in the Chapter 2 of this dissertation (Phalke et al., 2020). The entire data process ranging from Landsat data collection, preprocessing, indices calculation, and extraction was conducted on the Google Earth Engine (GEE) platform.

*Weather data*

This study included four primary weather-related data inputs: maximum temperature (°C), minimum temperature (°C), rainfall (mm), and wind speed (m/s). These inputs were extracted using a TerraClimate dataset available through the GEE archive. This dataset is 2.5 arc minutes (~4km at the equator) in resolution and includes monthly aggregated climate and climate water balance data for global terrestrial surfaces (Abatzoglou et al., 2018). This study extracted the dataset from January to August as well as the previous October to cover the cropping season cycle, along with the previous year's rainfall accumulations (Table 3.3). Final preparation of this data included masking the dataset to wheat area maps and then aggregating it to the respective statistical units.

*Soil and topographical data*

This study included soil moisture (mm), actual evapotranspiration (mm), and potential evapotranspiration (mm) variables derived using a one-dimensional soil water balance model from the TerraClimate dataset (Abatzoglou et al., 2018) from January to August and the previous October, similar to the weather data. Soil moisture content and water evaporation from the surface are effective to monitor crop growth and crop water stress, and they are widely used in the crop yield prediction models. Topographical variables such as slope were derived from the Shuttle Radar Topographic Mission (SRTM) digital elevation model (DEM) (http://www2.jpl.nasa.gov/srtm/) (Farr, 2007). Slope provides information about the inclination of the surface and is observed to be a suitable environmental variable for crop yield prediction

modeling. Slope values were extracted for the extent of wheat area masks and then aggregated to the selected statistical units (Table 3.3).

### 3.2.3 Modeling framework

The principal step in crop yield modeling is appropriate model selection according to data input characteristics and expected output requirements. This study used an empirical modeling approach due to suitable data availability compared to a data assimilation approach. We tested the simple as well as complex statistical models in the study area. Our previous study showed that simple statistical models can also be beneficial over machine learning models for classification or prediction problems with limited training data availability (Phalke and Ozdogan, 2018). With this context, we tested simple linear regression (SLR), Random Forest (RF), and multiple perceptron neural networks (MLP-NN) for predicting the wheat yield in the study area. Our primary results showed MLP-NN performed better over other algorithms, and therefore we selected MLP-NN for wheat yield predictions in the study area.

*Basics of multiple perceptron neural network*

Neural networks are supervised learning models with three important layers: i) input layer; ii) hidden layer; and iii) output layer. The input layer provides the dependent and independent variables information to the system. Each perceptron or learning node in the model is created from each independent variable input in the model and contains input value; weight and bias; summation function; and activation function (Figure 3.3). A neural network has the capability to learn from each given observation separately while understanding its relationship with neighboring nodes. In simple understanding, NN can be considered as a probabilistic model where Y is a dependent variable with Gaussian distribution and N as inputs weighted by hidden layers in the model. NN creates multiple matrices through its hidden layer learning, and each matrix represents the

individual weight calculated from its hidden layers. The bias value in the network quantifies the outlier or data noise of the model. Neural networks trained for more than one hidden layer are called deep learning models. Neural networks can also be studied through probabilistic function characteristics of each node output; they can then be called Bayesian Neural Networks. Data input characteristics decide the performance of each type of neural network. Deep neural networks are widely popular to have the best performance, but they are costly and dependent on large computing power. Complex problems like crop yield predictions exponentially benefit from neural networks as they scan all the complicated characteristics of the input independent variables in response to dependent variables and simplify them in each hidden layer matrix.

*Model data preparation*

Model input data is prepared to optimize the accuracy of the output over optimized speed. In the first step, data was screened for missing values and unique values, and the threshold for its selection was set. This study didn't exclude any data fields. Further, data are processed to improve its quality with suitable outlier handling mechanisms. There were 98 outliers identified in the dataset, which may add uncertainty in the output. But we kept all the outliers in the dataset because MLP-NN has better potential to handle outliers than other algorithms. We also tested several imputation algorithms for missing data replacement, and the time-series vegetation indices values were imputed for missing months. A total of 16 imputations were performed for time-series vegetation index variables. Lastly, the entire dataset is transformed using the Box-Cox transformation to normality.

*MLP-NN model architecture and setup*

In this study, our goal is to predict wheat yield in the study area. Therefore, the architecture design (Figure 3.2) has one endpoint and input layers from each statistical unit of each country.

After excessive testing of the model for various settings, we selected the model with depth of two hidden layers with sigmoid activation function. The threshold for minimum number of units in hidden layers is one and the maximum number of units is 50. The training is performed in batch size of 50 and 1000 epochs. The scaled conjugate gradient optimization algorithm was selected with initial lambda of 0.0000005 and initial sigma of 0.00005 with zero interval center and $\pm$ 0.5 interval offset.

### 3.2.4 Feature importance analysis

This study performed feature variable importance analysis based on two methods: i) sensitivity analysis; and ii) linear correlation between input variables and observed wheat yield records, also called as exploratory analysis. Sensitivity analysis is a powerful tool to interpret the variable importance by examining each feature variable effect on the output of the model. It basically transforms the testing variable value or simply removes it from the training set and analyzes its impact on the performance of the model trained with other remaining variables. The sensitivity analysis provides the variable importance values and normalized importance for each variable.

In the second method of variable importance, this study performed exploratory analysis of the data inputs. In order to understand the relationship between each variable, we performed bi-variate correlation analysis, and the results were analyzed for Pearson's correlation coefficients and a two-tailed test of significance. Both tests may provide different findings, but the combined variables according to both are found to be effective for optimum performance of the model.

### 3.2.5 Model evaluation

The developed MLP-NN model was thoroughly validated to assess its performance. The model was validated on the two levels and along the two dimensions. The two levels of model validations are: i) level 1, the country model; and ii) level 2, the entire study area model. In the country-model level, the model used training data from only one country. For example, the Turkey model will have its training data only from Turkey. Since the Bulgaria-side cross-border area had only data from two regions, we renamed the country model to the Turkey-data model. In the entire study area model (level 2), the training data was from the entire study area (i.e., from Turkey as well as Bulgaria). The two dimensions of model validations are: i) temporal validation (dimension 1); and ii) spatial validation (dimension 2). In temporal validation, the model is trained over all but one test year. For example, if the dataset ranges from 2004 to 2020, to test the wheat yield validations for year 2004, the model is trained based on all the remaining years (i.e., 2005 to 2020) and then applied to predict the 2004 wheat yield. In spatial validation, the model is trained with the dataset from selected statistical units and tested for the predictions of all the remaining statistical units in the area. For example, we have 26 district wheat yield records in Turkey; we selected 20 district records for training and the remaining six districts were kept for testing.

In summary, we carried the four evaluations as given in Table 3.4. And lastly, we tested the model for its aggregated prediction performance. For this purpose, we built the model using all the Turkey district datasets and all the regions from Bulgaria and applied it to all the Bulgaria municipals or LAU-1 units, then averaged the value of predictions to get the aggregate regional yield prediction for NUTS-2 units of Bulgaria. Then the observed and predicted aggregated regional yields were compared.

All the validations were evaluated for two matrices, $R^2$ and RMSE, as given in the below equations 5 and 6

$$R^2 = 1 - \frac{\sum_{i-1}^{n}(y_i - \hat{y}_i)^2}{\sum_{i-1}^{n}(y_i - \bar{y}_i)^2} \quad (5)$$

$$RMSE = \sqrt{\frac{1}{n}\sum_{i-1}^{n}(y_i - \hat{y}_i)^2} \quad (6)$$

where n is the number of samples; $y_i$ and $\hat{y}_i$ are the observed and estimated yield for the ith statistical unit; and $\bar{y}$ is the average of the observed yield values.

### 3.2.6 Wheat yield predictions

The main goal of this exercise was to demonstrate high-resolution wheat yield predictions of the study area using the final wheat model built in sections 2.2 to 2.4 and evaluate these high-resolution estimates. In this study, we chose village scale wheat yield as a sample scale for the demonstration. It is noted that the proposed model has the potential to predict yields from regional to field-scales but in this study, we will demonstrate village-scale predictions as an example. Village boundaries of Turkey were accessible through ancillary sources, but Bulgarian village boundaries were not accessible.

The first step of this exercise was to derive the equivalent boundaries of villages. Voronoi analysis allowed us to create polygons or area shapefiles equivalent to village areas of the study area using a human settlement layer. The accurate and high-resolution settlement layer was extracted from the recent Sentinel-2 based 10-m resolution land use and land cover map by ESRI (Karra and Kontgis, 2021). The centroid of the settlement polygons and the average area of Turkish villages were used as inputs to develop the Voronoi-based polygons. This method generated ~1000

village equivalent polygons for Turkey and ~2800 village polygons for Bulgaria. We named these polygons “villages” for ease of understanding.

In the next step, we extracted all satellite-based inputs for these villages and predicted the wheat yield using the final wheat yield model built in this study. The predicted wheat yield for these villages is validated by two methods. First, we compared the observed country yields with the predicted aggregate of country wheat yields through scatterplot and the paired t-test. A ‘t-test Paired Two Sample for Means’ tool is commonly used to compare two different methods of measurement and two populations of the same entity (Ross et al., 2017). In the second method, we analyzed the distributions of wheat yields in each year and each region while comparing the observed wheat yield of the specific region and specific year. For this purpose, we plotted the wheat distribution histograms of each region for each year along with the mean values for the same instance.

## 3.3. Results

### 3.3.1 Feature importance analysis

*Sensitivity analysis*

The results of the sensitivity analysis showed that vegetation indices such as GCI, NDVI and EVI are more important and receive higher weights over other environmental variables (Figure 3.3). Soil moisture is observed to be the least important variable compared to all. Figure 3.3a shows the top 10 variables out of hundreds of other variables in the input data cube. It is observed that mid to late-season values of vegetation indices are significant for the yield model over early season values. The latitude variable was observed to have greater importance over the longitude. NDWI had significant value in the early and late season compared to mid-season values. Maximum

temperature values had more significance over minimum temperature. Precipitation (in October) and maximum temperature (in March) were observed to be the most important variables compared to other weather variables. Wind speed in March and April had significant importance over other months. Potential evapotranspiration had more importance over actual evapotranspiration.

*Correlation analysis*

The results showed that the Pearson correlation coefficient values for the entire dataset vary from -0.5 to 0.5. The results for the 2-tailed significance test showed that most of the variables are significant at the level of P>0.01. For the satellite data-derived indices, NDVI in January, NDWI in January and February, and GCI in January were not significant, according to the significance test. Weather variables in August were observed to be non-significant as well.

GCI and EVI seasonal 95$^{th}$ percentile value observed to be the highly correlated sequential variable (Figure 3.4). GCI, NDVI and EVI values in the late season were observed to be highly correlated variables compared to other variables. Precipitation in October and maximum temperature in March are highly correlated weather variables compared to other weather variables. Longitude was observed to be positively correlated to the wheat yield and latitude was negatively correlated with wheat yield. Soil moisture was observed to be the least correlated variable compared to other variables. Potential evapotranspiration had a high positive correlation coefficient in the months of June and July compared to other months and was observed to be overall highly correlated to the yield compared to actual evapotranspiration values.

### 3.3.2 Model evaluation

*Spatial prediction performance*

The results for the first-level, first-dimension evaluation (i.e., all spatial data) model tested in each region of the Bulgaria showed average $R^2$ of ~0.75. The highest $R^2$ of ~0.81 was observed for northeast Bulgaria and the lowest $R^2$ of ~0.60 was observed for southcentral Bulgaria as the test region. The second level and first dimension (i.e., country data or Turkey-data) model, produced an average $R^2$ of 0.61 with a standard deviation value of 0.08, and an average RMSE value of 435 kg/ha with a standard deviation value of 42.6 kg/ha. The highest $R^2$ of 0.77 was noted for iteration 5, with the lowest of 0.53 for iteration 3. The highest RMSE (487 kg/ha) was observed in iteration 3, and the lowest (358 kg/ha) was observed in iteration 5 (Figure 3.5).

*Temporal prediction performance*

The results for first level and second dimension (i.e., all temporal data) model showed that the average value of $R^2$ for the 2004 to 2020 test years was 0.66 (0.09 standard deviation) and average RMSE for the same period was 537 kg/ha (180 kg/ha standard deviation) (Table 3.6). The highest $R^2$ (0.80) was observed in the year 2018 vs lowest (0.52) for 2005. The lowest RMSE (250 kg/ha) was observed in the year 2018 while the highest (932 kg/ha) was observed in 2020.

For the Turkey model, the average value of $R^2$ was observed to be 0.62 with standard deviation of 0.07, and the average value of RMSE was observed to be 515 kg/ha with standard deviation of 180 kg/ha. The highest $R^2$ (0.77) for the Turkey-data model was observed for the year 2014 and lowest (0.53) was observed in 2005. The lowest RMSE (268 kg/ha) was observed for 2014 and highest RMSE (842 kg/ha) was observed for 2008 (Figure 3.6a and 3.6b).

### 3.3.3 Wheat yield predictions

Voronoi analysis resulted in the creation of village-equivalent area boundaries in the study area (Figure 3.7). Turkey has ~1000 villages and Bulgaria has ~3600 villages with ~900 villages

in each region. This study predicted the village-scale wheat yield for the derived village boundaries and mapped the village-scale wheat yield from 2001 to 2020 for the entire study area (Figure 3.8).

*Comparison of the observed and the predicted wheat yield*

The first methods of comparison presented scatterplots of observed and predicted wheat to understand the trend between two estimates (Figure 3.9). The Turkish side has $R^2$ of ~0.86 with RMSE of 189 kg/ha, and the Bulgarian side had $R^2$ of ~0.78 with RMSE of 671 kg/ha when the observed wheat yield was compared with the predicted aggregate wheat yields. In Turkey, the Edirne province had the highest $R^2$ (0.82). The eastern regions in Bulgaria had the highest $R^2$ (0.73) compared to central regions. In Turkey, the Kirklareli province had the lowest RMSE (223 kg/ha), and in Bulgaria, the southcentral region had the lowest RMSE (297 kg/ha). Overall, the predicted wheat yield is significant and reliable when compared to observed statistics. It is observed that the predicted Bulgarian wheat yield is slightly lower than the observed yields, although the trends are significant and similar.

The second method of comparison in this study used a paired t-test. The results of this test presented statistics such as mean, variance, Pearson correlation, and t-stat. The results for the Turkey comparison had Pearson correlation coefficient of 0.93 and t-stat of -2.2. The results for the Bulgaria comparison had Pearson correlation coefficient of 0.88 and t-stat of -6.3 (Table 3.7). Overall, the predicted wheat yield was significantly closer to the observed yield as per its value as well as its trend. The results of the t-test are summarized in Table 3.7.

*Analyzing the wheat yield distributions*

This study analyzed all-year averages as well as annual wheat distribution plots of each region of the study area. First, we analyzed the overall average of observed as well as predicted

wheat distribution plots (Figure 3.10). Histograms for both the observed and the predicted yields were normally distributed and mostly overlapping (Figure 3.10). In southern Bulgaria and all districts of Turkey, the average observed wheat yield and predicted wheat yield lines are closely aligned with each other with minor differences. In the entire study area, the predicted wheat yields are slightly lower than the observed yields, and this difference is higher for northern Bulgaria compared to other regions (Figure 3.10).

The results for each year and each region's wheat yield distributions provided insights into the village-level wheat yield distributions of the region (Figure 3.11, 3.12, 3.13). In northcentral Bulgaria, the village-scale wheat yield distributions had gaussian shapes. The average predicted wheat yield of northcentral Bulgarian villages in years 2015 and 2017 did not match well with the observed wheat yield and are considered to be outliers. In case of southcentral Bulgaria, predicted wheat yield in 2008 was an outlier, but estimates for all other years were noted to be significant when compared to observed average yield values of the region. In Turkey, year 2010 wheat yield predictions for Edirne were different from the observed average, but all other regions and years had predictions in line with the observed average wheat yield quantities.

### 3.4. Discussion

Wheat yield prediction using an empirical modeling approach and remote sensing dataset presents several challenges, especially in data-limited areas. This study has estimated wheat yield with a detailed modeling framework at village or field-scale for Turkey and Bulgaria.

Wheat yield mapping model was trained with government statistics from Bulgaria (only at NUTS-2 units or planning region scale) and Turkey (only 36 LAU-1 unit or county-level). When compared to several statistical modeling approaches including linear regression and random forests and multilayer perceptron neural network (MLP-NN) produced the best estimates. The MLP-NN

architecture which allows deep learning to efficiently use every feature and reflect it to the outputs. The results of this study noted that, while performing simple data-cleaning techniques, our model performance didn't meet the expected outcomes. Advanced data-preparation methods (such as methods incorporating careful data cleaning, data structuring and careful handling of the outliers and if required data transformations) helped prepare the data for the model and further improve the model results. Different iterations of the model involving several combinations of inputs help to enhance the performance of the model. These iterations allowed the model to extract optimum information from each feature according to its importance and response to predictor function. We assessed the input features very carefully according to its importance (Figure 3.3 and Figure 3.4). GCI in April and June observed to be most important sequential variable for our model. End of April to July are the months when wheat is harvested in the region. Vegetation indices in the late growing period are observed to be important and they are positively correlated to the wheat yield. Precipitation in October is observed to be positively correlated with wheat yield, which is expected as wheat is generally planted in October in the region. Overall, growing season vegetation indices improve the performance of the model. Early and late season precipitation and temperature play important role in understanding the planting and harvesting conditions of the crop and therefore, these inputs are beneficial to the model.

Lastly, our proposed model was able to achieve $R^2$ of ~0.65 for both temporal and spatial predictions. The $R^2$ had a range of 0.5 to 0.6 for the test years 2001-2007, and after 2007 this range had improved to 0.6 to 0.8. We conclude that the model performance using only environmental and topographic variables without socio-economic input is limited. It is observed that Turkey had major agricultural reforms from 2001 to 2008 through the Agricultural Reform Implementation Project (ARIP), and that Bulgarian accession to the European Union in 2007, and the post-Soviet

era from 1991 forward, had underlying implications for the agriculture of this area. These socio-economic implications in the region are difficult to measure through only environmental changes.

It is also observed that the number of test samples to be predicted can have biased assessment of the performance of the model. In our case, we had relatively limited data for testing, and therefore the test results may have great uncertainty. For example, in the temporal prediction model, we had a test-data count of 26 (the number of LAU units in one year). In the case of spatial predictions, we had ~100 test cases, and the performance of the model was improved compared to the temporal prediction model test. The low correlation (~ -0.5 to 0.5) of the input features with the predicted variable was a major challenge to build the wheat yield model using a machine learning approach. This is another reason the performance of the model is limited compared to other crop yield modeling studies of other areas and/or crops.

We used village-scale administrative units to demonstrate how to effectively "downscale" disparate government statistics. It is noted that the proposed wheat-yield model can be downscaled to any required level from individual pixels to fields to statistical regions. However, it is expected the model uncertainty will increase as the granularity of desired predictions increase.

Overall, the proposed neural network approach allowed us to model a traditional difficult variable to estimate – crop yield. It is noted that the proposed methodological framework was found to be effective for the selected study area but its application in other regions may need further modifications.

### 3.5. Conclusions

This research provided a vigorous framework for reliable wheat yield mapping in the cross-border area between Turkey and Bulgaria using satellite observations, environmental variables,

and a neural network. In the preliminary tests, the capability of available and extracted input features was limited due to its low correlation with observed wheat yield statistics. An MLP-NN approach provided the opportunity to build a reliable model. We observed that the preliminary data preparation and the selection of appropriate inputs play a major role in the performance of machine learning models. In case of this study, the input feature set was not only limited in number, but also had a lot of noise and missing values. However, the MLP-NN was minimally impacted from noise or missing observations, and it allowed us to use as much available data for modeling. This study evaluated the model not only for temporal predictions of the wheat yield, but also for spatial predictions. The results showcase the only village-scale wheat yield dataset from 2001-2020 for the cross-border area between Turkey and Bulgaria with important implications to uncover policy implications on wheat production in the region.

**References**

Abatzoglou, J.T., S.Z. Dobrowski, S.A. Parks, K.C. Hegewisch, 2018, Terraclimate, a high-resolution global dataset of monthly climate and climatic water balance from 1958-2015, *Scientific Data 5*:170191, doi:10.1038/sdata.2017.191.

Alexandrov, V. A., & Hoogenboom, G. (2000). The impact of climate variability and change on crop yield in Bulgaria. *Agricultural and Forest Meteorology*, *104*(4), 315-327.

Alexandrov, V., Eitzinger, J., & Oberforster, M. (2001). Adaptation of crop-weather models in Austria and Bulgaria. In *Proceedings of the 5th European Conference on Applications of Meteorology.*

Anderson, M. C., Zolin, C. A., Sentelhas, P. C., Hain, C. R., Semmens, K., Yilmaz, M. T., ... & Tetrault, R. (2016). The Evaporative Stress Index as an indicator of agricultural drought in Brazil: An assessment based on crop yield impacts. *Remote Sensing of Environment*, *174*, 82-99.

Basso, B., & Liu, L. (2019). Seasonal crop yield forecast: Methods, applications, and accuracies. *Advances in Agronomy*, *154*, 201-255.

Bolton, D. K., & Friedl, M. A. (2013). Forecasting crop yield using remotely sensed vegetation indices and crop phenology metrics. *Agricultural and Forest Meteorology*, *173*, 74-84.

Branzova, P. (2015). Assess the economic imact of climate change on wheat, barley, maize and sunflower in Southeast Bulgaria. *Trakia Journal of Sciences*, *13*(supl 1), 4-7.

Bregaglio, S. U. M., Fischer, K., Ginaldi, F., Valeriano, T. T. B., & Giustarini, L. (2021). The HADES yield prediction system–a case study on the Turkish hazelnut sector. *Frontiers in Plant Science*, *12*, 1033.

Burke, M., & Lobell, D. B. (2017). Satellite-based assessment of yield variation and its determinants in smallholder African systems. *Proceedings of the National Academy of Sciences*, *114*(9), 2189-2194.

Cai, Y., Guan, K., Peng, J., Wang, S., Seifert, C., Wardlow, B., & Li, Z. (2018). A high-performance and in-season classification system of field-level crop types using time-series Landsat data and a machine learning approach. *Remote Sensing of Environment*, *210*, 35-47.

Çakır, Y., Kırcı, M., & Güneş, E. O. (2014). Yield prediction of wheat in south-east region of Turkey by using artificial neural networks. In *The Third International Conference on Agro-Geoinformatics* (pp. 1-4). IEEE.

Chen, Y., McVicar, T. R., Donohue, R. J., Garg, N., Waldner, F., Ota, N., ... & Lawes, R. (2020). To blend or not to blend? A framework for nationwide Landsat–MODIS data selection for crop yield prediction. *Remote Sensing*, *12*(10), 1653.

Chollet, F. (2017). The limitations of deep learning. Deep Learning With Python.

Daly, C., J.I. Smith, and K.V. Olson. 2015. Mapping atmospheric moisture climatologies across the conterminous United States. *PloS ONE 10*(10):e0141140. doi:10.1371/journal.pone.0141140.

Dang, C., Liu, Y., Yue, H., Qian, J., & Zhu, R. (2020). Autumn crop yield prediction using data-driven approaches:-Support vector machines, Random Forest, and deep neural network methods. *Canadian Journal of Remote Sensing*, 1-20.

Deryng, D., Sacks, W. J., Barford, C. C., & Ramankutty, N. (2011). Simulating the effects of climate and agricultural management practices on global crop yield. *Global Biogeochemical Cycles*, *25*(2).

Doraiswamy, P. C., Moulin, S., Cook, P. W., & Stern, A. (2003). Crop yield assessment from remote sensing. *Photogrammetric Engineering & Remote Sensing*, *69*(6), 665-674.

Duncan, J., Dash, J., & Atkinson, P. M. (2015). The potential of satellite-observed crop phenology to enhance yield gap assessments in smallholder landscapes. *Frontiers in Environmental Science*, *3*, 56.

FAOSTAT, R. "FAOSTAT database." (2017). United Nations Food and Agriculture Organization.

Farr, T. G., Rosen, P. A., Caro, E., Crippen, R., Duren, R., Hensley, S., Kobrick, M., Paller, M., Rodriguez, E., Roth, L., Seal, D., Shaffer, S., Shimada, J., Umland, J., Werner, M., Oskin, M., Burbank, D., & Alsdorf, D. (2007). The shuttle radar topography mission. *Reviews of Geophysics*, *45*(2).

Fuzzo, D. F. S., Carlson, T. N., Kourgialas, N. N., & Petropoulos, G. P. (2019). Coupling remote sensing with a water balance model for soybean yield predictions over large areas. *Earth Science Informatics*, 1-15.

Gibbs, H. K., Johnston, M., Foley, J. A., Holloway, T., Monfreda, C., Ramankutty, N., & Zaks, D. (2008). Carbon payback times for crop-based biofuel expansion in the tropics: the effects of changing yield and technology. *Environmental Research Letters*, *3*(3), 034001.

Gitelson, A. A., Vina, A., Ciganda, V., Rundquist, D. C., & Arkebauer, T. J. (2005). Remote estimation of canopy chlorophyll content in crops. *Geophysical Research Letters*, *32*(8).

Gómez, D., Salvador, P., Sanz, J., & Casanova, J. L. (2021). New spectral indicator Potato Productivity Index based on Sentinel-2 data to improve potato yield prediction: a machine learning approach. *International Journal of Remote Sensing*, *42*(9), 3426-3444.

Hansen, J. W., & Jones, J. W. (2000). Scaling-up crop models for climate variability applications. *Agricultural Systems*, *65*(1), 43-72.

Hunt, M. L., Blackburn, G. A., Carrasco, L., Redhead, J. W., & Rowland, C. S. (2019). High resolution wheat yield mapping using Sentinel-2. *Remote Sensing of Environment, 233*, 111410.

Iizumi, T., & Ramankutty, N. (2016). Changes in yield variability of major crops for 1981–2010 explained by climate change. *Environmental Research Letters, 11*(3), 034003.

Irons, J. R., & Masek, J. G. (2006). Requirements for a Landsat data continuity mission. *Photogrammetric Engineering & Remote Sensing, 72*(10), 1102.

Karra, Kontgis, et al. (2021). Global land use/land cover with Sentinel-2 and deep learning. IGARSS 2021-2021 *IEEE International Geoscience and Remote Sensing Symposium*.

Kaul, M., Hill, R. L., & Walthall, C. (2005). Artificial neural networks for corn and soybean yield prediction. *Agricultural Systems, 85*(1), 1-18.

Khaki, S., Wang, L., & Archontoulis, S. V. (2020). A cnn-rnn framework for crop yield prediction. *Frontiers in Plant Science, 10*, 1750.

Khosla, E., Dharavath, R., & Priya, R. (2019). Crop yield prediction using aggregated rainfall-based modular artificial neural networks and support vector regression. *Environment, Development and Sustainability*, 1-22.

Kogan, F., Popova, Z., & Alexandrov, P. (2016). Early forecasting corn yield using field experiment dataset and Vegetation health indices in Pleven region, north Bulgaria. *Ecologia i Industria (Ecology and Industry), 9*(1), 76-80.

Kumar, M. (2016). Impact of climate change on crop yield and role of model for achieving food security. *Environmental Monitoring and Assessment, 188*(8), 1-14.

Lobell, D. B. (2013). The use of satellite data for crop yield gap analysis. *Field Crops Research, 143*, 56-64.

Lobell, D. B., Thau, D., Seifert, C., Engle, E., & Little, B. (2015). A scalable satellite-based crop yield mapper. *Remote Sensing of Environment, 164*, 324-333.

Ma, Y., Zhang, Z., Kang, Y., & Özdoğan, M. (2021). Corn yield prediction and uncertainty analysis based on remotely sensed variables using a Bayesian neural network approach. *Remote Sensing of Environment, 259*, 112408.

Meyfroidt, P., Abeygunawardane, D., Ramankutty, N., Thomson, A., & Zeleke, G. (2019). Interactions between land systems and food systems. *Current Opinion in Environmental Sustainability, 38*, 60-67.

Moriondo, M., Giannakopoulos, C., & Bindi, M. (2011). Climate change impact assessment: the role of climate extremes in crop yield simulation. *Climatic Change, 104*(3), 679-701.

Muñoz Sabater, J., (2019): ERA5-Land hourly data from 1981 to present. Copernicus Climate Change Service (C3S) Climate Data Store (CDS). (<date of access>), doi:10.24381/cds.e2161bac.

Özdoğan, M. (2011). Modeling the impacts of climate change on wheat yields in Northwestern Turkey. *Agriculture, Ecosystems & Environment, 141*(1-2), 1-12.

Ozkan, B., & Akcaoz, H. (2002). Impacts of climate factors on yields for selected crops in the Southern Turkey. *Mitigation and Adaptation Strategies for Global Change, 7*(4), 367-380.

Panek, E., & Gozdowski, D. (2021). Relationship between MODIS derived NDVI and yield of cereals for selected European countries. *Agronomy, 11*(2), 340.

Phalke, A. R., & Özdoğan, M. (2018). Large area cropland extent mapping with Landsat data and a generalized classifier. *Remote Sensing of Environment, 219*, 180-195.

Phalke, A. R., Özdoğan, M., Thenkabail, P. S., Erickson, T., Gorelick, N., Yadav, K., & Congalton, R. G. (2020). Mapping croplands of Europe, Middle East, Russia, and Central Asia using Landsat, Random Forest, and Google Earth Engine. *ISPRS Journal of Photogrammetry and Remote Sensing, 167*, 104-122.

Ray, D. K., Gerber, J. S., MacDonald, G. K., & West, P. C. (2015). Climate variation explains a third of global crop yield variability. *Nature Communications, 6*(1), 1-9.

Ray, D. K., Ramankutty, N., Mueller, N. D., West, P. C., & Foley, J. A. (2012). Recent patterns of crop yield growth and stagnation. *Nature Communications, 3*(1), 1-7.

Rodell, M., P.R. Houser, U. Jambor, J. Gottschalck, K. Mitchell, C.-J. Meng, K. Arsenault, B. Cosgrove, J. Radakovich, M. Bosilovich, J.K. Entin, J.P. Walker, D. Lohmann, and D. Toll. (2004). The Global Land Data Assimilation System, *Bulletin of the American Meteorological Society, 85*(3), 381-394.

Ross, A., & Willson, V. L. (2017). Paired samples T-test. In *Basic and advanced statistical tests* (pp. 17-19). Brill Sense.

Roy, D. P., & Yan, L. (2020). Robust Landsat-based crop time series modelling. *Remote Sensing of Environment, 238*, 110810.

Satir, O., & Berberoglu, S. (2016). Crop yield prediction under soil salinity using satellite derived vegetation indices. *Field Crops Research, 192*, 134-143.

Sellam, V., & Poovammal, E. (2016). Prediction of crop yield using regression analysis. *Indian Journal of Science and Technology, 9*(38), 1-5.

Shao, Z., Cai, J., Fu, P., Hu, L., & Liu, T. (2019). Deep learning-based fusion of Landsat-8 and Sentinel-2 images for a harmonized surface reflectance product. *Remote Sensing of Environment, 235*, 111425.

Shook, J., Gangopadhyay, T., Wu, L., Ganapathysubramanian, B., Sarkar, S., & Singh, A. K. (2021). Crop yield prediction integrating genotype and weather variables using deep learning. *PLOS One, 16*(6), e0252402.

Srinivasan, R., Zhang, X., & Arnold, J. (2010). SWAT ungauged: hydrological budget and crop yield predictions in the Upper Mississippi River Basin. *Transactions of the ASABE, 53*(5), 1533-1546.

Stuart, A. M., Pame, A. R. P., Silva, J. V., Dikitanan, R. C., Rutsaert, P., Malabayabas, A. J. B., ... & Singleton, G. R. (2016). Yield gaps in rice-based farming systems: Insights from local studies and prospects for future analysis. *Field Crops Research, 194*, 43-56.

Vanli, Ö., Ahmad, I., & Ustundag, B. B. (2020). Area estimation and yield forecasting of wheat in southeastern Turkey using a machine learning approach. *Journal of the Indian Society of Remote Sensing, 48*(12), 1757-1766.

Verburg, P. H., Neumann, K., & Nol, L. (2011). Challenges in using land use and land cover data for global change studies. *Global Change Biology, 17*(2), 974-989.

Wang, X., Huang, J., Feng, Q., & Yin, D. (2020). Winter wheat yield prediction at county level and uncertainty analysis in main wheat-producing regions of China with deep learning approaches. *Remote Sensing, 12*(11), 1744.

Weiss, M., Jacob, F., & Duveiller, G. (2020). Remote sensing for agricultural applications: A meta-review. *Remote Sensing of Environment, 236*, 111402.

Xia, Y., Hao, Z., Shi, C., Li, Y., Meng, J., Xu, T., ... & Zhang, B. (2019). Regional and global land data assimilation systems: Innovations, challenges, and prospects. *Journal of Meteorological Research, 33*(2), 159-189.

Yildirak, K., Kalaylıoglu, Z., & Mermer, A. (2015). Bayesian estimation of crop yield function: drought based wheat prediction model for tigem farms. *Environmental and Ecological Statistics, 22*(4), 693-704.

Yolevski, M., Krastanov, S., Kabakciev, I., Georgieva, J., & Klevtsov, A. (1978). Wheat and maize yield prediction on the basis of soil climatic factors.[Conference paper]. In Meeting of the ISSS Working Group on Soil Information Systems. Varna/Sofia (Bulgaria).

## Figures

**Figure 3.1** Study area covering the cross-border area between Turkey and Bulgaria with average wheat yield in 26 districts (LAU-1) of northwest Turkey (period: 2004-2020) and four planning regions (NUTS-2) of Bulgaria (period: 2001-2017).

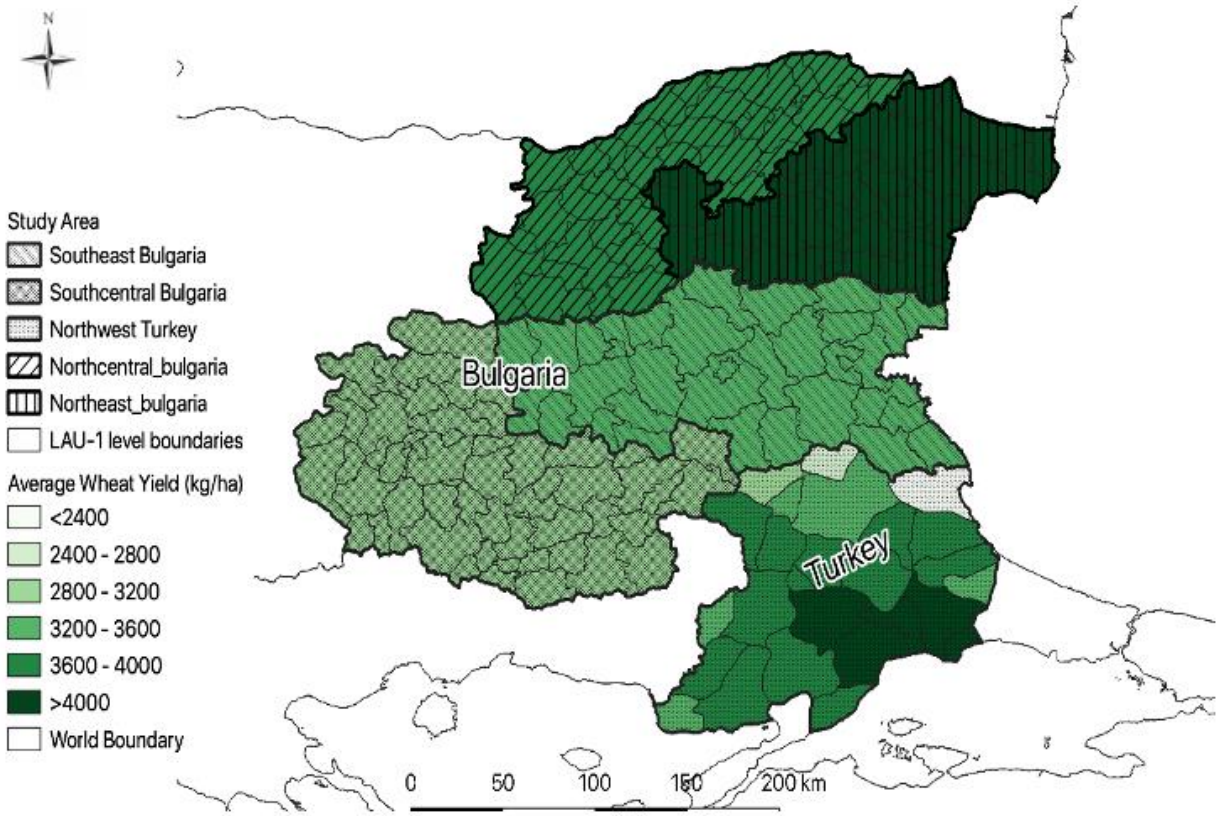

**Figure 3.2** MLP-NN model architecture. The first column on the left refers to the representative set of inputs to the model; the second column refers to the hidden layers of the model and bias which collects outlier observations; the third column refers to the second layer of hidden layers; and the fourth column is the response variable of the model. The connecting lines represent the relationships between each node; the width of the lines represents the importance. Synaptic weights are used for final predictions.

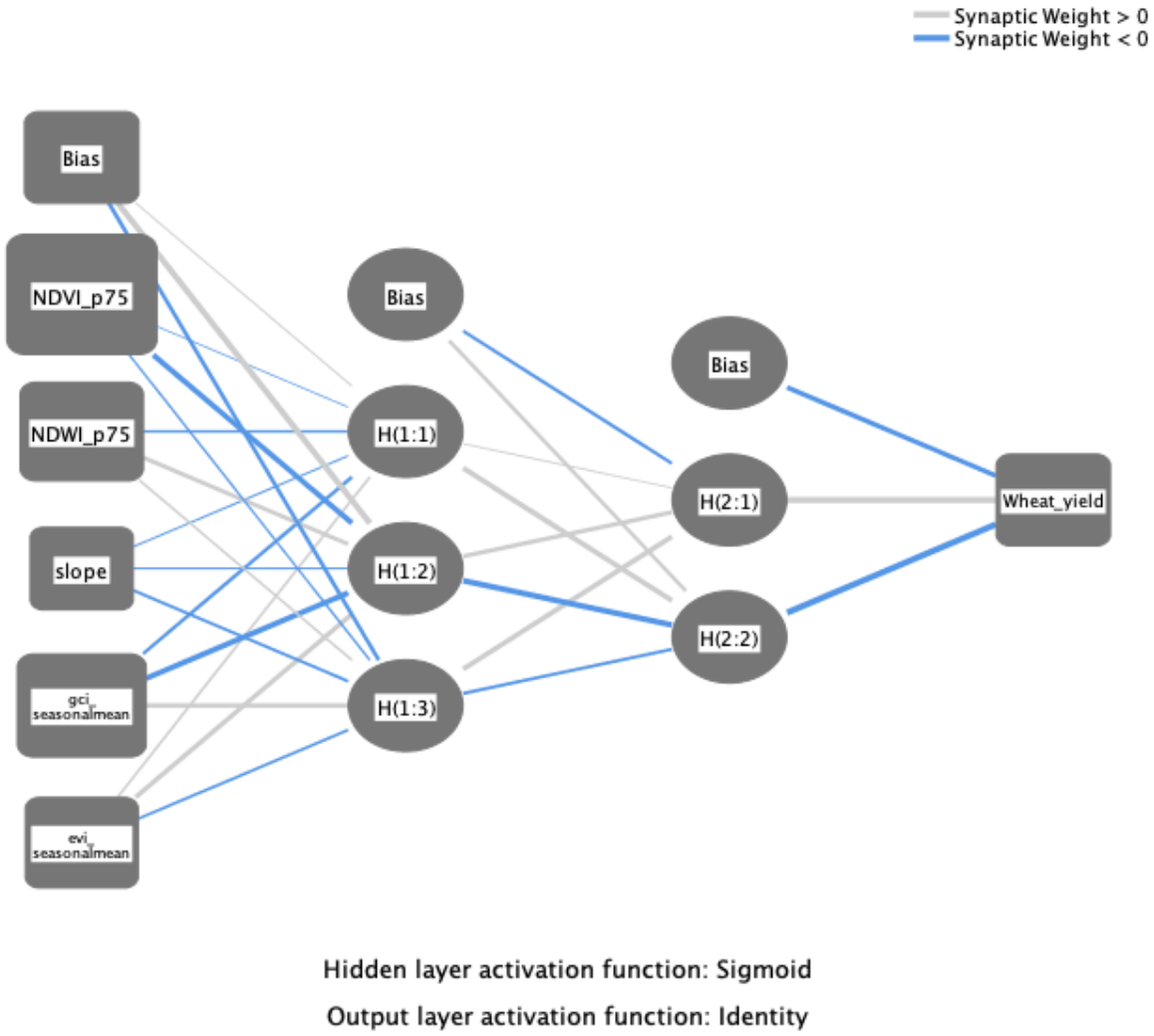

**Figure 3.3** Normalized importance of sequential variables (3.3a) and non-sequential (3.3b). Figure 3.3a refers to the top 10 sequential variables according to their overall importance values. Blue represents higher importance and brown represents lower importance values. The left panel consists of sequential variables in the model and right panel consists of non-sequential variables in the model.

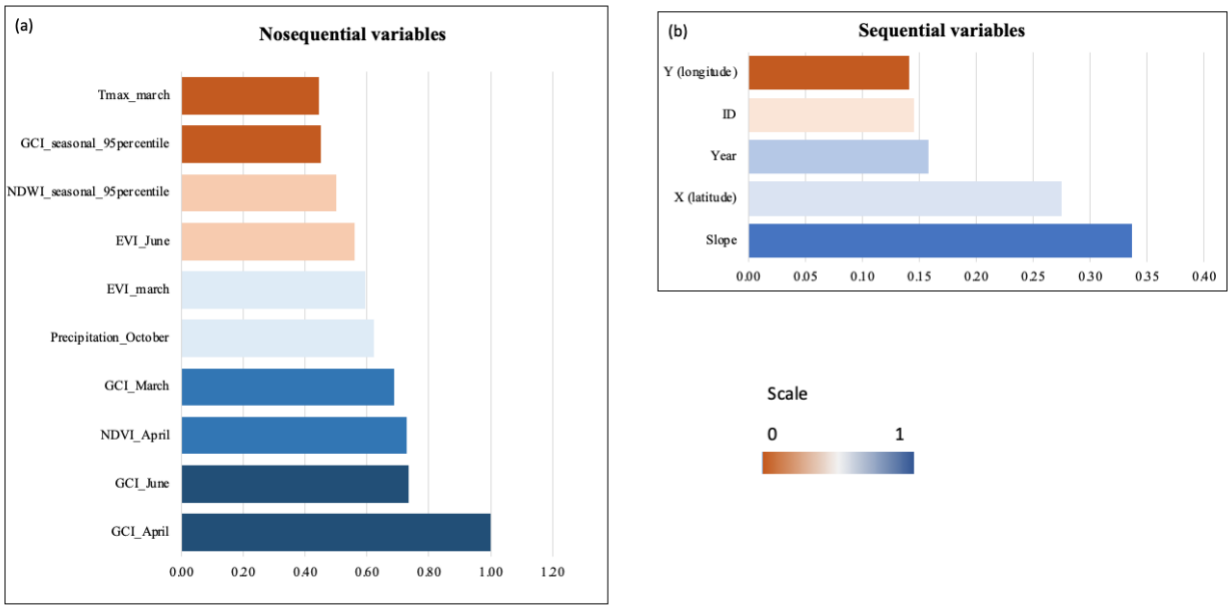

**Figure 3.4** Correlation coefficients of predictor variables when related to the response variable (wheat yield). Green and yellow represent high correlation (negative and positive, respectively), and the grey color code represents less or no correlation between yield and predictors. The left panel refers to the sequential variables, whereas the right panel refers to the non-sequential variables correlation coefficient values.

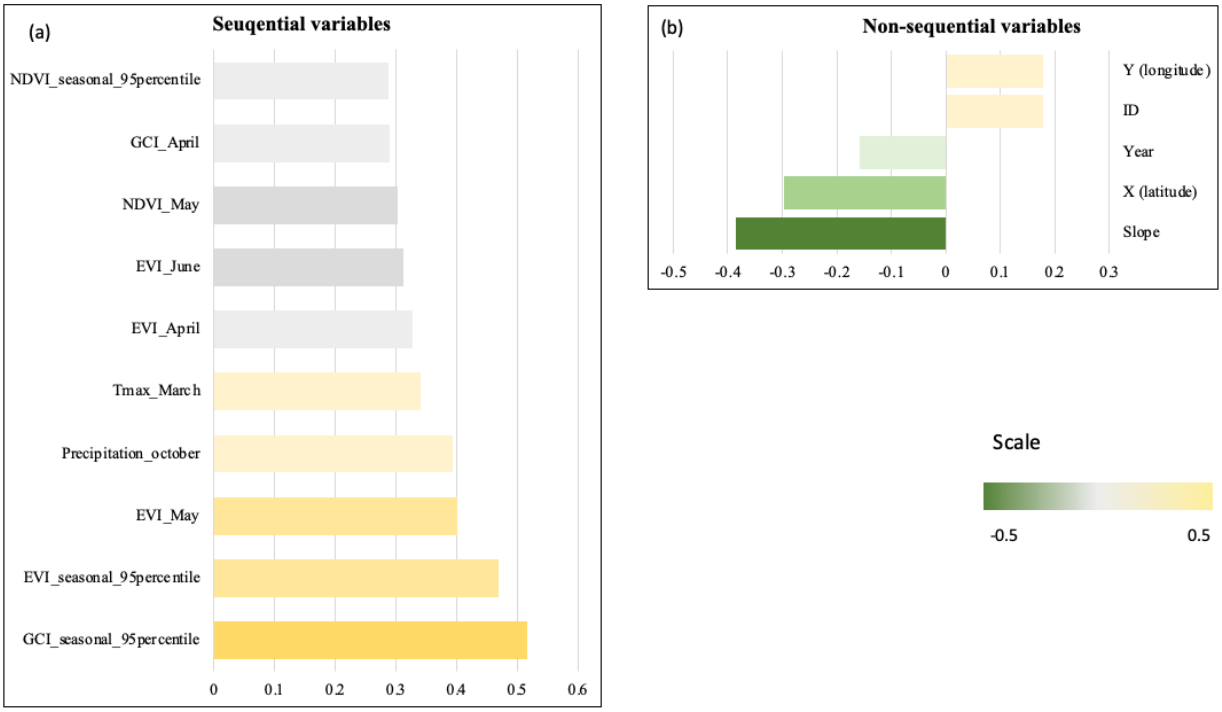

**Figure 3.5** Scatterplots of observed wheat yield vs predicted wheat yield in the test districts of Turkey. The X-axis refers to observed yield (kg/ha), and the Y-axis refers to predicted yield (kg/ha).

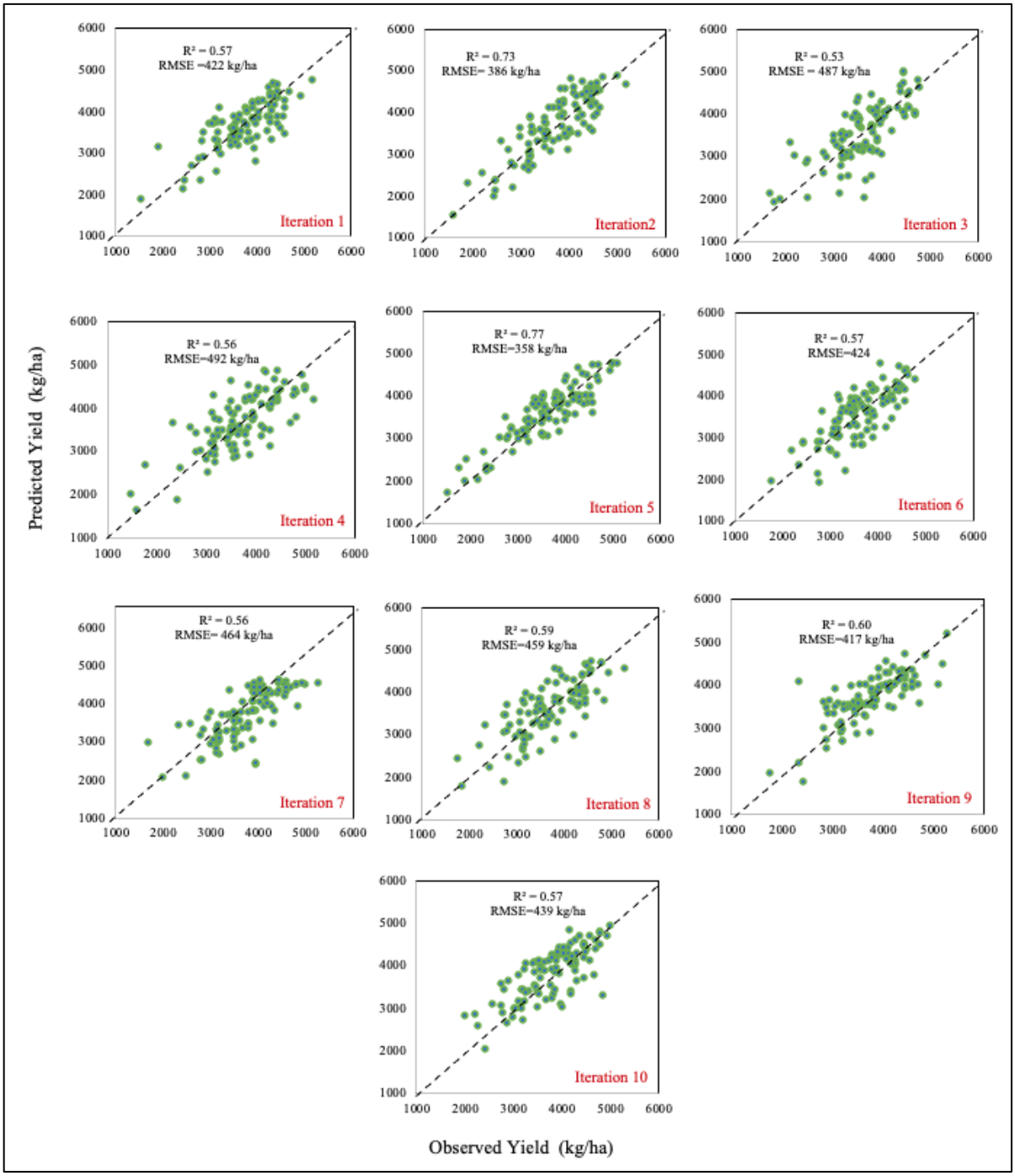

**Figure 3.6a** Scatterplots between observed and predicted yields for the 2005, 2007, and 2010 test years at the Turkey-data level and all-data level. The left column refers to the Turkey data model, and the right column refers to the all-data model; the X-axis refers to observed yield (kg/ha), and the Y-axis represents predicted yield (kg/ha)**.**

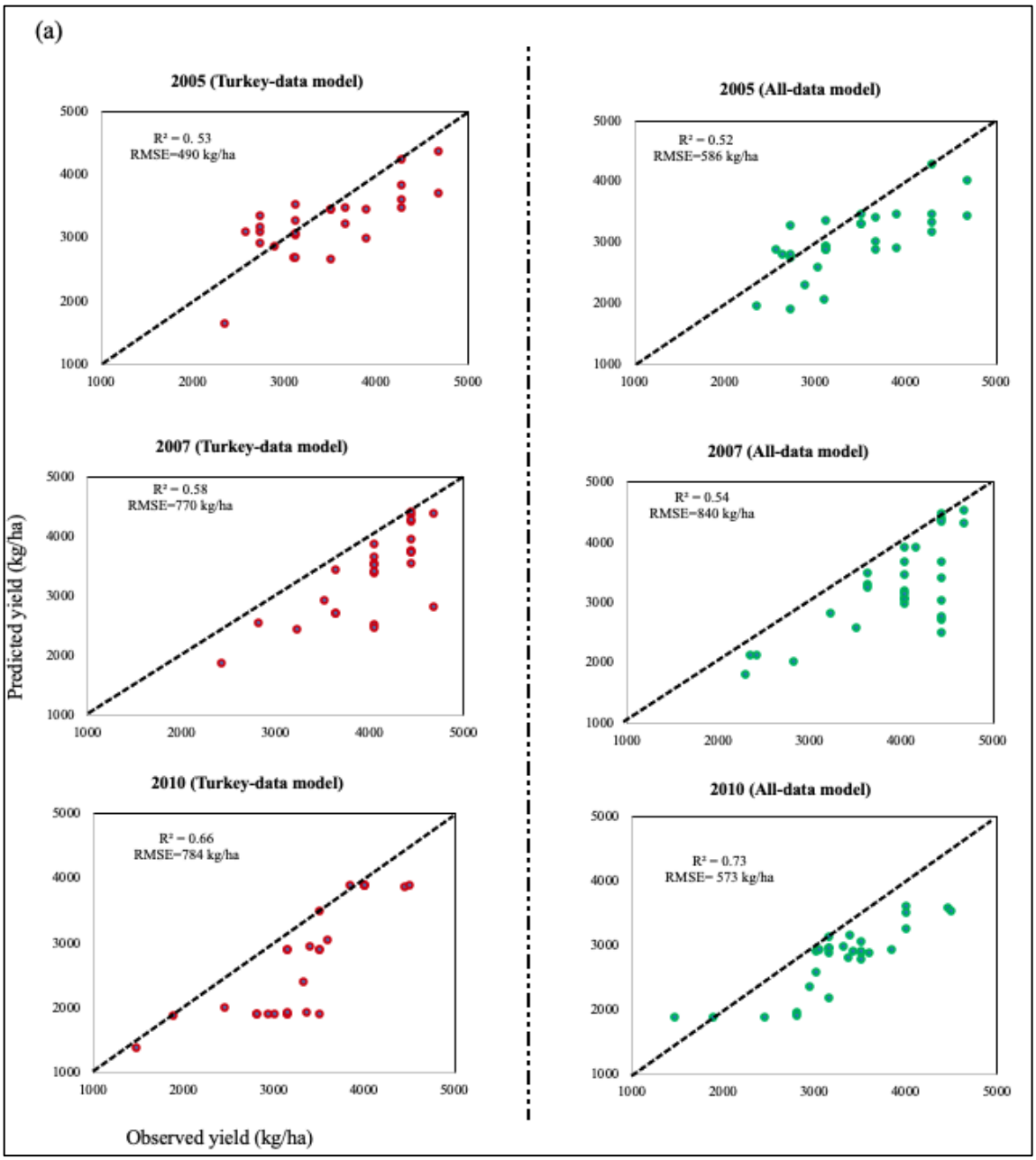

**Figure 3.6b** Scatterplots between observed and predicted yields for the 2014, 2018, and 2020 test years at the Turkey-data level and the all-data level. The left column refers to the Turkey data model, and the right column refers to the all-data model; the X-axis refers to observed yield (kg/ha), and the Y-axis represents predicted yield (kg/ha).

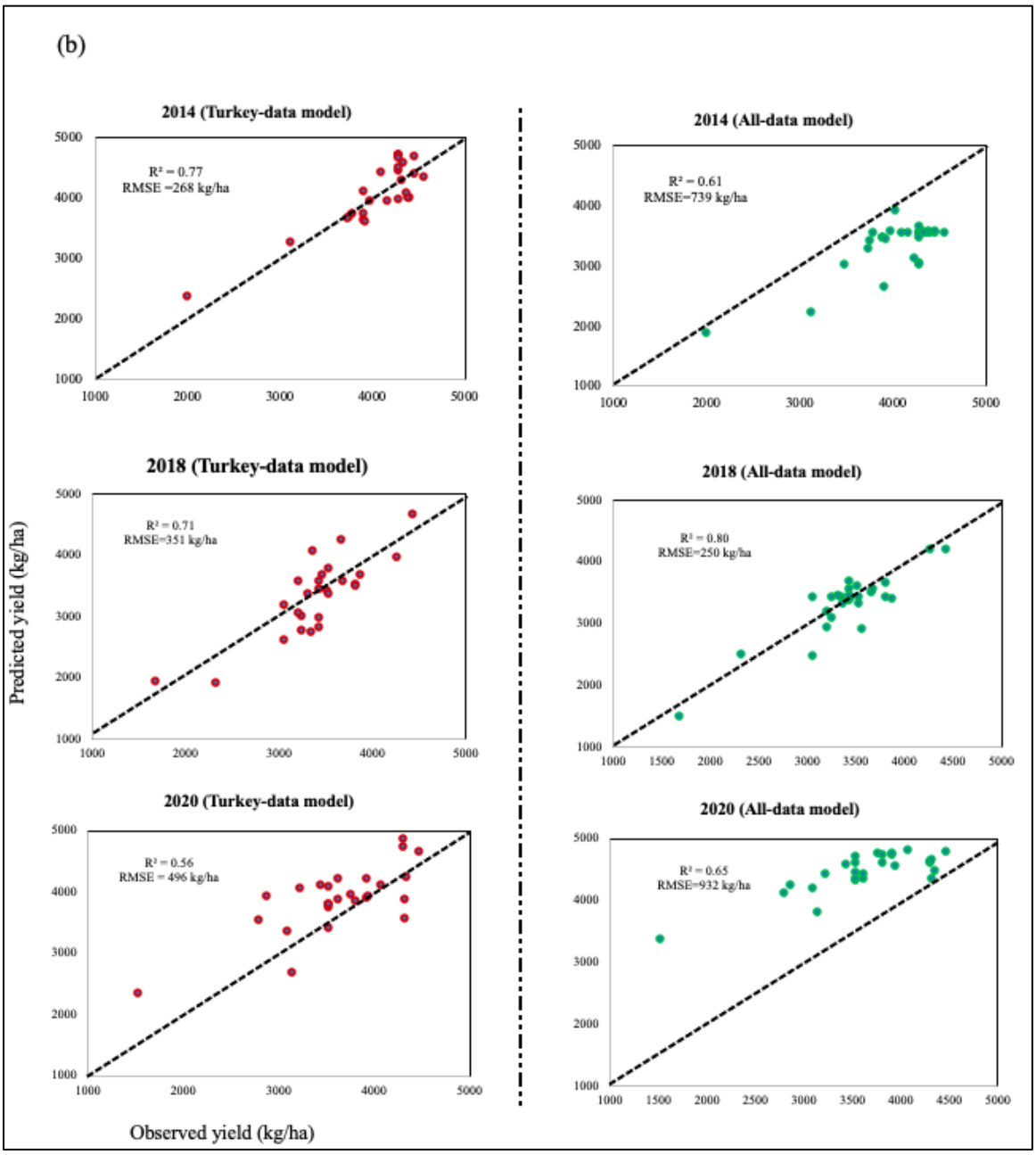

**Figure 3.7** Derived village boundaries in the study area using Voronoi analysis.

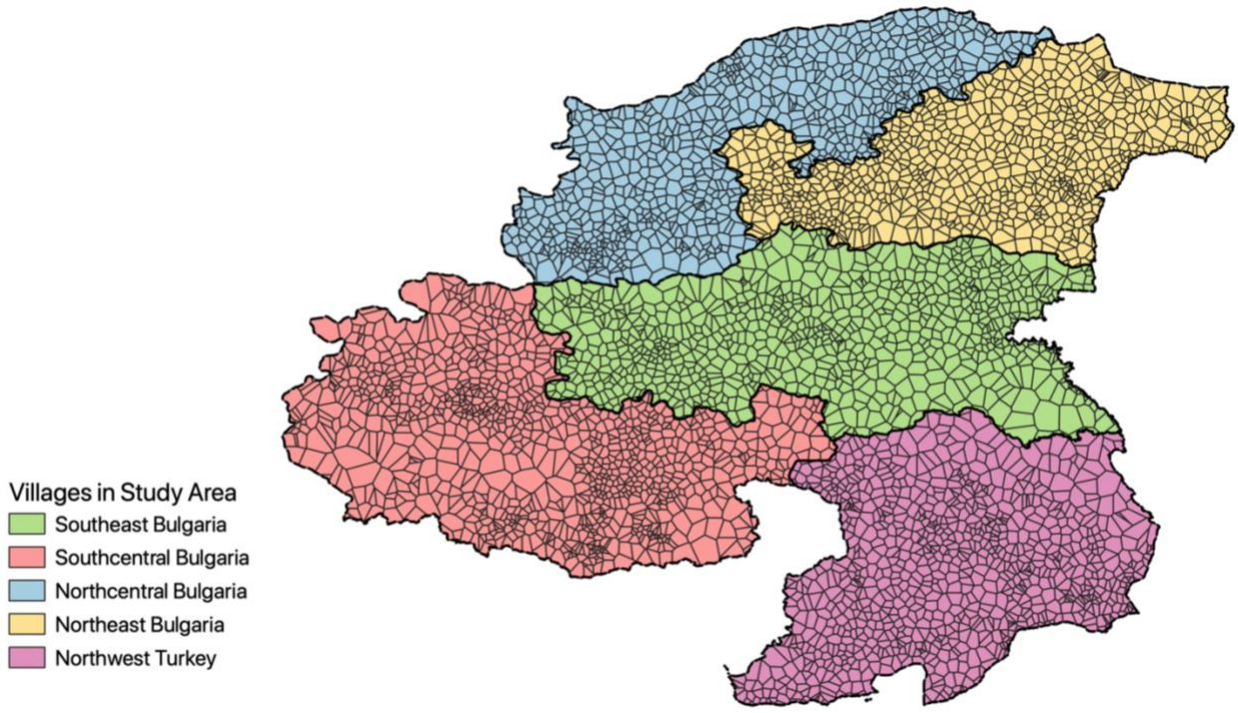

**Figure 3.8** Wheat yield predictions at village-scale using remotely sensed environmental variables and a neural network for the cross-border area between Turkey and Bulgaria.

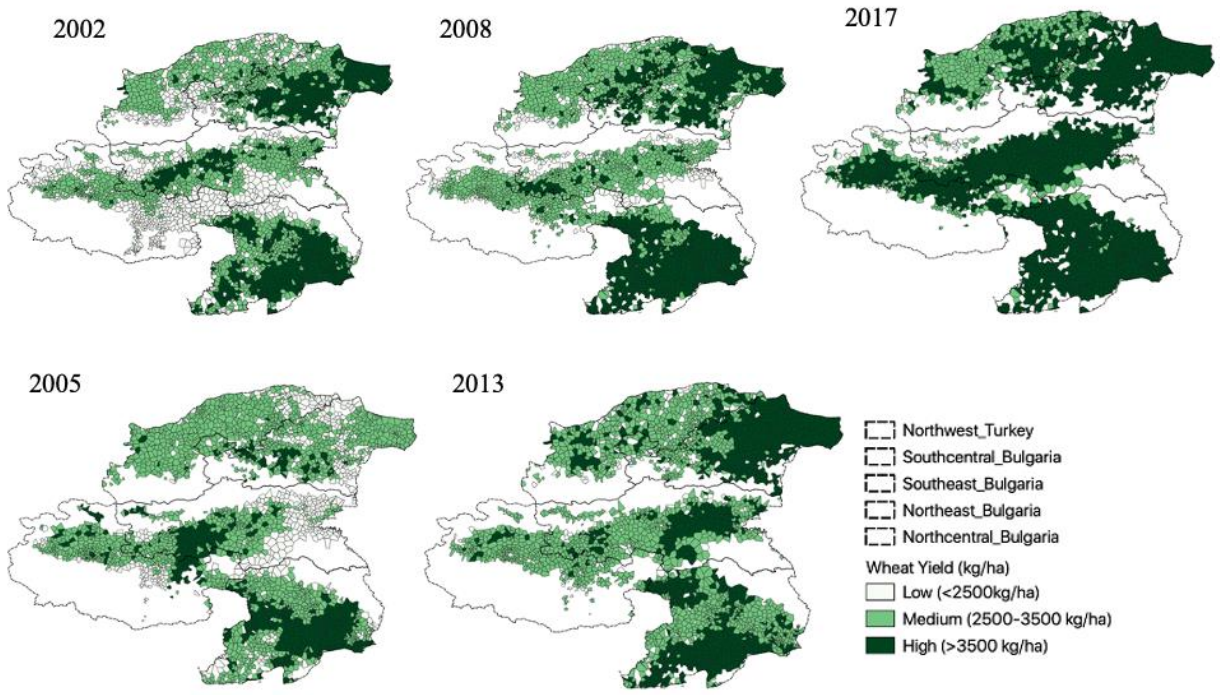

**Figure 3.9** Comparison of predicted and observed wheat yield estimates in the study area. The top panels with red point refers to country-level wheat yield comparisons; the middle panels with yellow points refer to the wheat yield comparison for planning regions (NUTS-2) in Bulgaria; and the bottom panels with green points refer to the wheat yield comparison for districts (NUTS-3) in Turkey. The X-axis is the observed yield, and the Y-axis is the predicted wheat yield.

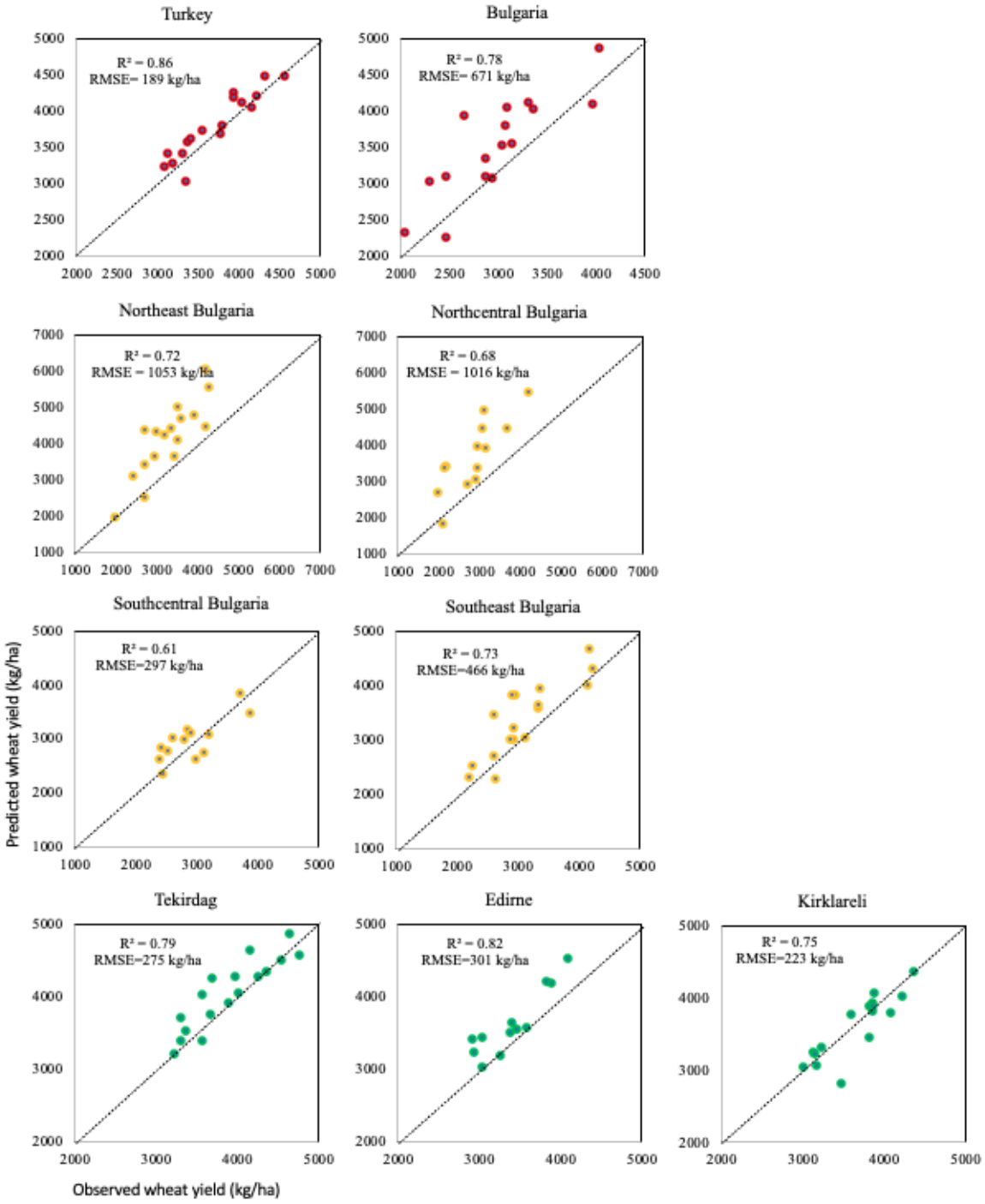

**Figure 3.10** Predicted and observed average wheat yield distributions (red line refers to average value of observed wheat yield, and blue line refers to the predicted wheat yield average).

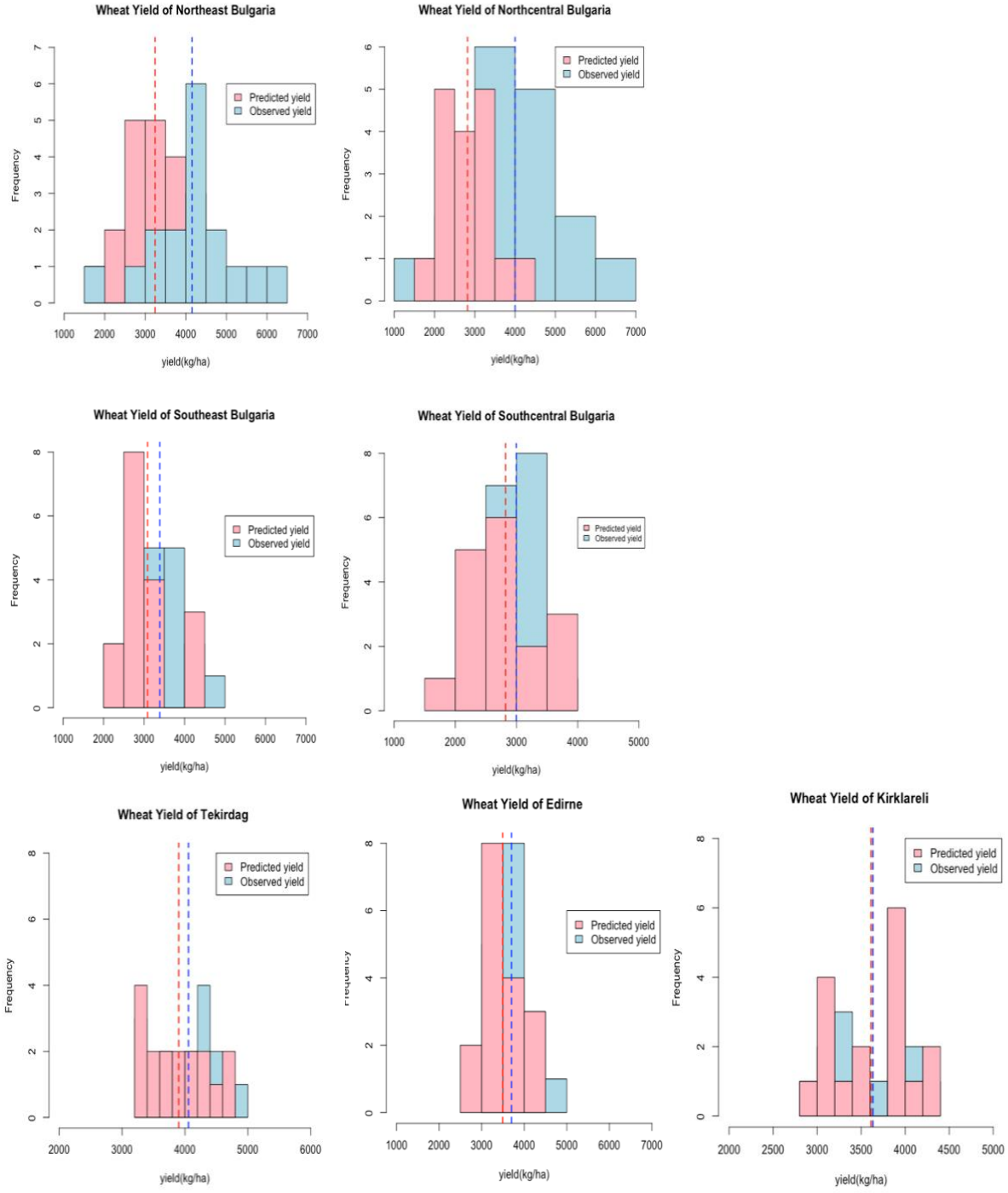

**Figure 3.11** Wheat yield predictions of northern Bulgaria (red line refers to observed wheat yield and blue line refers to predicted wheat yield).

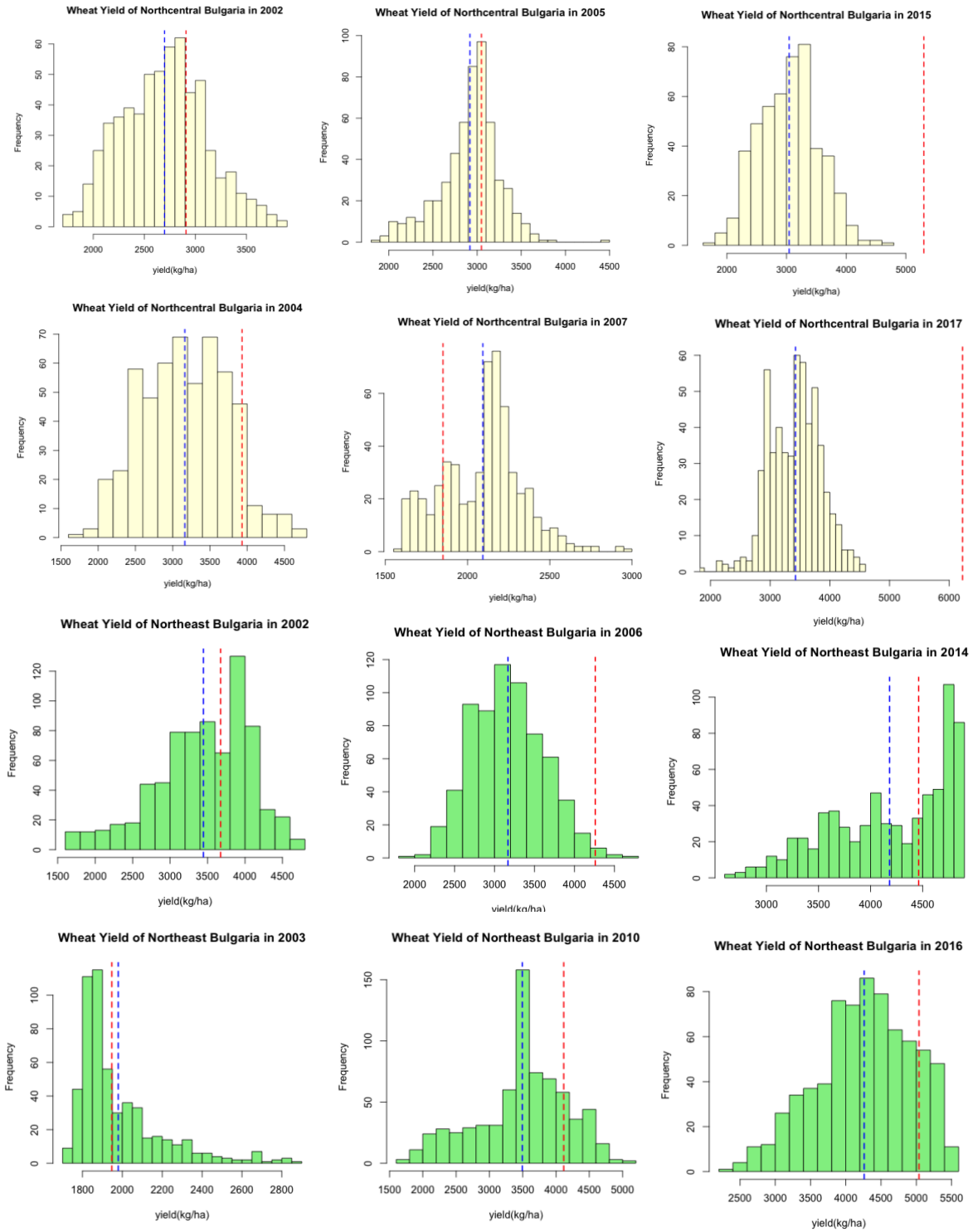

**Figure 3.12** Wheat yield predictions of southern Bulgaria (red line refers to observed wheat yield and blue line refers to predicted wheat yield).

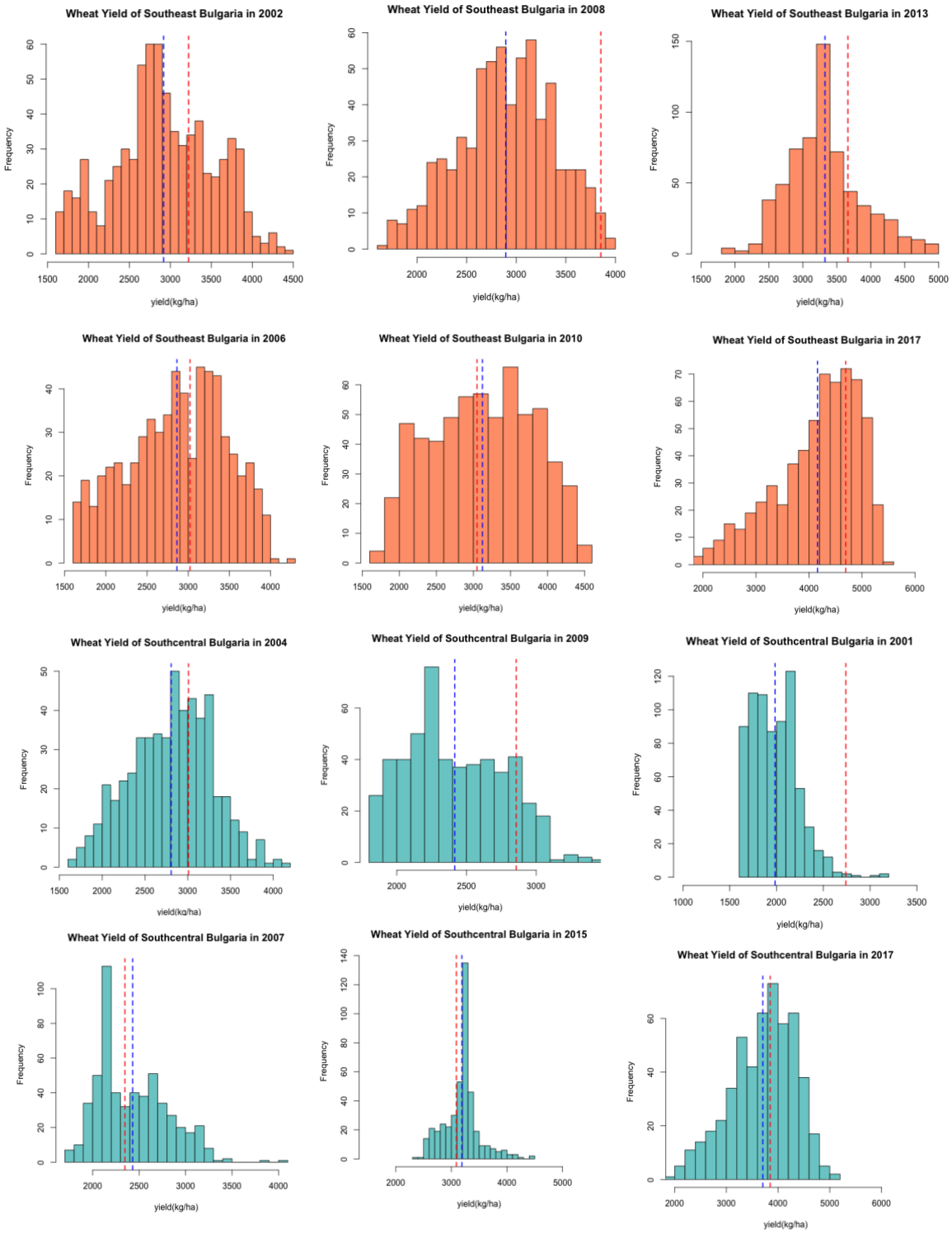

**Figure 3.13** Wheat yield predictions of Turkey districts (Edirne, Tekirdag and Kirklareli) (red line refers to observed wheat yield and blue line refers to predicted wheat yield).

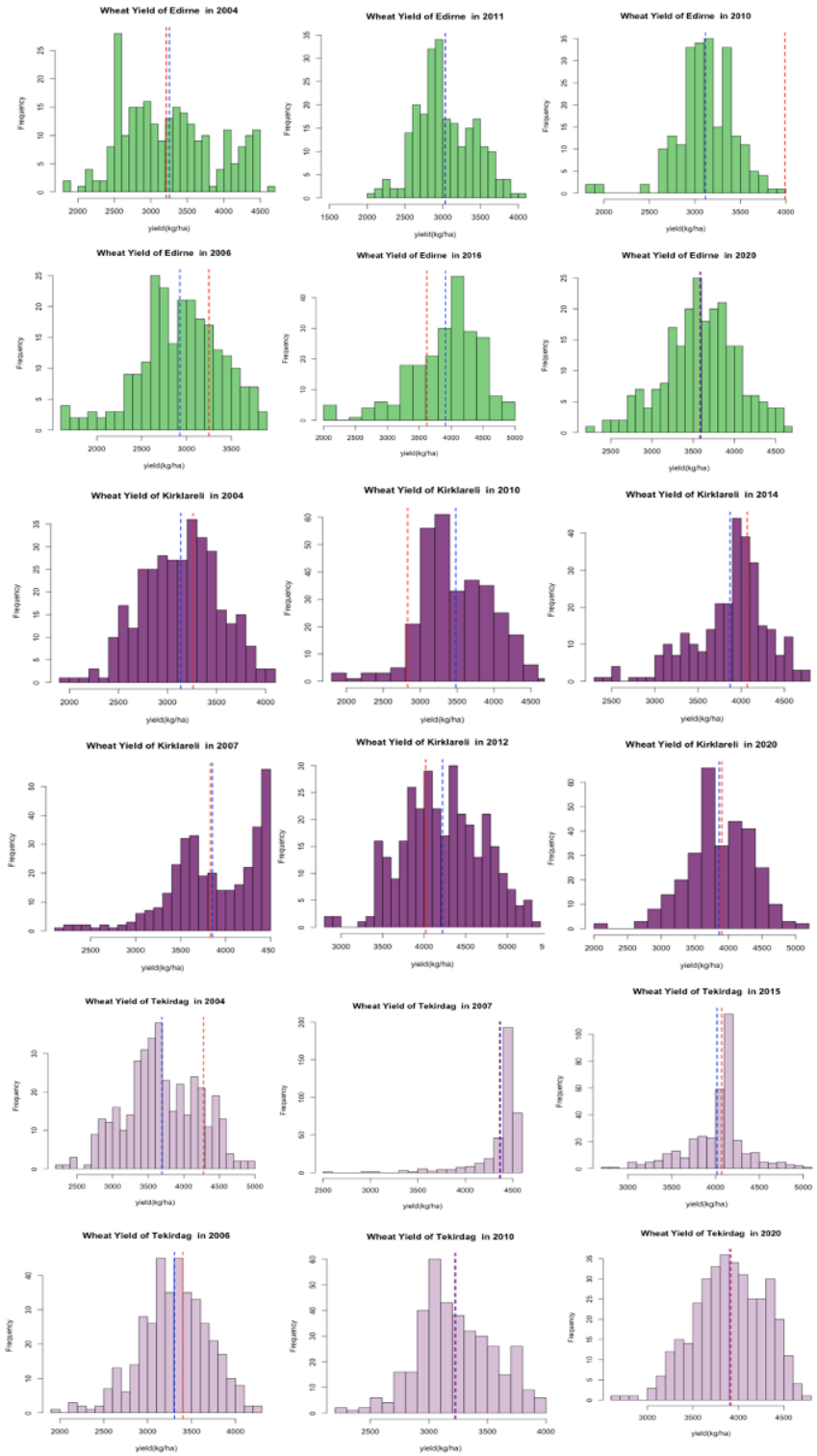

## Tables

**Table 3.1** Key similarities and differences between the two countries in a case study region.

| Sr. No. | Key data points | Northwestern Turkey (Cross-border area/ Northern Thracia) | Eastern Bulgaria (Cross-border area/ Eastern Thracia) |
|---|---|---|---|
| 1 | Provinces/regions covered | Edirne (West CB), Kirklareli (East CB), Tekirdag, | Northcentral, Northeast, Southcentral and Southeast |
| 2 | Rainfall | 603 mm (yearly average), 50 mm (monthly average) | 580 mm (yearly average), 48 mm (monthly average) |
| 3 | Average Max Temperature(0C) | ~19 | ~18 |
| 4 | Average Min Temperature(0C) | ~8 | ~8 |
| 5 | Length of growing period (days) | 90-179 | 90-179 |
| 6 | Moisture Regime | Mediterranean | Humid subtropical and Mediterranean |
| 7 | Population Density | 470 people per km² | 81.5 people per km² |
| 8 | Major crops | Winter wheat, corn, rice, sugar beet and sunflower. | Winter wheat, Barley, Corn, Sunflower, tobacco. |
| 9 | Agricultural value added (%GDP) | Decreased from ~10 to~ 8 since 2000 | Decreased from ~11 to~ 4 since 2000 |
| 10 | Wheat import value | Increased by ~17% since 2006 | Approximately stable since 2006 |
| 11 | Wheat export value | Increased by ~17% since 2007 | No major change in value from 2000 to 2017 |
| 13 | Wheat price index | Increased from 27 in 2000 to 246 in 2017 | Increased from 102 in 2000 to 158 in 2017 |
| 14 | All cropland area and yield | Increasing trend | Mixed trend until 2008 and then continuously increasing |
| 15 | Wheat crop area and yield | Decreased from 2000 to 2008 and then stabilized with minor fluctuations | Decreased from 2001 to 2003 and then slowly increased until 2009 and then stabilized with minor fluctuations |
| 16 | Employment in agriculture | Decreased from ~36% to~18% of total employment since 2000 to 2017 | Decreased from ~13% to~6% of total employment since 2000 to 2017 |

**Table 3.2** Input feature summary for model development.

| | | Feature dataset | Spatial Resolution | Temporal Interval | Time-period | Composites | Spatial Aggregation |
|---|---|---|---|---|---|---|---|
| **Sequential** | **Biomass** | Landsat EVI, NDVI and GCI | 30-m | Bi-weekly | 2001-2020 | Monthly | LAU-1 units/ NUTS-2 units |
| | | Landsat Surface Reflectance Band 1,2,3,4,5 and 7 | 30-m | Bi-weekly | 2001-2020 | Monthly | LAU-1 units/ NUTS-2 units |
| | **Water Stress** | Landsat NDWI | 30-m | Bi-weekly | 2001-2020 | Monthly | LAU-1 units/ NUTS-2 units |
| | **Weather** | TerraClimate maximum temperature (degree celcius), minimum tepmperature, precipitation (mm) | 2.5 arc min | Monthly | 2001-2020 | Monthly | LAU-1 units/ NUTS-2 units |
| | **Soil** | TerraClimate actual evapotraspiration (mm), potential evapotranspiration, soil moisture (mm), and wind speed (m/s) | 2.5 arc min | Monthly | 2001-2020 | Monthly | LAU-1 units/ NUTS-2 units |
| | **Crop yield statistics** | Government departments | Admin statistical unit | Yearly | 2001-2020 | Annual | LAU-1 units/ NUTS-2 units |
| **Non-sequential** | **Topography** | Slope | | | | | LAU-1 units/ NUTS-2 units |
| | **Location** | Latitude, Longitude | | | | | LAU-1 units/ NUTS-2 units |
| | **Technical** | Year | | | | | LAU-1 units/ NUTS-2 units |
| | **Technical** | ID (sequential code of each sample) | | | | | LAU-1 units/ NUTS-2 units |

**Table 3.3** Inputs used in the wheat yield model.

| | |
|---|---|
| Number of years/months | Number of years -20 (2001-2020)<br>Number of seasonal months- 8 (January, February, March, April, May, June, July, August) |
| Number of inputs bands | 1. Monthly EVI, NDVI, GCI, NDWI, Landsat Surface reflectance Band 1,2,4,5, and 7 (Each index and band – annual 7 bands each- 63 bands annually)<br>2. Seasonal average ($90^{th}$ percentile of seasonal dataset – 9 bands annually)<br>3. Monthly minimum temperature, maximum temperature, precipitation, actual evapotranspiration, soil moisture and wind speed (54 bands annually) and previous year October month average (6 bands annually)<br>4. Slope derived from SRTM DEM (1 band) |

**Table 3.4** Validation design.

| Model | Level | Dimension | Training data used | Testing data used | Number of predicted values |
|---|---|---|---|---|---|
| 1. | Country | Temporal | Turkey data from all the train years except one test year | Turkey data only from test year | 26 |
| 2 | Country | Spatial | Turkey data trained with random 20 districts out of total 26 (10 iterations) | Turkey data of 6 test districts from respective model iteration | 52 |
| 3 | Study area | Temporal | Entire study area data from all the train years except one test year | Entire study area data only from test year | 30 |
| 4 | Study area | Spatial | All the districts data from Turkey but only three region data from Bulgaria | One test region from Bulgaria | 17 |

**Table 3.5** Model evaluations for Turkey data for spatial predictions.

| Turkey Data (20 train /6 test districts) | | |
|---|---|---|
| Iteration | R2 | RMSE |
| 1 | 0.57 | 422 |
| 2 | 0.72 | 386 |
| 3 | 0.53 | 487 |
| 4 | 0.55 | 492 |
| 5 | 0.77 | 358 |
| 6 | 0.57 | 424 |
| 7 | 0.55 | 464 |
| 8 | 0.69 | 459 |
| 9 | 0.60 | 417 |
| 10 | 0.57 | 439 |
| Average | **0.61** | **435** |
| Stand. Dev. | **0.08** | **42.60** |

**Table 3.6** Model evaluation for Turkey-data model and all-data model for temporal predictions.

| Test Year | Turkey-data only | | All-data | |
|---|---|---|---|---|
| | R2 | RMSE | R2 | RMSE |
| 2004 | 0.60 | 445 | 0.58 | 466 |
| 2005 | 0.53 | 490 | 0.52 | 586 |
| 2006 | 0.57 | 736 | 0.54 | 526 |
| 2007 | 0.58 | 770 | 0.54 | 840 |
| 2008 | 0.55 | 842 | 0.58 | 670 |
| 2009 | 0.60 | 302 | 0.68 | 412 |
| 2010 | 0.66 | 784 | 0.73 | 573 |
| 2011 | 0.57 | 417 | 0.66 | 633 |
| 2012 | 0.66 | 617 | 0.77 | 402 |
| 2013 | 0.52 | 413 | 0.68 | 370 |
| 2014 | 0.77 | 268 | 0.61 | 739 |
| 2015 | 0.71 | 342 | 0.68 | 448 |
| 2016 | 0.69 | 382 | 0.68 | 396 |
| 2017 | 0.67 | 480 | 0.78 | 517 |
| 2018 | 0.69 | 351 | 0.80 | 250 |
| 2019 | 0.68 | 620 | 0.74 | 383 |
| 2020 | 0.56 | 496 | 0.65 | 932 |
| Average | **0.62** | **515.00** | **0.66** | **537.82** |
| Stand. Dev. | **0.07** | **180.73** | **0.09** | **180.35** |

**Table 3.7** Results of predicted and observed wheat yield comparisons using t-Test: Paired Two Sample for Means.

| | Bulgaria (2001-2017) | | Turkey (2004-2020) | |
|---|---|---|---|---|
| | *Variable 1* | *Variable 2* | *Variable 1* | *Variable 2* |
| Mean | 3047.51 | 3615.29 | 3710.39 | 3801.96 |
| Variance | 363844.97 | 599808.72 | 207369.37 | 200760.85 |
| Observations | 17.00 | 17.00 | 17.00 | 17.00 |
| Pearson Correlation | 0.89 | | 0.93 | |
| df | 16.00 | | 16.00 | |
| t stat | -6.33 | | -2.21 | |
| P(T<=t) one-tail | 0.00 | | 0.02 | |
| t Critical one-tail | 1.75 | | 1.75 | |
| P(T<=t) two-tail | 0.00 | | 0.04 | |
| t Critical two-tail | 2.12 | | 2.12 | |

## Appendix 3

**Figure A3.1** Predicted wheat yield distributions of northeast Bulgaria from 2001-2020 (red line refers to observed wheat yield and blue line refers to predicted wheat yield). X-axis refers to wheat yield (kg/ha) and Y-axis refers to number of villages.

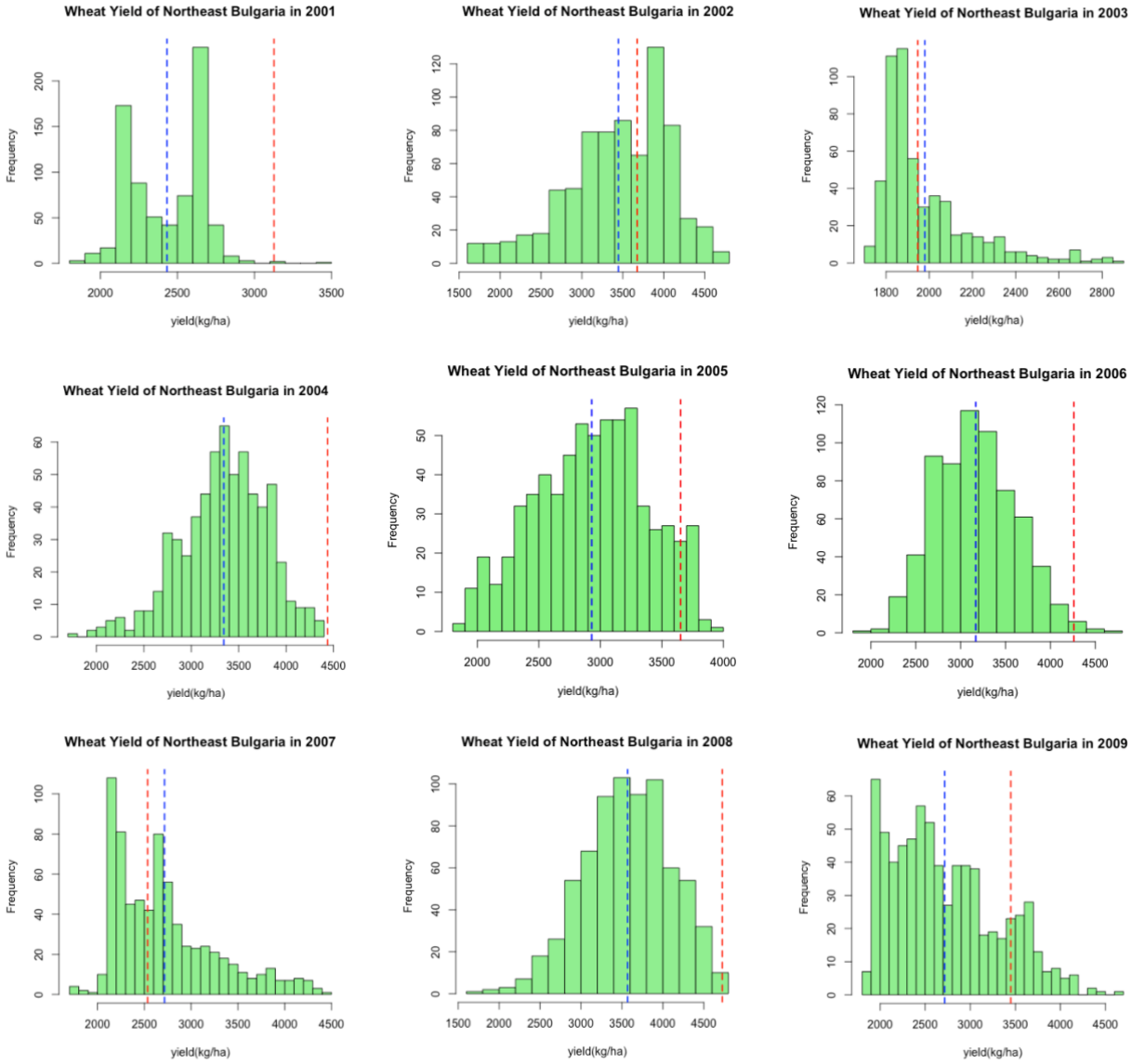

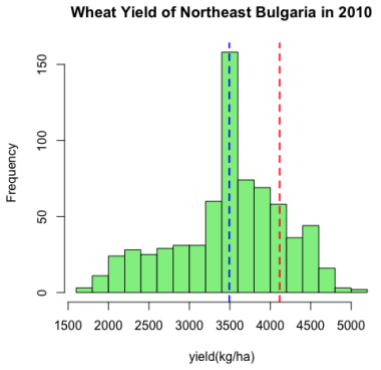
Wheat Yield of Northeast Bulgaria in 2010
Frequency
0
50
100
150
1500 2000 2500 3000 3500 4000 4500 5000
yield(kg/ha)

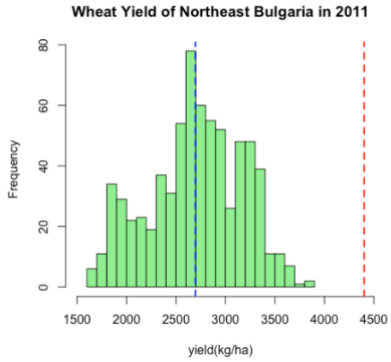
Wheat Yield of Northeast Bulgaria in 2011
Frequency
0
20
40
60
80
1500 2000 2500 3000 3500 4000 4500
yield(kg/ha)

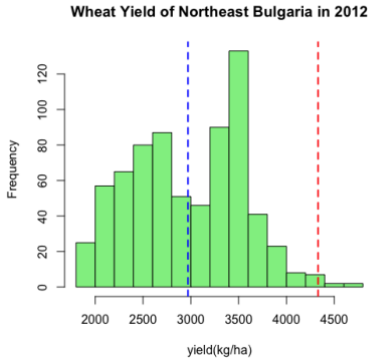
Wheat Yield of Northeast Bulgaria in 2012
Frequency
0
20
40
60
80
100
120
2000 2500 3000 3500 4000 4500
yield(kg/ha)

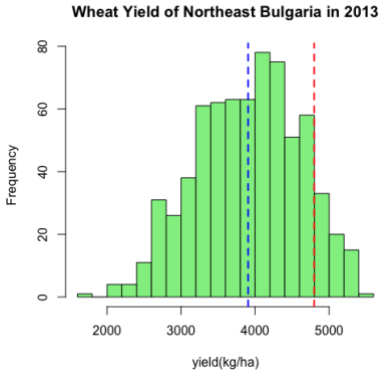
Wheat Yield of Northeast Bulgaria in 2013
Frequency
0
20
40
60
80
2000 3000 4000 5000
yield(kg/ha)

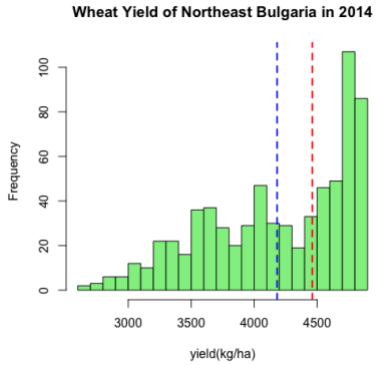
Wheat Yield of Northeast Bulgaria in 2014
Frequency
0
20
40
60
80
100
3000 3500 4000 4500
yield(kg/ha)

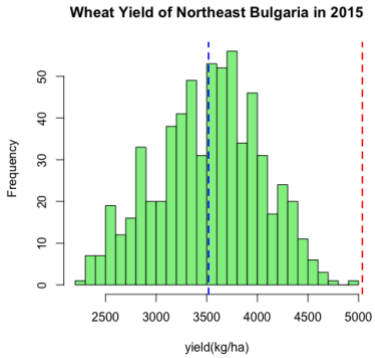
Wheat Yield of Northeast Bulgaria in 2015
Frequency
0
10
20
30
40
50
2500 3000 3500 4000 4500 5000
yield(kg/ha)

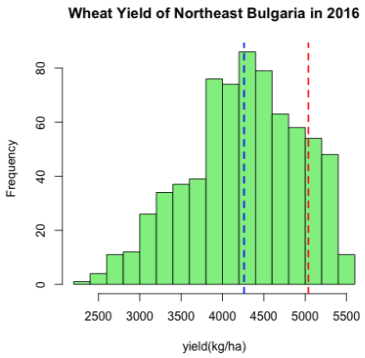
Wheat Yield of Northeast Bulgaria in 2016
Frequency
0
20
40
60
80
2500 3000 3500 4000 4500 5000 5500
yield(kg/ha)

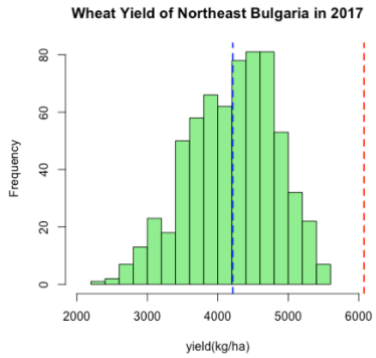
Wheat Yield of Northeast Bulgaria in 2017
Frequency
0
20
40
60
80
2000 3000 4000 5000 6000
yield(kg/ha)

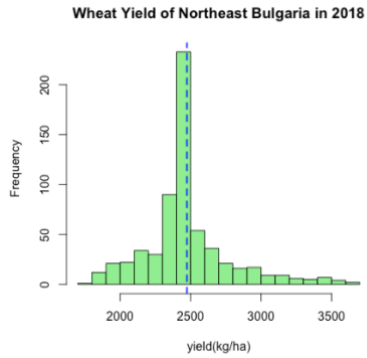
Wheat Yield of Northeast Bulgaria in 2018
Frequency
0
50
100
150
200
2000 2500 3000 3500
yield(kg/ha)

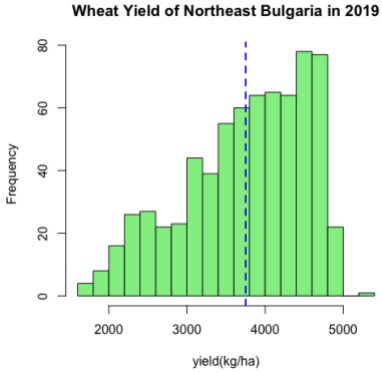
Wheat Yield of Northeast Bulgaria in 2019
Frequency
0
20
40
60
80
2000 3000 4000 5000
yield(kg/ha)

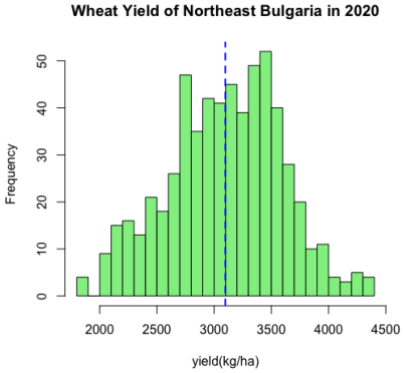
Wheat Yield of Northeast Bulgaria in 2020
Frequency
0
10
20
30
40
50
2000 2500 3000 3500 4000 4500
yield(kg/ha)

**Figure A3.2** Predicted wheat yield distributions of northcentral Bulgaria from 2001-2020 (red line refers to observed wheat yield and blue line refers to predicted wheat yield). X-axis refers to wheat yield (kg/ha) and Y-axis refers to number of villages.

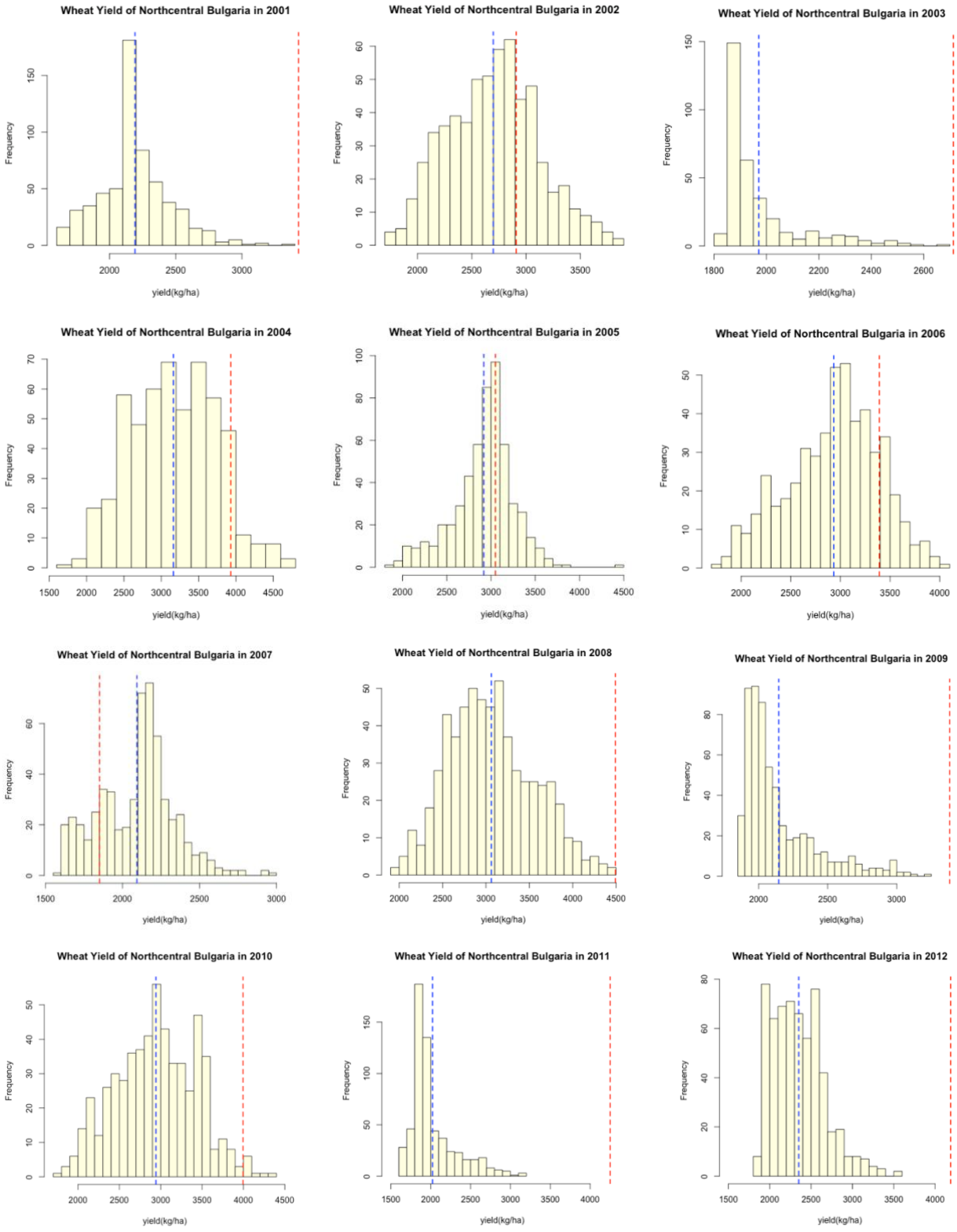

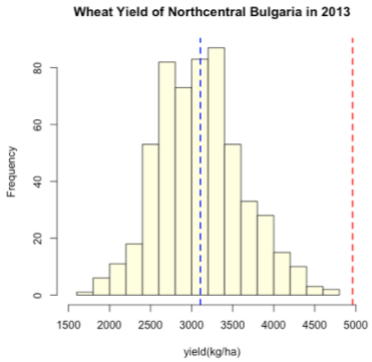
Wheat Yield of Northcentral Bulgaria in 2013
Frequency
yield(kg/ha)

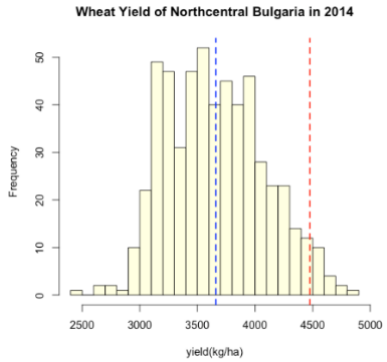
Wheat Yield of Northcentral Bulgaria in 2014
Frequency
yield(kg/ha)

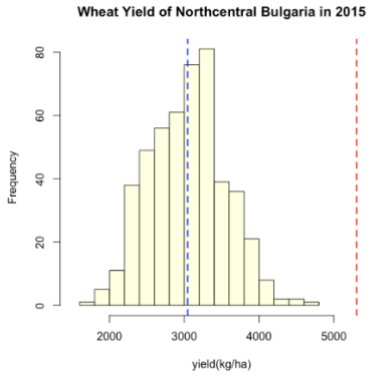
Wheat Yield of Northcentral Bulgaria in 2015
Frequency
yield(kg/ha)

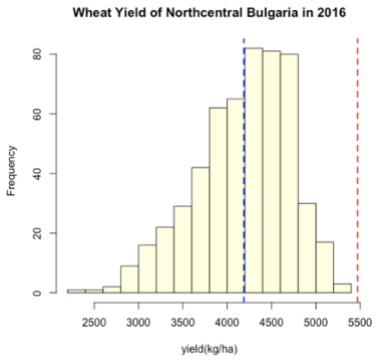
Wheat Yield of Northcentral Bulgaria in 2016
Frequency
yield(kg/ha)

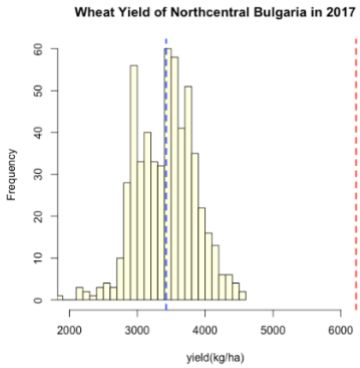
Wheat Yield of Northcentral Bulgaria in 2017
Frequency
yield(kg/ha)

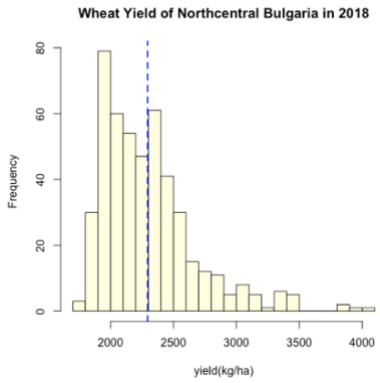
Wheat Yield of Northcentral Bulgaria in 2018
Frequency
yield(kg/ha)

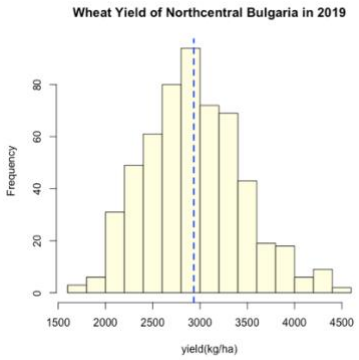
Wheat Yield of Northcentral Bulgaria in 2019
Frequency
yield(kg/ha)

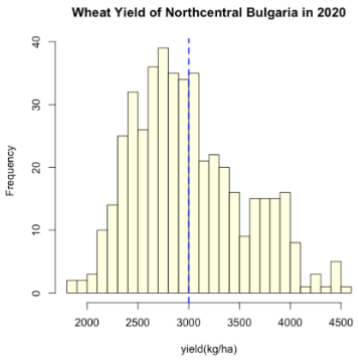
Wheat Yield of Northcentral Bulgaria in 2020
Frequency
yield(kg/ha)

**Figure A3.3** Predicted wheat yield distributions of southeast Bulgaria from 2001-2020 (red line refers to observed wheat yield and blue line refers to predicted wheat yield). X-axis refers to wheat yield (kg/ha) and Y-axis refers to number of villages.

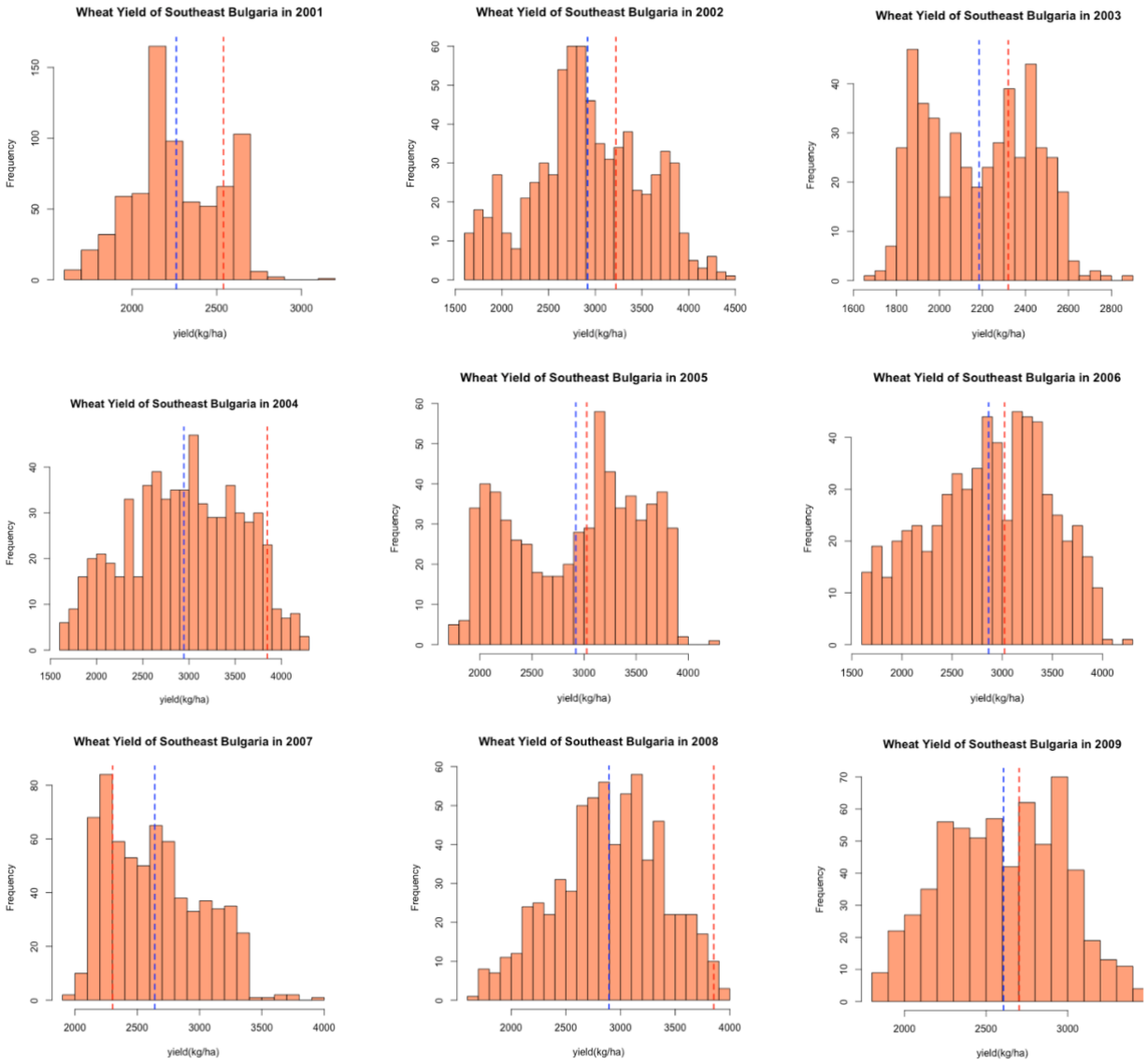

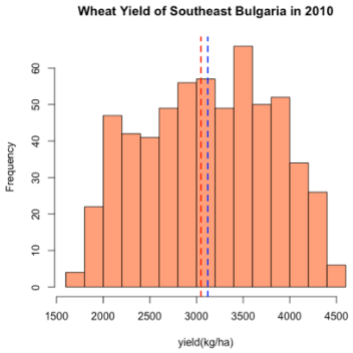
Wheat Yield of Southeast Bulgaria in 2010
Frequency
yield(kg/ha)

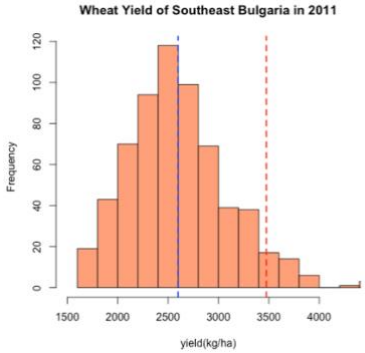
Wheat Yield of Southeast Bulgaria in 2011
Frequency
yield(kg/ha)

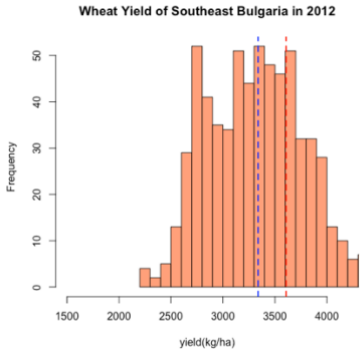
Wheat Yield of Southeast Bulgaria in 2012
Frequency
yield(kg/ha)

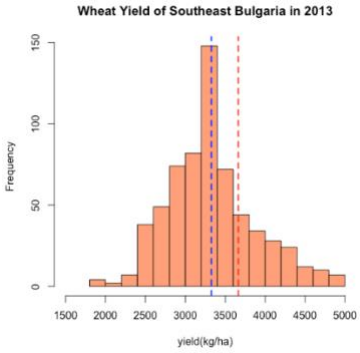
Wheat Yield of Southeast Bulgaria in 2013
Frequency
yield(kg/ha)

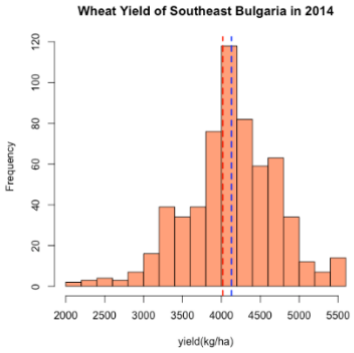
Wheat Yield of Southeast Bulgaria in 2014
Frequency
yield(kg/ha)

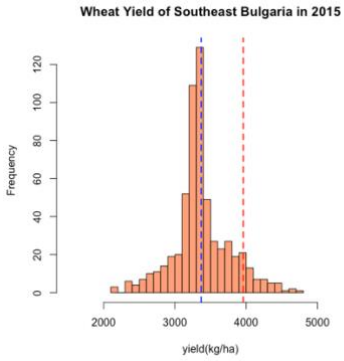
Wheat Yield of Southeast Bulgaria in 2015
Frequency
yield(kg/ha)

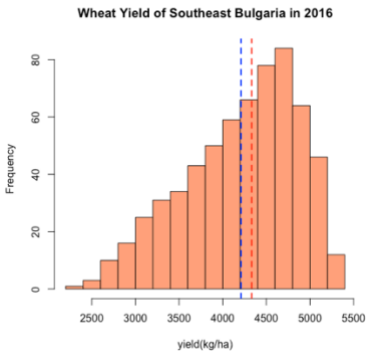
Wheat Yield of Southeast Bulgaria in 2016
Frequency
yield(kg/ha)

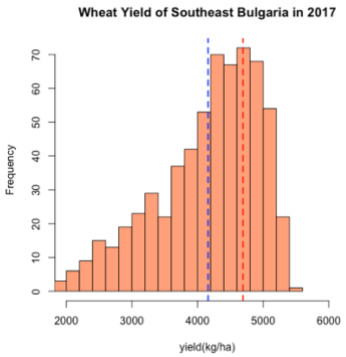
Wheat Yield of Southeast Bulgaria in 2017
Frequency
yield(kg/ha)

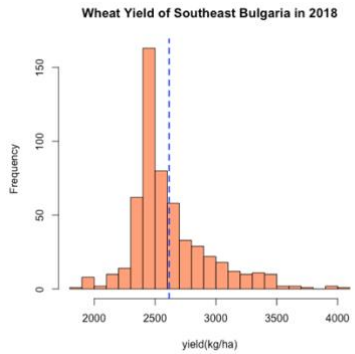
Wheat Yield of Southeast Bulgaria in 2018
Frequency
yield(kg/ha)

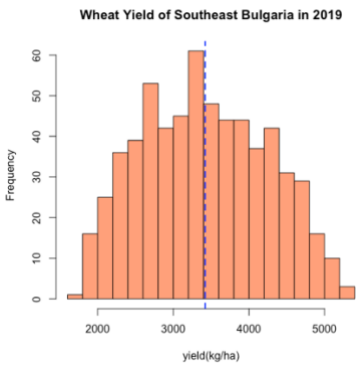
Wheat Yield of Southeast Bulgaria in 2019
Frequency
yield(kg/ha)

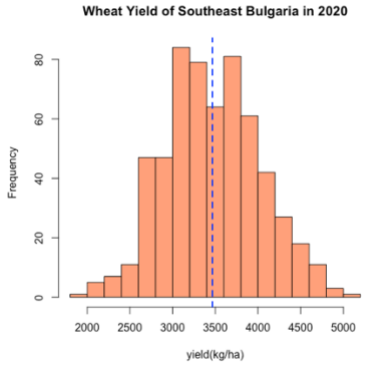
Wheat Yield of Southeast Bulgaria in 2020
Frequency
yield(kg/ha)

**Figure A3.4** Predicted wheat yield distributions of southcentral Bulgaria from 2001-2020 (red line refers to observed wheat yield and blue line refers to predicted wheat yield). X-axis refers to wheat yield (kg/ha) and Y-axis refers to number of villages.

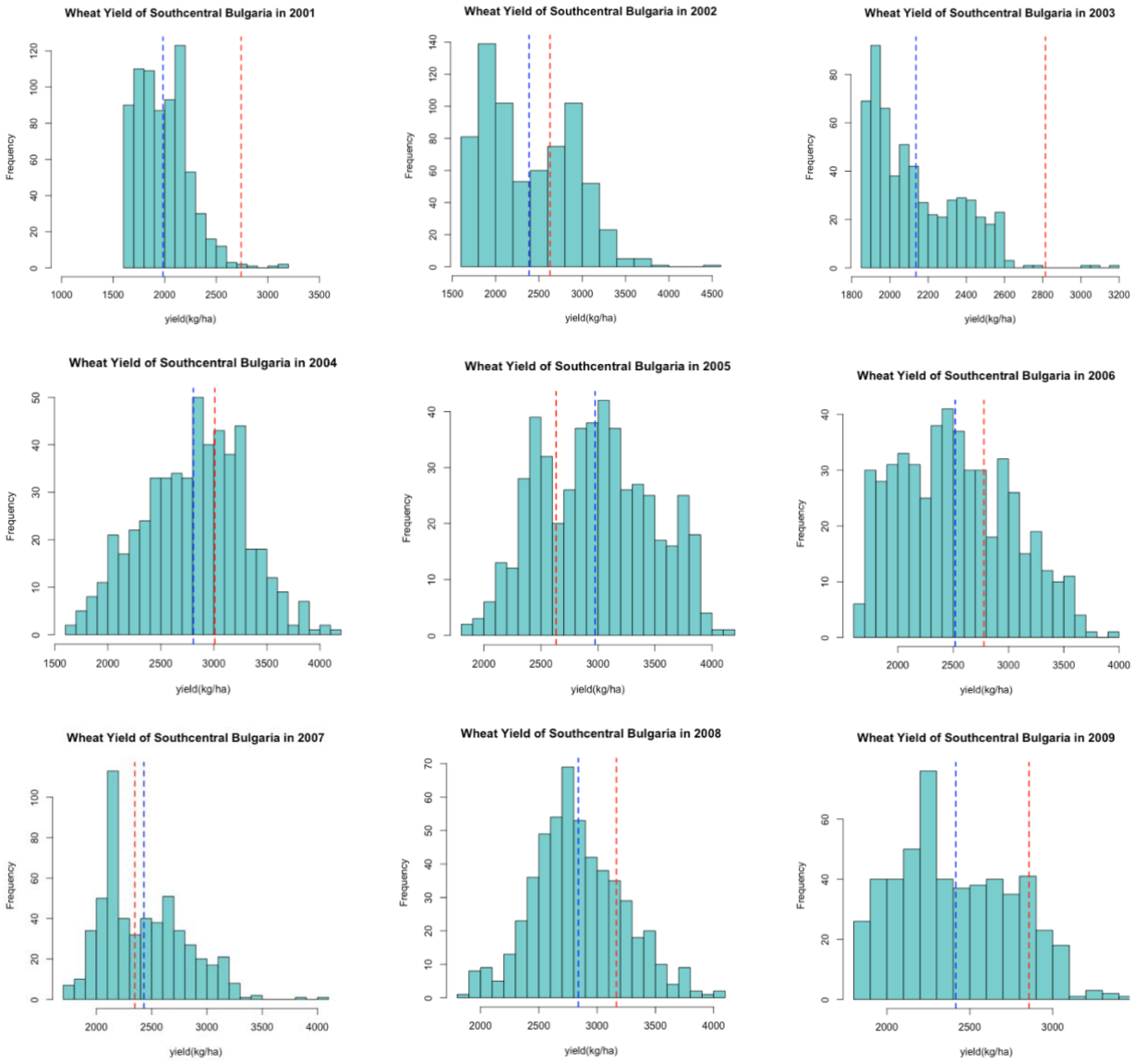

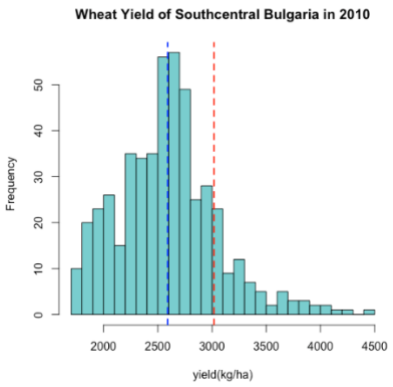
Wheat Yield of Southcentral Bulgaria in 2010
Frequency
yield(kg/ha)

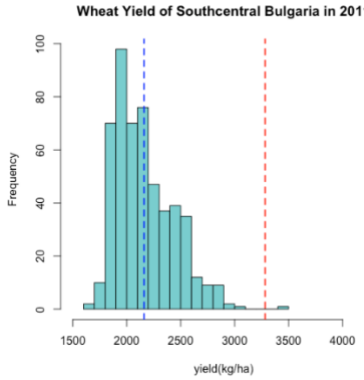
Wheat Yield of Southcentral Bulgaria in 2011
Frequency
yield(kg/ha)

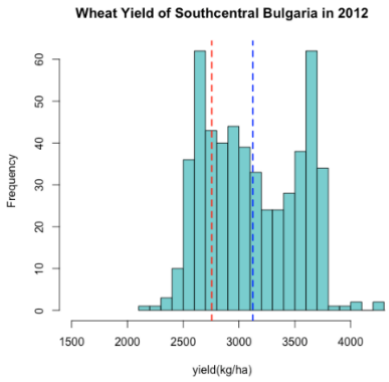
Wheat Yield of Southcentral Bulgaria in 2012
Frequency
yield(kg/ha)

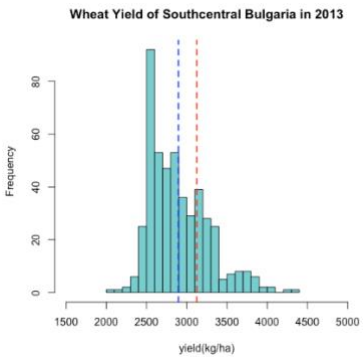
Wheat Yield of Southcentral Bulgaria in 2013
Frequency
yield(kg/ha)

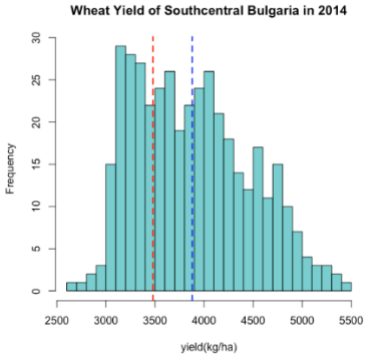
Wheat Yield of Southcentral Bulgaria in 2014
Frequency
yield(kg/ha)

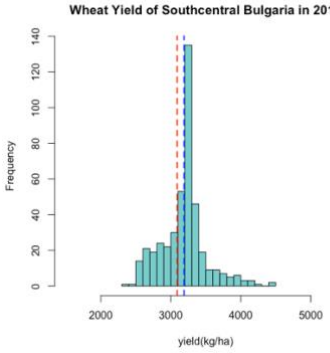
Wheat Yield of Southcentral Bulgaria in 2015
Frequency
yield(kg/ha)

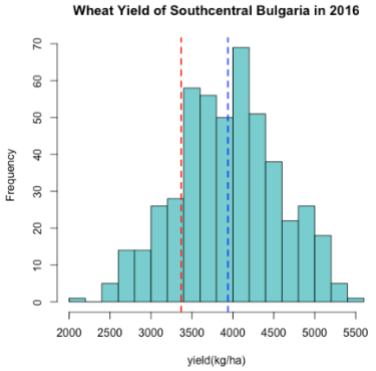
Wheat Yield of Southcentral Bulgaria in 2016
Frequency
yield(kg/ha)

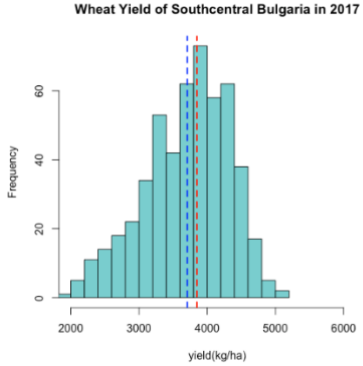
Wheat Yield of Southcentral Bulgaria in 2017
Frequency
yield(kg/ha)

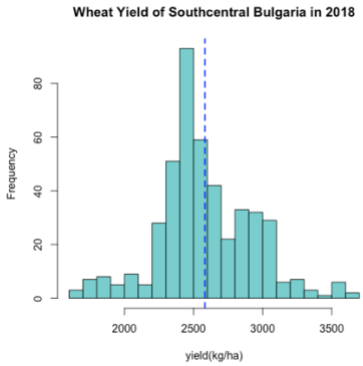
Wheat Yield of Southcentral Bulgaria in 2018
Frequency
yield(kg/ha)

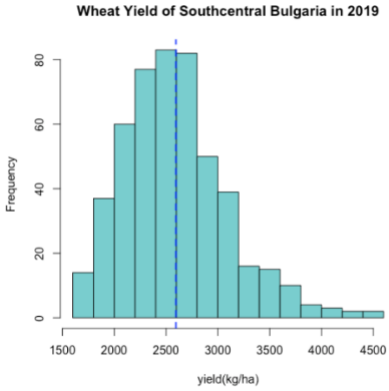
Wheat Yield of Southcentral Bulgaria in 2019
Frequency
yield(kg/ha)

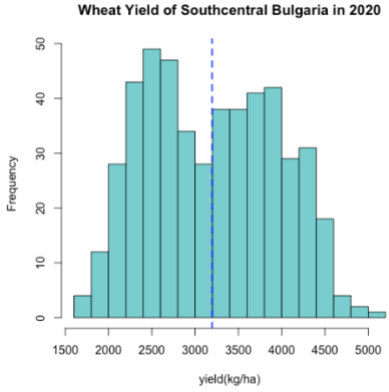
Wheat Yield of Southcentral Bulgaria in 2020
Frequency
yield(kg/ha)

**Figure A3.5** Predicted wheat yield distributions of Edirne (Turkey) from 2001-2020 (red line refers to observed wheat yield and blue line refers to predicted wheat yield). X-axis refers to wheat yield (kg/ha) and Y-axis refers to number of villages.

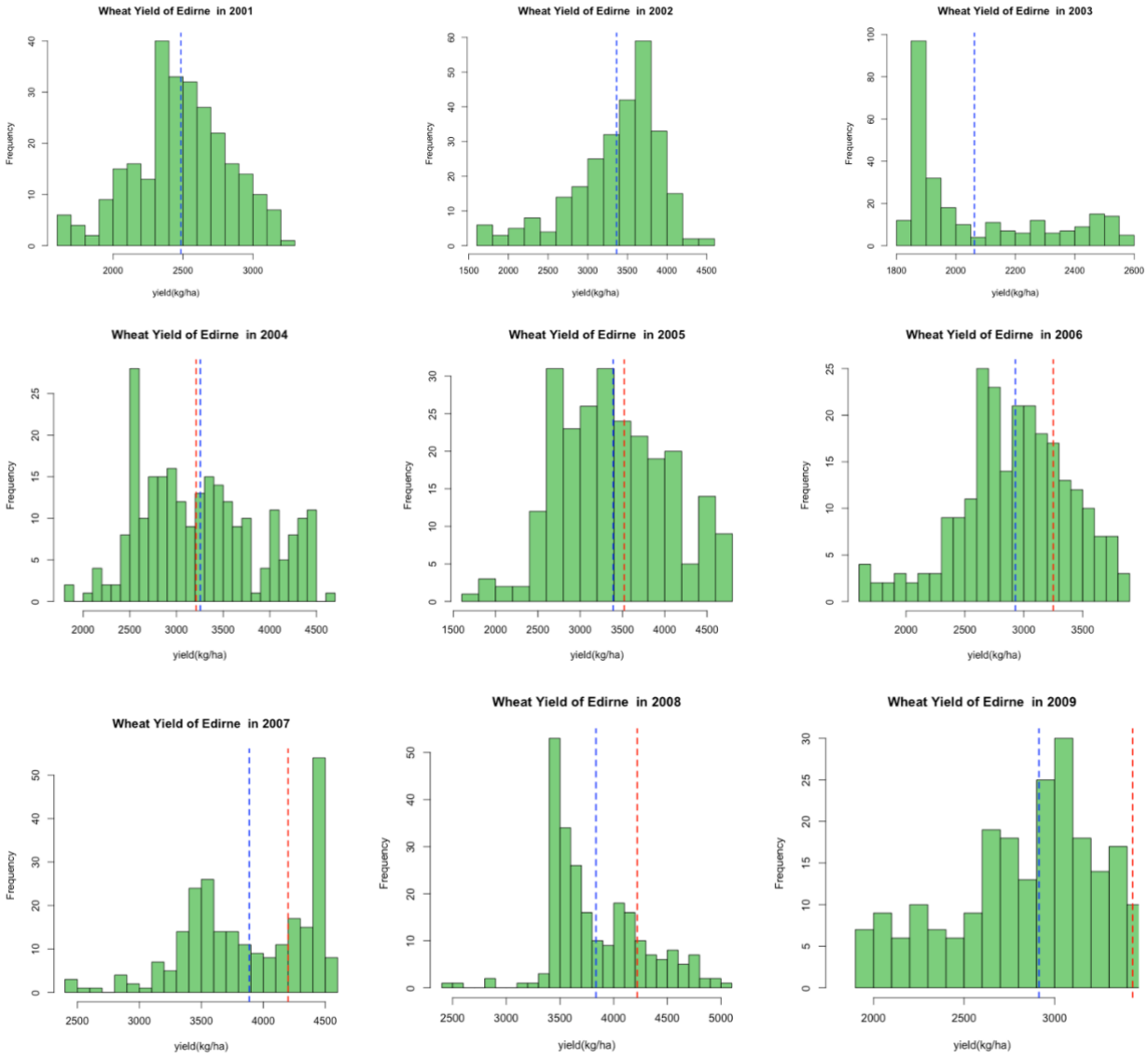

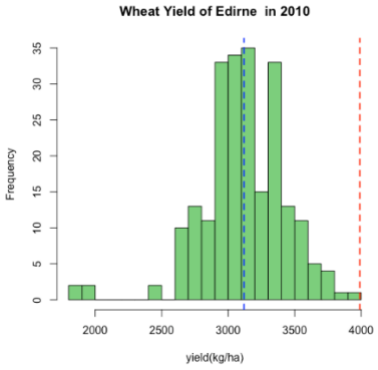
Wheat Yield of Edirne in 2010
Frequency
yield(kg/ha)

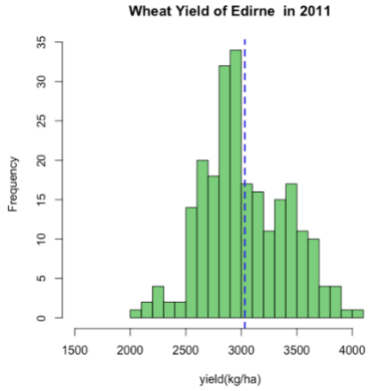
Wheat Yield of Edirne in 2011
Frequency
yield(kg/ha)

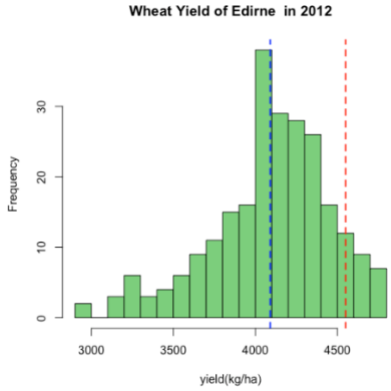
Wheat Yield of Edirne in 2012
Frequency
yield(kg/ha)

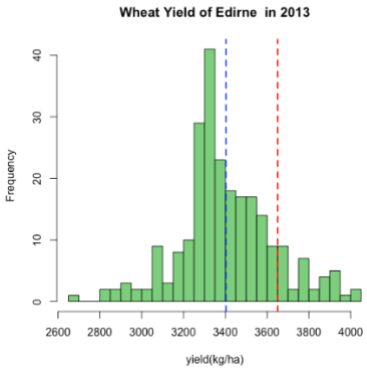
Wheat Yield of Edirne in 2013
Frequency
yield(kg/ha)

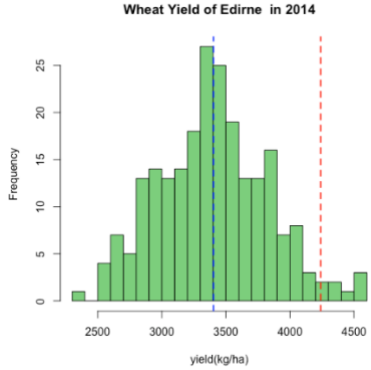
Wheat Yield of Edirne in 2014
Frequency
yield(kg/ha)

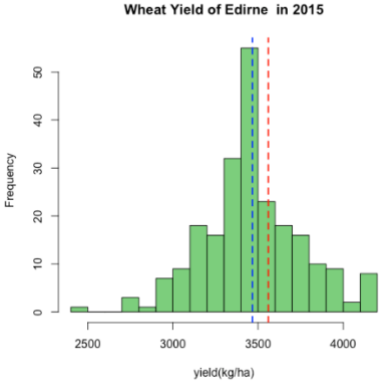
Wheat Yield of Edirne in 2015
Frequency
yield(kg/ha)

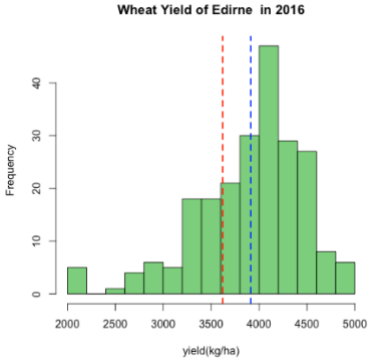
Wheat Yield of Edirne in 2016
Frequency
yield(kg/ha)

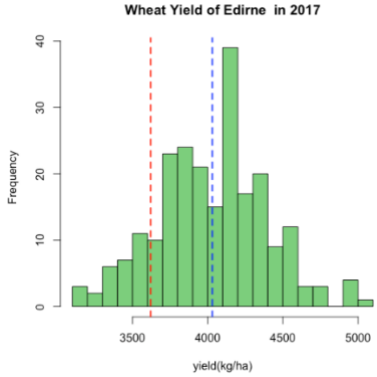
Wheat Yield of Edirne in 2017
Frequency
yield(kg/ha)

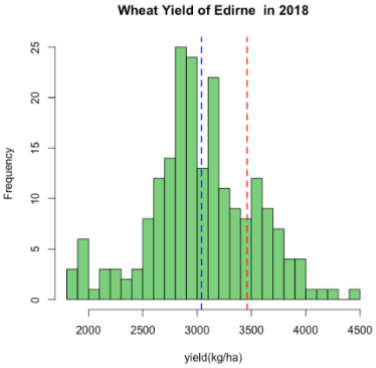
Wheat Yield of Edirne in 2018
Frequency
yield(kg/ha)

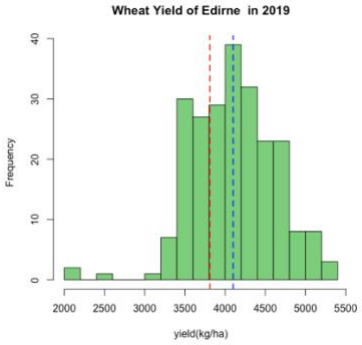
Wheat Yield of Edirne in 2019
Frequency
yield(kg/ha)

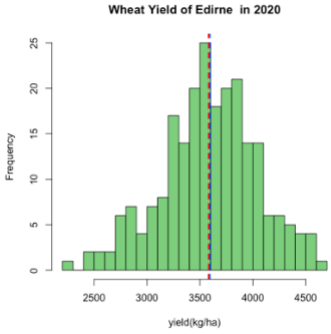
Wheat Yield of Edirne in 2020
Frequency
yield(kg/ha)

**Figure A3.6** Predicted wheat yield distributions of Kirklareli (Turkey) from 2001-2020 (red line refers to observed wheat yield and blue line refers to predicted wheat yield). X-axis refers to wheat yield (kg/ha) and Y-axis refers to number of villages.

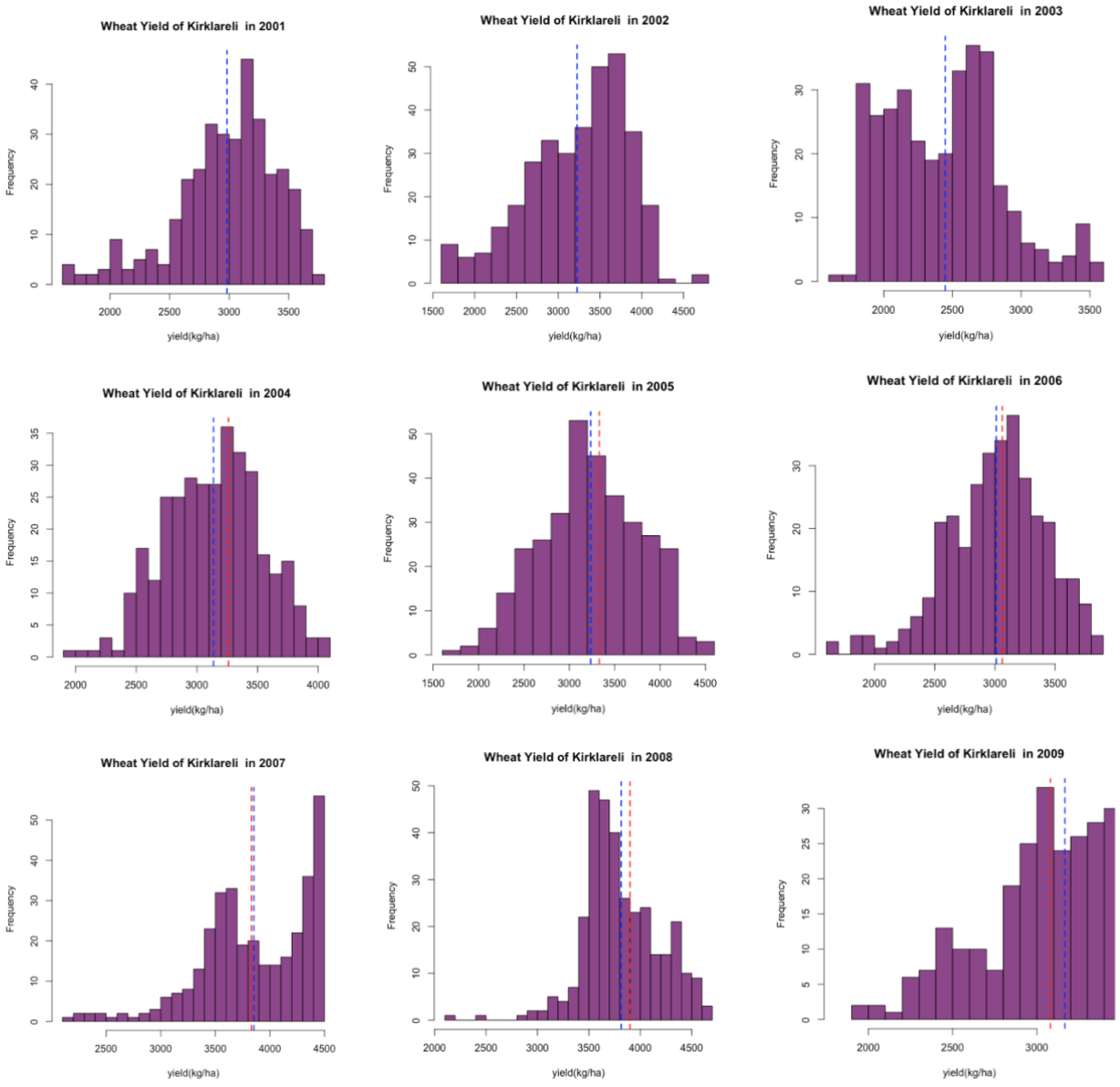

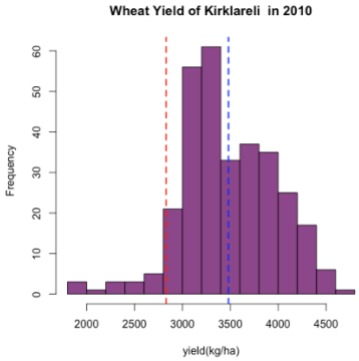
Wheat Yield of Kirklareli in 2010
Frequency
yield(kg/ha)

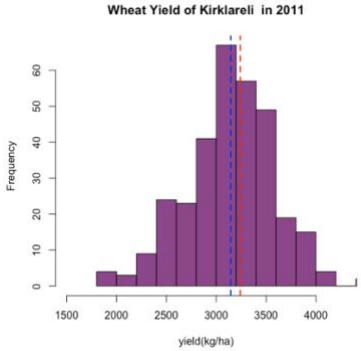
Wheat Yield of Kirklareli in 2011
Frequency
yield(kg/ha)

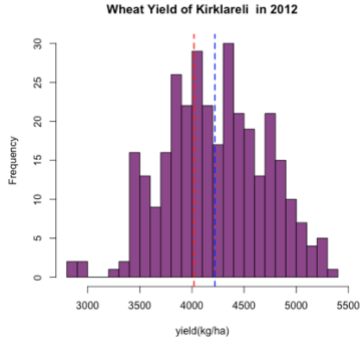
Wheat Yield of Kirklareli in 2012
Frequency
yield(kg/ha)

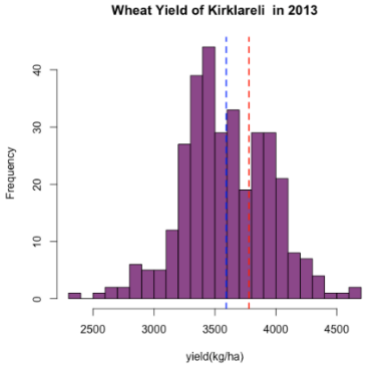
Wheat Yield of Kirklareli in 2013
Frequency
yield(kg/ha)

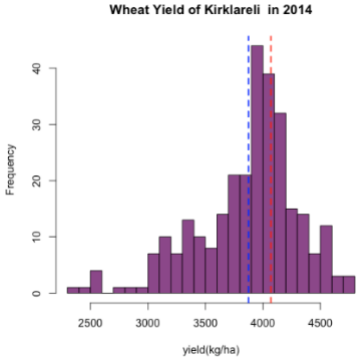
Wheat Yield of Kirklareli in 2014
Frequency
yield(kg/ha)

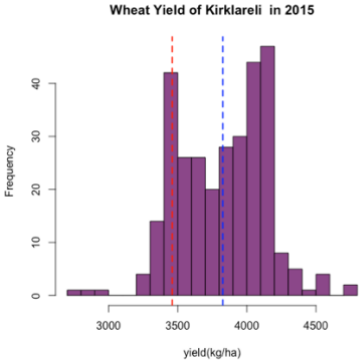
Wheat Yield of Kirklareli in 2015
Frequency
yield(kg/ha)

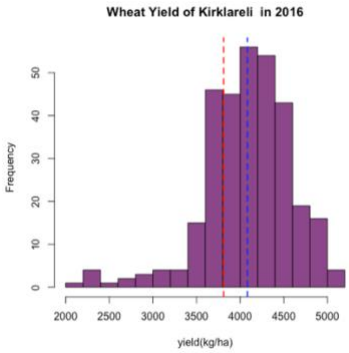
Wheat Yield of Kirklareli in 2016
Frequency
yield(kg/ha)

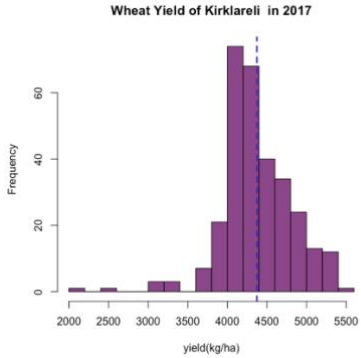
Wheat Yield of Kirklareli in 2017
Frequency
yield(kg/ha)

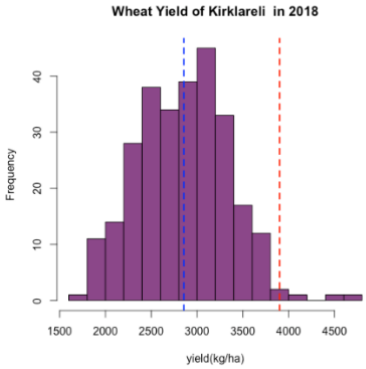
Wheat Yield of Kirklareli in 2018
Frequency
yield(kg/ha)

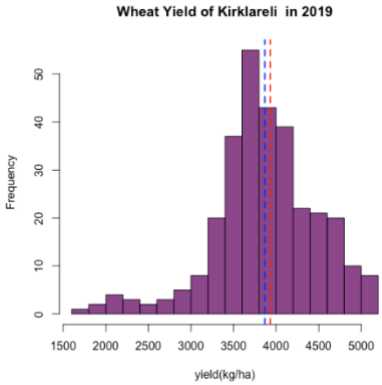
Wheat Yield of Kirklareli in 2019
Frequency
yield(kg/ha)

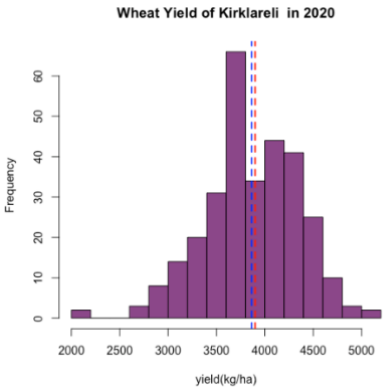
Wheat Yield of Kirklareli in 2020
Frequency
yield(kg/ha)

**Figure A3.7** Predicted wheat yield distributions of Tekirdag (Turkey) from 2001-2020 (red line refers to observed wheat yield and blue line refers to predicted wheat yield). X-axis refers to wheat yield (kg/ha) and Y-axis refers to number of villages.

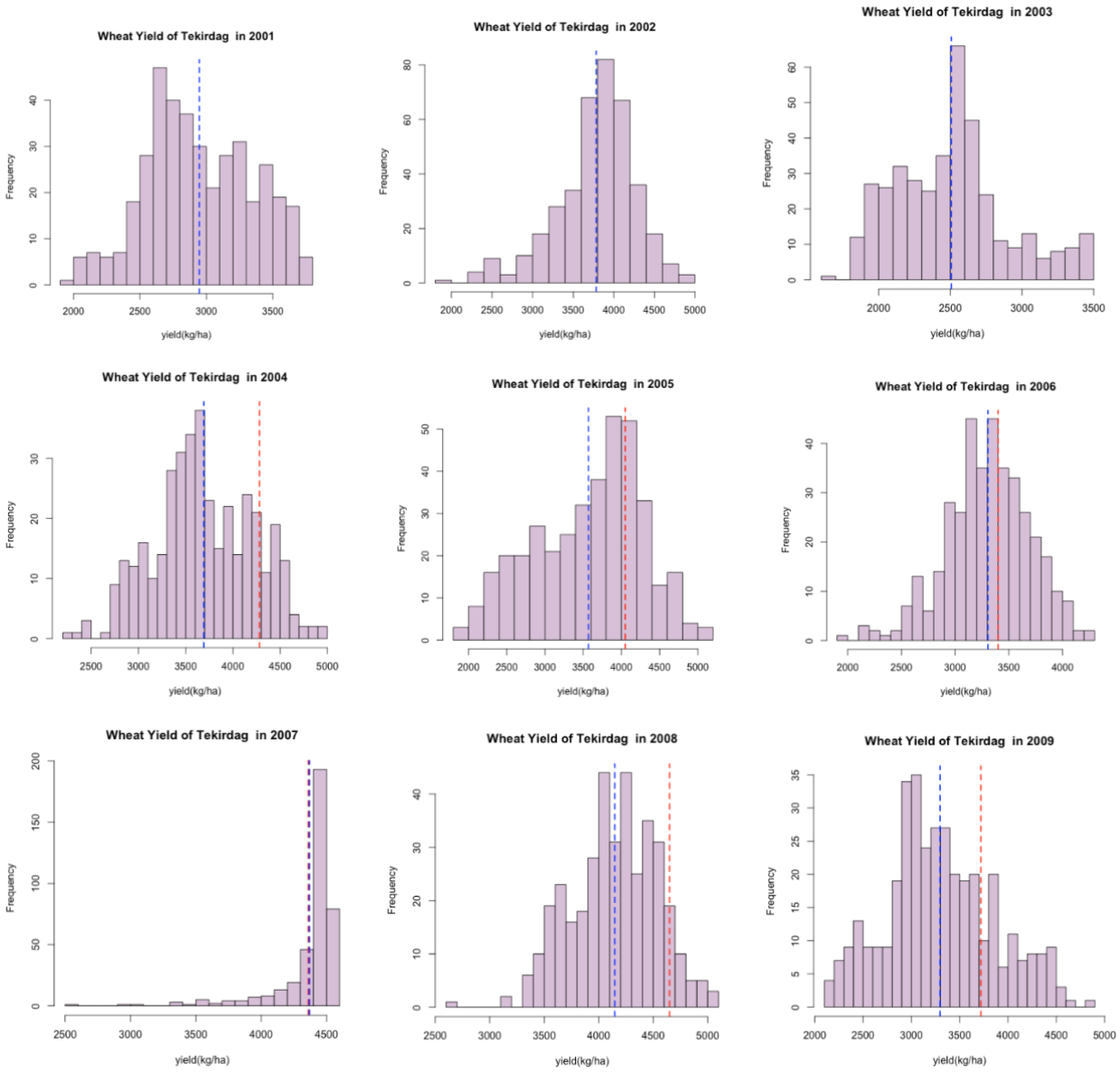

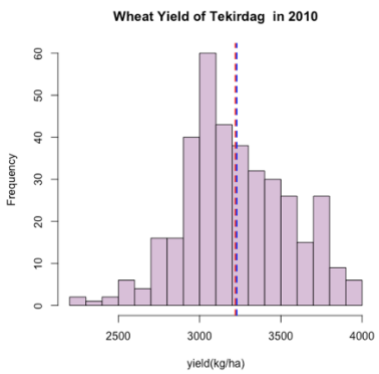
Wheat Yield of Tekirdag in 2010
Frequency
yield(kg/ha)

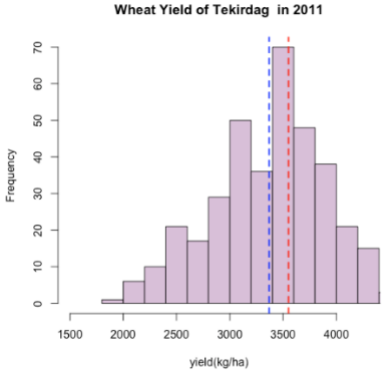
Wheat Yield of Tekirdag in 2011
Frequency
yield(kg/ha)

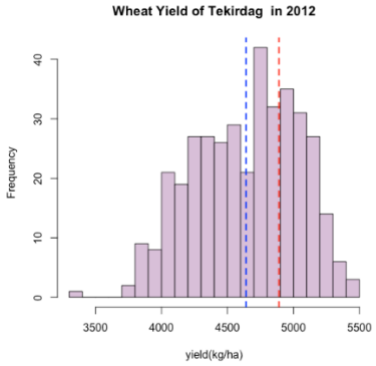
Wheat Yield of Tekirdag in 2012
Frequency
yield(kg/ha)

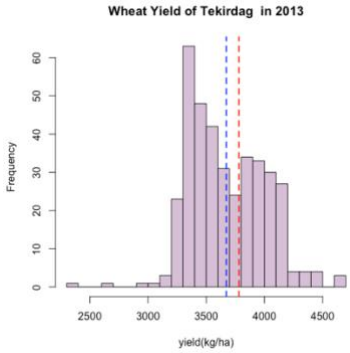
Wheat Yield of Tekirdag in 2013
Frequency
yield(kg/ha)

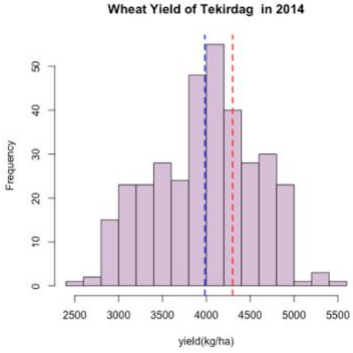
Wheat Yield of Tekirdag in 2014
Frequency
yield(kg/ha)

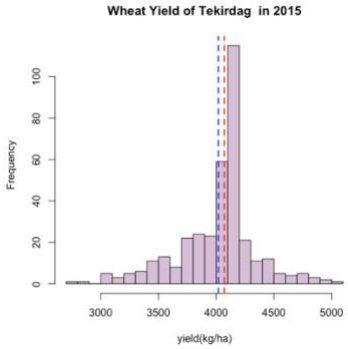
Wheat Yield of Tekirdag in 2015
Frequency
yield(kg/ha)

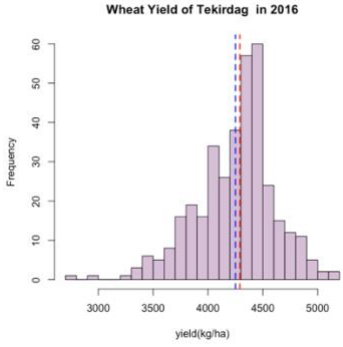
Wheat Yield of Tekirdag in 2016
Frequency
yield(kg/ha)

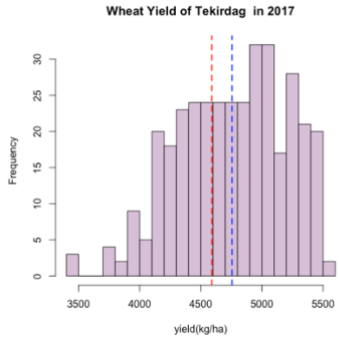
Wheat Yield of Tekirdag in 2017
Frequency
yield(kg/ha)

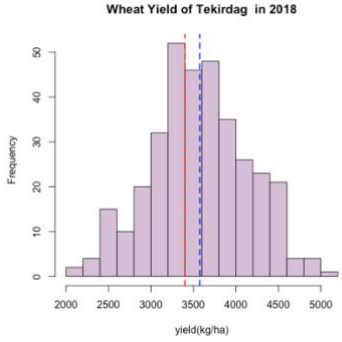
Wheat Yield of Tekirdag in 2018
Frequency
yield(kg/ha)

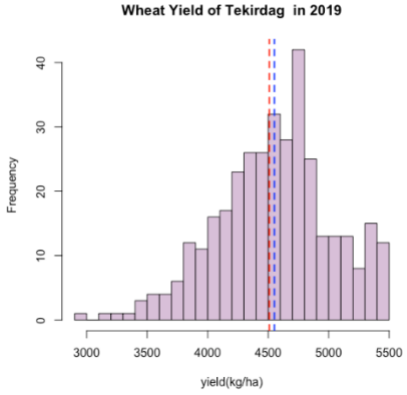
Wheat Yield of Tekirdag in 2019
Frequency
yield(kg/ha)

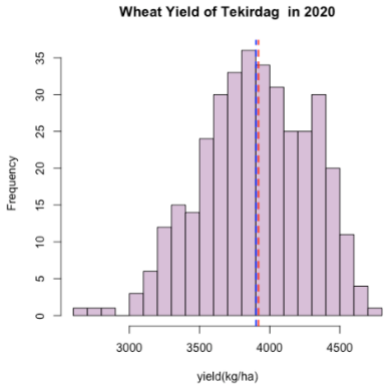
Wheat Yield of Tekirdag in 2020
Frequency
yield(kg/ha)

## Chapter 4

## Investigating local and regional drivers of agricultural land and production changes in the cross-border area between Turkey and Bulgaria


### Abstract

Agricultural lands with similar agroecological and climatic characteristics usually have equal capacity to produce but often don't because of various socio-economic underpinnings. This study presented one such example in the cross-border area between Turkey and Bulgaria, located in Mediterranean Europe. After the implementation of Common Agricultural Policies (CAP) of the European Union (EU) in Bulgaria in 2007, the agricultural sector underwent substantial changes: The rural development program was initiated, direct payments were distributed to farmers, and consolidation of agricultural lands was implemented. In contrast, Turkish side of the border had a stable agricultural sector for the last 30 years. To this date, there has been no quantitative assessment of the patterns, distributions, and drivers of agricultural production changes in the region. In this study, we investigated the staple crop (wheat) yield trends and patterns with respect to the socioeconomic changes in the study area using a simple statistical approach (using bins) and geospatial analysis. We quantified these trends using the Mann-Kendall trend test (MK-test). The results show that wheat yield in Bulgarian villages and regions changed considerably after the implementation of CAP. The number of villages with high wheat yield (>3500 kg/ha) increased (~4 times compared to before CAP) and the number of villages with low wheat yield (<2500 kg/ha) decreased significantly (~2.5 times compared to before CAP) after 2007. Even in locations with low suitability soils the number of villages with high wheat yield had considerable increases (from 10 to 100) after 2007 in Bulgaria. The results of MK-test showed that high yield villages increased by ~10% in number in post accession period compared to its decrease (~10%) in pre-accession

period (Sens' slope changed from -100 to 100) and low yield villages increased by ~10% in pre-accession period compared to its decrease by ~10% in post-accession period (Sens' slope changes from 100 to -100). Given the major changes in the socio-economic variables (such as increases in tractors and employment in agriculture) in Bulgaria after the CAP implementation, we can safely conclude that CAP implementation in 2007 had significant positive impact on wheat yield production in the country. Note that while we also observe important wheat yield changes in Turkey for the same period, the reasons were not related to CAP and appear to be a result of Turkey's own non-CAP agricultural policies. Overall, this study provided high-level reasons for wheat yield change in the study area at the village scale over the last 20 years. The results suggest that the support policy had different and significant impacts on agricultural production changes in each village and policy design should consider each farm or village capacity separately for equal benefit across the nation.

## 4.1 Introduction

Earth's biosphere has been consistently modified by human activities (Foley et al., 2005; Chhabra et al., 2006; Ramankutty et al., 2018). Agricultural land use is one such modification impacting food security, sustainable development, and environmental policies (DeFries et al., 1995; Godfray et al., 2010). In the near future, 70% more food will need to be produced to meet the calorific demands of rapidly increasing population, and that can be achieved either by expansion or intensification of agricultural lands (Maxwell, 1996; Godfray et al., 2010; Wheeler et al., 2013; Meyfroidt et al., 2017). The Green Revolution was one such historical event, which accelerated agricultural intensification and doubled the world's food production (from 1961 to 1996) with only a 10% increase in arable lands globally, but there was a rapid and negative impact on global ecosystem services and environmental footprint (Conway 1998; Roy et al., 2007; Thenkabail et al., 2010; Duncan et al., 2015). To this end, more studies are needed to better understand the drivers and consequences of land use transformations involving agricultural areas.

The geographic distribution of agricultural land use is a complex phenomenon and needs further exploration of its drivers (Lambin et al., 2003; Meyfroit et al., 2014). For example, croplands have decreased or have been abandoned due to forest transitions, urbanization, soil degradation, global warming, and desertification (Baumann et al., 2011; Prishchepov et al., 2013) in some locations, while in others they have expanded through slash-and-burn agriculture and cultivation of bio-fuel crops and boom crops (Kraemer et al., 2015; Hurni et al., 2017). Literature suggests that at local scales, land use decisions are made in hierarchical order where local actors and socio-economic factors are inter-dependent (Fernandez et al., 2007; Shen et al., 2009; Verburg et al., 2019), although socio-economic factors usually dominate (Dang et al., 2017; Therond et al., 2019). While local actors are responsible for decisions driven to change land use, data on local

actors is scarce (Prishchepov et al., 2017). Moreover, socio-economic and political changes are different for different locations or countries and regions (Kuemmerle et al., 2013), making it even more challenging to study the impact of support policies on land use change and crop production (Lambin, 2003). These and other studies suggest that to understand human dimensions in land use modeling, it is important to interlink the observed changes to underlying drivers, including the local actors. These local actors are shown to be highly influential in affecting agricultural land use and land cover changes at local scales. On the other hand, at broader scale, political and socio-economic factors (like policies) play a stronger role. Therefore, implementing a holistic approach that considers environmental, biophysical, and socio-economic variables and their interrelations is required to better understand the impact of human dimensions on land use and land cover changes. One approach to overcome these challenges is to focus on locations where rapid changes in socio-economic and political structures occurred in tandem with relatively stable socio-economic forces, creating "a natural experiment" (Prishchepov et al., 2013).

One example of such a natural experiment is at the cross-border area between Turkey and Bulgaria. This cross-border region has homogeneous agro-ecological and climatic characteristics, but the amount and patterns of agricultural land use change and production on each side of the border may be dramatically different. There is certainly evidence for such dramatic differences given the socialist history of Bulgaria that was replaced with accession to the EU in 2007. In contrast, Turkey has been a politically stable country for close to 100 years, without major socio-economic transformations. To this end, our study is focused on investigating how contrasting political changes are manifested in agricultural land use change in the study area.

Land use change is a function of environmental, biophysical, climatic, and socio-economic variables, and this function has different outcomes when observed for different geographic scales.

For example, the drivers of land use change at village scale are different than the drivers at the regional or national scale. The main limitation to study the drivers of land use change at village or field scale is availability of socio-economic data. Remote sensing provides an opportunity to derive biophysical or environmental datasets at field-scale through satellite image processing, but socio-economic drivers of land use change are usually available at national to sub-national scales.

With this context, the overarching goal of this study is to investigate if socio-economic changes in the study area have significant impact on a staple crop (wheat) yield change in the study area between 2001 and 2020. We used wheat yield estimates from Chapter 3 to investigate the policy implications in this chapter. We demonstrated three ways of assessing the village-scale wheat yield change patterns and distributions in relation to policy implications, including: i) a bin analysis approach; ii) geospatial modeling to understand the relation between soil quality and wheat yield; and iii) a Mann-Kendall trend test.

## 4.2 Study area

The study area is geographically situated in southeastern Europe (Figure 4.1) at the cross-border area between Turkey and Bulgaria. These cross-border areas are also known as Northern Thracia (Bulgaria) and Eastern Thracia (Turkey). The Bulgaria-side cross-border area covers 75,000 square kilometers of land and covers northcentral, northeast, southeast, and southcentral planning regions with 18 provinces and 177 municipalities. The Turkey-side cross border area covers the Northwest or Tekirdag subregion with three provinces (Edirne, Tekirdag, and Kirklareli) and 26 districts.

Agriculture is an important land use in the study region, covering more than 60% of the landscape in the study area, operated under very similar agro-ecological and climatic patterns

(FAO, 2019). Wheat is the major crop harvested in the winter, covering approximately 40% of the cultivated area in the region. This study area is situated on the border of the European Union.

The prominent topographical features defining Bulgaria's climate (mostly humid-continental, but sub-tropical in the southernmost part) are the Danubian Plain (in the north), the Balkan Mountains (in the center), the Thracian Plain (in the southeast) and the Rhodope Mountains (in the southwest) with elevation ranging from 0 m (Thracian Plain) to 2,900 m (Mount Musala in southwest Bulgaria). The major river flowing at the cross-border region between Bulgaria and Turkey is the Maritsa River with its tributaries. The average temperature and precipitation in Bulgaria are 3.45ºC and 630 mm, respectively. Northern Bulgaria is cooler and has higher precipitation compared to southern Bulgaria. Southern Bulgaria has 63% of total population, with population density of 81.5 people per km². Bulgaria's population rate has been continuously declining at a constant pace (Figure A4.1).

The cross-border area of Turkey is also known as European Turkey or Turkish Thrace. Although it covers only 3% of the total area (23,764 $km^2$) of Turkey, 14% of the total population lives here (about 11 million people), with average population density of 470 people per km² (compared to the highest in European Istanbul, which is1,564 people per km²). The total population of Turkey is rapidly increasing since 1950 (Figure A4.1). Eastern Thrace shares a border with Greece (212 km), Bulgaria (269 km), the Aegean Sea and the Black Sea. Because of its unique geographic location (at the transitional area between two continents), and its role as a sea-based trade corridor for many countries (Russia, Ukraine, Romania, Bulgaria, and Georgia), the region is the main connecting link for intercontinental and intercountry transports. Climatic conditions in the region are mostly Mediterranean, with the highest temperature of 35 ºC and lowest temperature of 12 ºC.

The key characteristics observed in agricultural land use change between the two countries are: i) agricultural land area and production in Bulgaria had increasing trends whereas Turkey had declining or mixed trends; ii) the number of farms with less than two hectares (smallholder) in size declined, and the number of farms with size >20 ha increased in Bulgaria after 2007; no such changes have been observed in Turkey except for the introduction of an indivisible parcel size law in 2007 that prevented further fragmentation of fields smaller than 0.5 ha; iii) wheat import was stagnant and exports increased in Bulgaria after 2007 while wheat import in Turkey had increased drastically with no changes in export; and iv) wheat area and yield in Bulgaria experienced a sudden increase after 2003, whereas Turkey continued to have the same pace in increasing yield with a slight reduction in wheat area (FAO, 2019 and EUROSTAT, 2019) (Table 4.1).

## 4.3 Agricultural socio-economic history in the study area

This study is focused on understanding the socio-economic dynamics in the study area and relating it to the food security of the region. For this purpose, we synthesized different agricultural policy and socio-economic-related literature to form a unique hypothesis. Agricultural socio-economic history for each country is given as follows.

### *Bulgaria*

Bulgarian farms tend to be larger than those of many other countries in Europe because of a collectivized farm system in earlier years (around the 1990s). However, one large farm is typically composed of a many small farms, ranging in size from 1.5 ha to 3 ha, most of which are often rented by landowners to other farmers for cultivation (Bachev, 2019). European subsidies provide guaranteed income to such landowners, and as a result, land prices and rent values have become the biggest expense for farmers. Farming structures in Bulgaria had major changes after EU accession in 2007 (Borisov et al., 2019). Utilized agriculture area in farms with size >30 ha to

49.9 ha increased by 50% from 2005 to 2013, and again increased by 60% from 2013 to 2016, whereas utilized agriculture area in smaller farms of less than 2 ha decreased by 28% from 2007 to 2016 (Figure 4.2a). The highest growth was observed in farms of size >30 ha to 49.9 ha, which was about 31% higher in 2016 compared to the number of farms in 2005, whereas smaller farms of size < 2 ha decreased in number by 60% from 2005 to 2016. Overall, smaller farms with size less than 9.9 ha decreased in numbers compared to large farms of size >10 ha from 2005 to 2013 (Figure 4.2b).

Agriculture in Bulgaria was the leading sector before the Bulgaria Communist Party (BCP) started collectivization of Bulgarian farms in 1958. Since then, agricultural land area and production in Bulgaria showed declining trends until the reform of agriculture in 1990 after the Soviet Union breakdown (Vassilev, 1999). Bulgaria has an upper-middle income range market economy with 70% of GDP from private sectors. The transition from a centralized to market-driven economy (1944-1989), the collapse of the Soviet Union after 1990, and joining the European Union in 2007 are the major socio-economic events in Bulgaria's recent history, directly affecting agricultural land use change. This study will focus particularly on support policy changes after 2000, when Bulgaria was in the pre-accession period and had implemented assistance programs such as the pre-accession financial instrument of the European Union (PHARE) in 1990. Under the new Special Accession Programme for Agricultural and Rural Development (SAPARD), Bulgaria had an annual indicative allocation over the period of 2000 to 2006.

After communism, collective farmland was resituated to Bulgarians and millions of other occupants of the post-communist nation in the 1990's. The significant policymakers in Eastern and Central Europe believed that the fragmentation of land was especially a vital impediment to the land market and the development of competitive products in the agricultural sector (Valdes,

2000). Since 2007, Common Agricultural Policy (CAP) determines agricultural decision making in the country. It involves a series of agreements that saw the nation receive significant numbers of grants and loans for a direct boost to the agricultural sector. After the creation and signing of the Common Agricultural Policy, the country received around EUR 7.4 billion for the farming sector in the seven years that would follow (Larson et al., 2014). The major priorities of the political system in Bulgaria include ensuring sustainability, job creation, innovation, modernization, and improvement of quality. The Common Agricultural Policy aids the nation in increasing its flexibility so that it can adapt both the direct payments and rural development projects to specific needs of the country.

*Turkey*

Agriculture is an important sector in Turkey with the highest share of the economy, but its share of the country's gross domestic product (GDP) has been decreasing from about 15% in 1999 to 6.8% in 2017 (Turkstat, 2019). The growth of the agricultural sector relative to population growth is unexpectedly slower. However, Turkey is self-sufficient in terms of food production with its highly fertile soil, rich water sources, and suitable climate. The study area of this research is focused on the Eastern Thrace region of Turkey, specifically on three provinces situated at the cross-border region: Kirklareli, Tekirdag, and Edirne. Edirne is an important contributor to the agriculturally based GDP of the country, with more than 70% of the population involved in agriculture for employment. The agricultural area in this region has doubled in the last decade, with an extensive area of wheat along with corn and sunflower (Turkstat, 2019). Tekirdag has the inland areas with fertile farmlands. Overall, the cross-border area is cultivated with winter wheat and sunflower as major crops. Tekirdag has the highest harvested area of all the major crops, whereas Edirne has the highest winter wheat area in 2004, but it declined after 2005.

According to the 2016 agricultural census, owner-occupied farms outpace tenants and sharecroppers, although their share is declining. Average farm=holding size in Turkey is 6-8 ha, with farm parcels of 0.5 ha (Table A.4.1). Approximately 65% of farmland falls into the 0 to 20 ha group of farm size. Farm sizes in Turkey, and especially in the northwestern areas, has not changed drastically in the last few decades mainly due to the fact that the majority of farms are owner-occupied. The complexities of the land tenure system and the principle of division of inheritance have hindered any real change in the patterns of landholdings. The central government recently enacted a series of regulations to prevent the fragmentation of agricultural lands, setting minimum field size requirements. According to this legal arrangement, marginal agricultural land with less than 2 ha, and cultivated land with less than 0.5 ha, has been prohibited from fragmentation since 2007.

Turkey is within the jurisdiction of policies imposed by the World Trade Organization because it was a founding member on March 26, 1995 (Larson et al., 2014). Hence, all agricultural policies shared by all members of WTO apply to Turkish land use and farming practices. The WTO influences agrarian systems in Turkey by sharing information with academia, the private sector, and public institutions. Another organization with significant influence in Turkish land and agricultural policies is the UN Food and Agriculture Organization (FAO). Turkey benefits from the technical assistance guaranteed by FAO. Additionally, the country makes significant technical and financial contributions which boost the efforts of FAO.

Turkey is also subject to policies dictated by the International Plant Protection Convention (IPPC). Turkey has been a member of the International Plant Protection Convention since July 11, 1988. However, the nation’s agricultural policies are mainly defined by the Agricultural Law No. 5488, which was adopted in 2006 (Akder, 2007). This legislation determines and regulates the

rules for agriculture and development in rural areas in line with the strategies and plans for the nation's development. This agricultural law also defines the scope, aims, and subjects of Turkey's agricultural policies. It describes the instruments for rural development and agricultural support. The law sets the legal, financial, and administrative structure of the primary research and development establishments in Turkey's agricultural sector. Major support tools in the period of 2006 to 2010 was direct income support (Table A.4.2).

Turkey's Ministry of Food, Agriculture, and Livestock selected some strategic areas on which to concentrate in the period between 2013 and 2017. These areas include food safety, plant health, welfare, animal health, rural development, agricultural infrastructure, security of supply, agricultural production, and institutional capacity. By 2023, Turkey targets an agrarian GDP of up to US$150 billion, with exports from agriculture exceeding US$150 billion (FAO, 2019). The country also wants to be in the top five states in the world as per its agricultural GDP. Land acquisition in Turkey by foreign investors does not have to be approved by the government. The acquisition is subject to the Foreign Direct Investment Law No.4875, which was enacted in 2003 (Hale, 2012). This law has assisted foreign investors who act in line with international investment standards to engage in various forms of investments in Turkey, especially in agriculture. Additionally, Article 3 of the Foreign Direct Investment Law treats foreign investors in the same way as domestic investors, especially if the investments are direct (Yilmaz, 2006). Table 4.2 provides specific socio-economic events regarding agricultural land use policies in each country.

**4.4 Methodology**

The purpose of this study was to investigate the socio-economic and environmental drivers of wheat yield and production changes in the study area. As a first step, we set up a hypothesis through detailed knowledge of the agricultural socio-economic history of the study area and by

considering the Bulgarian accession to European Union in 2007 as an important breakpoint. In second stage this study analyzed the trends and patterns of wheat yield at the village scale according to the hypothesis. In the third stage we simply observe the trends of socioeconomic variable changes in the study area and relate them to the changes in wheat yield patterns.

*Hypothesis*

First hypothesis of this study is: "While the cross-border area between Turkey and Bulgaria has similar agroecological characteristics, the current state and historical patterns of agricultural production are very different, fueled primarily by the break-neck pace of socio-economic changes in Bulgaria contrasted with relatively stable conditions in Turkey." With this hypothesis, we aim to address how the trends and patterns of wheat yield change in the 2001-2007 period are different compared to its changes in 2008-2020 due to implementation of the Common Agricultural Policy in Bulgaria in 2007.

The second hypothesis of this study is: "The trends and patterns of the wheat yield change in the different geographic regions of the study area are different in the last 20 years, and they have socio-economic underpinnings." With this hypothesis, we aim to address how the trends and patterns of wheat yield change in the 2001-2020 period are different in Turkey and Bulgaria according to the geographic location and socio-economics of the study area.

*Data*

This study used the wheat yield dataset from Chapter 3 (Table 4.3). This remote sensing-based village-scale data covers Turkey and Bulgaria and provides wheat yield dataset from 2001-2020. The soil suitability dataset for this study collected from the Food and Agricultural Organization (FAO) with three main suitability classes: high suitability (class 1 and 2); medium

suitability (class 3 and 4); and low suitability (class 5 and 6), collected from http://www.fao.org/nr/gaez/about-data-portal/agricultural-suitability-and-potential-yields/en/. To understand the socio-economic changes in the study area, this study collected different types of agricultural structure, policy, and inputs-related variables, along with a time dummy variable (Table 4.3). For the time dummy variable "0" value was set for the pre-accession period wheat yields (2001-2007) and "1" value for the post-accession period (2008-2020). The socio-economic variables were collected from each country's government statistical data sources. Socio-economic variables included population, gross domestic product (GDP), employment in agriculture, and unemployment rates. Agricultural input-related variables incorporated in this study are tractors, cattle, and irrigation. Agricultural policy-related variables were mainly the financial instruments used post- and pre-accession in Bulgaria such as single agricultural payments. Agricultural structure-related variables incorporated are the number of holdings, legal person holdings, and number of managers.

*Patterns and distributions of wheat yield change at village scale*

This study used three different ways of assessing the spatiotemporal wheat yield trends and patterns in respect to socio-economic changes using statistical and geospatial analysis.

The first method aimed to present and compare these distributions before and after 2007 (for hypothesis 1 test) and 2001 to 2020 (for hypothesis-2 test). This method used a binning approach performed separately for each country's data. The first step in the bin analysis was to measure the number of villages with the specific wheat yield range in each year and each country. Each bin consisted of 500 kg/ha wheat yield, starting from 0 kg/ha to 5500 kg/ha. In the next step, these bins across each year and each country were plotted using bar plots. Finally, these bin plots for each country were interpreted in order to understand its patterns and distributions for pre-

accession (before the CAP) and post-accession (after the CAP) changes and changes for entire time-period from 2001-2020.

The second method aimed to present the patterns and distributions of wheat yield according to its relation to soil suitability. In this method, bins were classified using wheat yield range as well as soil suitability type. Wheat yield had three ranges – high yield (>3500 kg/ha), medium yield (between 2500 kg/ha and 3500 kg/ha), and low yield (<2500 kg/ha). Soil suitability had three major types: high, medium, and low. In total, this analysis classified the villages into nine classes according to soil suitability and wheat yield values such as- i) high yield high suitability, ii) high yield medium suitability, iii) high yield low suitability, iv) low yield high suitability, v) low yield medium suitability, vi) low yield low suitability, vii) medium yield high suitability, viii) medium yield medium suitability and, ix) medium yield low suitability. We also analyzed the spatial and temporal distribution of each class for each country through mapping as well as bin analysis.

Third method aimed to quantify village-scale wheat yield trends and patterns in each country before and after 2007. For this purpose, we used a Mann-Kendall (MK) test on wheat yield time-series data. An MK test offers a statistical assessment of monotonic upward or downward trends of the variable of interest over time (Mann, 1945; Kendall, 1975; Gilbert, 1987). It is non-parametric and widely used in the field of hydrology and climate change. The main assumptions of this test are: i) time-series observations are independent where there is no trend; ii) the time-series is representative of the original conditions at sampling times; and iii) the sample collection, handling, and measurement methods provide unbiased and representative observations of the underlying populations over time.

The MK tests whether to reject the null hypothesis ($H_0$) and accept the alternative hypothesis ($H_a$), where

$H_0$: No monotonic trend

$H_a$: Monotonic trend is present

The initial assumption of the MK test is that the $H_0$ is true and that the data must be convincing beyond a reasonable doubt before $H_0$ is rejected and $H_a$ is accepted.

We calculated three statistics provided by MK-test: i) statistic S; ii) variance of S; and iii) test statistic Z. This study calculated Sen's slope to determine the magnitude of trend. The calculations of these statistics area as follows:

$$S = \sum_{k-1}^{n-1} \sum_{j-k+1}^{n} sgn(x_j - x_k) \tag{1}$$

$$sgn(x_j - x_k) = \begin{cases} +1, if(x_j - x_k) > 0 \\ 0, if(x_j - x_k) = 0 \\ -1, if\ (x_j - x_k) < 0 \end{cases} \tag{2}$$

where n is the length of sample, $x_k$ and $x_j$ are from k=1,2,..,n-1 and j=k+1,…n. If n is bigger than 8, statistic S approximates to normal distribution. The mean of S is 0 and the variance of S can be calculated as follows:

$$var\ (S) = \frac{n(n-1)(2n+5)}{18} \tag{3}$$

The test statistic Z is calculated by

$$Z = \begin{cases} \dfrac{S-1}{\sqrt{var\ (S)}}, if\ S > 0 \\ 0, \quad if\ S = 0 \\ \dfrac{S+1}{\sqrt{var\ (S)}}, if\ S < 0 \end{cases} \tag{4}$$

If Z>0, the trend is increasing and, vice versa. With confidence level α, the sequential data would be supposed to experience statistically significant trend if $|Z| > Z(1-\alpha/2)$, where $Z(1-\alpha/2)$ is the corresponding value of $P=\alpha/2$ following the standard normal distribution. In this study, 0.05 and 0.01 confidence levels were used.

The magnitude of a time series trend was evaluated by a simple non-parametric procedure developed by Sen. The trend is calculated by

$$\beta = Median\left(\frac{x_j - x_i}{j-i}\right), j > i \tag{5}$$

where $\beta$ is Sen's slope estimate, $\beta > 0$ indicates upward trend in a time-series, and vice versa.

In the last step, this study observed the trends of socioeconomic variables before and after the CAP implementation time-period as they relate to wheat yield changes in the study region. For this study, CAP implementation in 2007 in Bulgaria is a breakpoint event and the trends in the socio-economic variables may be influenced by this event. We only discuss Bulgarian socio-economic variable changes and its implication on agricultural production as CAP is implemented only in Bulgaria.

**4.5 Results and discussion**

*Patterns and distributions of wheat-yield change at village-scale*

The results of the bin analysis are discussed in two parts: i) wheat yield patterns and distributions before and after the CAP implementation (hypothesis-1 test); ii) overall wheat yield patterns and distributions (from 2001-2020) (hypothesis-2 test)

The results for the hypothesis-1 test showed that the number of villages with high yields (>3500 kg/ha) increased by four times and the number of villages with low yield decreased by ~2.5 times after the CAP implementation in Bulgaria. Medium-yield bins (1500 kg/ha-2500 kg/ha) had slight decrease in Bulgaria after 2007 (Figure 4.3). To this end, the hypothesis-1 appears to be accepted in the Bulgaria wheat yield dataset. Note that CAP had a direct positive impact on wheat yields in Bulgaria and this impact is further assessed through geospatial maps. The maps of wheat yield distribution in the pre- and post-accession periods showed that high-yield value farms are mostly distributed in eastern Bulgaria compared to central Bulgaria (Figure 4.4). The bin analysis suggested the amount of the quantities of the medium-yield farms in Bulgaria before and after the CAP implementation but the map of wheat yield presented the detailed locations where the change happened. In case of Turkey, the results showed that the number of villages with high yield increased by two times and the number of villages with low yield decreased by ~2 times. These changes in Turkey are mainly due to its own agricultural policies and hypothesis-1 test is not applicable to these data from Turkey.

The results for hypothesis-2 test suggested that wheat yield distributions in each country across the years were different in measurement and trends (Figure 4.5). The number of villages with high yield in Bulgaria started increasing around 2007 to 2017, whereas in Turkey the number of villages with high yield started increasing around 2001 to 2017. In Bulgaria, villages with medium yields had stable counts from 2004-2015, whereas in Turkey the number of villages with medium yield values had decreasing trends from 2010. It is observed that, Bulgaria had change

breakpoint around year 2007 whereas Turkey didn't have such breakpoint due to continuous trends. These results suggest that wheat yield changes in Bulgaria show abrupt positive changes from year 2007, most likely associated with CAP implementation in that year. In Turkey, the observed changes are primarily due its own agricultural policies. Overall, this distinct village-scale wheat yield bin distribution according to the number of villages in Turkey and Bulgaria from year 2001-2020 supported the second hypothesis in this study, which hypothesized that overall wheat yield trends in each country are different, although both countries have similar agroclimatic characteristics. These results also established that both cross-border countries have very different drivers of change.

*Patterns and distributions of wheat-yield change in relation to soil quality at village scale*

The results for pattern and distribution of wheat yield change in relation to soil quality are showed only for hypothesis-1 test. The number of villages with high-yield values in all three types of soils had increased after 2007 in Bulgaria (Figure 4.6). Note that villages with low soil suitability had less capacity to produce the wheat, but after CAP implementation, wheat yield in these villages had increasing trends. The results of the bin analysis provided changes in wheat yield for each time-period and country according to type of soil, the geospatial maps presented the spatiotemporal distribution of these changes in the study area according to soil suitability (Figure 4.7). The resulting maps showed that the villages with low yields in the pre-accession period were concentrated in southern Bulgaria. The same farms in the post-accession period have improved wheat yields from low to high values, and farms near the main settlement areas have been abandoned. It is observed that number of farms with high suitability have increased in number after 2007, but farms with low suitability and low yield have been abandoned in Bulgaria. High-yield value farms in the post-accession period were mainly concentrated in northeastern Bulgaria

after the CAP implementation. These results for Bulgaria data appear to support hypothesis 1. More specifically, CAP implementation in Bulgaria had increased the number of villages with high yield range in spite of any type of soil after 2007. In Turkey similar trends are also noted but the magnitude of change was less compared to Turkey and if we observe these changes separately for each year wheat yield distributions are completely different in both countries. Overall, this analysis indicted that the CAP implementation in Bulgaria had improved wheat yield in the region across all soil types.

*Quantifying the wheat trend and assessing its distribution through a Mann-Kendall test at village scale*

The main results of the Mann-Kendall test were the values of the direction of trend (positive, negative, or stable) through the statistic Z and measure of trend through Sen's slope estimate (Figure 4.8). In the pre-accession period, northeast Bulgaria had an overall negative trend in wheat yield, but in the post-accession period, northeast Bulgarian farms had a positive trend. The results showed that, in Bulgaria overall wheat yield decreased by 0.1% before CAP implementation and increased by 10% after CAP implementation (Sens' slope change from -10 to 100). The map of Sen's slopes (Figure 4.8) located those villages with improved wheat yield and also those villages which were abandoned after 2007. Note that in Turkey, the overall trend was positive but the amount of trend was completely different than Bulgaria and reasons of change were not related to the CAP. The reason of including Turkey in this discussion is that Turkey already had better agricultural economy while running under its own government policies. To this end, this study is inconclusive in answering if future CAP-style policy implementations in Turkey could produce the same positive impact as in Bulgaria.

*Socio-economic variable trends and its possible impact on wheat yield change*

The results for the socio-economic variable trends were mainly discussed with respect to the impact on wheat yield change in Bulgaria. We will discuss trends of total population, GDP, employment in agriculture, unemployment rates, tractors, cattle, number of holdings and agricultural land owned by companies. We observed the trends of these socioeconomic variables and checked if they had the breakpoint corresponds to CAP implementation in 2007. If their breakpoint is 2007 then these variables had impacted the wheat yield change in the study area too (as our previous results reported that CAP implementation had positive impact on wheat yield in Bulgaria).

Population in Bulgaria is continuously decreasing from 2001 and is not affected by CAP. GDP in Bulgaria had increasing trends 2001 and had slight stable stage during 2007. Employment in Bulgaria was decreasing before CAP implementation, but it was stabilized after CAP implementation. Before CAP, unemployment rates were slightly increased from 2003 to 2007 but after 2007 these rates were slightly decreased and stabilized. The number of tractors and cattle in Bulgaria were increased after CAP implementation. Number of holdings in Bulgaria were decreased in Bulgaria from 2001. These different trends in socioeconomic changes had implications on agricultural production in the region and they may have impacted food security of the region.

**4.6 Conclusions**

The overarching goal of this study was to investigate the impact of agricultural support policies on the drivers of wheat yield change for the last 20 years in the cross-border area between Turkey and Bulgaria. The study started out with two hypotheses. The first was aimed to assess the impact of CAP implementation on the wheat yield change of the study area, and the second sought to assess overall wheat yield changes of the study area. In this chapter, we discussed the results of

hypothesis testing in three steps: i) only in Bulgaria; ii) only in Turkey; and iii) between the two countries.

For Bulgaria, the results provided evidence that wheat yield change in the pre-accession period (2001-2007) had different amounts and patterns than the post-accession period (2008-2020). Specifically, the villages with high-yield values increased in number, low-yield value villages decreased in number, and medium-yield value villages had a slight decrease in number in the post-accession period (Figure 4.3 and 4.4). These results support both hypotheses for Bulgaria. The visualization of wheat yield maps and the changes in the pre- and post-accession periods provided a detailed picture of wheat yield changes in the region and helped us conclude that entering the EU had strong positive effects on wheat yield and production in Bulgaria.

Wheat yields in Turkey also increased in the same period, but this was due to its own agricultural policies. However, these results do not support the idea that future CAP-style policy implementations in Turkey could produce the same positive impact as in Bulgaria.

This study observed the socioeconomic variable trends in Bulgaria. It is noted that, CAP and other agricultural policies in Bulgaria are the main reasons of the changes in socio-economic variables. For example, number of tractors have been increasing in Bulgaria after 2007, most likely associated with CAP implementation in the country. Overall, this study showed that CAP implementation in Bulgaria have improved wheat production and the improved agricultural inputs is the most likely cause and that Bulgaria's agriculture generally benefitted from CAP implementation. While we analyzed the impact of policy changes at the village scales, same conclusions can also be drawn at the field-scale as well given the field-scale data input using similar methods.

We found that bin analysis helps to understand the patterns and distributions of wheat yield across the villages in the study area, and the MK test helped to quantify the wheat yield change and interpret the results in relation to the socio-economic history of the region. The spatiotemporal maps of wheat yield change helped to highlight the locations impacted due to policy. This study also discussed different socioeconomic variable trends in the study area and these variable trends further related to the changes in wheat yield in the study region. Overall, this work presented novel approach where observed agricultural production trends and patterns at granular level were assessed with respect to major socioeconomic breakpoint event. The results of this experiment provided details about the wheat yield changes and its locations while linking them to policy according to its time-periods. Outcomes of this study can be used for food security analysis of the region and also policy designs.

**References**

Agricultural Statistical Reports of Bulgaria from 2000-2020, Ministry of Agriculture, Bulgaria. https://www.mzh.government.bg/bg /

Akder, A. H. (2007). Policy formation in the process of implementing agricultural reform in Turkey. *International Journal of Agricultural Resources, Governance and Ecology*, *6*(4-5), 514-532.

Bachev, H. (2019). *Sustainability of farming enterprises in Bulgaria*. Cambridge Scholars Publishing.

Bastiaanssen, W. G., Molden, D. J., & Makin, I. W. (2000). Remote sensing for irrigated agriculture: Examples from research and possible applications. *Agricultural Water Management*, *46*(2), 137-155.

Baumann, M., Kuemmerle, T., Elbakidze, M., Ozdogan, M., Radeloff, V. C., Keuler, N. S., ... & Hostert, P. (2011). Patterns and drivers of post-socialist farmland abandonment in western Ukraine. *Land Use Policy*, *28*(3), 552-562.

Baumann, M., Ozdogan, M., Wolter, P. T., Krylov, A., Vladimirova, N., & Radeloff, V. C. (2014). Landsat remote sensing of forest windfall disturbance. *Remote Sensing of Environment*, *143*, 171-179.

Chhabra, A., Geist, H., Houghton, R. A., Haberl, H., Braimoh, A. K., Vlek, P. L., ... & Lambin, E. F. (2006). Multiple impacts of land-use/cover change. In *Land-use and land-cover change* (pp. 71-116). Springer, Berlin, Heidelberg.

Conway, G. (2019). *The doubly green revolution: Food for all in the twenty-first century*. Cornell University Press.

Dang, A. N., & Kawasaki, A. (2017). Integrating biophysical and socio-economic factors for land-use and land-cover change projection in agricultural economic regions. *Ecological Modelling*, *344*, 29-37.

DeFries, R. S., Field, C. B., Fung, I., Justice, C. O., Los, S., Matson, P. A., ... & Vitousek, P. M. (1995). Mapping the land surface for global atmosphere-biosphere models: Toward continuous distributions of vegetation's functional properties. *Journal of Geophysical Research: Atmospheres*, *100*(D10), 20867-20882.

Duncan, J. M., Dash, J., & Atkinson, P. M. (2015). Elucidating the impact of temperature variability and extremes on cereal croplands through remote sensing. *Global Change Biology*, *21*(4), 1541-1551.

European Commission Report, (2016) retrieved from https://ec.europa.eu/info/publications/2016-commission-report-and-factsheets-monitoring-application-eu-law_en

Eurostat, (2019). *Europe in figures: Eurostat yearbook 2019* (Vol. 1). Office for Official Publications.

FAO, U., (2019). FAOstat. *Retrieved Feb*. *2019*.

Fernández, J. L., Kendall, J., Davey, V., & Knapp, M. (2007). Direct payments in England: Factors linked to variations in local provision. *Journal of Social Policy*, *36*(1), 97-121.

Fischer, G., Nachtergaele, F., Prieler, S., Van Velthuizen, H. T., Verelst, L., & Wiberg, D. (2008). Global agro-ecological zones assessment for agriculture (GAEZ 2008). *IIASA, Laxenburg, Austria and FAO, Rome, Italy*, *10*.

Foley, J. A., DeFries, R., Asner, G. P., Barford, C., Bonan, G., Carpenter, S. R., ... & Snyder, P. K. (2005). Global consequences of land use. *Science*, *309*(5734), 570-574.

Gao, F., Anderson, M. C., Zhang, X., Yang, Z., Alfieri, J. G., Kustas, W. P., ... & Prueger, J. H. (2017). Toward mapping crop progress at field scales through fusion of Landsat and MODIS imagery. *Remote Sensing of Environment*, *188*, 9-25.

Gilbert, R. O. (1987). *Statistical methods for environmental pollution monitoring*. John Wiley & Sons.

Godfray, H. C. J., Beddington, J. R., Crute, I. R., Haddad, L., Lawrence, D., Muir, J. F., ... & Toulmin, C. (2010). Food security: The challenge of feeding 9 billion people. *Science*, *327*(5967), 812-818.

Hale, W. (2012). *Turkish foreign policy since 1774*. Routledge.

Hurni, K., Schneider, A., Heinimann, A., Nong, D. H., & Fox, J. (2017). Mapping the expansion of boom crops in mainland Southeast Asia using dense time stacks of Landsat data. *Remote Sensing*, *9*(4), 320.

Jensen, J. R. (2009). *Remote sensing of the environment: An earth resource perspective 2/e*. Pearson Education India.

Kendall, M. G. (1948). Rank correlation methods.

Kraemer, R., Prishchepov, A. V., Müller, D., Kuemmerle, T., Radeloff, V. C., Dara, A., ... & Frühauf, M. (2015). Long-term agricultural land-cover change and potential for cropland expansion in the former Virgin Lands area of Kazakhstan. *Environmental Research Letters*, *10*(5), 054012.

Lambin, E. F., Geist, H. J., & Lepers, E. (2003). Dynamics of land-use and land-cover change in tropical regions. *Annual Review of Environment and Resources*, *28*(1), 205-241.

Larson, D., Martin, W., Sahin, S., & Tsigas, M. (2016). Agricultural policies and trade paths in Turkey. *The World Economy*, *39*(8), 1194-1224.

Mann, H. B. (1945). Nonparametric tests against trend. *Econometrica: Journal of the Econometric Society*, 245-259.

Maxwell, S. (1996). Food security: A post-modern perspective. *Food Policy*, *21*(2), 155-170.

Mayaux, P., Eva, H., Gallego, J., Strahler, A. H., Herold, M., Agrawal, S., ... & Roy, P. S. (2006). Validation of the global land cover 2000 map. *IEEE Transactions on Geoscience and Remote Sensing*, *44*(7), 1728-1739.

Meyfroidt, P. (2018). Trade-offs between environment and livelihoods: Bridging the global land use and food security discussions. *Global Food Security*, *16*, 9-16.

Meyfroidt, P., Carlson, K. M., Fagan, M. E., Gutiérrez-Vélez, V. H., Macedo, M. N., Curran, L. M., ... & Robiglio, V. (2014). Multiple pathways of commodity crop expansion in tropical forest landscapes. *Environmental Research Letters*, *9*(7), 074012.

Myers, V. I. (1983). Remote sensing applications in agriculture. *Manual of Remote Sensing*, 2111-2228.

NSI (National Statistical Institute of Bulgaria) (2020). https://www.nsi.bg/en

Ozdogan, M., & Woodcock, C. E. (2006). Resolution dependent errors in remote sensing of cultivated areas. *Remote Sensing of Environment*, *103*(2), 203-217.

Ozdogan, M., Yang, Y., Allez, G., & Cervantes, C. (2010). Remote sensing of irrigated agriculture: Opportunities and challenges. *Remote Sensing*, *2*(9), 2274-2304.

Phalke, A. R., & Özdoğan, M. (2018). Large area cropland extent mapping with Landsat data and a generalized classifier. *Remote Sensing of Environment*, *219*, 180-195.

Phalke, A. R., Özdoğan, M., Thenkabail, P. S., Erickson, T., Gorelick, N., Yadav, K., & Congalton, R. G. (2020). Mapping croplands of Europe, middle east, russia, and central asia using landsat, random forest, and google earth engine. *ISPRS Journal of Photogrammetry and Remote Sensing*, *167*, 104-122.

Phalke, A., Ozdogan, M., Thenkabail, P. S., Congalton, R. G., Yadav, K., Massey, R., ... & Smith, C. (2017). NASA Making Earth System Data Records for Use in Research Environments (MEaSUREs) Global Food Security-Support Analysis Data (GFSAD)@ 30-m for Europe. *Middle-East, Russia and Central Asia: Cropland Extent Product (GFSAD30EUCEARUMECE)*.

Pittman, K., Hansen, M. C., Becker-Reshef, I., Potapov, P. V., & Justice, C. O. (2010). Estimating global cropland extent with multi-year MODIS data. *Remote Sensing*, *2*(7), 1844-1863.

Prishchepov, A. V., Müller, D., Baumann, M., Kuemmerle, T., Alcantara, C., & Radeloff, V. C. (2017). Underlying drivers and spatial determinants of post-soviet agricultural land abandonment in temperate Eastern Europe. In *Land-cover and land-use changes in Eastern Europe after the collapse of the Soviet Union in 1991* (pp. 91-117). Springer, Cham.

Prishchepov, A. V., Müller, D., Dubinin, M., Baumann, M., & Radeloff, V. C. (2013). Determinants of agricultural land abandonment in post-Soviet European Russia. *Land Use Policy*, *30*(1), 873-884.

Ramankutty, N., Mehrabi, Z., Waha, K., Jarvis, L., Kremen, C., Herrero, M., & Rieseberg, L. H. (2018). Trends in global agricultural land use: implications for environmental health and food security. *Annual Review of Plant Biology*, *69*, 789-815.

Roy, S. S., Mahmood, R., Niyogi, D., Lei, M., Foster, S. A., Hubbard, K. G., ... & Pielke Sr, R. (2007). Impacts of the agricultural Green Revolution–induced land use changes on air temperatures in India. *Journal of Geophysical Research: Atmospheres*, *112*(D21).

Schneider, A. (2012). Monitoring land cover change in urban and peri-urban areas using dense time stacks of Landsat satellite data and a data mining approach. *Remote Sensing of Environment*, *124*, 689-704.

Shen, Q., Chen, Q., Tang, B. S., Yeung, S., Hu, Y., & Cheung, G. (2009). A system dynamics model for the sustainable land use planning and development. *Habitat International*, *33*(1), 15-25.

Thenkabail, P. S., Hanjra, M. A., Dheeravath, V., & Gumma, M. (2010). A holistic view of global croplands and their water use for ensuring global food security in the 21st century through advanced remote sensing and non-remote sensing approaches. *Remote Sensing*, *2*(1), 211-261.

Therond, O., Debril, T., Duru, M., Magrini, M. B., Plumecocq, G., & Sarthou, J. P. (2019). Socio-economic Characterisation of agriculture models. In *Agroecological transitions: From theory to practice in local participatory design* (pp. 21-43). Springer, Cham.

TURKSTAT. (2019). Database, Turkish Statistical Institute. (http://www.turkstat.gov.tr/Start.do

Vassilev, R. (1999). Modernization theory revisited: The case of Bulgaria. *East European Politics and Societies*, *13*(3), 566-599.

Verburg, P. H., Alexander, P., Evans, T., Magliocca, N. R., Malek, Z., Rounsevell, M. D., & van Vliet, J. (2019). Beyond land cover change: Towards a new generation of land use models. *Current Opinion in Environmental Sustainability*, *38*, 77-85.

Waldner, F., Fritz, S., Di Gregorio, A., & Defourny, P. (2015). Mapping priorities to focus cropland mapping activities: Fitness assessment of existing global, regional and national cropland maps. *Remote Sensing*, *7*(6), 7959-7986.

Wheeler, T., & Von Braun, J. (2013). Climate change impacts on global food security. *Science*, *341*(6145), 508-513.

Yilmaz, H., 2006. Policies and transition problems of agriculture in Turkey. *Journal of Applied Sciences*, *6*(15), pp.3052-3059.

**Figures**

**Figure 4.1**. Map of villages in the study area (derived in Chapter 3 of this dissertation). The color of village polygons represents different regions in the study area.

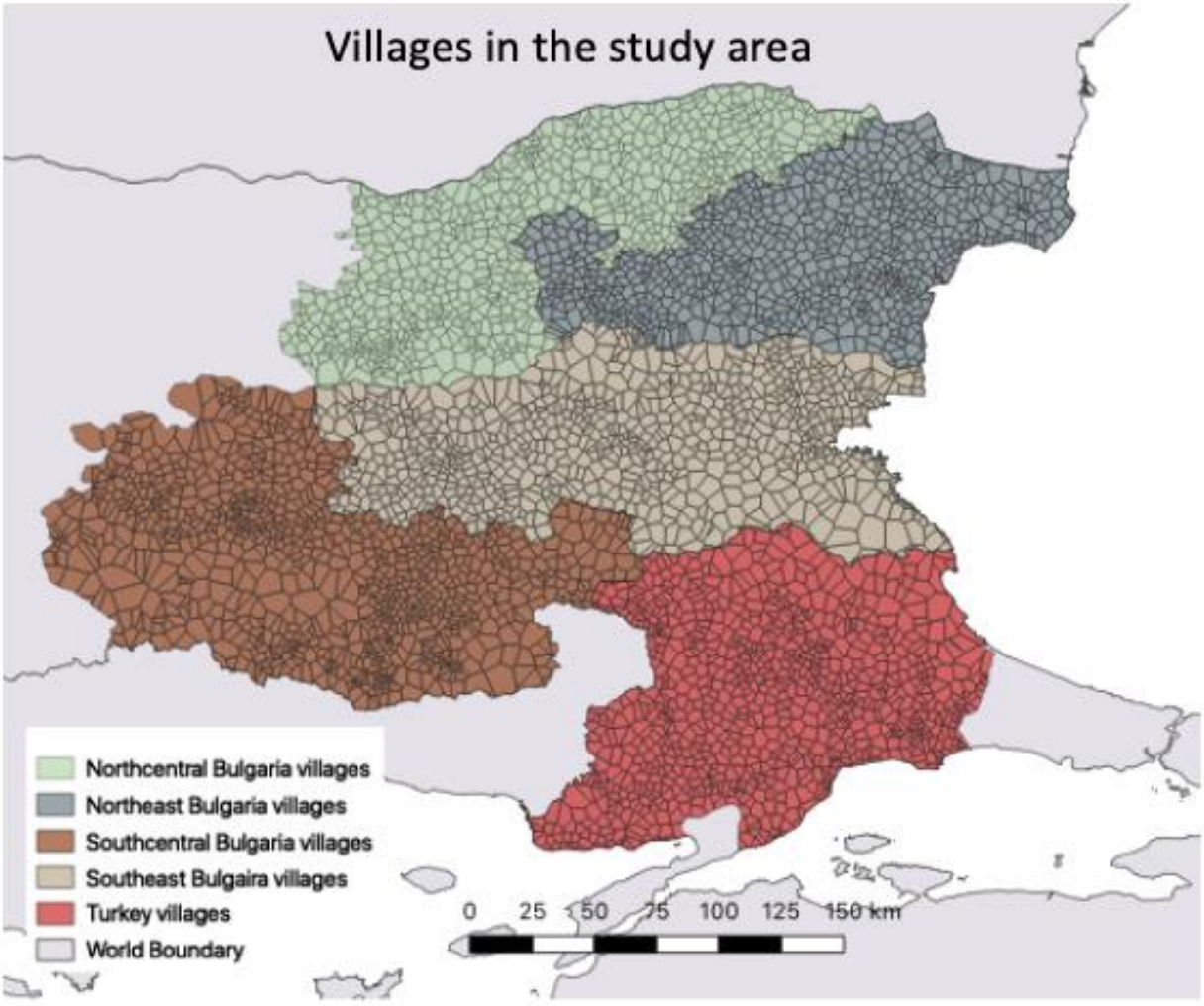

**Figure 4.2a** Utilized agricultural area in Bulgaria as per farm size (source: Eurostat, 2019).

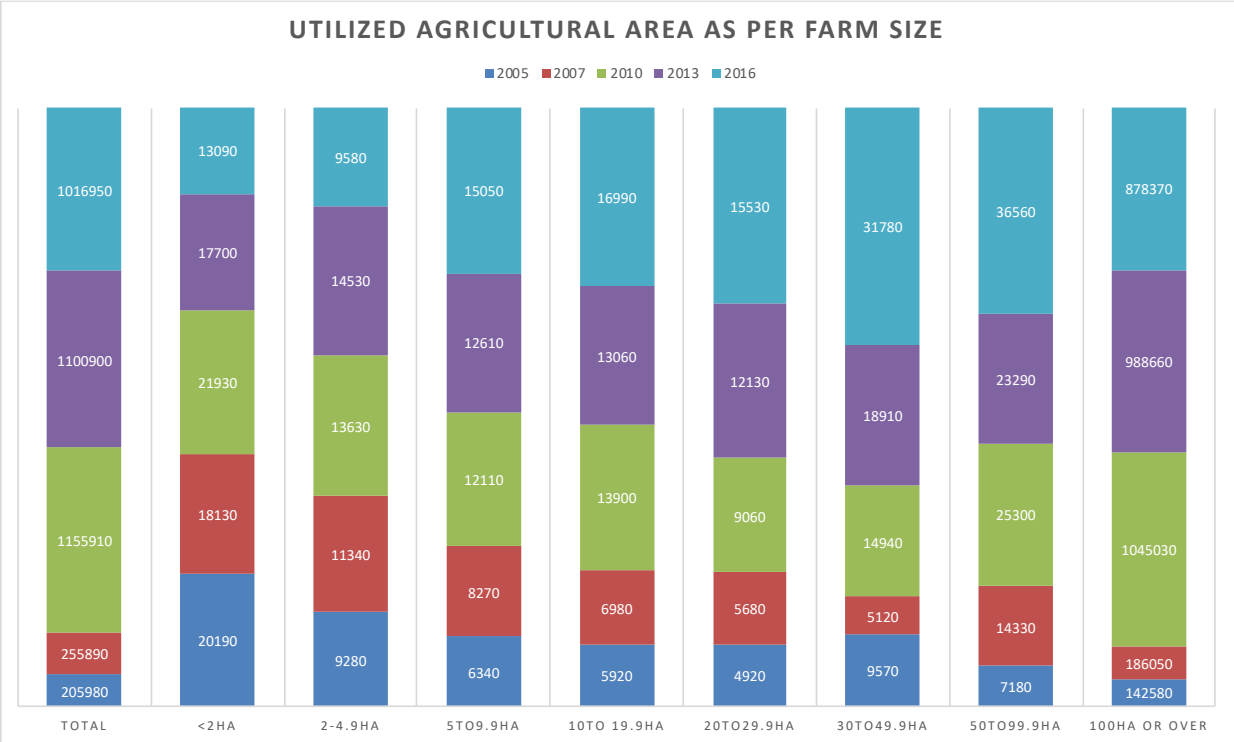

**Figure 4.2b** Farm number in Bulgaria as per farm size (source: Eurostat, 2019).

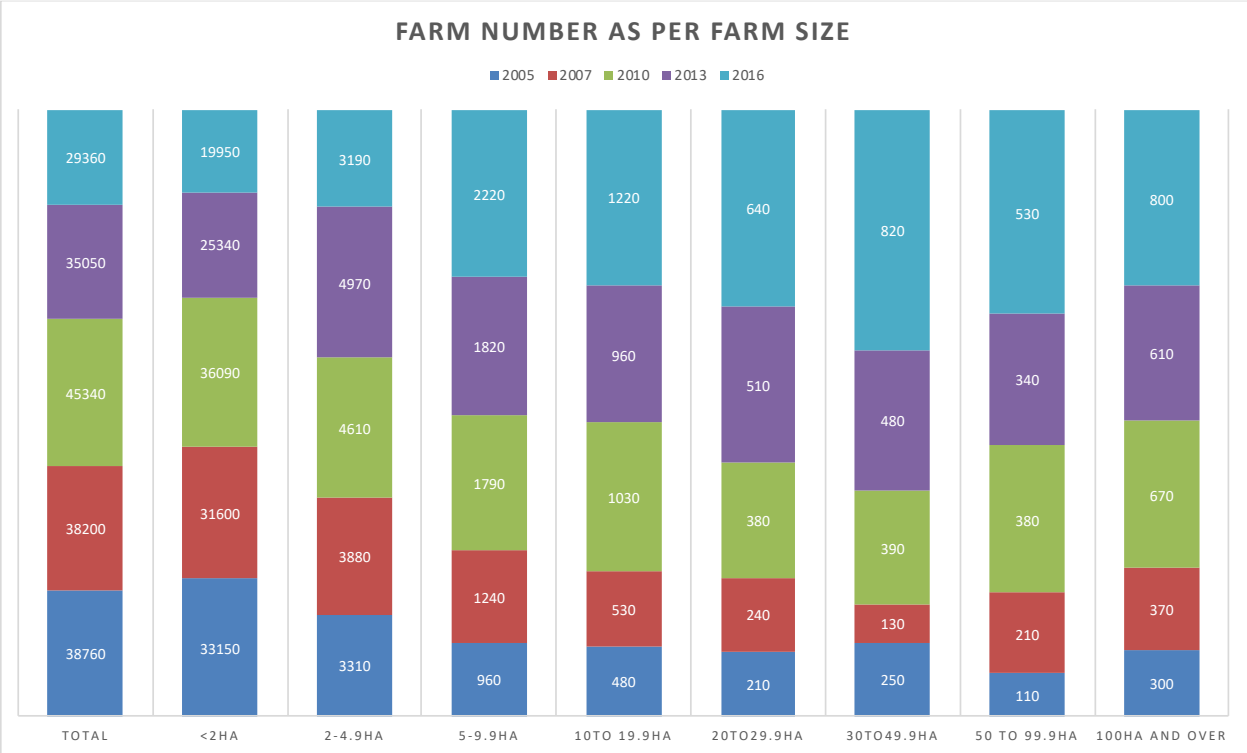

**Figure 4.3** Wheat yield bins in the pre-accession (2001-2007) and post-accession (2008-2020) periods in each country according to the number of villages. Dark color bins are for the post-accession period, and the light color bins are for pre-accession period wheat yield estimates. Note that Turkey has not entered the EU, therefore the figure to the right is for reference only.

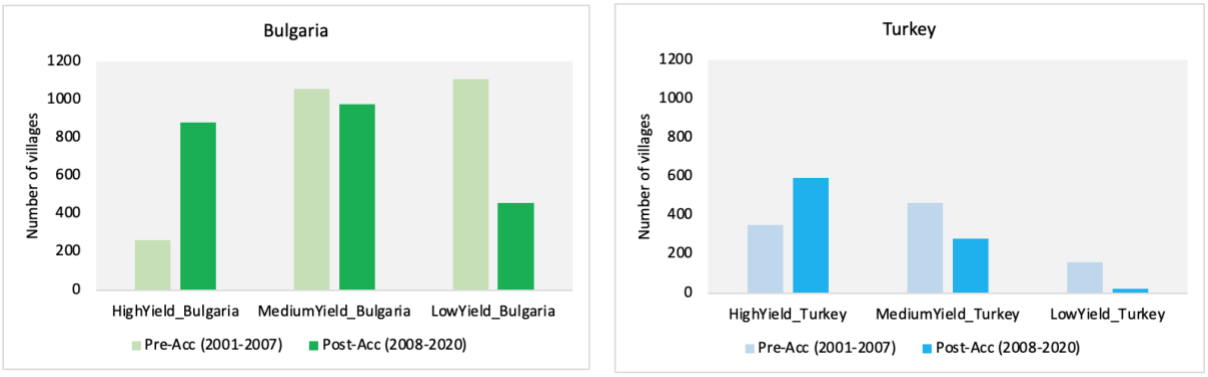

**Figure 4.4** Maps of wheat yield patterns and distributions in the study area before and after CAP implementation. The top map refers to the period before CAP implementation, and the bottom map refers to the period after CAP implementation. Yellow indicates high-yields, and blue indicates low-yields.

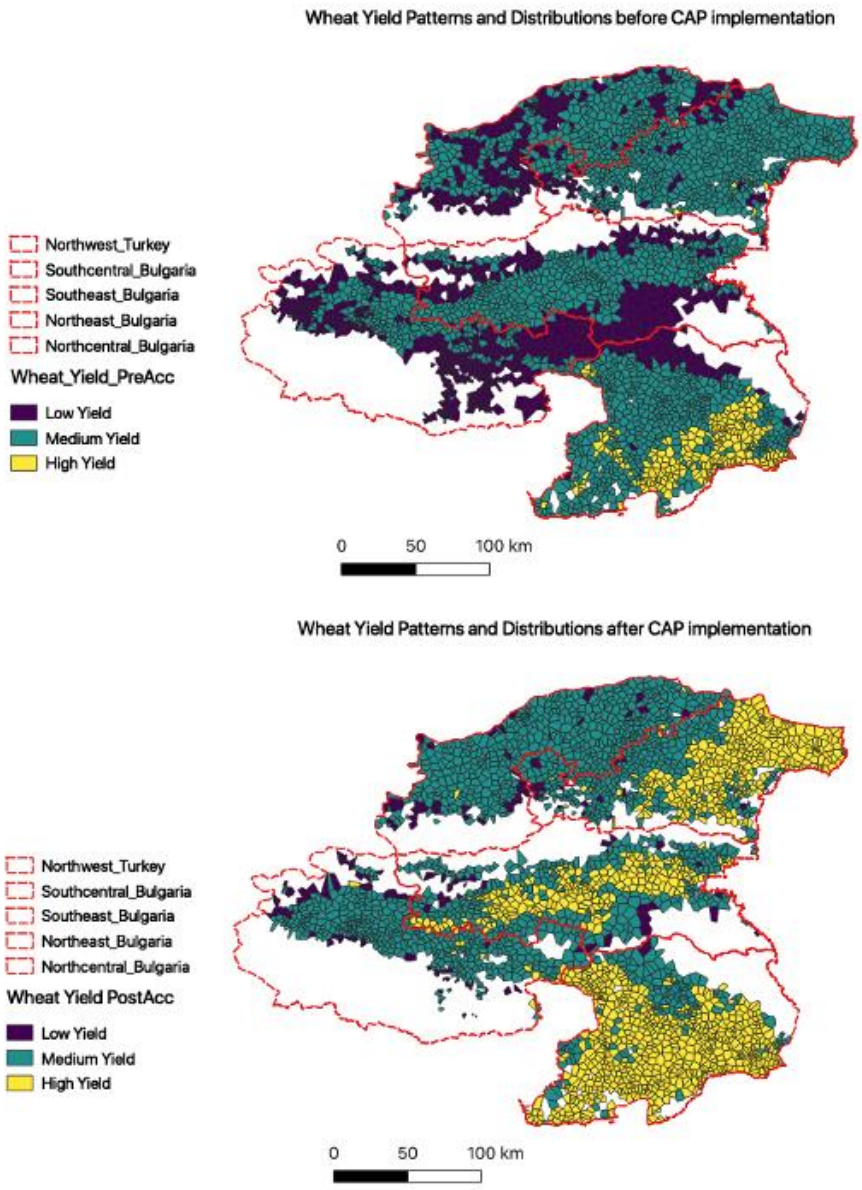

**Figure 4.5** Wheat yield bins in the study region according to the number of villages in each country. The X-axis refers to the year, and the Y-axis refers to the number of villages in each year and each wheat yield range. Top panel refers to Bulgaria with blue color bins and bottom panel refers to Turkey with orange color bins. Left panel refers to high-yield village distribution and right panel refers to low yield village distribution.

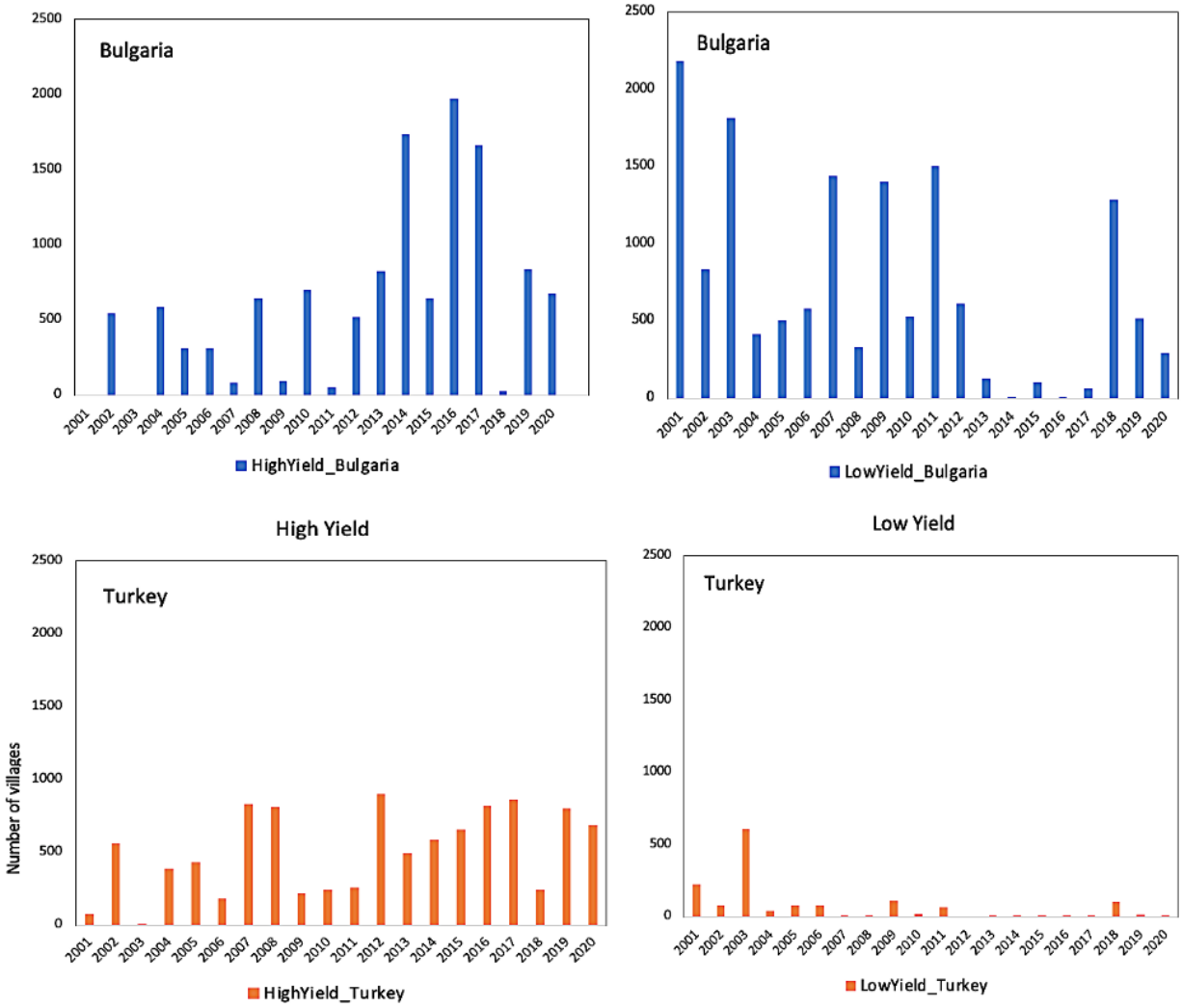

**Figure 4.6** Patterns of wheat yield distribution in Turkey and Bulgaria before and after Bulgarian accession to the EU according to the soil quality in the region. The X-axis refers to the wheat yield range, and the Y-axis refers to number of villages. Pre-Acc refers to the pre-accession period and Post-Acc refers to the post accession period. Green color bins refers to Bulgaria and blue color bins refer to Turkey. Light color of bins refers to Pre-Acc period and dark color of bins refers to Post-Acc period.

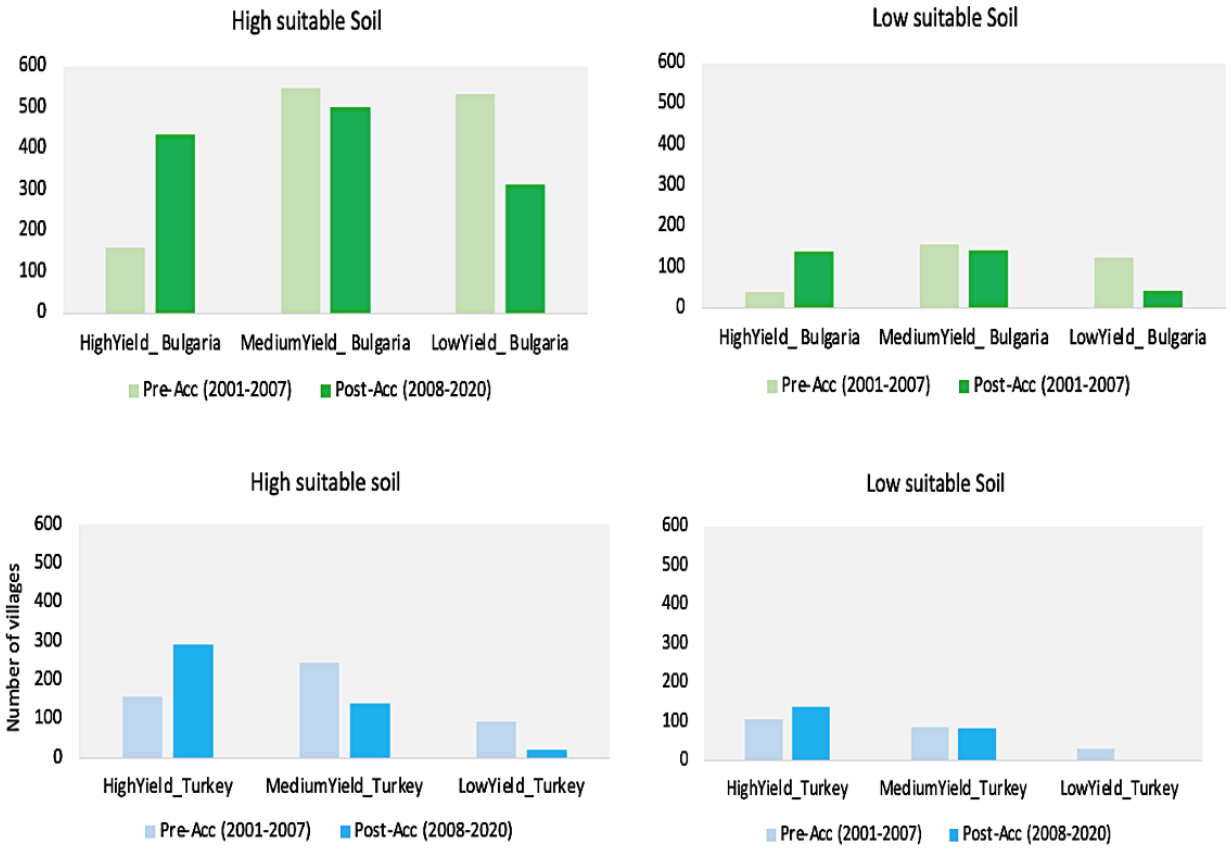

**Figure 4.7** Maps of wheat yield distributions as per soil quality in the region before and after CAP implementation. The top panel refers to the period before CAP (2001-2007), and the bottom panel refers to the period after CAP (2008-2020).

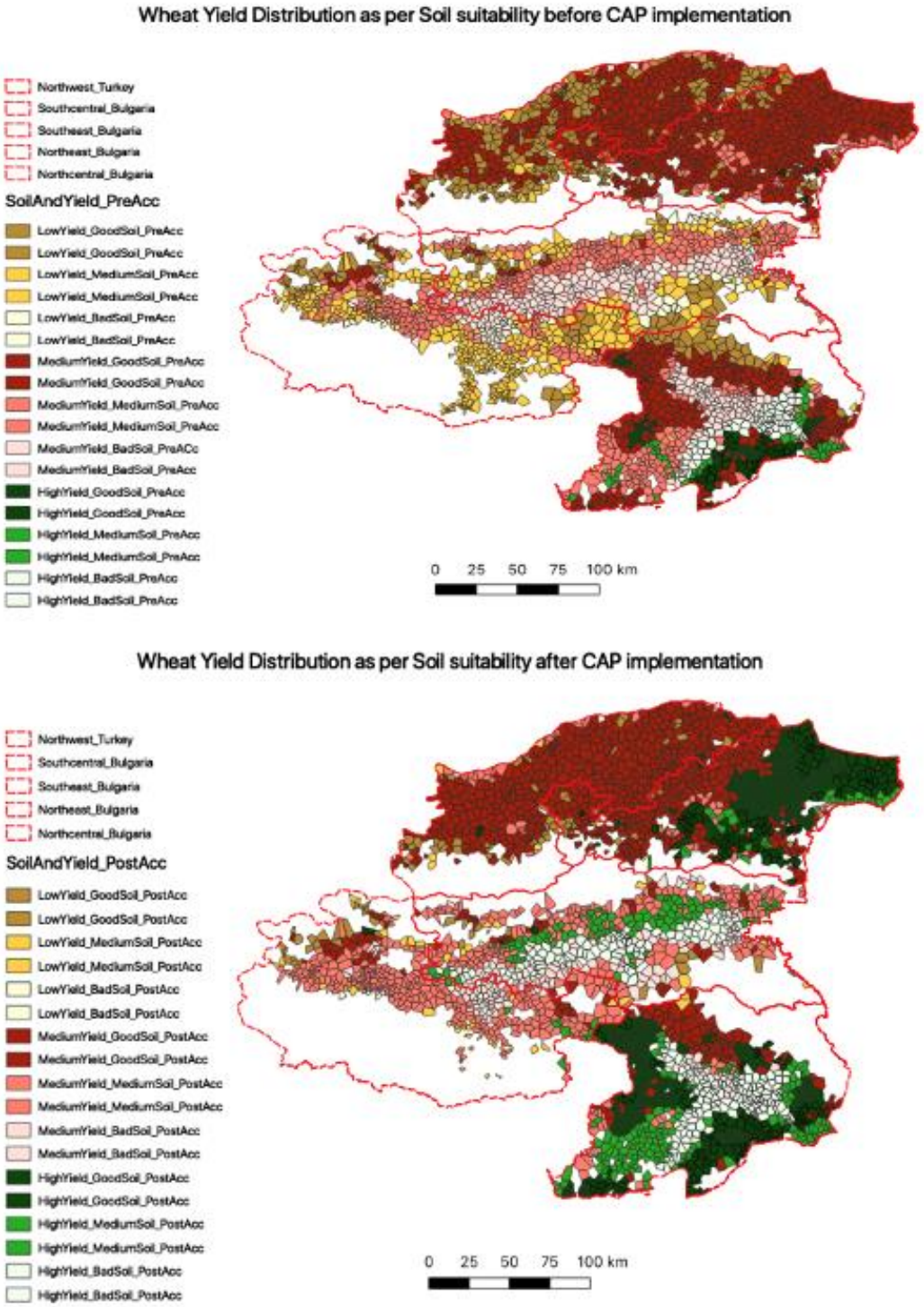

**Figure 4.8** Maps of wheat yield trend measure and distribution across the study area. The top panel refers to the period before CAP (2001-2007), and the bottom panel refers to the period after CAP (2008-2020).

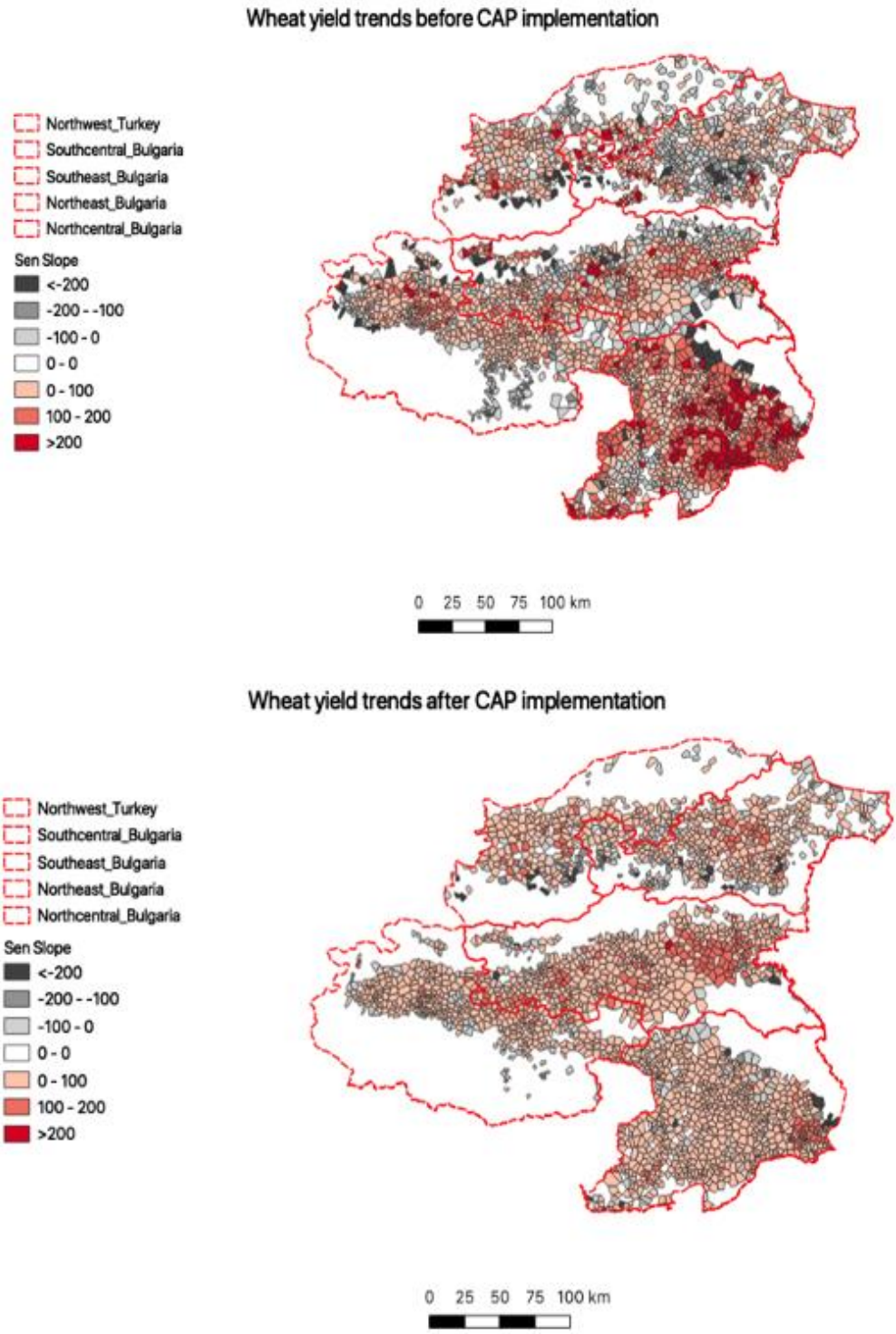

**Figure 4.9** Socioeconomic variable trends in Bulgaria. Data is derived from government statistics. Green bars refer to tractors, yellow bard refer to employment in agriculture, blue bars refer to population and red bars refer to agricultural holdings. Dotted circle represents the CAP implementation even in Bulgaria. X-axis refers to year and Y-axis refers to average value for regions in Bulgaria.

Tables

**Table 4.1** Key similarities and differences between the two countries in a case study region.

| Sr. No. | Key data points | Northwestern Turkey (Cross-border area/ Northern Thracia) | East and Central Bulgaria (Cross-border area/ Eastern Thracia) |
|---|---|---|---|
| 1 | States/provinces covered | Edirne , Kirklareli, Tekirdag, | Southcentral Bulgaria, Southeast Bulgaria, Northcentral Bulgaria, Northeast Bulgaria |
| 2 | Rainfall | 603 mm (yearly average), 50 mm (monthly average) | 580 mm (yearly average), 48 mm (monthly average) |
| 3 | Average Max Temperature(0C) | ~19 | ~18 |
| 4 | Average Min Temperature(0C) | ~8 | ~8 |
| 5 | Length of growing period (days) | 90-179 | 90-179 |
| 6 | Moisture Regime | Mediterranean | Humid subtropical and Mediterranean |
| 7 | Population Density | 470 people per km² | 81.5 people per km² |
| 8 | Major crops | Winter wheat, corn, rice, sugar beet and sunflower. | Winter wheat, Barley, Corn, Sunflower, tobacco. |
| 9 | Agricultural value added (%GDP) | Decreased from ~10 to~ 8 since 2000 | Decreased from ~11 to~ 4 since 2000 |
| 10 | Wheat import value | Increased by ~17% since 2006 | Approximately stable since 2006 |
| 11 | Wheat export value | Increased by ~17% since 2007 | No major change in value from 2000 to 2017 |
| 13 | Wheat price index | Increased from 27 in 2000 to 246 in 2017 | Increased from 102 in 2000 to 158 in 2017 |
| 14 | All cropland area and yield | Increasing trend | Mixed trend until 2008 and then continuously increasing |
| 15 | Wheat crop area and yield | Decreased from 2000 to 2008 and then stabilized with minor fluctuations | Decreased from 2001 to 2003 and then slowly increased until 2009 and then stabilized with minor fluctuations |
| 16 | Employment in agriculture | Decreased from ~36% to~18% of total employment since 2000 to 2017 | Decreased from ~13% to~6% of total employment since 2000 to 2017 |

**Table 4.2** Socio-economic and institutional change-related events in Turkey and Bulgaria.

| Year | Event | Outcome |
|---|---|---|
| Bulgaria | | |
| 1990-2005 | Post-communist transition period | |
| 1990 | Restitution and privatization | After 1990, large scale restitution of collectivized or nationalized farmland was undertaken affecting 85% of farmlands and turning three quarter of Bulgarian households into owners of farmlands. It took almost 10 years to complete and was associated with big technical difficulties. Besides a significant part of agrarian assets (irrigation facilities, wine yards, orchards, destroyed and almost one third of cultivated land left unused for a long period of time) |
| 1990 | Market liberalization and regulations | After 1990, there was fundamental liberalization of markets and prices in Bulgaria |
| 1992 | Privatization of state famers and agro-companies | Most agrarian assets were sold to managerial workers team or private entrepreneurs. |
| 2000 | Formation of public support to agrarian sectors | support in the form of subsidies, preferential credits, investment subsidies and price guarantee formed since 2000. thus, improvement in technological factors happened like, application of chemicals exceeded with 68%, irrigation 126%, and new machineries 42% |
| 2000 | National Agricultural and Rural Development Plan for the period 2000-2006 under SAPARD | |
| 2001 | start of SAPARD | Pre-accession to EU policy |
| 2004 | Bulgaria Joined NATO | |
| 2007 | EU CAP implementation | |
| 2014 | Agricultural Land Protection Act (ALPA) | ALPA contains a legal framework covering some of the activities envisaged for the Agriculture sector in the NAPCC, such as counteracting the burning of stubble and plant waste and promoting agricultural practices aimed at reducing greenhouse gas emissions. |
| 2015 | Agricultural Producers Support Act (APSA) | APSA regulates some of the activities through which the measures envisaged for the Agriculture sector of the NAPCC can be implemented, as well as the activities related to biofuel production. APSA is the law regulating the key financial mechanism for management of agricultural activities. Most of the proposals – whether introduction of best practices for rice production or for encouragement of crop rotation, especially with nitrogen-fixing crops, for restoration of degraded agricultural lands, or |

| | | |
|---|---|---|
| | | the introduction of water saving irrigation technologies – can be applied using the financial mechanisms regulated by APSA. |
| Turkey | | |
| Year | Event | Outcome |
| 1990 | Privatization in agriculture | |
| 1999 | Agreement with IMF | The Turkish Government signed a stand-by Agreement with IMF in December 1999 committing itself to gradually phase out existing agricultural support and credit subsidy to farmers and replace them with a direct income support system targeted at poor farmers and to meanwhile rationalize the agricultural policies commensurably. |
| 2001-2008 | Agricultural Reform Implementation Project (ARIP) | Its main objective was to bring about a move market-oriented agricultural policy, through; the abolition of the administered output price and the elimination of input subsidies, including credit; the restructuring of state-owned enterprises and ASCUs; and the introduction of direct income support (DIS) , decoupled from commodity production |
| 2006 | Agricultural law implemented | Producer support based on commodity output increased, while DIS payments decreased and were eventually abolished in 2009. |
| 2014-2020 | Instrument for Pre-Accession Assistance Rural Development (IPARD) Programme | |

**Table 4.3** Socioeconomic data and its scale in Turkey and Bulgaria .

| Variable Group | Variable Name | Time-period covered | Source | Aggregated Scale |
|---|---|---|---|---|
| **Agricultural productivity** | Wheat yield (village scale) | 2001-2020 | Author created | Village/Muncipalty/District |
| **Socioeconomic variable** | Total Population | 2001-2020 | Government | District/Region |
| | Gross Domestic Product (GDP) | 2001-2020 | Government | Region |
| | Employment in Agriculture | 2001-2020 | Government | Region |
| | Unemployment rate | 2001-2020 | Government | Region |
| | Employment rate | 2001-2020 | Government | Region |
| | Human Resource in Science and Technology | 2001-2020 | Government | Region |
| **Agricultural Inputs** | Tractors | 2001-2020 | Government | District/Region |
| | Cattles | 2001-2020 | Government | District/Region |
| | Fertilizer | 2001-2020 | Government | Country |
| | Irrigation | 2001-2020 | Government | Region |
| **Agricultural policy** | Direct Agricultural Support | 2001-2020 | Government | District/Region/Muncipalty |
| | Single Agricultural Payments (SAP) | 2001-2020 | Government | District/Region/Muncipalty |
| **Agricultural Structure** | Number of holdings | 2001-2020 | Government | Region |
| | Average Used Agricultural Area (UAA) | 2001-2020 | Government | Region |
| | Managers | 2001-2020 | Government | Region |
| | Legal person holdings (Natural Person) | 2001-2020 | Government | Region |
| | Legal person holdings (Sole traders) | 2001-2020 | Government | Region |
| | Legal person holdings (Co-operative) | 2001-2020 | Government | Region |
| | Legal person holdings (Companies) | 2001-2020 | Government | Region |
| | Legal person holdings (Civil Associations and others) | 2001-2020 | Government | Region |
| **Time Dummy** | Takes a value" 0 " for 2000-2007 (pre-accession period) and value "1" for 2008-2020 (Post accession period) | | Author created | |

## Appendix 4

**Figure A.4.1** Total population of Bulgaria and northern Turkey (Edirne, Tekirdag and Kirlareli) from 2000 to 2017 (retrieved from FAOSTAT, 2019).

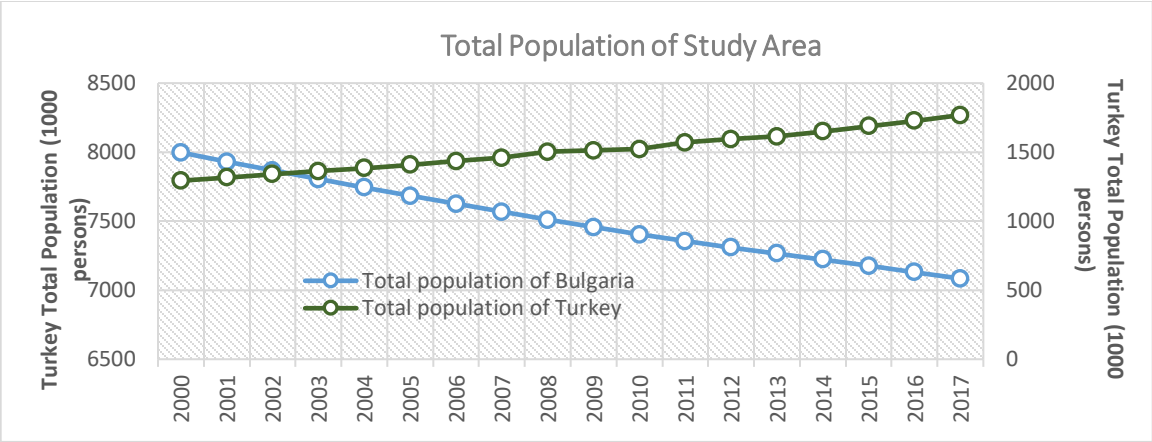

**Figure A.4.2** Wheat yield patterns and distributions at village scale for sample years 2002, 2005, 2008, 2013, and 2017.

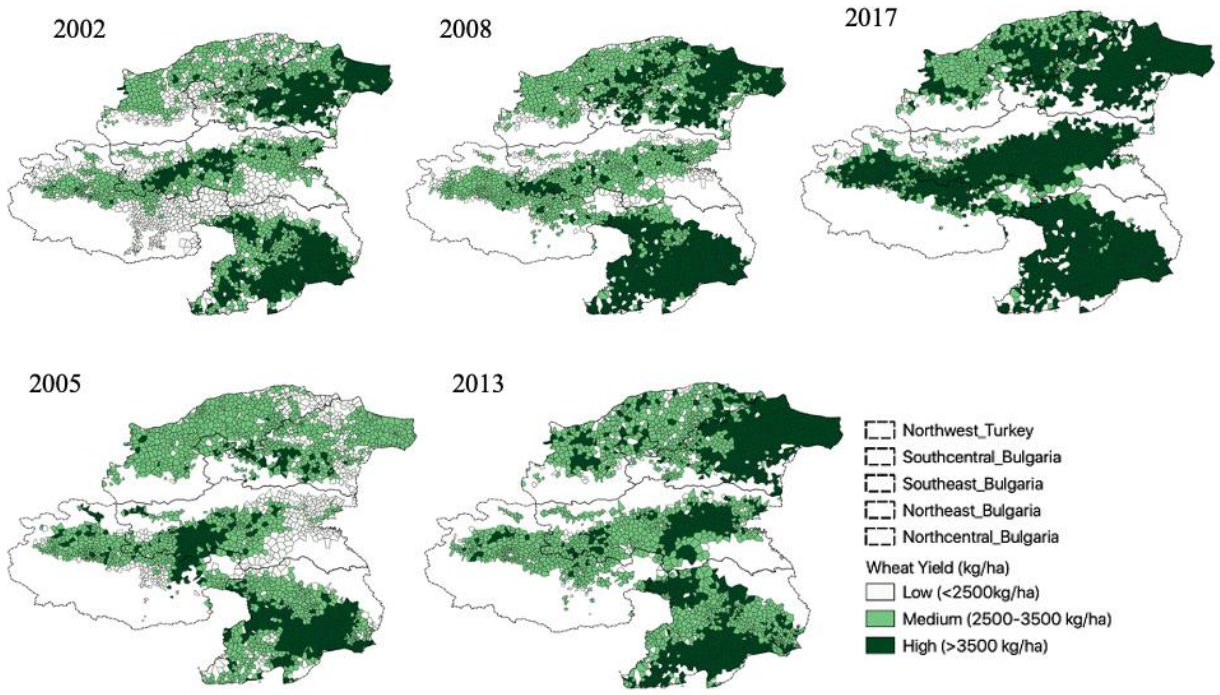

**Figure A.4.3** Village-scale soil suitability map of the study area derived from FAO. Red refers to highly suitable soil for agriculture, and blue refers to low soil suitability for agriculture.

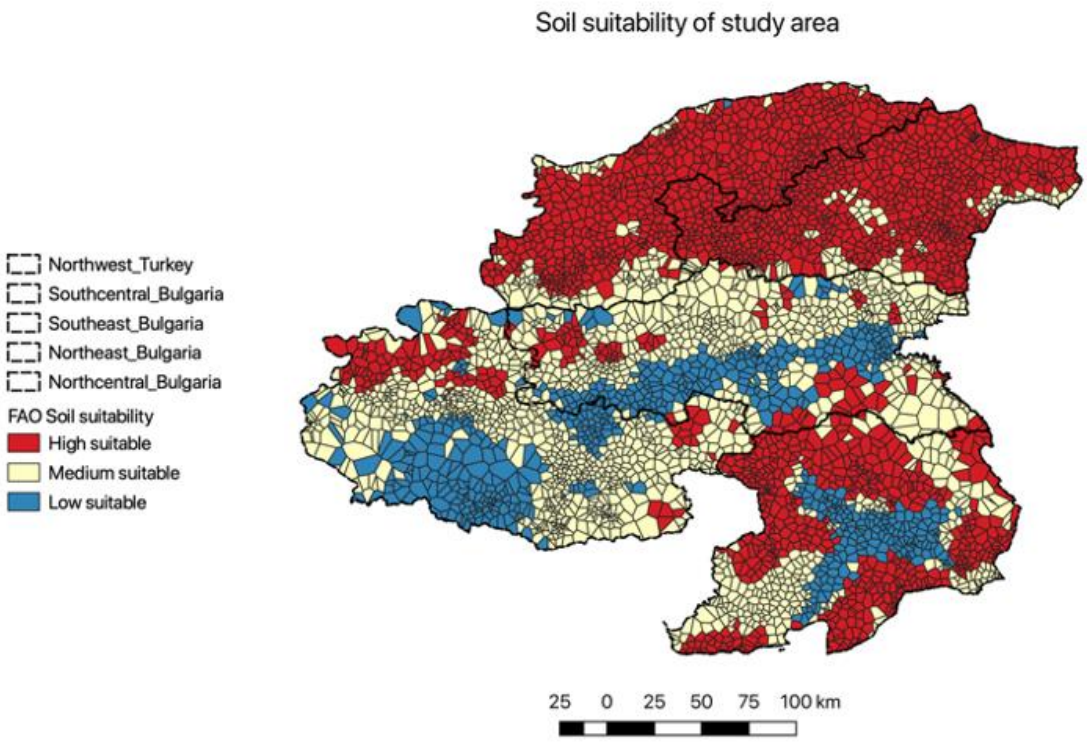

**Figure A.4.4** Wheat yield distributions in high, medium, and low soil quality from 2001-2020 in each country.

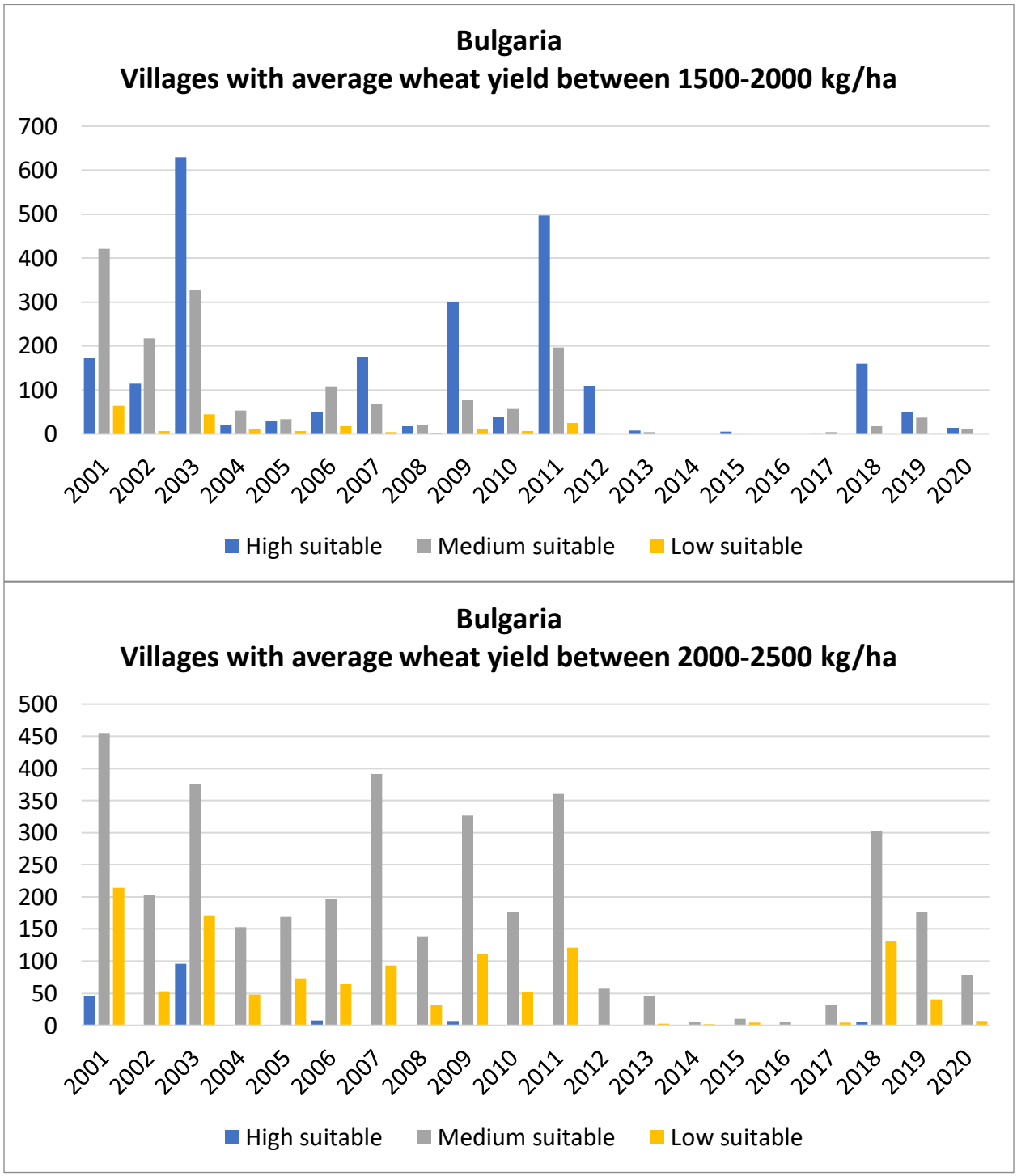

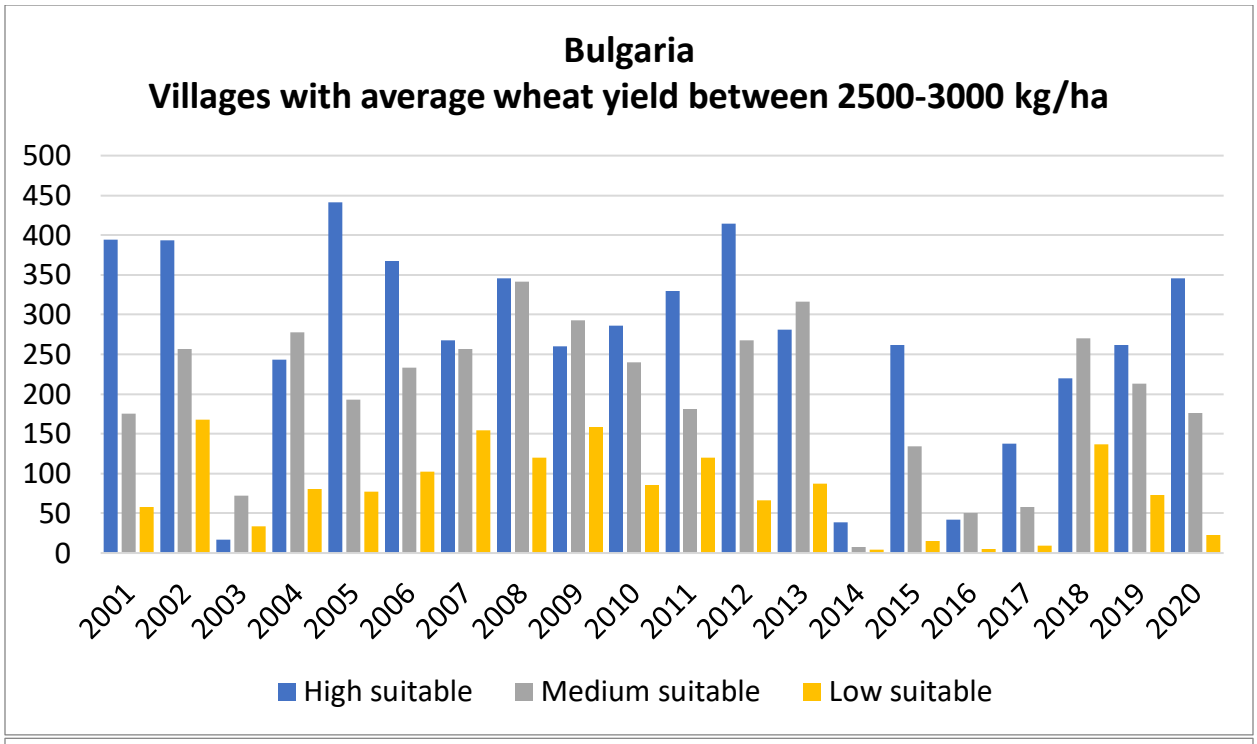
Bulgaria
Villages with average wheat yield between 2500-3000 kg/ha
500
450
400
350
300
250
200
150
100
50
0
2001
2002
2003
2004
2005
2006
2007
2008
2009
2010
2011
2012
2013
2014
2015
2016
2017
2018
2019
2020
High suitable
Medium suitable
Low suitable

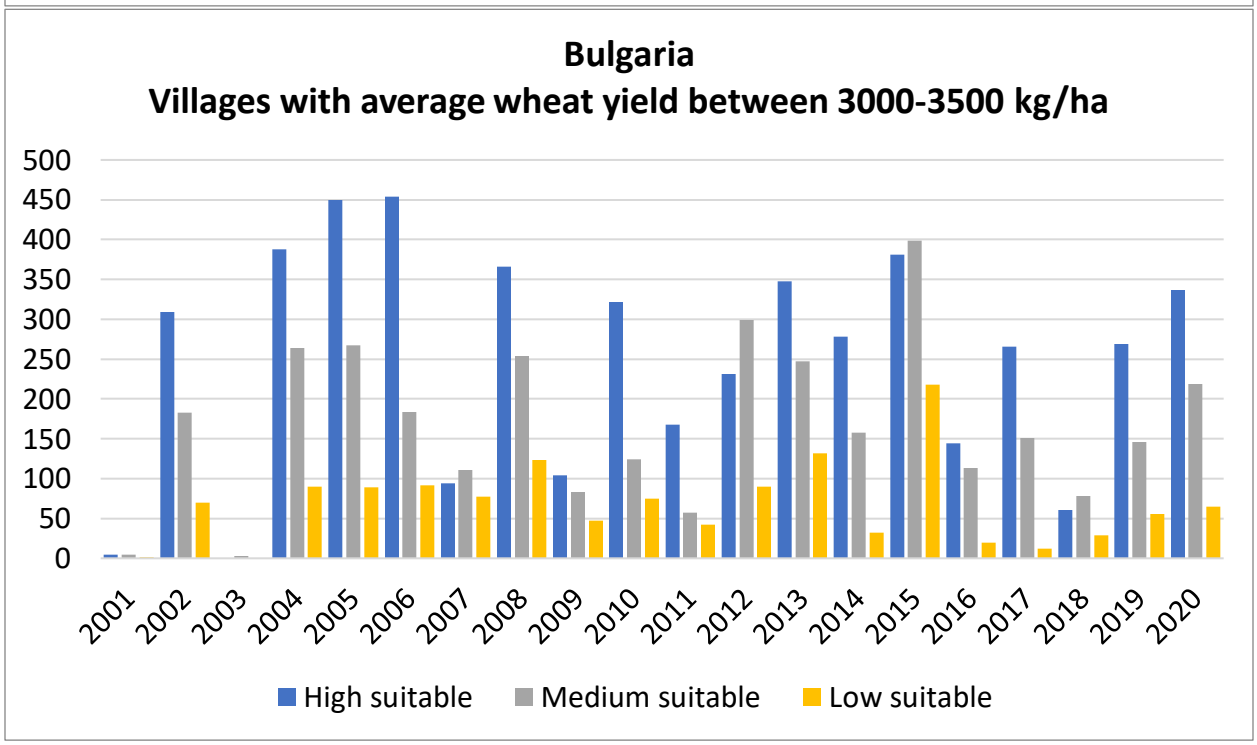
Bulgaria
Villages with average wheat yield between 3000-3500 kg/ha
500
450
400
350
300
250
200
150
100
50
0
2001
2002
2003
2004
2005
2006
2007
2008
2009
2010
2011
2012
2013
2014
2015
2016
2017
2018
2019
2020
High suitable
Medium suitable
Low suitable

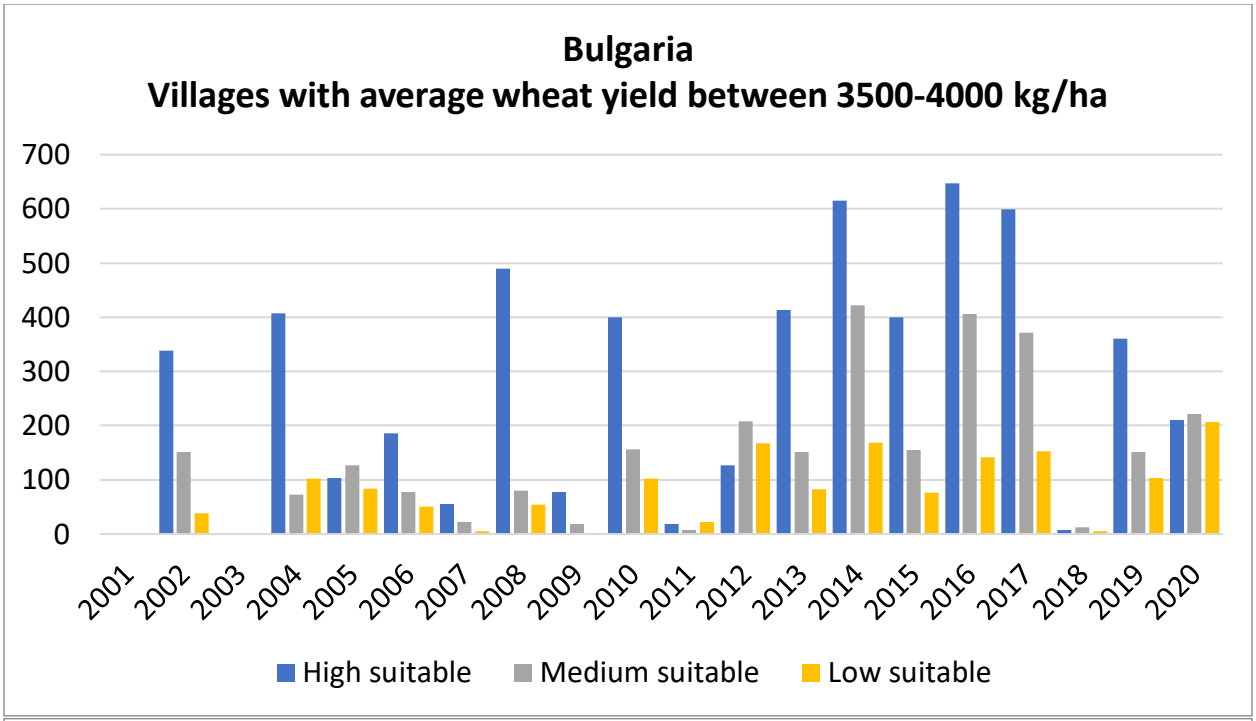
Bulgaria
Villages with average wheat yield between 3500-4000 kg/ha
700
600
500
400
300
200
100
0
2001
2002
2003
2004
2005
2006
2007
2008
2009
2010
2011
2012
2013
2014
2015
2016
2017
2018
2019
2020
High suitable
Medium suitable
Low suitable

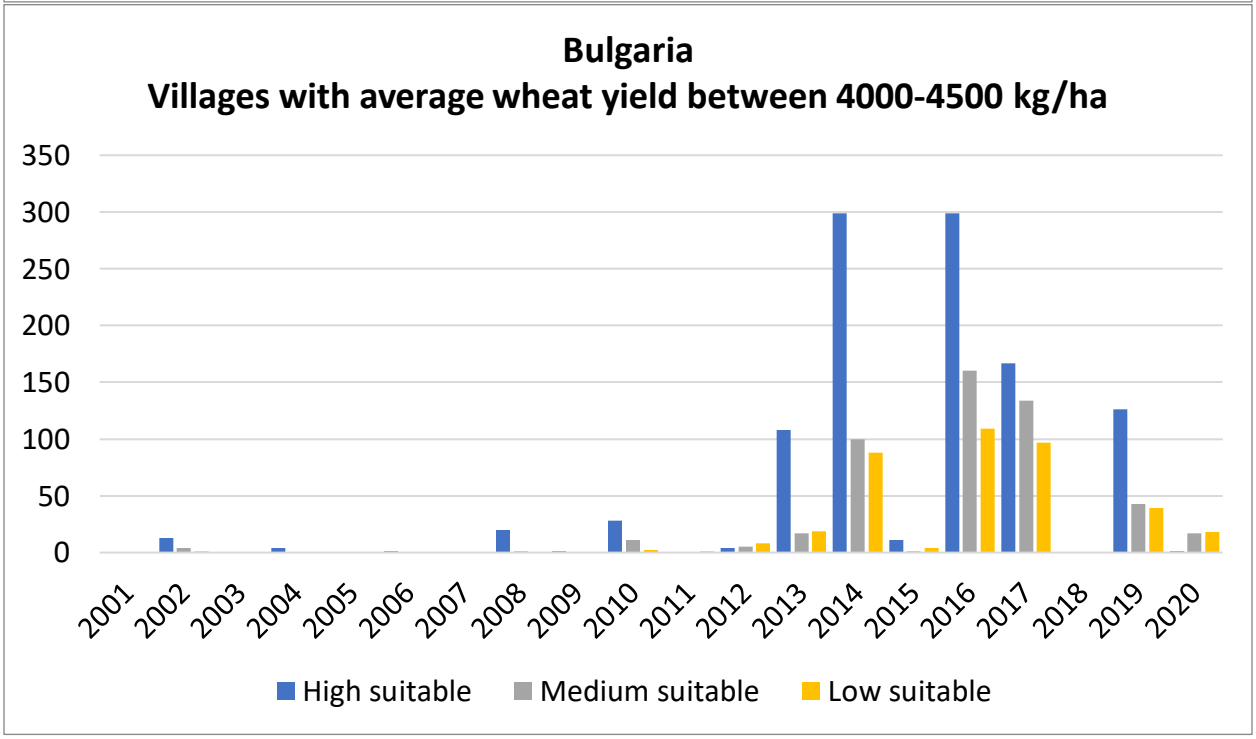
Bulgaria
Villages with average wheat yield between 4000-4500 kg/ha
350
300
250
200
150
100
50
0
2001
2002
2003
2004
2005
2006
2007
2008
2009
2010
2011
2012
2013
2014
2015
2016
2017
2018
2019
2020
High suitable
Medium suitable
Low suitable

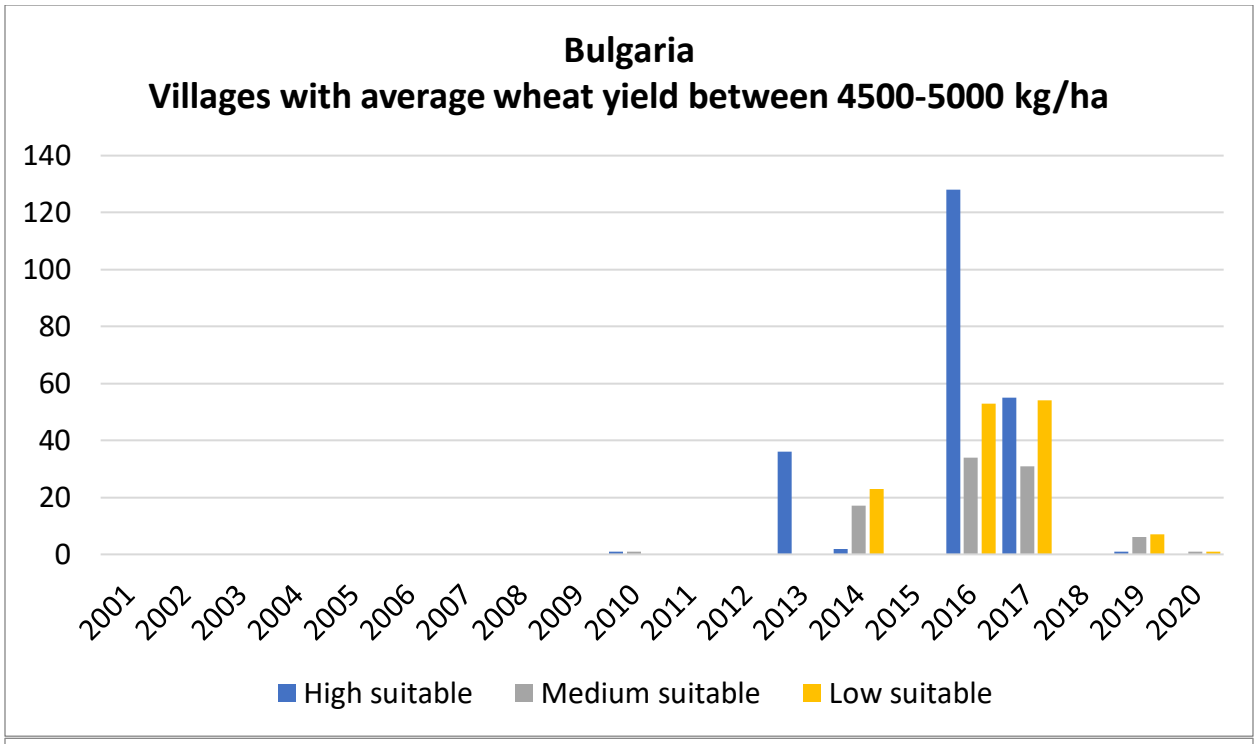
Bulgaria
Villages with average wheat yield between 4500-5000 kg/ha
140
120
100
80
60
40
20
0
2001
2002
2003
2004
2005
2006
2007
2008
2009
2010
2011
2012
2013
2014
2015
2016
2017
2018
2019
2020
High suitable
Medium suitable
Low suitable

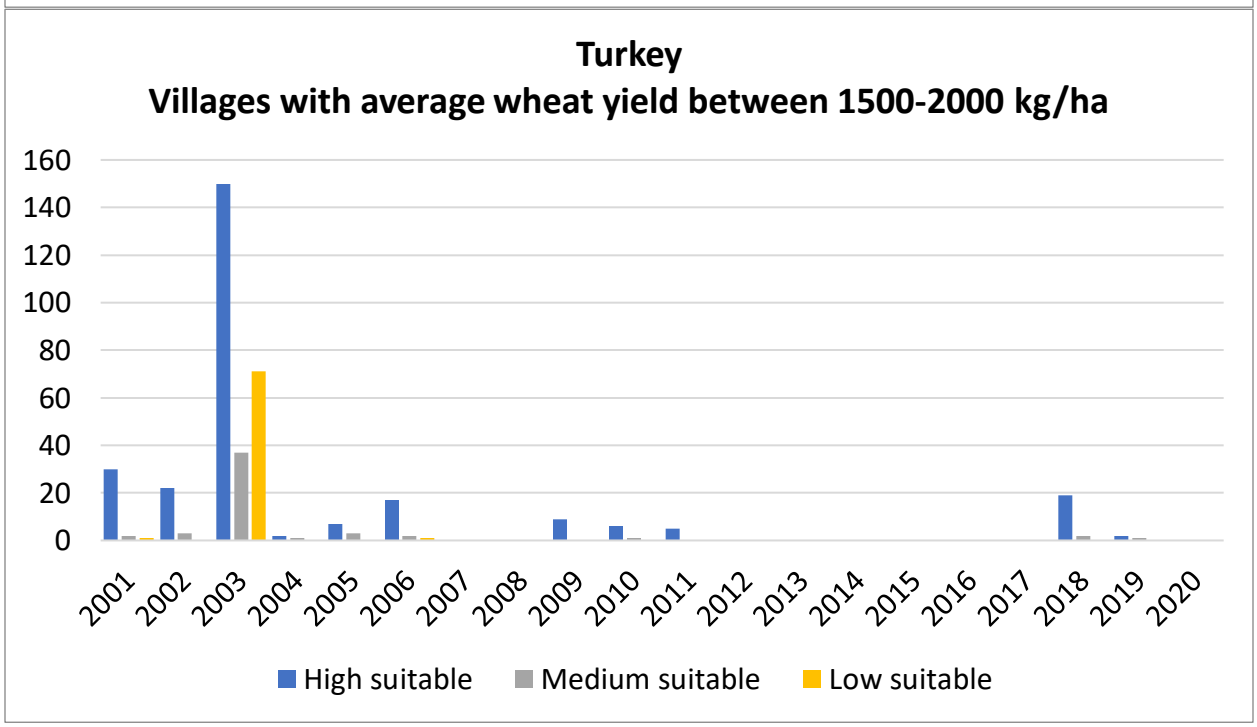
Turkey
Villages with average wheat yield between 1500-2000 kg/ha
160
140
120
100
80
60
40
20
0
2001
2002
2003
2004
2005
2006
2007
2008
2009
2010
2011
2012
2013
2014
2015
2016
2017
2018
2019
2020
High suitable
Medium suitable
Low suitable

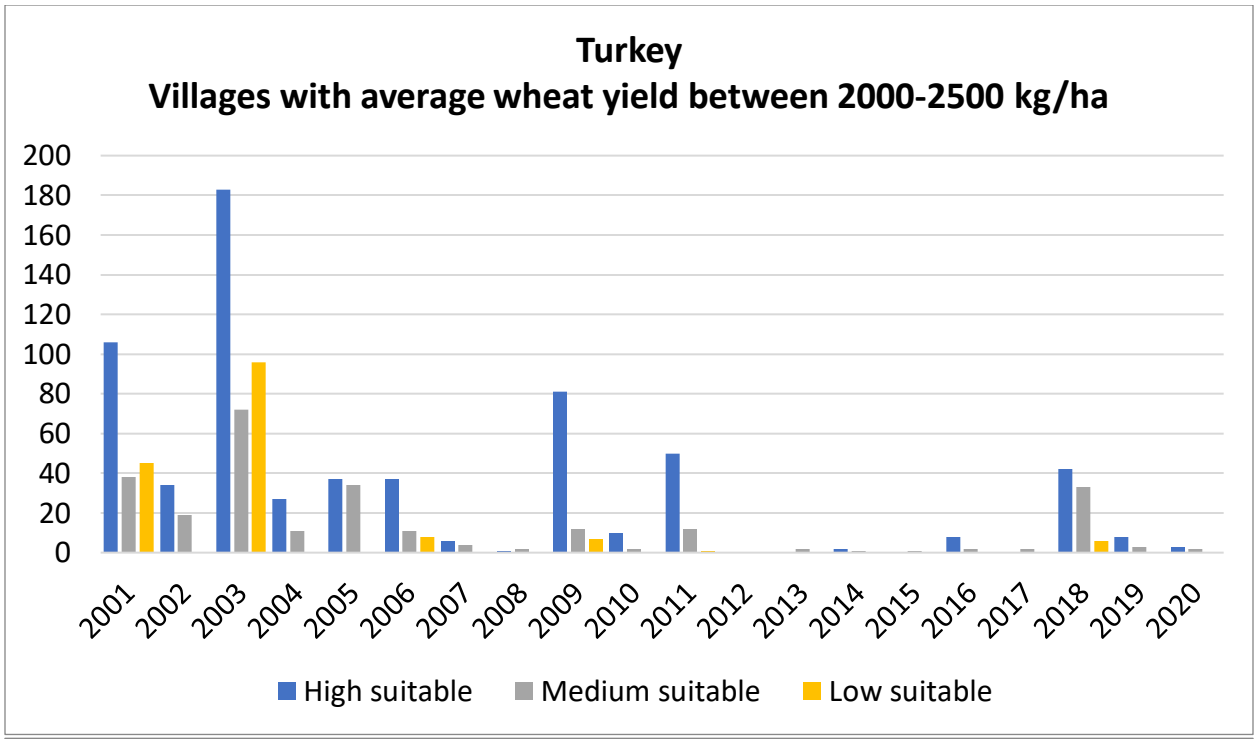
Turkey
Villages with average wheat yield between 2000-2500 kg/ha
200
180
160
140
120
100
80
60
40
20
0
2001
2002
2003
2004
2005
2006
2007
2008
2009
2010
2011
2012
2013
2014
2015
2016
2017
2018
2019
2020
High suitable
Medium suitable
Low suitable

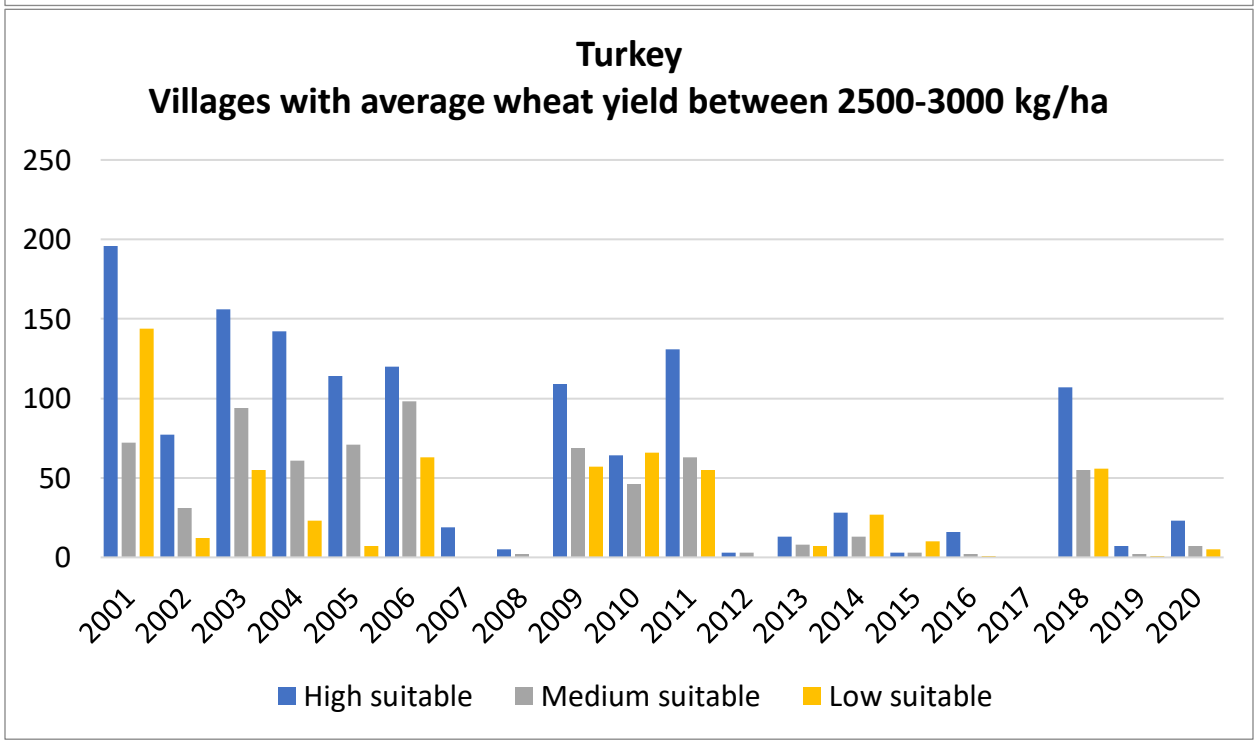
Turkey
Villages with average wheat yield between 2500-3000 kg/ha
250
200
150
100
50
0
2001
2002
2003
2004
2005
2006
2007
2008
2009
2010
2011
2012
2013
2014
2015
2016
2017
2018
2019
2020
High suitable
Medium suitable
Low suitable

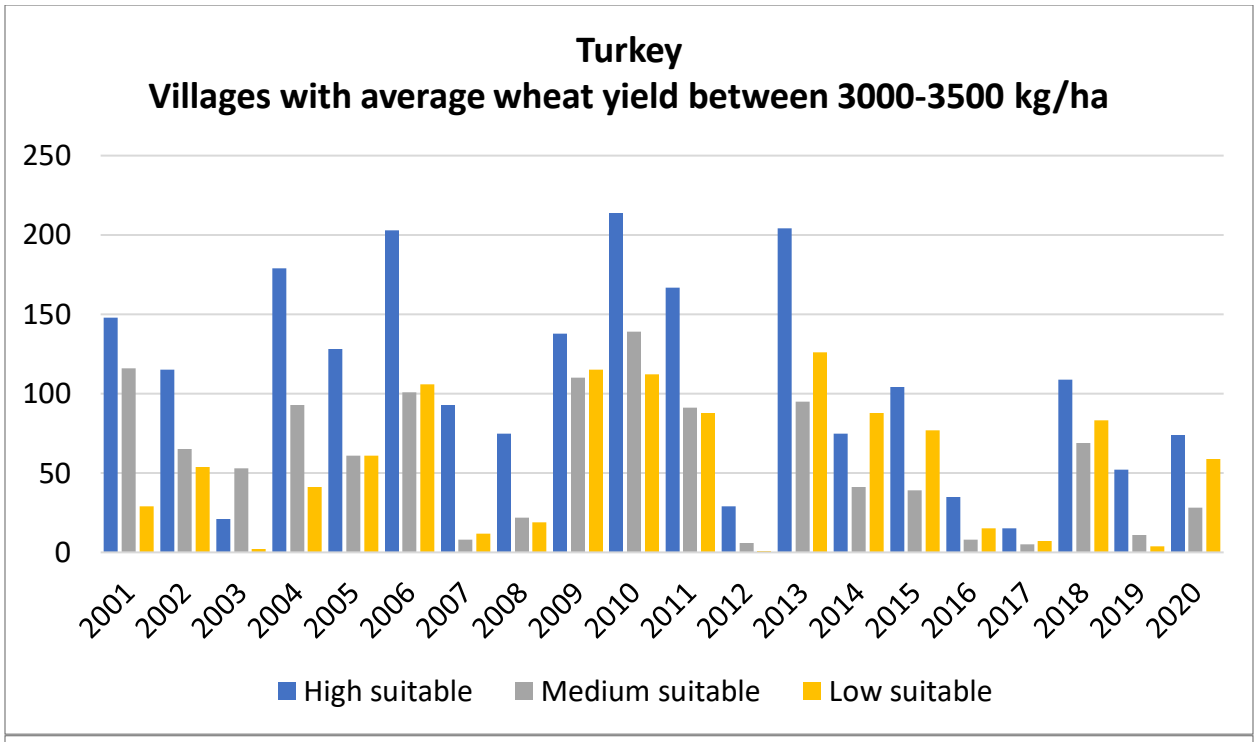
Turkey
Villages with average wheat yield between 3000-3500 kg/ha
250
200
150
100
50
0
2001
2002
2003
2004
2005
2006
2007
2008
2009
2010
2011
2012
2013
2014
2015
2016
2017
2018
2019
2020
High suitable
Medium suitable
Low suitable

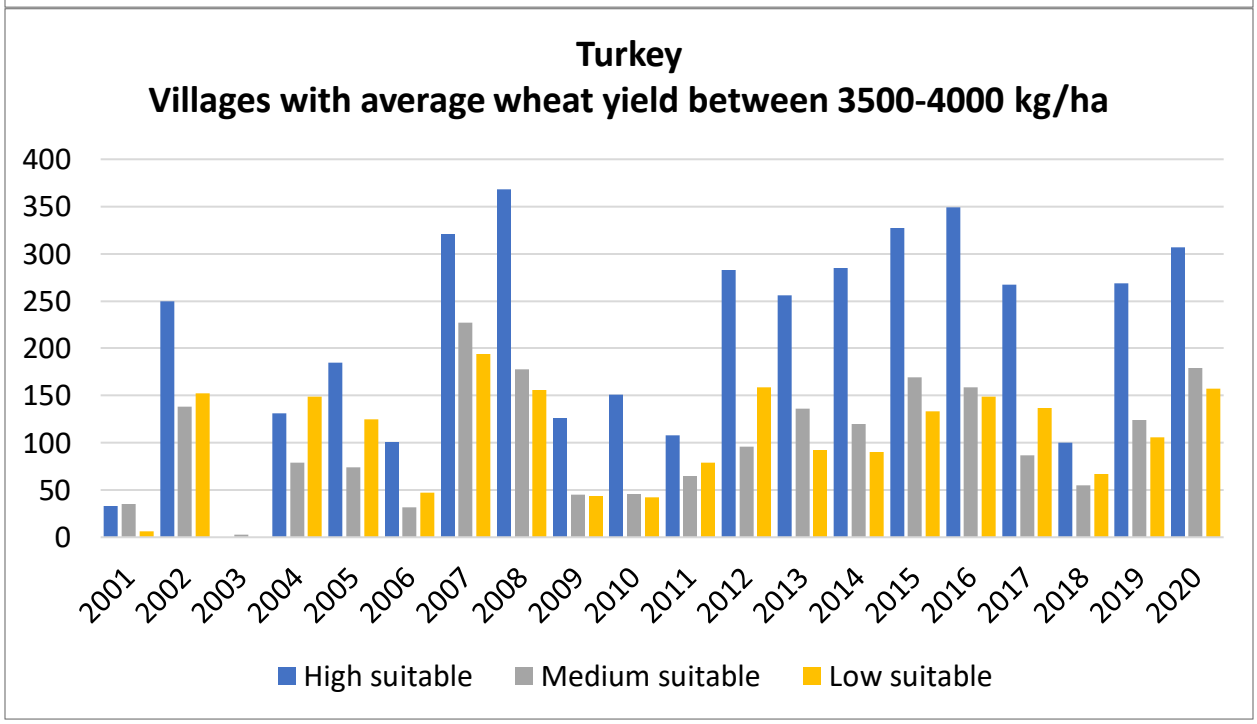
Turkey
Villages with average wheat yield between 3500-4000 kg/ha
400
350
300
250
200
150
100
50
0
2001
2002
2003
2004
2005
2006
2007
2008
2009
2010
2011
2012
2013
2014
2015
2016
2017
2018
2019
2020
High suitable
Medium suitable
Low suitable

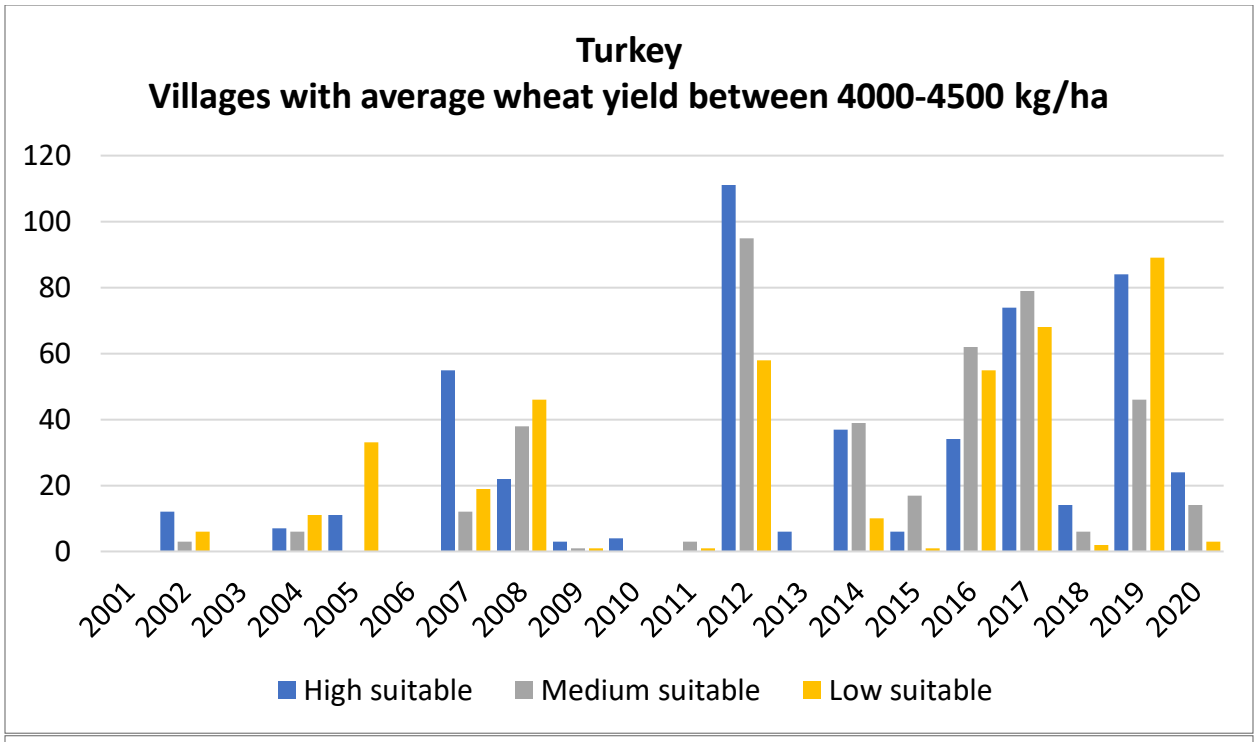
Turkey
Villages with average wheat yield between 4000-4500 kg/ha
120
100
80
60
40
20
0
2001
2002
2003
2004
2005
2006
2007
2008
2009
2010
2011
2012
2013
2014
2015
2016
2017
2018
2019
2020
High suitable
Medium suitable
Low suitable

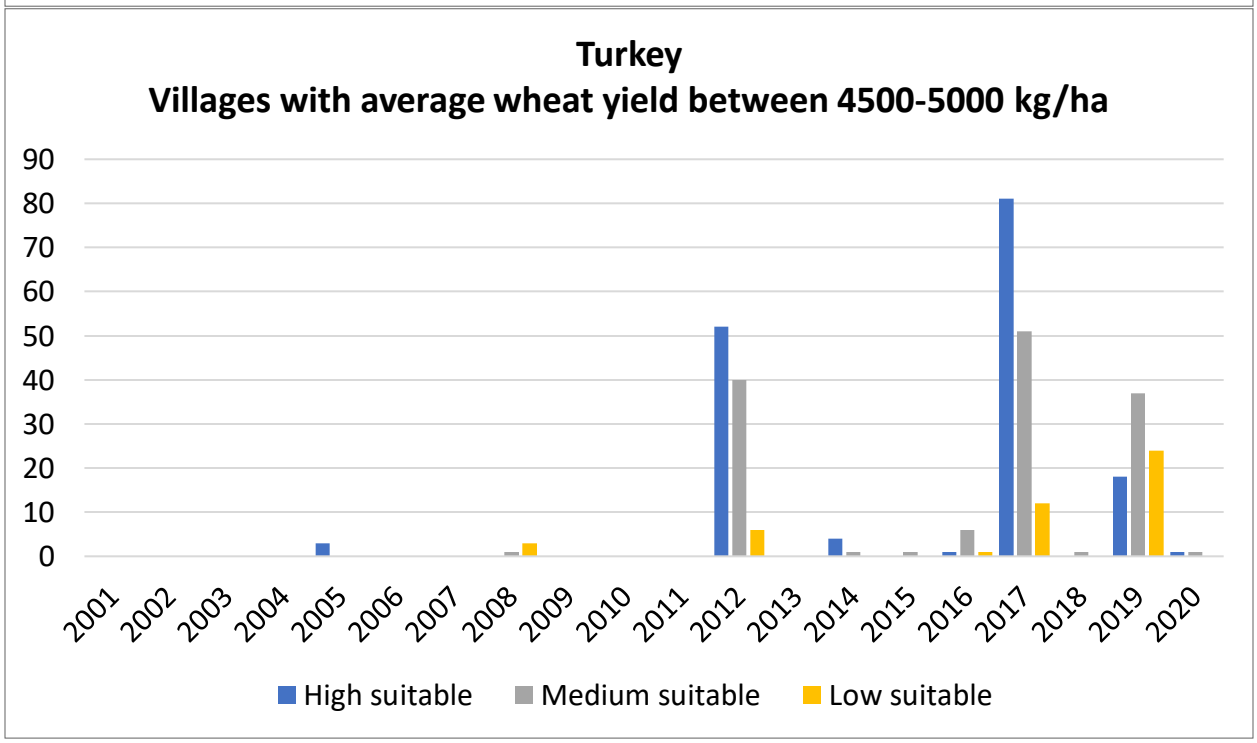
Turkey
Villages with average wheat yield between 4500-5000 kg/ha
90
80
70
60
50
40
30
20
10
0
2001
2002
2003
2004
2005
2006
2007
2008
2009
2010
2011
2012
2013
2014
2015
2016
2017
2018
2019
2020
High suitable
Medium suitable
Low suitable

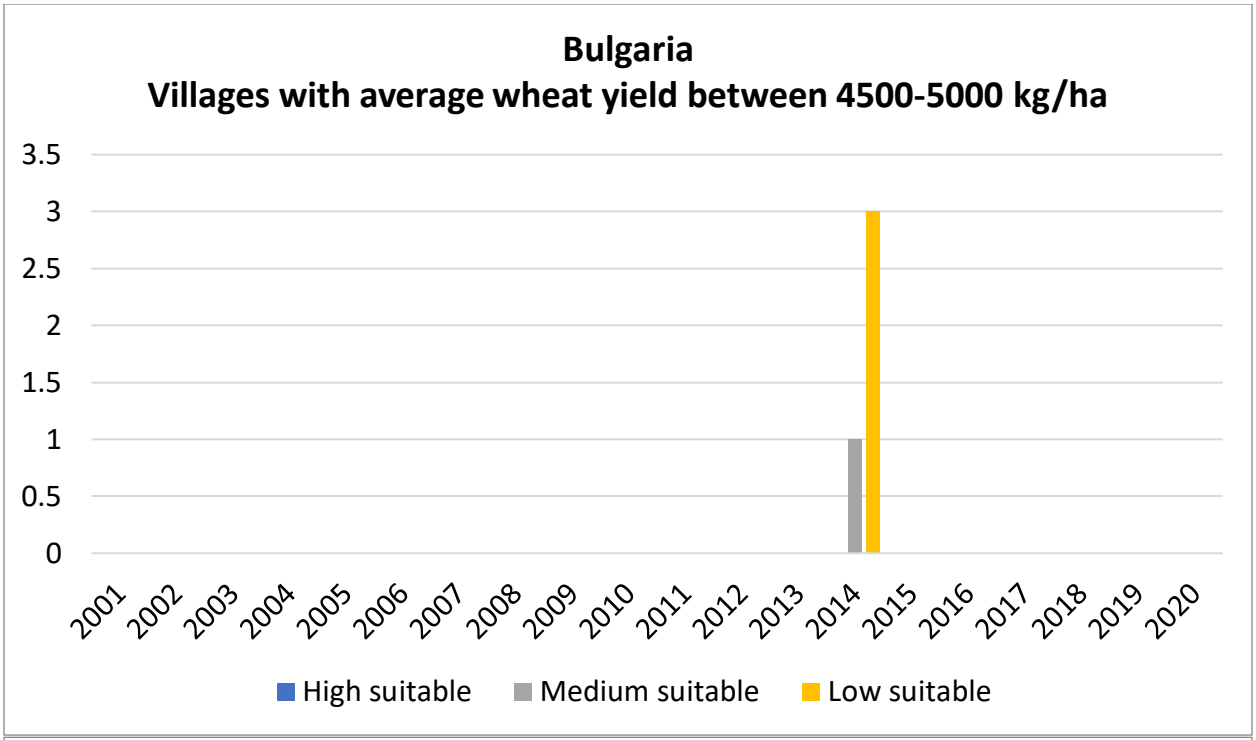
Bulgaria
Villages with average wheat yield between 4500-5000 kg/ha
3.5
3
2.5
2
1.5
1
0.5
0
2001
2002
2003
2004
2005
2006
2007
2008
2009
2010
2011
2012
2013
2014
2015
2016
2017
2018
2019
2020
High suitable
Medium suitable
Low suitable

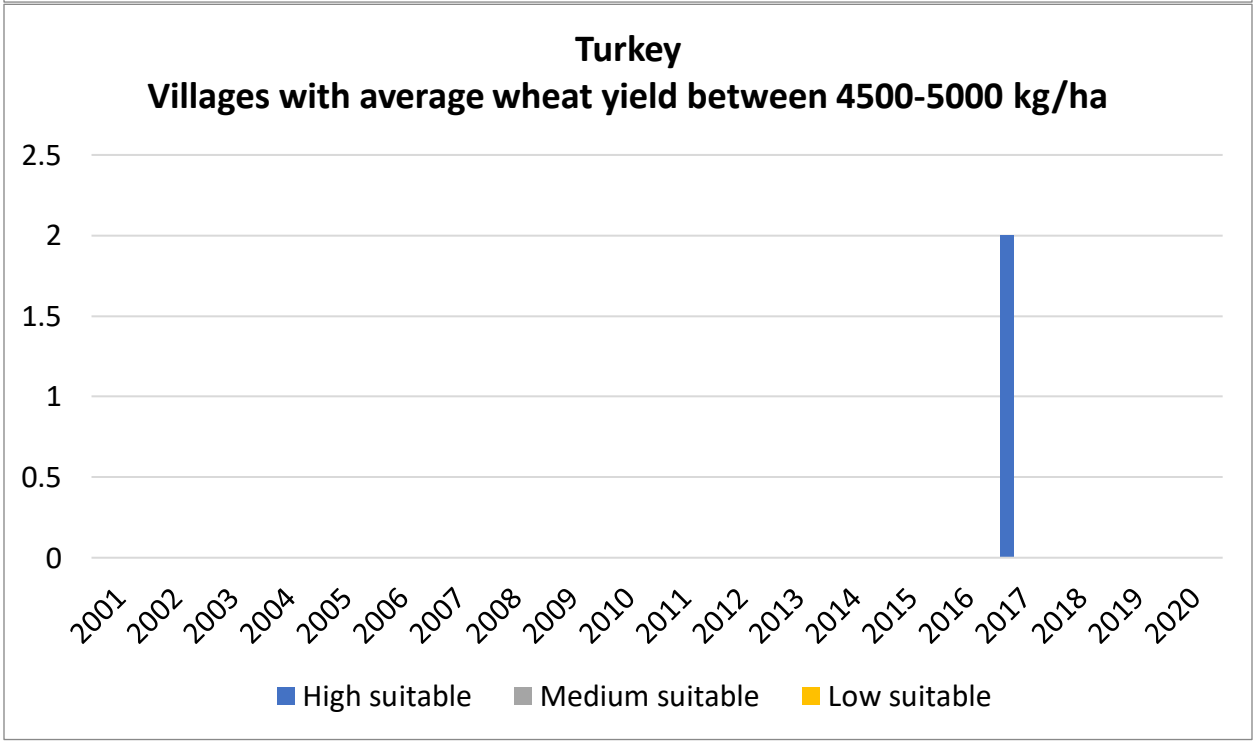
Turkey
Villages with average wheat yield between 4500-5000 kg/ha
2.5
2
1.5
1
0.5
0
2001
2002
2003
2004
2005
2006
2007
2008
2009
2010
2011
2012
2013
2014
2015
2016
2017
2018
2019
2020
High suitable
Medium suitable
Low suitable

**Table A.4.1** Number of parcels of agricultural land per holding, and average parcel size of agricultural land in Turkey in 2016 (source: Turkstat).

| Holding size (decares) | Number of parcels of agricultural land per holding | Average parcel size of agricultural land (decares) |
|---|---|---|
| Total | 5.9 | 12.9 |
| -5 | 1.5 | 1.6 |
| 5 - 9 | 2.4 | 2.7 |
| 10 - 19 | 3.4 | 3.8 |
| 20 - 49 | 4.7 | 6.4 |
| 50 - 99 | 6.9 | 9.4 |
| 100 - 199 | 10.1 | 12.9 |
| 200 - 499 | 13.7 | 20.6 |
| 500 - 999 | 21.1 | 30.3 |
| 1000+ | 36.9 | 60.3 |

**Table A.4.2** Support tools from the agricultural support policies of Turkey in the period of 2006 to 2010 (Faccio and Masulis, 2005).

| Support Tools | (%) |
|---|---|
| Direct Income Support | 45 |
| Deficiency payments | 13 |
| Livestock supports | 12 |
| Rural development supports | 10 |
| Alternative crop support | 5 |
| Crop insurance premium supports | 5 |
| Environmentally based agricultural land protection support (CATAK) | 5 |
| Other supports | 5 |
| Total | 100 |

# Chapter 5

# Main contributions and Conclusions

## 5.1 Synthesis

This dissertation started with a simple question of how humans use the land, particularly for agricultural activities, and examined challenges such as acquiring basic agricultural land use datasets (Chapter 2, Part 1); limitations in producing such datasets from individual fields to entire continents using advanced remote sensing technology and cloud platforms (Chapter 2, Part 2); constraints in accessing the historical datasets of major food crops (Chapter 2, Part 3); understanding the productivity of main food-crop farms through cutting-edge machine learning prototypes (Chapter 3); and interpreting this large-scale high-resolution agricultural intelligence to investigate broad-scale (national to sub-national) policy instruments through a top-to-bottom approach (Chapter 4) in order to assess the basic capability of farms under support-policy designs.

To demonstrate this, the cross-border area between Turkey and Bulgaria was used as a case study, mainly due to its rare geography with different nations (political units) and similar agroecosystems on each side of cross-border area. Under controlled situations, these areas would have similar agricultural production, but the national crop estimates suggested different trends in each country. This dissertation investigated the reasons behind these differences while considering the impact of humans or socio-political instruments on land-use decisions. Bulgarian accession to the EU followed by CAP implementation in 2007 was the major breakpoint of changes in the agricultural sector of Bulgaria, while Turkey had a stable democracy and business-as-usual scenario towards its agricultural development. To investigate if the changes in agricultural land and production have socio-economic underpinnings in the study area, this dissertation carried a detailed research program using remote sensing and statistical approaches.

The first step of this study was to acquire a detailed agricultural land use data of the study area. We observed that the cross-border region had only administrative-level datasets. This created the need to develop high-resolution datasets using satellite remote sensing. Wheat is the main crop in the study area and a major exported commodity. The data on wheat area and yield estimates were also available at the administrative units. Chapter 2 provided validated methods for mapping croplands and crop type (wheat only) that could be applicable from individual fields to entire regions. Chapter 3 demonstrated field-scale wheat yield estimation methods using a neural network and Landsat images. The results of Chapter 2 and Chapter 3 provided highly granular data on cropland extent, wheat area, and wheat yields from 2001 to 2020, covering the entire study area.

Although Chapters 2 and 3 developed new remote sensing methods to create high-resolution agricultural parameters of the study area, socio-economic data cannot be created through such tools. This dissertation faced major challenges in collecting high-resolution socio-economic data of the study area because the regional-level statistics were the highest administrative unit-level data we could collect.

Chapter 4 explored an approach to study the patterns and distributions of wheat yield through a bin analysis and geospatial mapping techniques along with a statistical Mann-Kendall trend test to quantify the wheat yield trends at the village scale. Chapter 4 was a sincere attempt to provide different ways of assessing the impact of socio-economic variables related to soil quality on the village-scale patterns and distributions of wheat yield. This study provided high-level insights on the drivers of wheat yield change in the study area. This study also tested the direct impact of the CAP implementation event in 2007 on the wheat yield of the study area at regional scales and found support for the hypotheses using village-level data in Bulgaria. We were partly

able to provide the answers about human impacts on agricultural land and production in the cross-border area between Turkey and Bulgaria.

In summary, this dissertation exploited the power of remote sensing to study agriculture at local to regional scales (in Chapters 2 and 3), and Chapter 4 explored the ways in which this high-resolution dataset can be used to investigate the drivers of land use and land cover change. One implication of this research is that national policies could have outsized impacts on land use decisions and ultimately the economics of the farm. To this end, the results presented here could supplement food security and sustainability questions of the study area with the hope that it could benefit the farmers and the policy makers towards a well-being of all the elements in the society in both countries.

**5.2 Implications**

Information on the location and extent of croplands has important food security, economic, and policy implications at local to regional scales (Lambin and Meyfroidt, 2011; Thenkabail et al., 2012; See et al., 2015). Remote sensing, either alone or in combination with statistical field surveys, has been at the core of identifying and mapping croplands over large areas (Myers et al., 1983; Jensen, 2009; Gao et al., 2017). Mapping of croplands over large areas using multi-date and multi-spectral remotely sensed data remains elusive, partly due to geographic variation in cultivation practices; spatial resolution requirements in areas with small parcel size distributions; large volumes of data; inconsistent availability of data across footprints; and most importantly, the need for a large number of training samples (Pax-Lenny et al., 2001; Mayaux et al., 2006; Ozdogan, 2010; Immitzer et al., 2016). To overcome these cropland extent mapping challenges, Chapter 2 (Part 1) of this dissertation introduced a generalized image classifier based on the Linear Discriminant Analysis (LDA) algorithm to map cropland extent over large scales using a simple

statistical tool. This classification model was built on training data from one location and period and applied to other times and locations without the need for additional training data. This method demonstrated the automatic application of quickly and efficiently mapping large areas of cropland without having to re-train and re-parameterize a model. The expected decrease in accuracy as we generalize from a single scene to a zone and to regions appeared to be within acceptable levels for large-scale mapping. The demonstrated generalization approach, while only tested with the LDA model, can be applied with any classification algorithm of choice. The developed approach in this study provided an automatic and scalable method of continent-scale cropland mapping using a platform like GEE without training data. The introduced generalization framework had important implications for cropland mapping over large areas at 30-meter spatial resolution while requiring very little user input.

While developing a simple algorithm with minimum inputs to demonstrate large-scale remote sensing-based cropland extent mapping was one challenge, another challenge was to produce a wall-to-wall seamless cropland extent mapping product at global scale. Chapter 2 (Part 2) of this dissertation presented a machine learning tool to produce the first cropland extent map at 30-m using Landsat-7 and Landsat-8 data for the year 2015 over 64 countries of Europe, the Middle East, Russia, and Central Asia. The resulting cropland map with ~94% overall accuracy suggested that the study area has a total 546 Mha net cultivated area, which is 17.8% net land area of the study region and nearly 30% of all global croplands. The current map showed that vast flat topographic areas of Central, Eastern, and Western Europe, irrigated zones in Central Asia and the Middle East, and highly productive soils of southwestern Russia had the highest concentrations of croplands. In contrast, Northern Europe, large parts of the Middle East, and far eastern Russia have very little agriculture. Nevertheless, the high-resolution nature of the developed map allowed us

to capture narrow concentrations of cultivated areas even in these locations. The classification approach used in this study has the potential to be replicated to map net croplands for other years in the same study area as well as in any other region, given the required inputs. The developed dataset and mapping code in this chapter is publicly available to download through NASA's Land Processes Distributed Active Archive Center (LP DAAC) at https://doi.org/10.5067/MEaSUREs/GFSAD/GFSAD30EUCEARUMECE.001 The results presented in this chapter are crucial for the societal use and scientific community, especially in studies related to agriculture, water, food security, land use and land cover change, climate change, environmental monitoring, and policy development. To date, ~4.5 million people had downloaded and used the developed cropland map (http:/croplands.org) as a base dataset for different environmental applications.

In the next step (Chapter 2, Part 3), this dissertation developed a new classification method to identify and map crop types (wheat in this case). To keep the study area aligned with the overall goal of this dissertation – to investigate the human impact on agricultural lands – this study used the cross-border area between Turkey and Bulgaria as a case study. Wheat as a staple crop, with 60% coverage of the cultivated area in the study region, plays a significant role in the livelihood and sustainability of the region (NSI, 2020; TurkStat, 2020). The two main challenges in crop type mapping in the study area were: i) need for extensive training data; and ii) lack of consistent satellite observations. Chapter 2 (Part 3) of this dissertation demonstrated an automated wheat area mapping algorithm named 'Peak Value Method" (PVM) and generated reliable wheat area maps covering the last 20 years using Landsat satellite data. The results of this study add great value to areas including food security, climate change, environment, and sustainability studies of the region.

Crop yield is a key indicator of support policy and global food security-related studies (Gibbs et al., 2008; Deryng et al., 2011; Ray et al., 2012). Accurate and timely crop yield estimates help to understand environmental stress and design the suitable adaptation framework for sustainable livelihood (Weiss et al., 2020; Ma et al., 2021). Administrative unit-level crop estimate datasets can be easily available from government statistical departments, but they come with certain disadvantages. Chapter 3 of this dissertation provided a framework for reliable wheat yield mapping in the cross-border area between using satellite observations, environmental variables and a neural network. This study evaluated a multilayer perceptron neural network (MLP-NN) model not only for temporal predictions of the wheat yield but also for the spatial predictions. This systematic model evaluation helped us to build a model based on the data from one country and apply it to the other. To date, this work presents the only village-scale (or field-scale) wheat yield dataset for the 2001-2020 time period for the cross-border area between Turkey and Bulgaria. The wheat yield dataset developed in this study is the main input for investigating the impact of policies on food security on the study area (Chapter 4).

Agricultural lands with similar agroecological and climatic characteristics usually have equal capacity to produce unless changes in agricultural input due to socio-economic transformations. Chapter 4 of this dissertation presented one such example in the cross-border area between Turkey and Bulgaria. After the implementation of Common Agricultural Policies (CAP) of the European Union (EU) in Bulgaria in 2007, the agricultural sector in Bulgaria underwent substantial changes: The rural development program was initiated, direct payments were distributed to farmers, and consolidation of agricultural lands was implemented. The Turkish side of the cross-border area has had a stable agricultural sector over the last 30 years. In this study, we analyzed regional- to village-scale staple crop (wheat) yield trends and patterns using advanced

statistical analysis, remote sensing and geospatial analysis. Results of this study provided insights about the importance of environmental and socio-economic drivers in each region of the study area and explained their impacts on wheat yield at regional to village scale. The key contribution of this research is to explain the high-level drivers of wheat yield changes since the year 2000. The main benefit of this work is its granularity and multi-scale approach. This study is the first to understand the drivers of wheat yield change in the study area and has the potential to provide new insights to policy makers and environmental investigations.

Overall, this dissertation study provided a large archive of field-scale cropland data for regional as well as specific-area case studies. Specific crop parameters mapped and validated in this study are: cropland extent, crop type (wheat), and crop yield (wheat yield) from 2001 to 2020. Along with the detailed agricultural data production, this research work developed algorithms to automatically map this detailed cropland information. In the next step, this dissertation provided an example of application of the field-scale remote sensing dataset to investigate the impact of policies in order to assess global food security. In summary, this dissertation developed and synthesized agricultural data intelligence and utilized it for the investigation of the impact of support policies on agricultural land and production with novel statistical as well as remote sensing methods. This study has discussed the advantages and disadvantages of the methods and provided a direction for its future adaptation in each chapter. We believe the findings of this research are useful for different stakeholders ranging from farmers and policy makers to environmental scientists and government officials. At the core of this dissertation, our hope is to help farmers and policy makers to make informed decisions about the farmland and to have better yields and improve the economics of the land while maintaining sustainability, the environment, and food security.

## 5.3 Future research

This dissertation emphasized agricultural data development and its social science applications. The way people farm is changing every day and there is a continuous need to provide science-driven information to keep pace with the changing environment. This motivates us to explore the following agricultural remote sensing-related questions:

1. *Continue monitoring the agricultural areas towards agricultural data bank archives*.

   Chapters 2 and 3 provided detailed agricultural data archives from 2000 to 2020 for the cross-border area between Turkey and Bulgaria. To stay up to date on these data archives and expand them, future research will be focused on: i) improving the current mapping products; and ii) developing new maps. The generalization scheme presented in Chapter 2 can be scaled to develop a new global model with the same methodological framework, and this model can be further used to automatically map large-area croplands. The cropland extent mapping product in Chapter 2 could be updated for past and future years using the same methodology and for the same area. Wheat-area mapping products can be further improved through up-to-date satellite inputs from the upcoming Landsat-9 or Sentinel datasets. Wheat-yield datasets provided in the Chapter 4 could use more detailed knowledge on reference data to improve the predictions. Given the new growth, if governments release the improved reference data, these datasets can be updated using similar methodology. Lastly, impact policies in the region are elastic, and therefore, elastic land use and land cover frameworks need to be produced to investigate those minor changes and their impact on farmers. This research dataset could use detailed socio-economic data if it is released by respective governments. The fusion approach of geospatial land use pattern analysis and statistical models would improve the

investigational framework and may provide detailed insights on the impact of support policies in the study area.

2. *Continue improving the machine learning and deep learning algorithms*.

   Every method comes with caveats and advantages. In this new era of easy access to advanced technology – the power of the current dataset used in this research can be improved through excessive testing of deep neural networks, and also improving the input datasets through new libraries of data could be helpful.

3. *Expanding the agricultural monitoring to other regions*.

   Farmers are the backbone of half of the world's economy. This dissertation's research methods can be expanded to other regions of the world to fill the data gap and improve the agricultural monitoring of those regions.

4. *Provide an automatic and scalable tool to investigate and quantify policy impact on agricultural land use and land cover.*

   To date, policy frameworks are highly manual, and they have the capability to automate if focused on specific regions. Future research in this direction can be useful to society to bring accurate, data-driven tools to farmers in order to make suitable decisions for their farms according to current subsidies, environmental change, and requirements of the market.

References

Lambin, E. F., & Meyfroidt, P. (2011). Global land use change, economic globalization, and the looming land scarcity. *Proceedings of the National Academy of Sciences*, *108*(9), 3465-3472.

Thenkabail, P. S., & Wu, Z. (2012). An automated cropland classification algorithm (ACCA) for Tajikistan by combining Landsat, MODIS, and secondary data. *Remote Sensing*, *4*(10), 2890-2918.

See, L., Fritz, S., You, L., Ramankutty, N., Herrero, M., Justice, C., ... & Obersteiner, M. (2015). Improved global cropland data as an essential ingredient for food security. *Global Food Security*, *4*, 37-45.

Myers, V. I. (1983). Remote sensing applications in agriculture. *Manual of remote sensing*, 2111-2228.

Jensen, J. R. (2009). *Remote sensing of the environment: An earth resource perspective 2/e*. Pearson Education India.

Gao, F., Anderson, M. C., Zhang, X., Yang, Z., Alfieri, J. G., Kustas, W. P., ... & Prueger, J. H. (2017). Toward mapping crop progress at field scales through fusion of Landsat and MODIS imagery. *Remote Sensing of Environment*, *188*, 9-25.

Pax-Lenney, M., Woodcock, C. E., Macomber, S. A., Gopal, S., & Song, C. (2001). Forest mapping with a generalized classifier and Landsat TM data. *Remote Sensing of Environment*, *77*(3), 241-250.

Mayaux, P., Eva, H., Gallego, J., Strahler, A. H., Herold, M., Agrawal, S., ... & Roy, P. S. (2006). Validation of the global land cover 2000 map. *IEEE Transactions on Geoscience and Remote Sensing*, *44*(7), 1728-1739.

Ozdogan, M. (2010). The spatial distribution of crop types from MODIS data: Temporal unmixing using Independent Component Analysis. *Remote Sensing of Environment*, *114*(6), 1190-1204.

Immitzer, M., Vuolo, F., & Atzberger, C. (2016). First experience with Sentinel-2 data for crop and tree species classifications in central Europe. *Remote Sensing*, *8*(3), 166.

National Statistical Institute (NSI), Bulgaria, (2020) https://infostat.nsi.bg/infostat/pages/module.jsf?x_2=6.

Turkish Statistical Institute (TURKSTAT), Turkey, (2020) https://www.tuik.gov.tr/Home/Index.

Khan, A., Hansen, M. C., Potapov, P., Stehman, S. V., & Chatta, A. A. (2016). Landsat-based wheat mapping in the heterogeneous cropping system of Punjab, Pakistan. *International Journal of Remote Sensing*, *37*(6), 1391-1410.

Qiu, B., Luo, Y., Tang, Z., Chen, C., Lu, D., Huang, H., ... & Xu, W. (2017). Winter wheat mapping combining variations before and after estimated heading dates. *ISPRS Journal of Photogrammetry and Remote Sensing*, *123*, 35-46.

Zhong, L., Hu, L., Zhou, H., & Tao, X. (2019). Deep learning based winter wheat mapping using statistical data as ground references in Kansas and northern Texas, US. *Remote Sensing of Environment, 233*, 111411.

Ramankutty, N., & Foley, J. A. (1999). Estimating historical changes in global land cover: Croplands from 1700 to 1992. *Global Biogeochemical Cycles*, *13*(4), 997-1027.

Gibbs, H. K., & Salmon, J. M. (2015). Mapping the world's degraded lands. *Applied Geography*, *57*, 12-21.

Ozdogan, M., Yang, Y., Allez, G., & Cervantes, C. (2010). Remote sensing of irrigated agriculture: Opportunities and challenges. *Remote Sensing*, *2*(9), 2274-2304.

Mulla, D. J. (2013). Twenty five years of remote sensing in precision agriculture: Key advances and remaining knowledge gaps. *Biosystems Engineering*, *114*(4), 358-371.

Roy, P. S., Behera, M. D., & Srivastav, S. K. (2017). Satellite remote sensing: sensors, applications and techniques. *Proceedings of the National Academy of Sciences, India Section A: Physical Sciences volume 87*, 465–472.

Gibbs, H. K., Johnston, M., Foley, J. A., Holloway, T., Monfreda, C., Ramankutty, N., & Zaks, D. (2008). Carbon payback times for crop-based biofuel expansion in the tropics: the effects of changing yield and technology. *Environmental Research Letters*, *3*(3), 034001.

Deryng, D., Sacks, W. J., Barford, C. C., & Ramankutty, N. (2011). Simulating the effects of climate and agricultural management practices on global crop yields. *Global Biogeochemical Cycles*, *25*(2).

Ray, D. K., Ramankutty, N., Mueller, N. D., West, P. C., & Foley, J. A. (2012). Recent patterns of crop yield growth and stagnation. *Nature Communications*, *3*(1), 1-7.

Weiss, M., Jacob, F., & Duveiller, G. (2020). Remote sensing for agricultural applications: A meta-review. *Remote Sensing of Environment, 236*, 111402.

Ma, Y., Zhang, Z., Kang, Y., & Özdoğan, M. (2021). Corn yield prediction and uncertainty analysis based on remotely sensed variables using a Bayesian neural network approach. *Remote Sensing of Environment, 259*, 112408.

Doraiswamy, P. C., Moulin, S., Cook, P. W., & Stern, A. (2003). Crop yield assessment from remote sensing. *Photogrammetric Engineering & Remote Sensing*, *69*(6), 665-674.

Iizumi, T., & Ramankutty, N. (2016). Changes in yield variability of major crops for 1981–2010 explained by climate change. *Environmental Research Letters, 11*(3), 034003.

Meyfroidt, P., Abeygunawardane, D., Ramankutty, N., Thomson, A., & Zeleke, G. (2019). Interactions between land systems and food systems. *Current Opinion in Environmental Sustainability, 38*, 60-67.

Verburg, P. H., Neumann, K., & Nol, L. (2011). Challenges in using land use and land cover data for global change studies. *Global Change Biology*, *17*(2), 974-989.

Burke, M., & Lobell, D. B. (2017). Satellite-based assessment of yield variation and its determinants in smallholder African systems. *Proceedings of the National Academy of Sciences, 114*(9), 2189-2194.

Hunt, M. L., Blackburn, G. A., Carrasco, L., Redhead, J. W., & Rowland, C. S. (2019). High resolution wheat yield mapping using Sentinel-2. *Remote Sensing of Environment, 233*, 111410.

Ray, D. K., Gerber, J. S., MacDonald, G. K., & West, P. C. (2015). Climate variation explains a third of global crop yield variability. *Nature Communications*, *6*(1), 1-9.

Lobell, D. B. (2013). The use of satellite data for crop yield gap analysis. *Field Crops Research, 143*, 56-64.